AD-A054 239 NAVAL POSTGRADUATE SCHOOL MONTEREY CALIF F/G 13/2
EXPERIMENTAL INVESTIGATION OF THE MARINE BOUNDARY LAYER IN SUPP--ETC(U)
FEB 78 G E SCHACHER, C W FAIRALL
UNCLASSIFIED NPS61-78-002 NL

1 OF 3
AD A054239

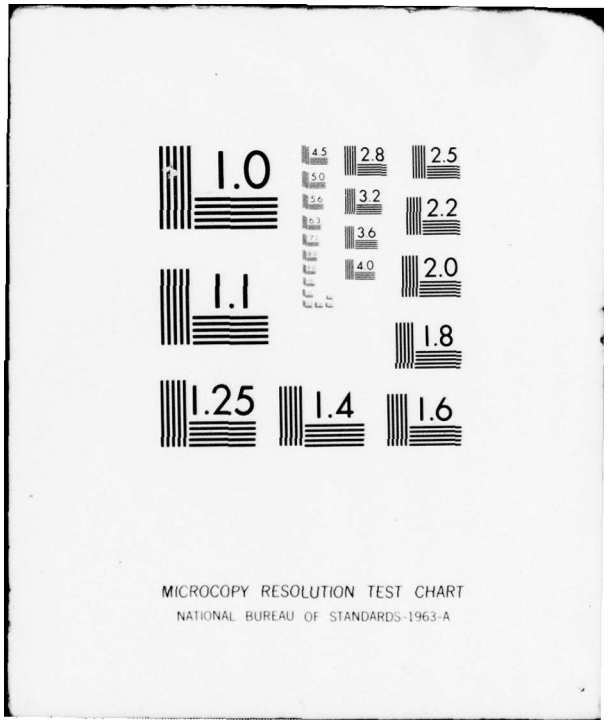
1.0
1.1
1.25
1.4
1.6
1.8
2.0
2.2
2.5
2.8
3.2
3.6
4.0
4.5
5.0
5.6
6.3
MICROCOPY RESOLUTION TEST CHART
NATIONAL BUREAU OF STANDARDS-1963-A

NPS61-78-002

NAVAL POSTGRADUATE SCHOOL

Monterey, California

EXPERIMENTAL INVESTIGATION
OF THE MARINE BOUNDARY LAYER
IN SUPPORT OF AIR POLLUTION STUDIES
IN THE LOS ANGELES AIR BASIN

G. E. Schacher, C. W. Fairall,
K. L. Davidson, and T. M. Houlihan

February 1978

Prepared for: California Air Resources Board
Sacramento, California 95814

NAVAL POSTGRADUATE SCHOOL
Monterey, California

Rear Admiral I. W. Linder
Superintendent

J. R. Borsting
Provost

The work reported herein was supported in part by the California Air Resources Board, Sacramento, California.

This report was prepared by:

G. E. Schacher
Associate Professor of Physics

C. W. Fairall
Assistant Professor of Physics

K. L. Davidson
Associate Professor of Meteorology

T. M. Houlihan
Associate Professor of
Mechanical Engineering

Approved by:

K. E. Woehler, Chairman
Department of Physics and Chemistry

William M. Tolles
Acting Dean of Research

NPS61-78-002

UNCLASSIFIED

SECURITY CLASSIFICATION OF THIS PAGE (When Data Entered)

REPORT DOCUMENTATION PAGE

READ INSTRUCTIONS BEFORE COMPLETING FORM

1. REPORT NUMBER: NPS61-78-002
2. GOVT ACCESSION NO.:
3. RECIPIENT'S CATALOG NUMBER:
4. TITLE (and Subtitle): Experimental Investigation of the Marine Boundary Layer in Support of Air Pollution Studies in the Los Angeles Air Basin.
5. TYPE OF REPORT & PERIOD COVERED: Technical Report
6. PERFORMING ORG. REPORT NUMBER:
7. AUTHOR(s): G.E. Schacher, C.W. Fairall, K.L. Davidson, and T.M. Houlihan
8. CONTRACT OR GRANT NUMBER(s):
9. PERFORMING ORGANIZATION NAME AND ADDRESS: Naval Postgraduate School, Monterey, CA 93940
10. PROGRAM ELEMENT, PROJECT, TASK AREA & WORK UNIT NUMBERS: N622717WE70081
11. CONTROLLING OFFICE NAME AND ADDRESS: California Air Resources Board, 1709 11th Street, Sacramento, CA 95814
12. REPORT DATE: February 1978
13. NUMBER OF PAGES: 257 (12) 253 p.
14. MONITORING AGENCY NAME & ADDRESS (if different from Controlling Office):
15. SECURITY CLASS. (of this report): UNCLASSIFIED
15a. DECLASSIFICATION/DOWNGRADING SCHEDULE:
16. DISTRIBUTION STATEMENT (of this Report): Approved for public release; distribution unlimited.
17. DISTRIBUTION STATEMENT (of the abstract entered in Block 20, if different from Report):
18. SUPPLEMENTARY NOTES:
19. KEY WORDS (Continue on reverse side if necessary and identify by block number): Marine Boundary Layer, Air Pollution, Turbulence
20. ABSTRACT (Continue on reverse side if necessary and identify by block number):

A four level shipboard system has been used to obtain profiles of mean wind, temperature, and humidity and to obtain distributions of temperature and wind speed fluctuations. These data have been used to characterize the marine boundary layer in the Los Angeles air basin and to obtain turbulence fluxes of momentum and sensible heat. The data show that the overwater mixing rates are much smaller than those observed on land, even though land influence can be seen as far as 30 miles from shore. Parameters have over

DD FORM 1 JAN 73 1473 EDITION OF 1 NOV 65 IS OBSOLETE S/N 0102-014-6601

UNCLASSIFIED

SECURITY CLASSIFICATION OF THIS PAGE (When Data Entered)

251 457

been obtained which can be used as inputs for the land-sea boundary descriptions involved in current air pollution analyses.

"The statements and conclusions in this report are those of the contractor and not necessarily those of the California Air Resources Board. The mention of commercial products, their source or their use in connection with material reported herein is not to be construed as either and actual or implied endorsement of such products."

TABLE OF CONTENTS

LIST OF TABLES

LIST OF FIGURES

I. Introduction

In July 1977 the Naval Postgraduate School (NPS) conducted a cruise aboard the R/V Acania of approximately two weeks duration (7/17 to 7/28) to the Los Angeles air basin. The basin is of great interest for meteorological studies because of its configuration, which, in conjunction with the prevalent marine inversion causes a severe air pollution problem. The purpose of this cruise was to conduct initial overwater studies of the area within 40 nautical miles of shore from Santa Barbara to Long Beach. There is a need for this type of work since very little data has been collected on the seaward boundary of the air basin. This means that there is insufficient data available to establish boundary conditions for current air pollution models. Since the westward boundary of the area is far out to sea, data must be collected from some type of overwater platform.

One of the main purposes of this cruise was to collect turbulence data on the boundaries of the California Air Resources Board (CARB) numerical air pollution diffusion model and at several locations within the boundary. This data was to be collected at several different times of day, and if possible, under different meteorological conditions. At the same time a fairly complete set of parameters were measured in order to specify the local atmospheric conditions. These data will be used to adjust the parameterization of the CARB model.

The second main endeavor of the NPS effort was to participate in an air flow trajectory experiment conducted by the California Institute of Technology (CIT). In this experiment a tracer gas (SF_6) was released from the smoke stacks of the El Segundo power plant and the air flow was traced by monitoring stations along the shore and by the R/V Acania. Thus, the ship

provided a portion of the tracer effort and the overwater meteorological support. Of course, the meteorological data was also used to expand the data base for the model studies.

A complete list of the various activities performed on the cruise is given in Section II.

This report will describe in detail, and report the results for the NPS effort on this cruise. Other groups, in particular the Air Resources Board, were major participants in the cruise and their results are reported elsewhere. Here we describe the other projects only very briefly, and no results are reported. Of course, the R/V Acania was the vehicle for all overwater experiments.

This was planned as the first of a number of cruises whose purpose would be to collect overwater data which would directly relate to air pollution studies. The period of time chosen was not necessarily the best for performing some of the studies (in particular the release of SF_6 from the power plant) but was a target of opportunity. However, since we hope to conduct several such cruises during different times of the year in order to test a wide range of conditions, the dates used are entirely appropriate. Also, as shall be seen below, the prevailing conditions were excellent for all of the experiments planned.

II. Participants, Experiments Performed

The various organizations other than NPS which participated in this cruise were:

California Air Resources Board (CARB)

Calspan Corporation

California Institute of Technology (CIT)

Naval Weather Service Facility (NWS)

Science Application, Inc. (SAI)

Western Oil & Gas Association (WOGA)

The principal activities of these groups were as follows:

CARB: Collect data on air pollutants, coordination between shipboard and shore personnel, logistic support in the Southern California area.

Calspan: Collect aerosol data, maintain meteorological conditions log.

CIT: Conduct release and collection of tracer gases both on ship and shore.

NWS: Perform radiosonde releases twice daily.

SAI: Observe shipboard operations and maintain a log for WOGA.

WOGA: Coordinate with oil tankers and drilling platforms.

The various experiments and the dates and times on which they were performed were:

17/0900 - 18/0230 Monitor open ocean aerosol and pollutant background levels.

18/0300 - 18/1000 Monitor aerosol and pollutants in Santa Barbara Channel, measure oil platform emission levels.

	18/1945 - 19/0345	Near shore turbulence studies in Santa Monica Bay.
T1	19/1100 - 19/1200	Monitor tanker emissions during non-transfer period.
	19/1430 - 19/1500	Cross check ship and shore instruments at Catalina.
M1	19/1545 - 19/1730	At sea turbulence data.
T2	20/0430 - 20/0820	Monitor emissions during tanker transfer operation.
P	20/1710 - 20/1800	Monitor drilling platforms.
M2	20/1820 - 20/2200	Turbulence data on Southern edge of CARB model.
M3	21/0000 - 21/2115	Santa Monica Bay CARB model studies.
G1	21/2300 - 22/1100	Track tracer gas released from power plant on shore.
T3	22/1700 - 22/2100	Monitor emissions during tanker transfer operation.
	22/2100 - 23/0830	Monitor pollutants and aerosols along coast from Del Mar area to Long Beach area.
S	23/1400 - 23/1800	Check turbulence results for various ship maneuvers.
G2	23/2300 - 24/1030	Track tracer gas released from power plant on shore.
	25/2100 - 26/0320	Turbulence study during light wind conditions.
G3	26/0530 - 26/1730	Release of tracer gas from ship along shipping lanes west of Los Angeles up to Santa Barbara area.
	27/0000 - 27/0445	Monitor oil drilling platforms in Santa Barbara Channel.
	27/2030 - 27/2230	Monitor aerosols and natural pollutants in vicinity of coal oil point.
	28/0500 - 28/0715	Release of tracer gas from ship west of Santa Barbara.

The letters and numbers preceding some of the times are codes used below for easy reference to the various experiments.

III. Equipment and Data Acquisition

The R/V ACANIA is 126 ft. long, and of narrow beam and low profile, which makes it ideal for meteorological work since disturbance of the local air flow is minimal. Sensors are located at four levels on two masts, one at the tip of the bow, and the second 15 ft. aft of bow. The forward mast has sensors located at 4.2 meters and 7 meters, those on the rearward mast are at 14.7 meters and 20.5 meters, where all heights are measured above the mean water line. Each level contains sensors for detecting both mean and fluctuating parameters, and on the top two levels the mean sensors are 0.7 meters below the fluctuation sensors.

A sea surface temperature sensor was suspended from a pole which extended 10 ft. beyond the tip of the bow. This sensor is mounted in a 300 gram brass plug in the end of a 6 ft. long by 3/4 inch piece of tygon tubing. The tubing floats and keeps the sensor on the surface (a depth of approximately 1 ft. is averaged because of bobbing caused by the ship's motion) and also protects the sensor from the sea water. The brass plug has a high heat capacity and smooths fluctuations in temperature that would be caused by the bobbing of the sensor.

An acoustic sounder for monitoring the temperature inversion was mounted on the ship's fantail. A special enclosure and mounting were constructed to attenuate the rather severe shipboard acoustic noise, which limits the usefulness of the device when the ship is underway. The normal range of the sounder is 1 kilometer, which is limited to approximately 500 meters when the ship is at full speed.

The mean sensors at the four levels above the surface are for wind speed, temperature and humidity. Wind speed is measured with cup anemometers

which have a threshold of 0.5 knots. Humidity sensors are Li Cl cells which have an accuracy of 3%. The temperature sensors are quartz thermometers (including the sea surface) which have an accuracy of 0.01°C. The temperature and humidity sensors are placed in aspirators which protect them from the environment. The aspirators include radiation shields so that the temperature sensors are protected from both direct and reflected radiation from the sun and also from heat radiated from the ship. With this system the precision of temperature measurements is about 0.07°C.

Fluctuations of temperature and wind speed are detected with cold wires and hot wires respectively. The cold wires are 2.5 μ x 2 mm platinum. The hot wires are 60 μ x 2 mm platinum film on a quartz substrate and are operated at 20% overheat, which is high enough to make them insensitive to temperature fluctuations. The wind speed bridges are constant temperature anemometers. The temperature bridges are operated at 3 kHz and very low current so that the wires are not heated, thus, they are not sensitive to wind speed fluctuations. The hot wires are aligned with their axes vertical so that they are sensitive only to the horizontal component of the wind.

The mean signals are averaged for times that are determined by the conditions (usually either 10 or 20 min.). Acquisition, averaging, and recording on a teletype and magnetic tape are accomplished by an NPS developed system, designated MIDAS.

Fluctuation data was acquired in two forms, using either a single sensor, or paired sensors at a separation of 0.3 meters. We used paired sensors for temperature and a single sensor for wind speed. Paired sensors result in spatial filtering of the signal. When a single sensor was used, the resulting signal was attenuated above 200 Hz and below 5 Hz giving temporal filtering which is equivalent to the spatial filtering with paired sensors.

The resultant signals were recorded on magnetic tape for later processing in the laboratory. The signals were also processed to give the RMS values which were acquired and recorded by MIDAS and also recorded on strip charts. The strip charts are used on shipboard to obtain real time ε and C_T^2 values.

The acoustic sounder output is a strip chart record of the height from which the return echo occurs, giving a real time presentation of the inversion height. This height is compared with the twice a day radiosonde results which identify both the height and strength of the inversion. Agreement to within 20 meters was consistently obtained.

Even though the R/V ACANIA is very well suited to meteorological measurements its presence can disturb the local air flow sufficiently to compromise acquired data. This effect can be reduced sufficiently to be negligible by keeping the ship pointed into the wind. Of course, this cannot always be done so we acquire data only when the relative wind is within 30° of the bow. The second problem with a ship platform is motion due to roll. Roll can cause two adverse effects: introducing an extra component to the wind speed fluctuations and increasing the rotation rate of the cup anemometers. Since fluctuation signals are analyzed only at frequencies above 5 Hz and ship motions are much less than 1 Hz, there is no observable affect on the fluctuation signal. Under conditions of severe roll (20° roll, 4 sec. period) the mean wind speed measured at level 4 is elevated by about 1 knot when the relative wind is from the bow. When the relative wind is from 90° off the bow this effect is reduced to zero. The wind speed results given in this report are not corrected for this effect.

Complete descriptions of the NPS shipboard equipment and the analysis methods can be found in the references.

IV. Data Reduction

As described in the previous section the data acquired includes: Profiles of temperature, humidity, and wind speed, sea surface temperature, and records of the temperature and wind speed fluctuations. This data is reduced to obtain the following parameters:

U_*	Friction velocity
ε	Dissipation rate of turbulent kinetic energy
C_T^2	Temperature structure function
D	Diffusivity
Ri	Richardson Number
F_H	Sensible Heat Flux
F_M	Momentum Flux

There are several possible methods to evaluate these parameters by utilizing both the profile and fluctuation data. Here we describe only the method used to process the data presented in this report.

All of the data collected have not been analyzed. There were many time periods when the relative wind was from an unfavorable direction, and these data were not analyzed. Also, there are periods when the results obtained are obviously in error and they have been discarded. These errors are due to extraneous noise, such as ship radio transmission and power surges.

We use the profiles to obtain potential temperature (°C)

$$\theta = T + 0.0098\ Z \quad , \tag{1}$$

and the virtual potential temperature

$$\theta_v = \theta + 0.61\ q\ T \quad , \tag{2}$$

and their gradients with height. T is the absolute temperature, Z the height above the mean sea surface in meters, and q the specific humidity in grams of water vapor per gram of dry air. The gradients are obtained by fitting θ and θ_v with a log profile and then evaluating the gradients at a height of 10 meters.

The specific humidity is found from

$$q = 6.5 \times 10^{-6} H \exp_{10}[A - \frac{B}{T} - C \log T] \quad , \tag{3}$$

where H is the relative humidity (%), A = 23.84, B = 2984, and C = 5.03.

In calculating q for the various heights we use a single value of H which is the average of the four measured values. Thus, the dependence of q on height comes from the temperature variation. This is done because the humidity sensors are not accurate enough to allow a profile to be specified.

Three methods have been used to analyze the fluctuation data: difference, RMS, and spectral. The structure functions C_T^2 and C_U^2 are obtained directly from the analysis, and ε is found from

$$C_U^2 = 2 \varepsilon^{2/3} \quad . \tag{4}$$

In the difference method the structure function is found by measuring the variance of the difference in the variable x at two points separated a known distance, d:

$$C_x^2 = < [x(r) - x(r + d)]^2 > d^{-2/3} \quad . \tag{5}$$

The spectral method is based upon the assumption of "local isotropy" and the Kolmogorov -5/3 slope of the one-dimensional power spectral density, $\phi_x(k)$:

$$\phi_x(k) = 0.25\, C_x^2\, k^{-5/3} \quad , \tag{6}$$

where k is the wave number. Using Taylor's "frozen turbulence" hypothesis ($k = 2\pi f/\overline{U}$) we can find C_x by performing a fourier spectrum analysis of a signal in the frequency domain (f):

$$f\,\phi_x(f) = k\,\phi_x(k) = 0.25\, C_x^2 \left(\frac{2\pi f}{\overline{U}}\right)^{-2/3} \quad . \tag{7}$$

Therefore,

$$C_x^2 = 4 \left(\frac{2\pi}{\overline{U}}\right)^{2/3} [f^{5/3}\,\phi_x(f)] \quad . \tag{8}$$

Here $\overline{U}$ is the mean wind speed averaged over the analysis time to perform the spectral analysis. This expression is expected to be valid in the inertial subrange, which covers a frequency range of approximately 0.1 to 100 Hz.

The RMS method is based upon measuring the variance of the signal fluctuations between selected frequency limits:

$$\int_{k_\ell}^{k_u} \phi_x(k)\, d\,k = \overline{x'^2} = (x'_{rms})^2 \tag{9}$$

where x' is the fluctuating component of x. The upper and lower frequency limits, f_u and f_ℓ, are determined by a filter, and are related to the respective wave numbers by Taylor's hypothesis. Using equations (6) and (9):

$$C_x^2 = \frac{8}{3} \left(\frac{2\pi}{U}\right)^{2/3} \frac{(x'_{rms})^2}{(f_\ell^{-2/3} - f_u^{-2/3})} \tag{10}$$

The advantages of the difference and RMS methods are that the output voltage can be presented and averaged on a strip chart for real time analysis. The spectral method is more time consuming and is normally performed in the laboratory from tape recorded signals. However, it has one distinct advantage in that the spectrum can be viewed and obvious noise can be ignored (such as 60 Hz and its harmonics).

For the data presented in this report C_T^2 was found using the difference method, and ε was found both from the RMS and spectral methods.

Using ε, θ_*, and θ_{v*} the other parameters are obtained from the following equations:

$$U_* = (k\ Z\ \varepsilon)^{1/3} \quad , \tag{11}$$

$$D = k\ Z\ U_* \quad \text{(neutral stability)} \quad , \tag{12}$$

$$R_i = \frac{g}{T}\ k\ Z\ \frac{\theta_{v*}}{U_*^2} \quad , \tag{13}$$

$$F_H = \rho\ C\ (\theta_*\ U_*) \quad , \tag{14}$$

and

$$F_M = \rho\ (U_*)^2 \quad , \tag{15}$$

where ρ is the density of air at STP (1.29 kg/m^3), C the heat capacity of air ($\rho C = 1.31 \times 10^3$ Joule/K m^3), g the acceleration of gravity (9.8 m/sec^2), and k is Von Karmans constant (0.35).

Most of the above parameters depend on height. We arrive at final values for all of the parameters for an assumed height of 10 meters. To be specific, θ and θ_v are fitted by a log profile, C_T^2 is fitted by $Z^{-2/3}$, and ε by Z^{-1}. The 10 meter values for ε, θ_* and θ_{v*} are calculated, then D, R_i, F_H and F_M are calculated directly.

V. Results

A. Acoustic Sounder and Radiosonde

The acoustic sounder and radiosonde soundings show the presence of a strong marine inversion for the full cruise. The height and strength of the inversion varied with time and/or location. The bottom of each acoustic sounder strip chart (Figures 2a - 2d) is marked with letters which correspond to radiosonde graphs (Figures 3a - 3u) to show the times at which the radiosondes were released. Examination of both sets of data shows good agreement, except for 0200 PDT on 7/24, for which the radiosonde shows the inversion base approximately 150 m higher than the sounder. The reason for the discrepancy is not known but we assume that an error was made in reducing the radiosonde data.

In Table I we list the height of the base of the inversion and the strength of the inversion, taken from the radiosonde data. The data are coded with letters A thru U. Examination of the graphs shows that it is difficult, in many cases, to identify accurately the height and strength of the inversion since temperature changes occur gradually. In general the base of the inversion is taken to be the height at which the minimum temperature occurs; the strength is from minimum to maximum temperature regardless of the height difference, unless there is a subsequent increase in temperature identifying a second inversion. Good examples of difficult to interpret profiles are Figures 3b and 3c. There are several inflections on each profile and interpretation is very subjective.

The acoustic sounder is most useful for continually monitoring the inversion height, and hence the mixing depth. Figure 2a shows the beginning portion of the cruise, including the initial investigation of the Santa Barbara Channel. The inversion was quite stable for the entire time,

TABLE I

Height and Strength of the Marine Inversion taken from Shipboard Radiosonde Data

Times are PDT

Code	Date/Time	Inversion Height (m)	Inversion Strength (°C)
A	7/17/1700	360	14.5
B	7/18/0500	0	0.5
		240	13.
C	7/19/0200	280	6.7
		850	2.5
D	7/19/1900	450	0.4
		640	9.3
E	7/20/0200	0	0.5
		680	9.3
F	7/20/1900	200	2.1
		650	1.8
G	7/21/0200	450	10. +
H	7/21/1900	200	7.8
		470	4.2
I	7/21/2300	330	0.2
		440	7.1
		610	4.6
J	7/22/0200	240	13.3
K	7/22/1900	380	11.9
L	7/23/0200	360	13.4
M	7/23/1900	360	9.5
N	7/23/2300	520	5.8
		700	3.0
O	7/24/0200	650	~ 8.
P	7/26/0200	170	8.3
Q	7/27/1900	100	12.6
		530	1.2
R	7/28/0200	110	14.8
S	7/28/0500	20	2.8
		180	10.5
T	7/28/1700	230	16.3
U	7/29/0500	120	13.5
		~ 500	1.8

varying from 200 m to 400 m. The exception was when the ship rounded Pt. Conception at 0230 on 7/18. The presence of very intense thermal plumes indicates the region of mixing of marine air and air that has passed over land and been warmed. The region of disturbed air extends well into the channel from Pt. Conception.

From approximately 0900 to 1300 on 7/19 an oil tanker which was not in the process of transfering oil was monitored. The inversion height was approximately 600 m for the first 3 hours, then dropped to 200 m during the last hour. At 2130 of the same day the monitoring was resumed, but during lightering operation, and continued until 0930 on 7/20. The inversion height was 600 m to 800 m. The lightering operation was approximately 50 kmi from shore and the inversion was much higher than that found near shore.

During the monitoring of platform Eva the inversion was below 100 m. The change in inversion height appears to have been a geographical effect since the height was greater both as the ship approached and left the shoreline.

We then proceeded to do a thorough study of the turbulence in the Santa Monica Bay, the study taking approximately 24 hours. The inversion was at 200 m to 400 m during all but the last 5 hours, when it dropped to the surface, split into more than one level, and became difficult to interpret, (around 1900 on 7/21).

The first power plant SF_6 release at 0100 on 7/22 occurred when the inversion was 150 m high and not sharp. (See Figure 2a). Multiple returns were obtained from complex thermal structure up to 700 m. At 0400 the inversion either dropped to the surface or a new inversion rose from the surface, reaching an elevation of 250 m by 0600. This variation in the inversion

height appears to be a change with time rather than position since the ship was in the same locations at different times, with different inversion heights being obtained. The height and intensity of the inversion remained stable through the remainder of the SF_6 tracer experiment, which ended at $\sim$ 1200.

The sounder was not in operation during the period when data was being taken along the coast from Del Mar to Long Beach. The one radiosonde taken during this period (Figure 2e) shows an inversion height of approximately 450 m.

When SF_6 was released from the power plant the second time the inversion height was approximately 600 m ($\sim$0200 on 7/24). The inversion remained fairly high until 0800, at which time it was $\sim$ 500 m, thereupon it dropped to 200 m by the end of the experiment at 1100. Again the changes that occurred were temporal rather than spatial.

The remainder of the experiments were performed under similar conditions. The inversion was near the surface (within 200 m) and for much of the time it was difficult to distinguish an inversion from thermal plumes.

B. Calculated Results

Appendix B presents a table of the results that were computed from the basic data (Table VI). The data includes dissipation rate, temperature structure function, turbulent eddy diffusivity, Richardson's number, momentum flux, and heat flux. Figures 4a and 4b show plots of Richardson's number and the momentum flux versus time for most of the cruise. The codes on the time axis refer to the various experiments listed in Section II. It must be emphasized that these numbers give estimates of flux parameters,

based on measurements of inertial subrange parameters, not direct measurements.

Difficulty can be encountered in evaluating temperature profiles to obtain θ_* and θ_{v*}. The following two examples for temperatures obtained from the four levels have been taken from Table V and illustrate the problem.

T_1	T_2	T_3	T_4
17.85	17.79	17.70	17.54
17.72	17.52	<u>17.85</u>	17.46

The first set of temperatures shows a good profile and it is easy to fit θ with a log profile to obtain θ_*. T_3 for the second set (underlined) appears to be in error since it certainly does match the gradient shown by the other temperatures. The reason for this discrepancy could be ship influence, or it could be real, this is unknown but ship influence is most likely. However, it would be inappropriate to include the value when fitting the log profile, so the point was discarded. Level 3 temperature data was not used for calculations for a large percentage of the data.

Discarding experimental data is a hazardous thing to do and raises questions about the validity of the final results. To this point we must recall that we are trying to make flux estimates, and determine the stability of the atmosphere in a land sea boundary region. The data we have taken indicates that the land influence extends well out to sea in this area. We did not encounter the homogenous, equilibrium atmosphere on which the theory, and hence data evaluation methods are based. However, reasonable estimates can be obtained by fitting an averaged profile, and this is what we have done by discarding level 3. We expect a 50% error in the final result for measurements made this close to land, and on a non-stationary platform.

A few general conclusions can be drawn for the cruise as a whole. The Z = 10 m value of Richardson's number varied from slightly positive to as low as -1.3, and was in the range of -.1 to -.5 the majority of the time. Hence, conditions were generally slightly unstable (the sea surface was warmer than the air within the first 20 meters for the full time the ship was in the Southern California area). Since small temperature gradients were present small errors in temperature measurements, such as those due to ship influence, could have resulted in large perturbations in the final results. This could account for some of the fluctuations evident in Figure 4.

Note that Table VI contains a dashed line at 0420 on 7/26. This is due to the poor quality of the data that was obtained at subsequent times. The waves were extremely high during this period; part of level 1 had been destroyed by waves breaking over the bow, and all of level 1 was removed. The table shows positive Richardson's numbers from 0725 to 1030, but the numbers are undoubtedly too large. The zeroes indicated for heat flux are due to the fact that for Ri > 0.2 heat flux will be zero. The numbers given for momentum flux for this period are good estimates.

Because of the variations in the data Figure 4 shows two superimposed representations of the data. Individual data points are shown, which are fit by an average curve (heavy lines), and are also fit by a curve which shows fluctuations about the average (light lines). Note that the curve for fluctuations is only used in those regions of the graphs where fluctuations were quite rapid. Where the fluctuations can be easily identified from the individual points no curve is included to reduce the clutter on the graph. The average is an estimate, not a computed curve.

Refering to Equations 11 through 15 we see that all of the calculated results depend on two parameters, θ_* and ε. (In actuality C_T^2 was derived directly from fluctuation data, not from θ_*, although it would have been possible to do so). Examination of Figure 4 illustrates the manner in which Ri and F_m are related. A large temperature gradient (unstable case) results in a large negative Richardson's number (Ri α θ_{v*}), whereas a large momentum flux (F_M α u_*^2) results in a small Richardson's number (Ri α u_*^{-2}). Thus, when the flux is large Ri will be small unless compensated by large temperature or humidity gradients. This behavior is evident in the figures.

Not all of the fluctuation evident in the results are measurements effects. The most striking example is shown from 0400 to 1100 on 7/21. Ri and F_m vary in somewhat of an oscillatory manner, the variations being almost a factor of 4. The values obtained during this time are reasonable estimates, for 20 minutes averages. However, a more reasonable estimate of the flux, for example, would be obtained from an hourly average. As has been pointed out by others, any averaging time shorter than one hour is probably too short for processing atmospheric turbulence data. We use the shorter averaging time out of necessity because of the shipboard platform and changes in course, position, and conditions. Longer averaging times could be used for those periods when conditions remain constant. Because of the short experimental averaging time it is more appropriate to use the average curve through the data shown in Figures 4, than the individual points in order to obtain final results.

C. Diurnal Variation and Land Influence

In Figure 5 we have plotted momentum flux versus time for the 24 hour day, where data from all time periods of the cruise have been averaged. The

numbers that were used to obtain this figure were obtained from the average curves in Figures 4, not from the individual data points. One expects very little diurnal variation for open ocean conditions, and this has been confirmed on previous cruises. In Figure 5 we see a significant diurnal variation of the flux.

Data was taken on this cruise for a wide range of distances from shore, as close as 1/2 mile and as far as 30 miles when the ship was south of Catalina Island. In Figure 5 we divide the averaged data into two groups, all data, and at sea data. The at sea data is that taken in the neighborhood of Catalina Island. The at sea data shows a much smaller diurnal variation, but the variation is large enough to indicate significant land influence in the area.

In Figure 6 we show the variation of momentum flux with wind speed. The points on the graph were computed directly from the data in Table VI and then averaged. When there was not much data available at a particular wind speed, data from more than one speed were averaged in order to improve the statistics. The error bars were obtained from the square root of the number of points in each sample. The solid points are for data near the shore, the open points are for at sea (south of Catalina Island). The two solid lines are theoretical curves obtained from

$$F_m = \rho \, [kU/\ell n(Z/Z_o)]^2 \quad , \tag{16}$$

for values of the roughness length $Z_o = 0.01$ and $Z_o = 0.1$ cm. Previous measurements over the open ocean give values of Z_o near 0.1 cm and the results presented in Figure 6 are somewhat in agreement with this value.

The data is much higher than the prediction for wind speeds below 5 knots. Obviously the shear produced momentum flux would be zero at zero wind speed, but we measure values of the order 10^{-2} kg/msec^2. The measurements can be partially explained by convective flow and the roll of the ship. The convective flow could be enhanced by the ship's presence since its mean temperature is greater than the water temperature. Quantitative comparison with the results are not feasible.

Careful evaluation of the results shows that some, but not all, of the diurnal effect is due to an increased wind speed near land during those periods when high values of F_m were obtained. The data base reported here is not sufficiently large to separate the effect of wind speed from the influence of the nearby land mass.

It is interesting to note that these data imply that the "Los Angeles air basin" is an area that extends at least 30 miles to sea.

D. Pollution Model Parameters

Figure 1d shows the course followed by the ship to obtain parameters for the CARB air pollution model. Data taken on the westward leg on the lower part of the figure is labeled M2 on Figure 4a. The remainder of the data is labeled M3. In addition the data labeled M1 was obtained in the neighborhood of Catalina Island in the hope of finding open ocean conditions for comparison purposes. The model experiment was performed on 7/21. On 7/22 and 7/24 we performed the tracer experiments in the same area and the parameters presented here are averages for all of the data. Comparing all of the data shows that the variations in the parameters which we observed were temporal rather than spatial.

We cannot stress too strongly that the parameters presented below are averages that were obtained during a particular time of the year, under a particular set of circumstances. As the weather changes the parameters will change. The following are our best estimates:

Ri: The water was warmer than the air leading to slightly unstable conditions. Expected values are in the range $-0.3 \leq Ri \leq -0.05$. This is consistent with the Richardson's numbers obtained for other overwater experiments which average to $\overline{Ri} = -0.08$ (open ocean).

F_m: Figures 5 and 6 can be used, recalling that the solid curve in Figure 5 includes at sea data and that values as high as 6×10^{-2} kg/msec^2 were obtained near land in the late afternoon. The diurnal/wind speed variation is significant and should be taken into account. For simplification one could use $F_m = 1.5 \times 10^{-2}$ for all periods except 1400-1800 where a value of 4×10^{-2} would be appropriate. Alternately, Figure 6 can be used to obtain F_m as a function of wind speed.

D: The turbulent eddy diffusivity can be found from F_m using Equations 12 and 15 (assuming near neutral stability and a height of 10 meters). We obtain:

$$D = (F_m/0.105)^{1/2} \quad . \tag{17}$$

Near land this gives the range $0.3 \leq D \leq 0.8$ m^2/sec. This is much lower than overland values.

ε: The dissipation rate can also be found easily from F_m. Using Equations 11 and 15, for a height of 10 meters, we obtain:

$$\varepsilon = (F_m/2.97)^{3/2} \quad . \tag{18}$$

F_H: The sensible heat flux varies quite widely since it depends both on the turbulence and on the temperature profile. Of course F_H can be either positive or negative depending on the direction of the gradient. We obtained values that ranged from -50 to +20 watts/m^2. A reasonable average would be -4 watt/m^2 for $F_m \sim 1.5 \times 10^{-2}$ and Ri ~ -.3. For the same stability a momentum flux of 6×10^{-2} will give a heat flux of ~ -20 watt/m^2. For a much larger thermal gradient (Ri ~ -3) a momentum flux of ~ 1×10^{-2} will produce the same heat flux. Further extrapolations can be made but it is best to refer to Table VI.

E. Stability Corrections

As has been described above, the data was reduced assuming neutral stability. Conditions were slightly unstable, the average Richardson's number being -0.3. This value of Richardson's number leads to a stability correction of 20 to 30% for the calculated results, depending on the parameter. This correction is within the errors associated with the measurements and has, hence, not been applied.

Acknowledgements:

This work was supported by the California Air Resources Board. We wish to thank Mr. Jeff Phillips who accompanied us on the cruise and participated in collecting the data. Miss Estelle Garner and Mr. Derek Porter did much of the initial data reduction. The aerosol results presented in Appendix C were evaluated by LT Alan Simoncek, USN from data gathered by Calspan Corporation.

APPENDIX A: BASIC DATA

In this appendix we present data on a) the ship's speed and course and cruise charts, b) wind speed and direction, c) acoustic sounder strip charts and interpretation, d) radiosonde results, e) sea surface temperature and air temperature and humidity.

A. Ship Course

Table II lists changes in the ship's heading and speed, the information being obtained from the ship's log and the NPS scientific log. The ship's normal cruising speed is approximately 9 1/4 knots and is designated as full ahead in the table. No correction is made for currents or winds. Charts of the ship's position are shown in Figures 1a - 1j. Small course changes which are occasionally necessary for maneuvering purposes are not shown in either the table or the charts.

TABLE II

Changes in Ship's Speed and/or Course

7/17/77	0815	Departed
	0850	c/c 210°
	0924	c/c 168°
	1126	c/c 150°
	1400	c/c 148°
	1500	c/c 143°
	1655	c/c 144°
7/18/77	0100	c/c 126°
	0220	c/c 079°
	0335	Downwind leg of platform Helen run
	0345	Start 360° pass of platform
	0355	Underway to Holly c 100°
	0615	Stop for true wind, maneuvering near Holly
	0654	c/c 105° Depart Holly
	0815	Stop for true wind, 1.5 mi from platform C
	0822	c 090°, 1/2 ahead near platforms
	0835	c/c 145° into clean air
	0855	c/c 070°, 1/2 ahead run by platform
	0915	c 133°, full ahead
	1135	c/c 115°
	1230	c/c 110°
	1355	c/c 104°
	1550	Drifting
	1630	Head into wind, 1 engine dead slow
	1845	c/c 060°
	1930	c/c 270°, port engine slow ahead
	2242	c/c 080°
	2350	c/c 270°, starboard engine slow ahead
7/19/77	0215	Underway to beach
	0255	Drifting
	0345	Underway to Catalina
	0500	c/c 148°
	0750	c/c 205°
	0900	maneuvering near Edinburgh
	0945	c/c 345°, full ahead
	1120	Downwind Edinburgh, 160° at 2 knots
	1140	Finished downwind leg
	1149	Upwind, 160° at 2 knots
	1205	Finished tanker data, underway to Isthmus
	1425	In fisherman's cove
	1455	Underway easterly
	1545	Heading into wind
	1730	Underway to tanker
	1800	c 133°, full ahead
	1935	c/c 165°
	2120	Drift neighborhood of tanker

7/20/77	0820	c 348°, full ahead
	1015	c/c 345°
	1445	Underway to platform Eva
	1710	Arrive at Eva
	1800	c 210°, half ahead
	1815	c/c 270°
	2200	Stop for true wind
	2205	c 030°, full ahead
	2300	Stop for true wind
	2325	c 000°, full ahead
7/21/77	0010	c/c 345°
	0100	Stopped for true wind
	0250	Stopped
	0315	Underway, c 180°
	0345	Stopped
	0410	Underway, c 177°
	0445	Stopped
	0510	Underway, c 175°
	0540	Stopped
	0606	c 180°, full ahead
	0635	Stopped
	0640	c 240°, dead slow
	0700	Stopped
	0810	c 090°, 2/3 ahead
	0900	c/c 000°
	1110	Stopped
	1245	Underway, c 265°, 1/2 ahead
	1410	c/c 182°, full ahead
	1440	At position, head into wind
	1515	Underway to new position, full ahead
	1555	At new position, head into wind
	1620	Underway to new position, full ahead
	1700	At position, head into wind
	1725	Underway to new position, full ahead
	1800	At position
	1823	Underway, c 078°
	1925	At position, dead slow into wind, c 270°
	1947	Underway, c 000°, full ahead
	2011	At position, c 235°, dead slow into wind
	2038	Full ahead, c 010°
	2110	At position
	2135	Full ahead, c 053°
	2212	Stop for true wind
	2217	Resume course and speed
	2305	Stop for true wind
	2310	c 000°, full ahead
	2333	c/c 180°, 1/2 ahead
	2350	Stopped
7/22/77	0001	c 350°
	0050	c 009°
	0055	c 026°
	0115	c/c 168°
	0150	c/c 208°
	0200	c 200°

	0211	c/c 336°
	0222	Underway, c 336°
	0258	c/c 023°
	0330	c/c 012°
	0350	c/c 270°
	0415	Stop for true wind
	0420	Underway, c 216°, full ahead
	0450	c/c 200°
	0510	Stop for true wind
	0530	Underway, c 135°
	0615	Stop for true wind
	0634	c 000°, full ahead
	0710	Stop for true wind
	0756	Stop for true wind
	0759	c 000°, 1/2 ahead
	0805	c/c 150°, full ahead
	0818	c/c 170°
	0831	2/3 ahead
	0835	c/c 090°, 1/2 ahead
	0845	Full ahead
	0850	c/c 180°
7/22/77 (cont'd)	0910	c/c 270°
	0945	Stop for true wind
	0948	c 260°, full ahead
	1005	Stop for true wind
	1040	Stop for true wind
	1044	c 122°, full ahead
	1130	Stop for true wind
	1150	c 085°
	1305	Rendevous at Redondo Beach
	1315	Underway to Catalina, c 215°
	1405	c/c 155°
	1700	c/c 180°
	1800	Drifting near Edinburgh
	2100	Underway, c 100°, full ahead
7/23/77	0100	c 095°
	0200	c/c 085°
	0235	Stop for true wind
	0245	Underway, c 325°, full ahead
	0500	c 300°
	0530	c/c 304°
	0625	c/c 292°
	0845	c/c 240°
	0915	c/c 305°
	1130	Reduce speed to slow ahead
	1150	Drifting
	1420	Ship stationary pointing into wind
	1450	Underway, c 215°, 1/2 speed into wind
	1510	Full ahead into wind
	1530	c 035°, full ahead
	1550	c 000°
	1630	Stop for true wind
	1650	No motion, point into wind

	1720	c 265°, 1/2 ahead into wind
	1745	c 265°, full ahead into wind
	1810	Stop for true wind
	1812	c 025°, full ahead
	1820	c/c 100°
	1932	c/c 090°
	1943	Stopped
	2315	Underway, c 316°, 1/2 ahead
7/24/77	0100	Drifting
	0110	Underway, c 092°, 1/2 ahead
	0150	Dead in water
	0210	Move closer to beach
	0240	Underway, c 245°, 1/2 ahead
	0300	c 245°, full ahead
	0450	Stop for true wind
	0455	Underway, c 050°, full ahead
	0530	c/c 038°
	0548	Stop for true wind
	0600	c 150°, full ahead
	0707	Stop for true wind
	0745	Underway, c 150°, full ahead
	0855	Stop for true wind
	0905	c 055°, full ahead
	0946	Stop for true wind
	0951	Underway, c 330°
	1112	Stop for true wind
	1130	Underway, c 265°, full ahead
	1140	c/c 220°
	1150	c/c 100°
	1245	Drifting
	1330	Underway to LA Seabuoy
	1800	Maneuvering in LA harbor
7/25/77	1900	Depart pier LA harbor
	1938	Clear harbor entrance, c 198°
	2027	Stop engines
7/26/77	0100	Drifting
	0345	Underway to Pt Fermin
	0445	Arrive at station
	0530	Underway, c 270°, full ahead
	0630	c/c 300°
	0930	Stop for true wind
	1200	c 298°, speed 9 knots
	1210	c/c 285°
	1310	Stop for true wind
	1330	c/c 278°
	1425	Reduce speed to 1/2 ahead
	1430	Resume speed
	1501	Stop for true wind
	1530	Reduce speed to 8 knots
	1645	Dead slow
	1650	Resume full ahead
	1700	Speed 8 knots
	1735	c/c 080°, 1/2 ahead
	1800	c 075°, slow ahead
	2312	1/2 ahead for oil platforms
	2400	Nearing platforms

7/27/77	0448	Complete working platforms Underway, c 185°, full ahead
	0535	Drifting
	1145	Underway, c 122°, full ahead
	1345	Arrive channel island harbor
	1630	Underway for Coal Oil Point
	1800	c 292°, full ahead
	2020	Stop for true wind, near Holly
	2235	Leave Coal Oil Point area, c 180°, slow ahead
7/28/77	0100	Drifting
	0420	Underway to station, c 245°
	0500	Drifting on station
	0719	Underway, c 292°
	1055	c/c 303°
	1225	c/c 330°
	1255	Heavy seas, 3/4 ahead
	1435	Heavy seas, 1/2 ahead
7/29/77	0245	c/c 320°
	0340	c/c 325°, speed 5 knots
	0600	c/c 349°
	1200	At Cypress Point

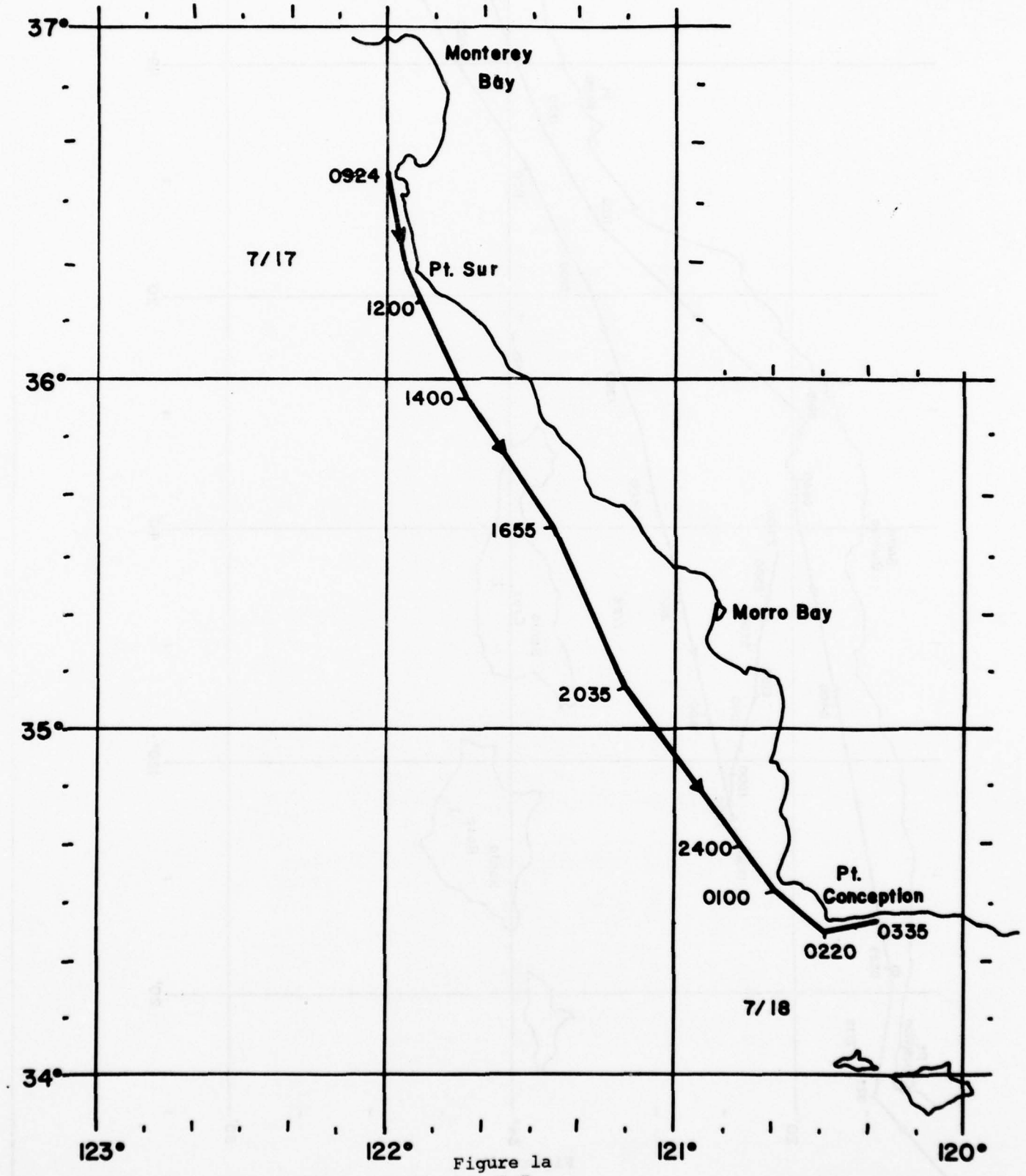
37°
36°
35°
34°
123°
122°
121°
120°
Monterey Bay
0924
7/17
Pt. Sur
1200
1400
1655
Morro Bay
2035
2400
0100
Pt. Conception
0335
0220
7/18

Figure 1a

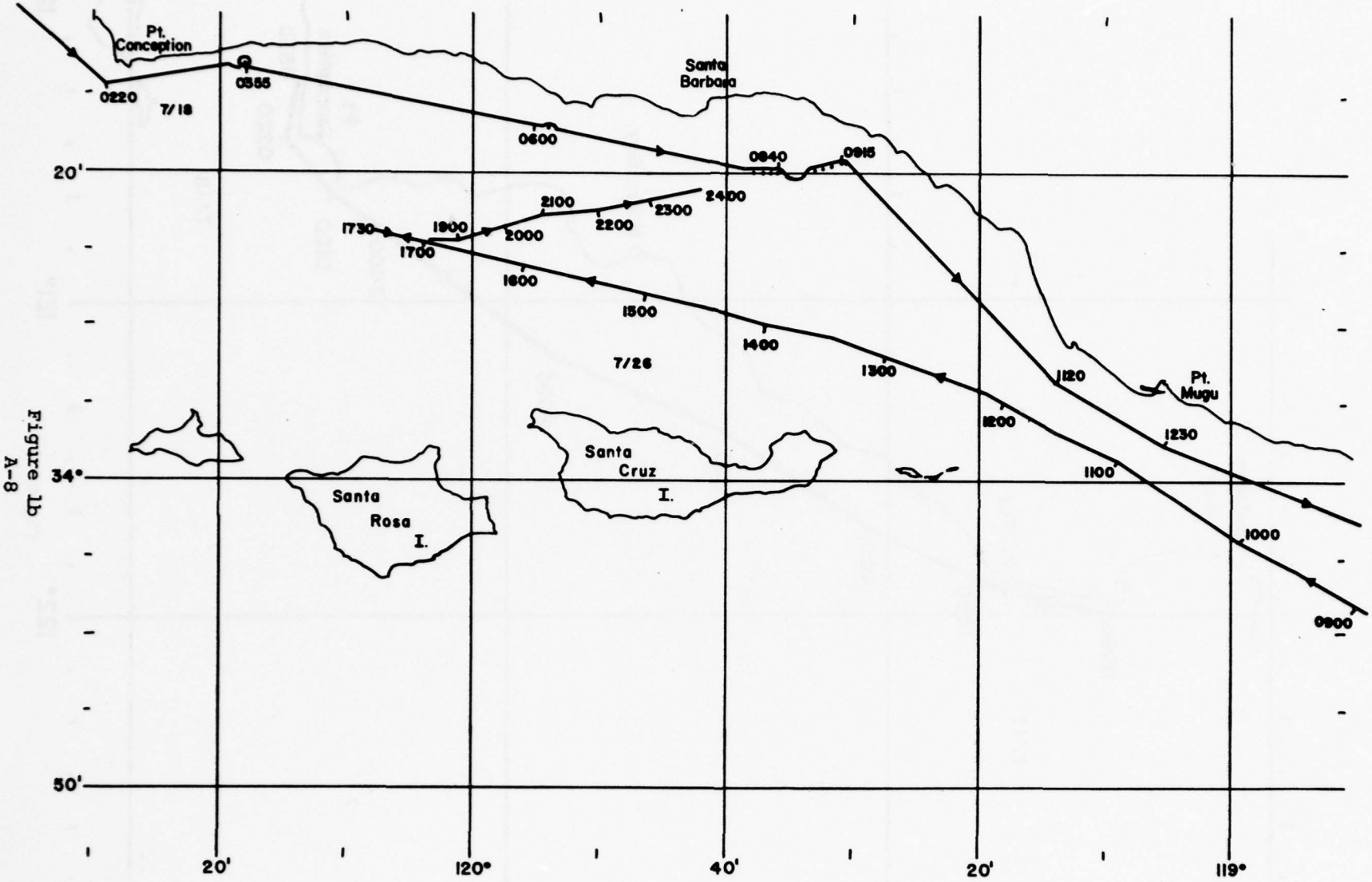
Pt.
Conception
0220
7/18
0555
0600
Santa
Barbara
0840
0915
20'
2100
2400
2300
2200
2000
1900
1730
1700
1600
1500
1400
7/26
1300
1120
Pt.
Mugu
1200
1230
Santa
Cruz
I.
1100
34°
Santa
Rosa
I.
1000
0900
50'
20'
120°
40'
20'
119°

Figure 1b
A-8

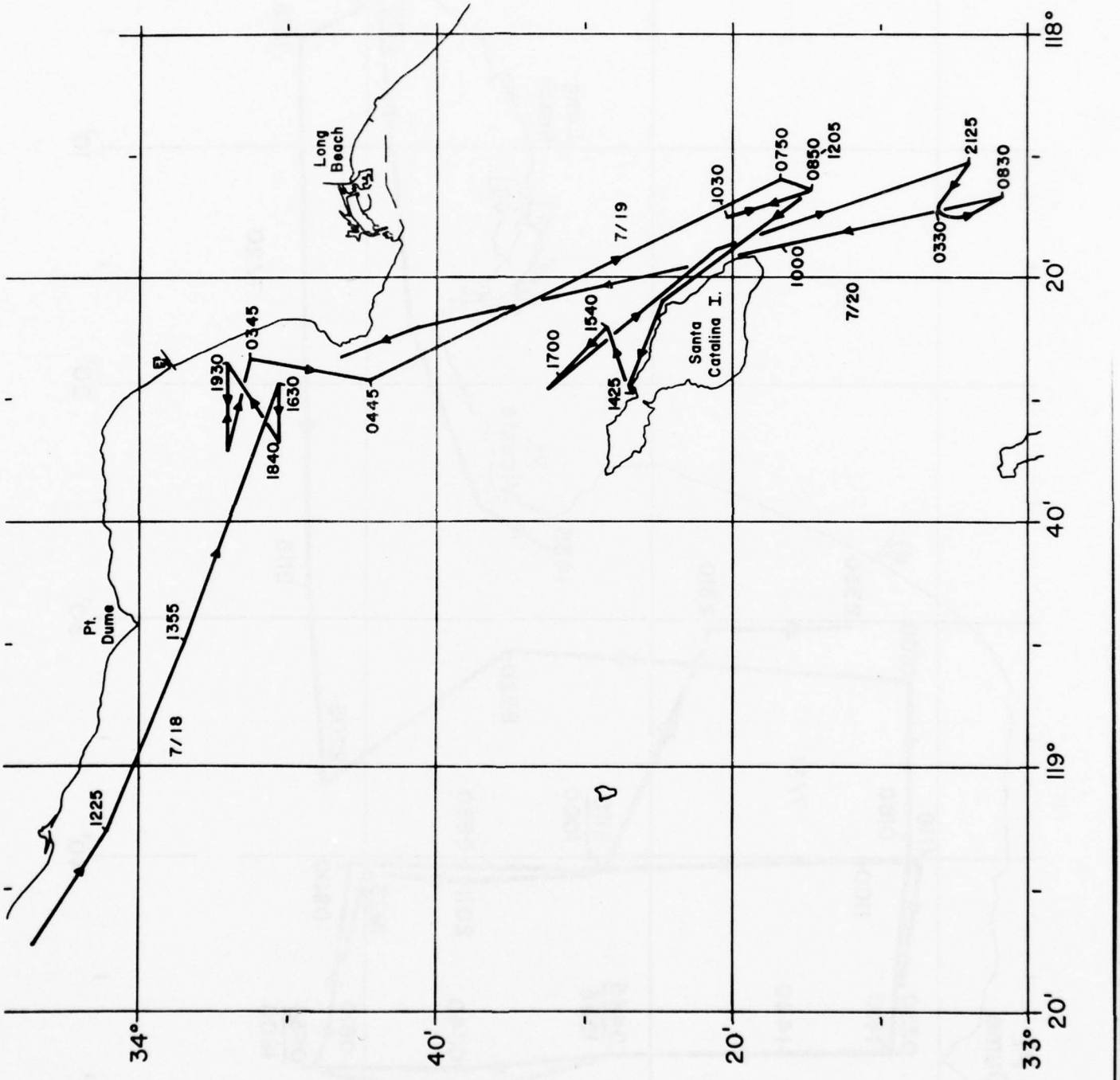
Long Beach
Pt. Dume
Santa Catalina I.
1225
1355
7/18
1840
1630
1930
0345
0445
1700
1540
1425
7/19
1030
0750
0850
1205
1000
7/20
0330
2125
0830
34°
40'
20'
33°
20'
40'
119°
118°

Figure 1c
A-9

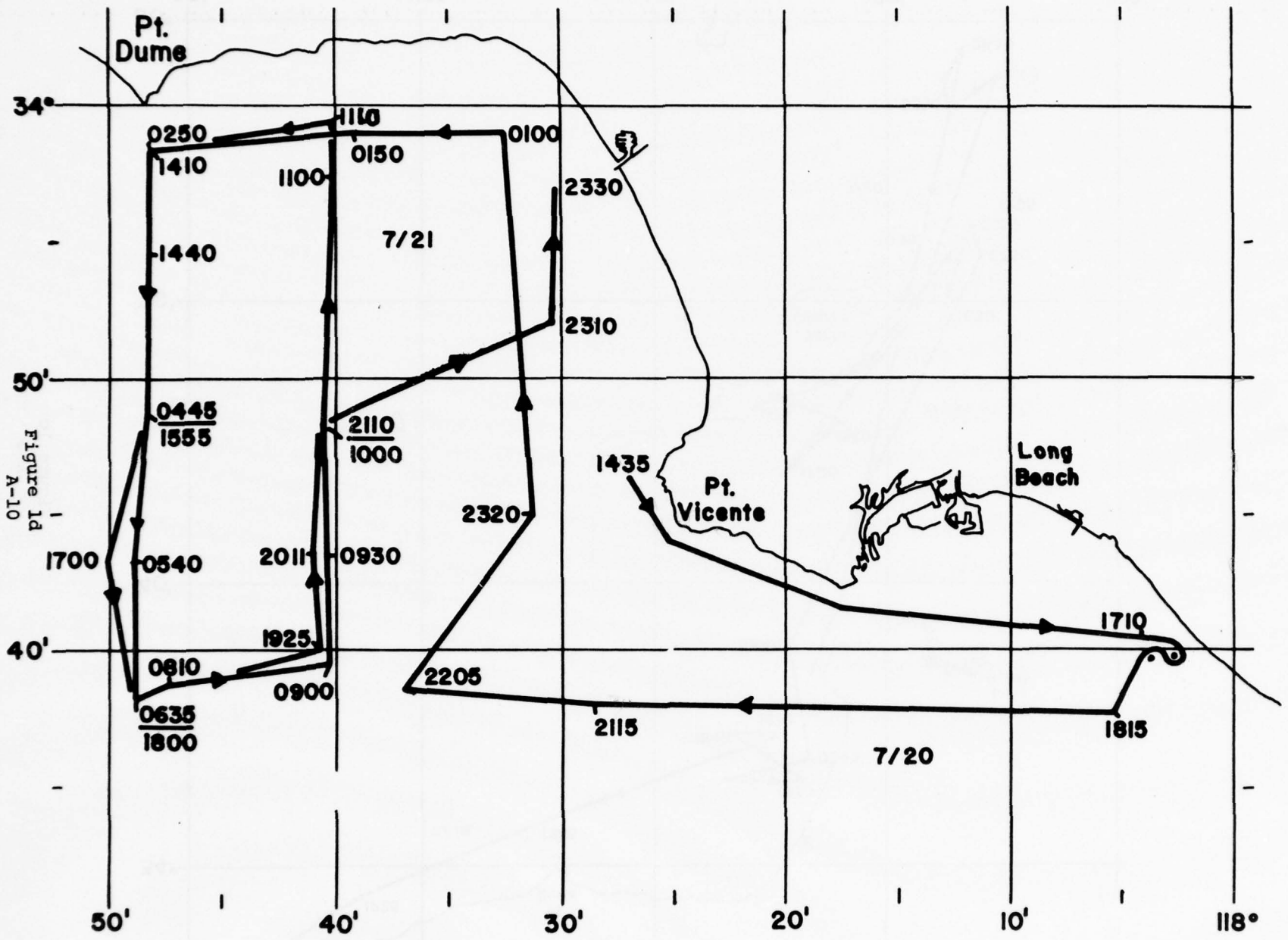

Figure 1d
A-10

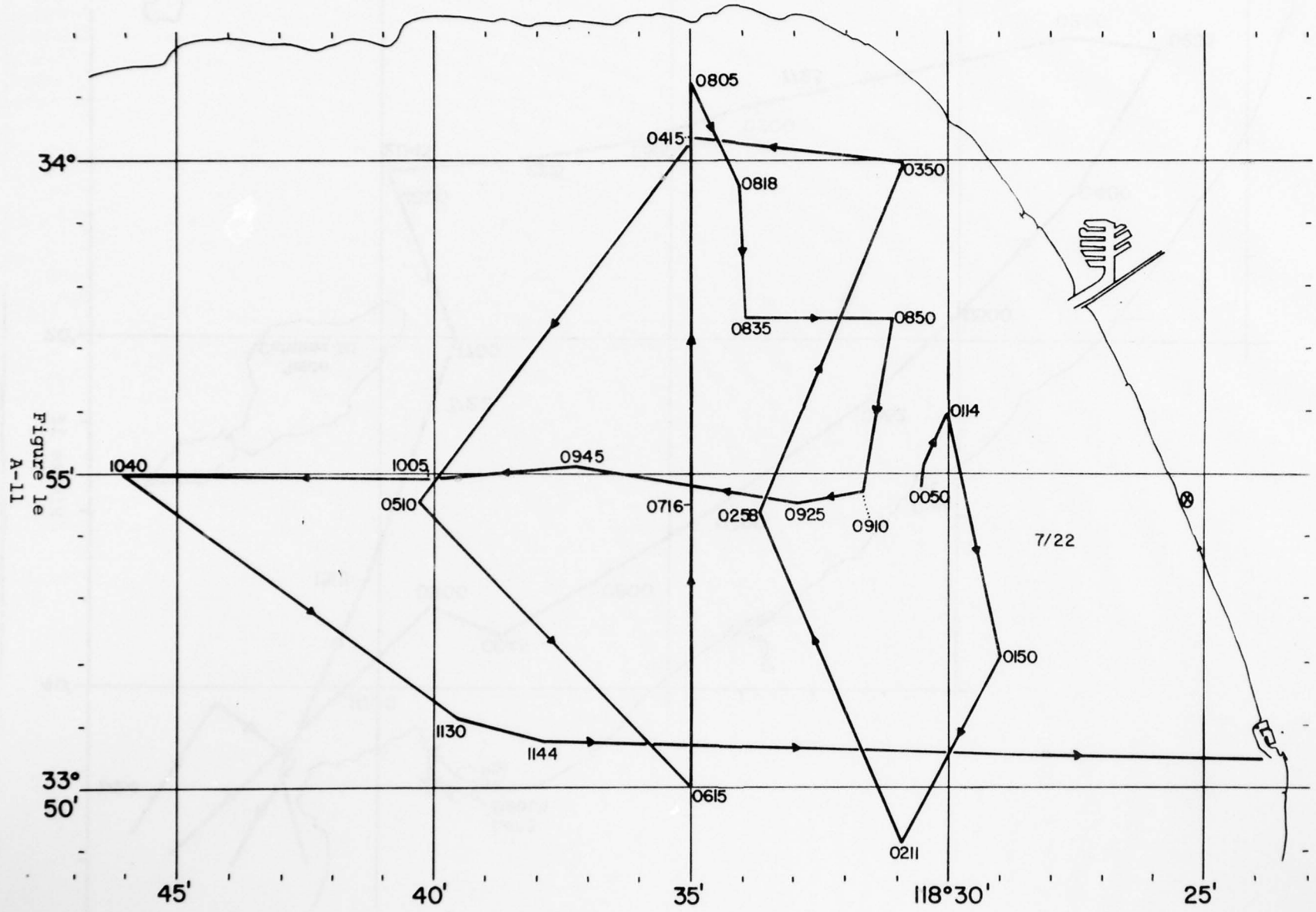

Figure 1e
A-11

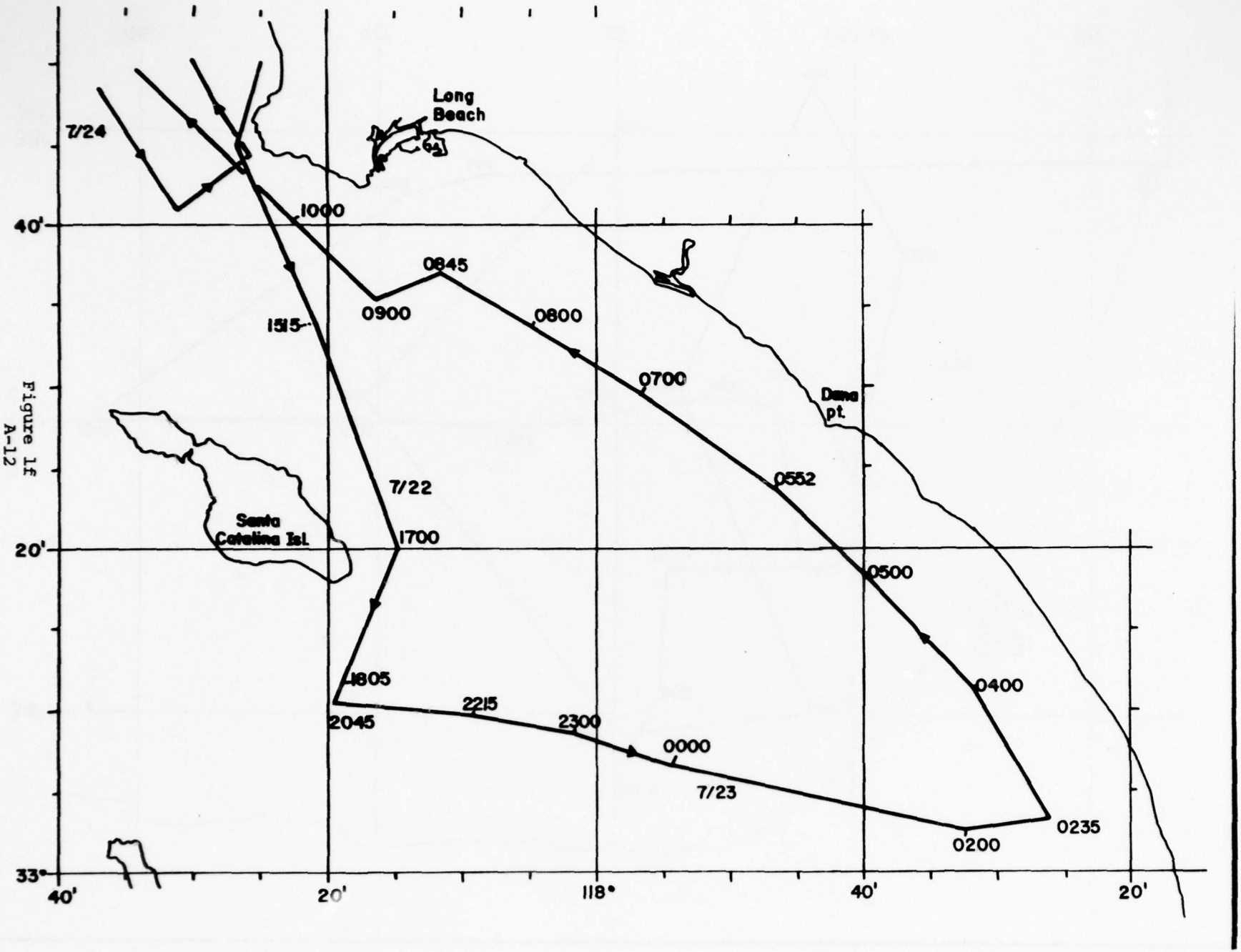

Figure 1f
A-12

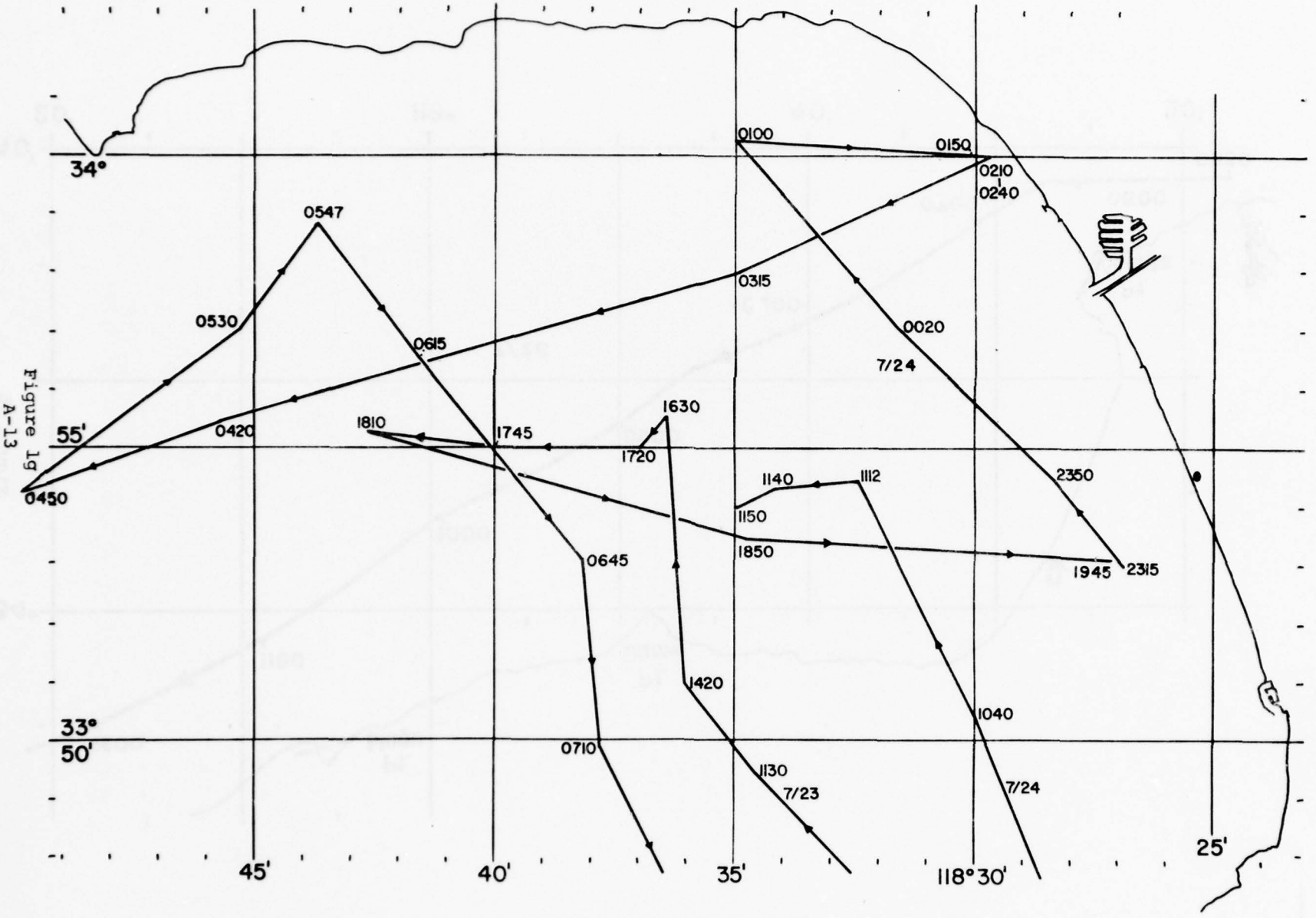

Figure 1g
A-13

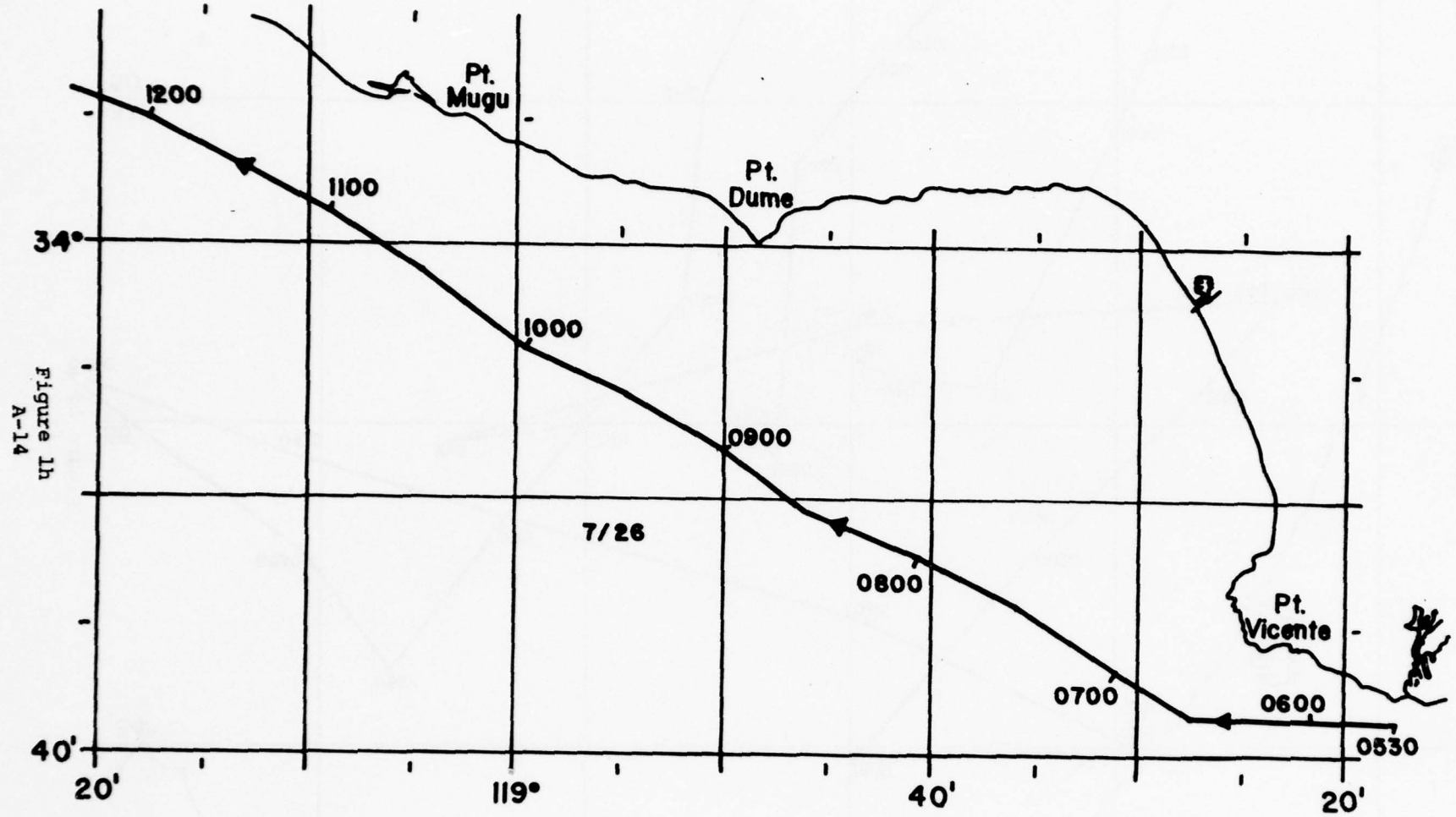

Figure 1h
A-14

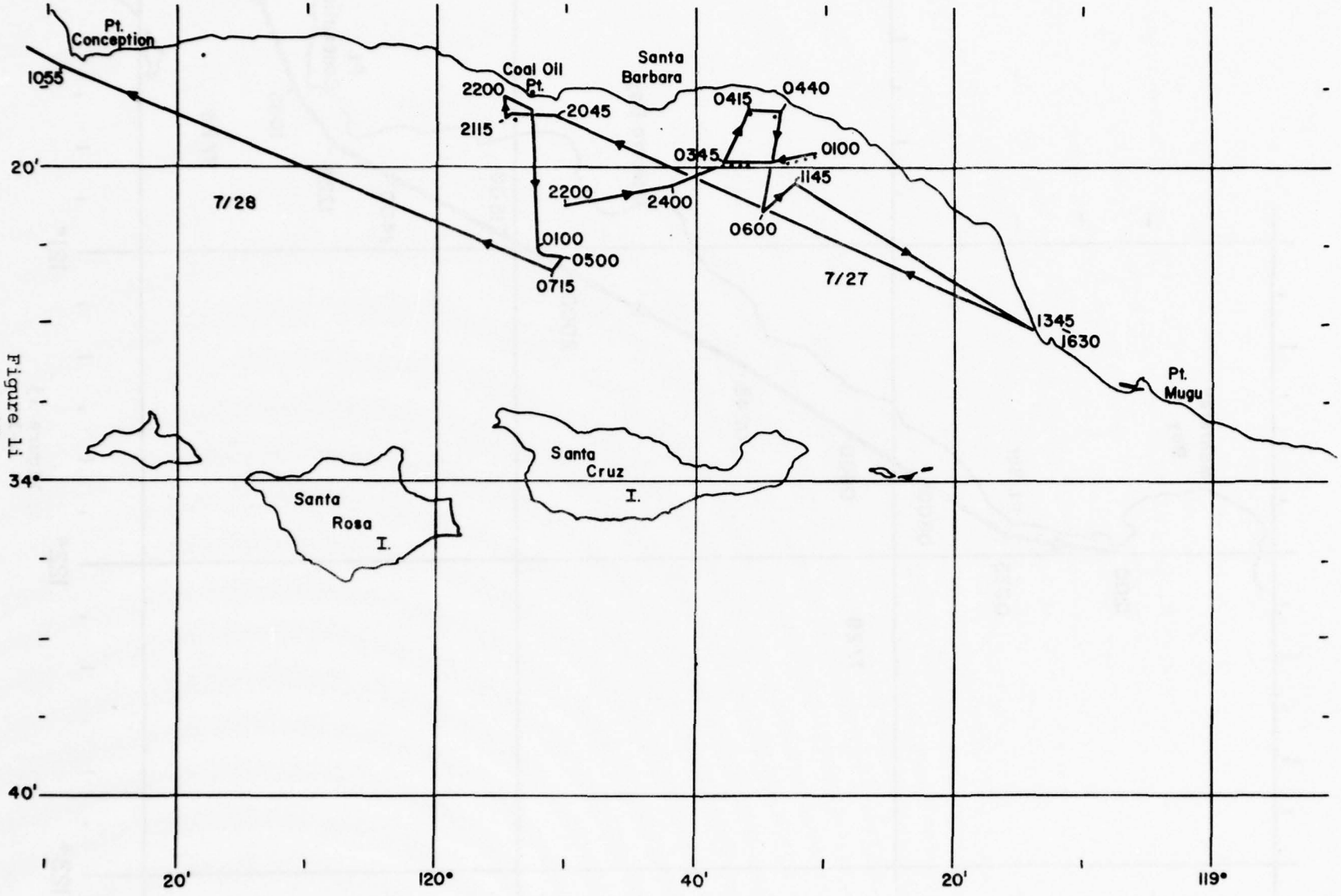

Figure 11
A-15

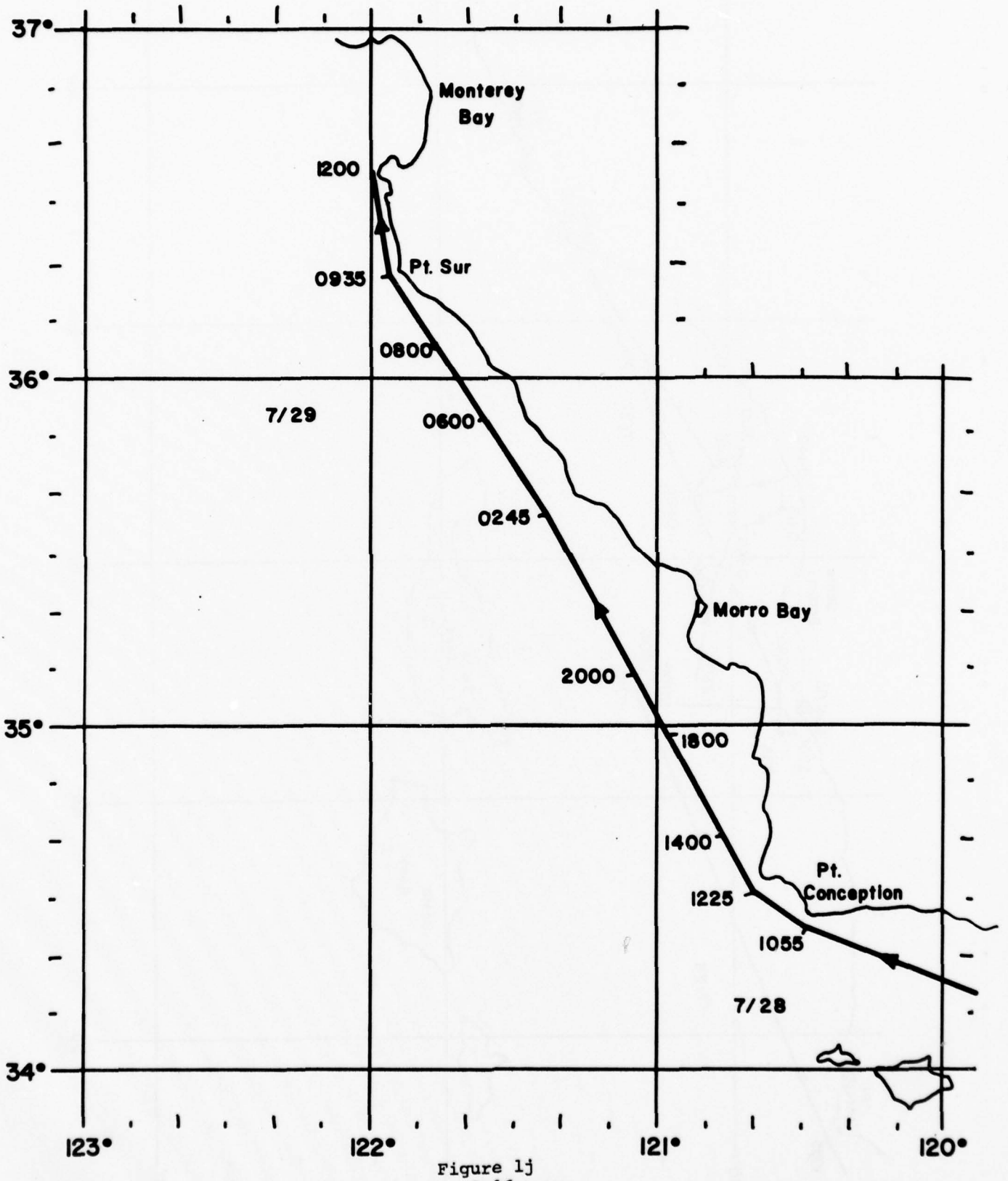

Figure 1j
A-16

B. Wind Speed and Direction

Table III lists ship's heading and speed, relative wind direction and speed, and true wind direction and speed. All speeds are in knots, and directions are in degrees measured clockwise from true North for the ship heading and true wind, and clockwise from the ship's bow for the relative wind. The ship speed was obtained from the bridge and is based on the speed of the ship's screws. Relative wind was measured both from the ship's anemometer and from the cups on level 4 of the NPS scientific equipment. True wind was calculated from the other data and is no more accurate than $\pm$ 1 knot and $\pm$ 20°, especially at low wind speeds.

TABLE III

Relative and True Wind

	Ship		Relative Wind		True Wind	
Time	Heading	Speed	Direction	Speed	Direction	Speed
7/17						
1000	168	10	013	12.5	220	4
1100	168	10	010	9.5	279	2
1200	150	10	010	6	316	4
1300	150	10	030	5	306	6
1400	148	10	020	5	310	6
1500	143	9	038	3	307	7
1600	143	9	087	2	310	9
1700	144	9	092	3.5	303	10
1800	144	9	082	4.5	296	9.5
1900	144	9	090	4	300	9.8
2000	144	9	006	2	322	7.0
2100	144	9	349	1.5	326	7.5
2200	144	9	011	3	319	6
7/18						
0000	144	9	300	5.5	001	8
0300	079	9	001	4	258	5
0330	-				295	4
0400	100	9	012	8.5	211	2
0500	102	9	028	9	206	4
0600	075	9	000	16.5	075	7.5
0630	-				075	9
0800	097	9	023	13.5	154	6
0830	095	2.5	020	7	125	5

7/18						
0900	070	3	020	6.5	106	4
1000	133	9	032	6.2	272	5
1100	133	9.5	047	3	297	8
1200	113	9.5	047	4	270	7
1300	111	9.5	019	6	264	4
1400	104	9.5	031	2	276	8
1600	-				265	7
1700	277	2	063	10	351	9
1800	275	2	075	8.5	004	8
1900	073	9	079	3	234	9
2000	264	2	345	8	244	6
2100	265	2	340	3.5	222	2
2120	265	2	000	4	265	2
2140	265	2	000	5	265	3
2220	260	2	315	4	186	3
7/19						
0000	265	2	010	4.5	283	3
0020	270	2	020	4	308	2
0040	270	2	018	3	317	1
0100	270	2	018	3	317	1
0120	265	2	060	2	025	2
0140	275	2	012	2	011	0.5
0200	270	2	350	3	241	1
0220	090	9	270	8	312	1
0300	-				194	3

7/19						
0400	180	9	000	11	180	2
0440	180	9	355	12	161	3
0500	150	9	000	10	150	1
0520	148	9	004	11.5	166	3
0600	140	9	350	9	045	2
0700	140	9	355	9	048	1
0900	-				200	4
1000	353	2	226	3	201	5
1100	175	9	357	11.5	161	3
1140	155	2	017	3.5	192	2
1200	168	2	000	5	168	3
1330	305	9	000	0	125	9
1430	254	0	340	9	234	9
1540	-				328	4
1550	320	2	000	7	320	5
1610	320	2	340	8	294	6
1630	290	2	355	8	283	6
1650	285	2	350	9.5	272	7.5
1710	275	2	000	9	275	7.0
1800	133	9	058	2	301	8
1900	133	9	327	4.5	338	6
2000	167	9	053	10	277	8.5
2100	147	9	028	6	290	5
2120	-				005	3
2140	350	0	328	3	318	3
2300	-				315	~0

7/20						
0000	-				183	1.5
0100	-				067	4
0200	-				290	4
0300	-				090	6
0400	-				280	7
0500	-				280	6
0555	-				270	5
0640	295	0	000	6	295	6
0700	-				285	7
0830	345	9	340	7	210	3
0850	350	9	340	9	250	3
0920	350	9	335	9	248	4
1000	350	9	315	10	245	7
1020	345	9	340	7.5	218	3
1100	343	9	040	6.5	117	6
1200	340	9	345	5	177	4
1220	340	9	340	6	193	4
1300	332	9	338	7.5	206	3.5
1400	-				280	4
1500	152	9	068	9.5	274	10
1600	102	9	181	6.5	282	15
1700	094	9	146	5.5	261	14
1710	-				260	12
1720	187	0	068	4	255	4
1740	350	0	285	11.5	275	11.5

7/20						
1800	210	5	342	19	186	14
1820	270	5	000	17	270	12
1840	275	5	359	16	274	11
1900	275	5	000	17	275	12
1920	250	5	000	14	250	14
1940	270	5	000	14	270	14
2000	270	5	000	16	270	11
2020	270	5	000	15	270	10
2045	-				280	7
2050	270	5	000	11	270	6
2100	270	5	000	14	270	9
2120	270	5	000	12	270	7
2200	-				280	4
2300	-				302	4.5
2325	000	9	000	6	180	3
7/21						
0000	000	9	330	9	255	5
0040	345	9	333	10.5	259	5
0100	-				305	3.5
0120	270	9	350	8	141	2
0140	270	9	348	6	112	3
0200	270	9	350	5	102	4
0215	-				120	5
0250	-				100	5
0345	100	2	000	7	100	5
0350	095	0	350	6	085	6
0447	-				142	5

0500	-				125	4
0545	-				160	3
0635	-				calm	
0830	095	7	350	12	072	5
0850	095	7	360	13	095	6
0900	360	7	030	8	091	4
0930	360	9	010	8	129	2
1000	360	9	020	7	135	3
1030	330	9	000	9		~0
1050	330	9	350	9	235	1.6
1115	-				270	7
1220	-				270	10
1245	265	5	000	16	265	11
1300	265	5	355	19	258	14
1400	260	5	018	18	285	13
1445	-				280	15
1600	-				260	14
1700	-				270	11
1800	-				265	11
1925	-				250	8
2010	-				225	9
2115	-				220	2
2215	-				120	4
2300	-				100	3
2320	000	9	015	10	076	3
2350	-				050	2

7/22						
0004	-				040	2
0030	-				010	1
0045	-				025	2
0100	-				020	2
0130	170	9	340	10	087	3
0211	-				180	1
0215	-				calm	
0245	-				095	7
0300	025	9	035	10	123	6
0330	-				122	5
0415	-				015	3
0515	-				120	4.5
0615	-				130	3
0645	000	9	010	8.5	113	2
0715	-				calm	
0800	-				calm	
0825	170	5	004	9	179	4
0910	180	9	011	8	307	2
0930	270	9	000	10	270	1
0950	-				260	3
1010	-				260	5
1045	-				240	4
1055	125	9	000	8	305	1
1130	-				230	3
1200	052	0	126	4	178	4
1307	-				250	10

7/22						
1430	155	9	052	7.5	278	10
1500	155	9	066	9	278	10
1600	155	9	006	3.5	331	5.5
1640	155	9	341	6.5	012	4
1700	179	9	036	9.5	282	6
1910	-				145	7.5
1950	-				150	4.5
2120	100	9	033	11.5	184	6
2200	100	9	015	16.5	132	8
2220	100	9	042	17	172	12
2300	100	9	035	13.5	175	8
2320	100	9	047	16	181	12
7/23						
0000	100	9	035	13.5	175	8
0100	095	9	040	12	184	8
0200	090	9	045	9.5	199	7
0235	-				160	4
0315	325	9	005	5	139	4
0400	324	9	016	5.5	122	4
0450	325	9	353	4.5	152	5
0630	300	9	025	4.5	099	5
0730	300	9	010	4	112	5
0830	290	9	025	5	085	5
0900	335	9	030	3.5	139	6
1000	300	9	030	5	092	5
1100	320	9.1	290	3	159	9

7/23						
1200	-				200	7
1300	-				290	9
1400	-				250	6.5
1425	-				260	6
1450	215	5	000	9	215	4
1510	215	4.5	000	12	215	7.5
1540	-				240	7.5
1600	000	9	300	8.5	237	9
1630	-				275	9
1650	-				255	9
1720	270	5	355	14.5	262	9.5
1745	260	9	355	13	244	4
1805	-				205	4.5
1815	025	9	000	3.5	205	5.5
1900	102	9	028	6	245	5
2000	-				250	3
2002	-				240	3.5
2100	-				calm	
2200	-				330	1
2300	-				200	3
7/24						
0000	316	4	343	7.5	281	4
0030	316	4	344	7	281	3
0100	-				270	3.5
0115	090	7	022	4.7	236	3
0150	-				180	3.5
0210	-				170	4

7/24						
0300	245	9	340	8.5	136	3
0330	-				135	3.5
0400	245	9	345	7.5	113	3
0430	246	9	354	10.5	209	2
0450	-				210	2
0500	050	9	010	6.5	207	3
0530	038	9	347	5.5	237	4
0550	-				310	4.5
0600	150	9	025	9	253	4
0630	147	9	023	8	265	3.5
0700	167	9	353	9.5	097	1
0720	-				130	2
0800	150	9	350	10	086	2
0825	150	9	000	8	330	1
0900	-				075	4
0945	-				300	2
1000	325	9	350	10	261	2
1100	330	9	350	13	299	4.5
1200	100	9	035	3	265	7
1300	-				275	9.5
1400	195	2.5	060	10	269	9
1500	193	2.5	307	10	127	9
1600	115	4	185	4.5	298	8.5
1700	080	8	205	11	275	18.5
7/25						
2100	295	1	340	13	273	12
2200	285	1	340	8	262	7

7/25						
2300	-				280	12
7/26						
0000	285	1	000	8	285	7
0100	-				045	1
0200	-				225	1
0300	-				240	3
0400	340	9	000	11	340	2
0500	-				300	4
0530	270	9	000	11	270	2
0600	270	9.4	000	7	090	2
0700	297	9.4	333	7	162	4.5
0730	295	9.4	000	7	115	2
0800	295	9.4	020	10.5	018	4
0900	295	9.2	005	12	315	3
0930	-				315	4
1000	295	9.2	005	13.5	310	4
1100	295	9.4	005	13.5	311	4
1200	295	9	355	18.5	285	10
1305	-				285	11.5
1400	280	9	352	18.5	265	10
1500	-				245	16.5
1600	278	8	317	13.5	200	9
1700	278	8	342	23	251	15.5
1800	-				315	18
1900	070	2	235	16	300	17

7/26						
2000	070	2	235	13	298	14
2100	070	3	255	14	314	15
2200	080	3	245	10	311	11.5
2300	080	3	245	5	302	7
7/27						
0000	090	2	060	4.5		
0100	-				130	5.5
0156	-				210	3
0218	-				240	3
0300	-				calm	
0412	-				030	3
0500	-				275	6
0600	-				270	4
0700	-				255	4
0800	-				250	4
0900	-				225	6
1000	-				250	5
1100	-				260	3
1200	117	9	038	7	246	5.5
1300	113	9	047	8.5	230	7
1400	-				230	4
1500	-				160	5.5
1600	-				260	1
1700	295	9	015	12.5	341	4.5
1800	-				260	5
1900	290	9.2	325	8.5	175	5
2000	280	9	005	5	094	4

7/27						
2045	-				100	4
2115	-				085	3.5
2155	-				085	9
2230	-				095	7
2300	180	3.5	325	7.5	122	5
7/28						
0000	180	3.5	025	5.5	237	3
0100	-				210	8.5
0200	-				210	6.5
0300	-				215	6.5
0400	-				250	6
0500	-				255	6
0600	-				265	4.5
0700	-				230	5
0800	290	9.2	000	9	110	~ 0
0900	290	9	355	8	144	1
1000	290	9	350	5	122	4
1100	290	9	005	19	299	10
1200	300	7.5	030	14	357	8
1300	330	5.5	015	15	353	10
1400	330	6	345	25	310	19
1700	330	4	345	27	312	23
2200	330	4.2	010	22	342	18

7/29						
0600	325	8	355	19	316	11
0700	325	8.2	355	23	317	15
0900	325	8.8	000	19	325	10
1000	347	8.8	343	18	315	10
1100	347	9	353	15	330	6
1200	022	9	323	15	310	9.5

C. Acoustic Sounder

Reproductions of the acoustic sounder strip charts are shown in Figures 2a - 2d. Each strip in the photographs shows a 24 hour period and the vertical span is 1000 meters. Return echos are readily apparent and in most cases one strong return identifies the presence of a temperature inversion. The height of the base of the inversion is identified on the charts from the lower most portion of the return echo signal (dark horizontal band on chart). The vertical dark areas on the charts are caused by the increased noise when the ship is in motion. Thermal plumes are evident on many of the charts and can be identified by a return at the surface and extending upward, at times to heights of nearly 300 meters. The times at which radiosondes were launched are shown at the bottom of each chart by a letter, which corresponds to the letter designation on the radiosonde graphs. Experiment codes are also shown.

Table IV is a compilation of data taken from the acoustic sounder charts. We present this table because it is much more difficult to identify weak returns on the reproductions of the charts than on the originals, and at times as many as 5 or 6 distinct returns can be identified. The table lists the height of top of thermal plumes, when present, and the height of the base of non-surface return regions, all heights being in meters. There are also code letters associated with the listed heights. The letters "W" and "S" refer to weak and strong return echos, respectively, when they precede a number. A "W" following the listed height for a return height indicates that echos are obtained over a wide band. "Dark" means that there is too much background noise, giving a dark trace, to allow determination of the presence of a return.

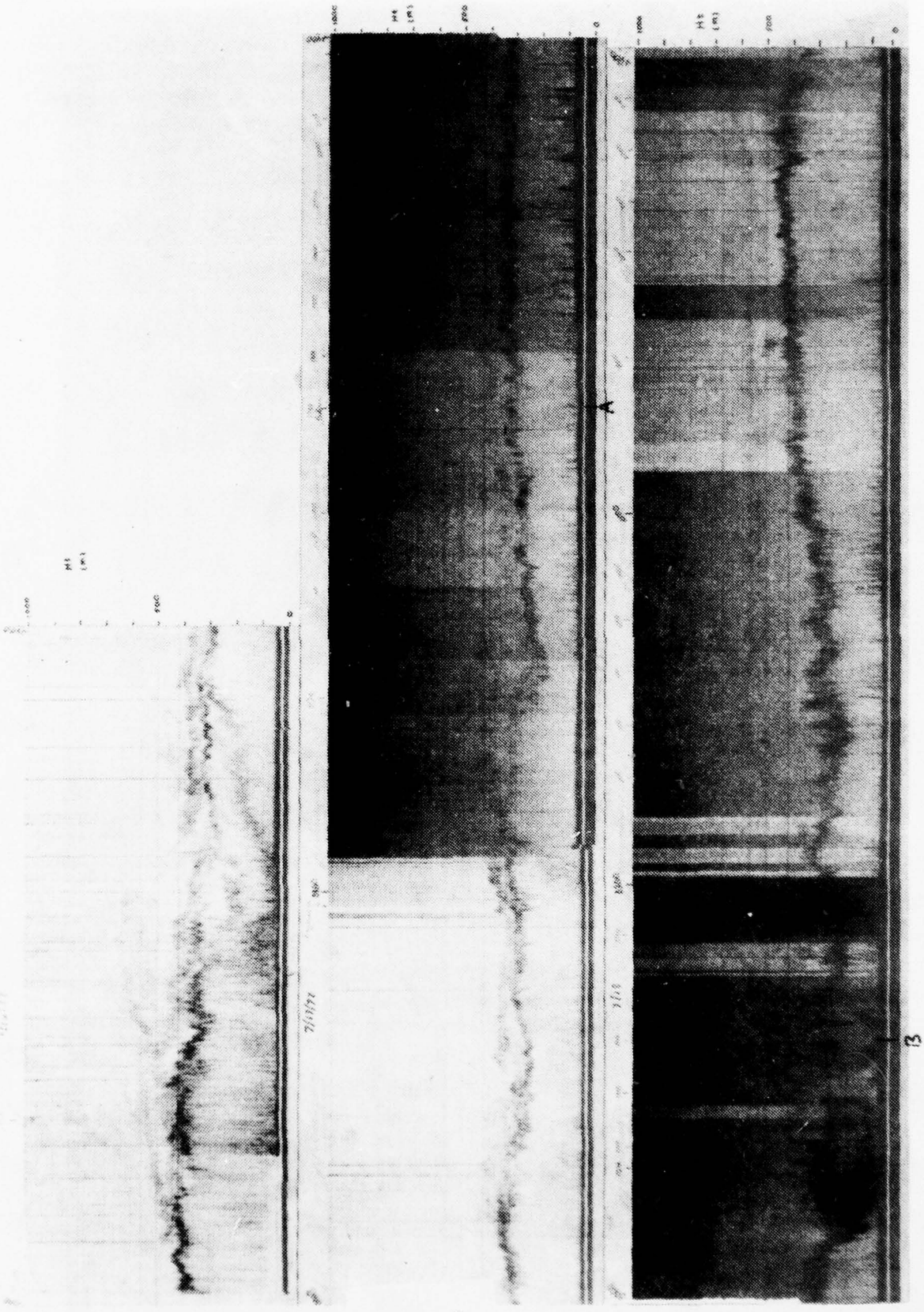

Figure 2a

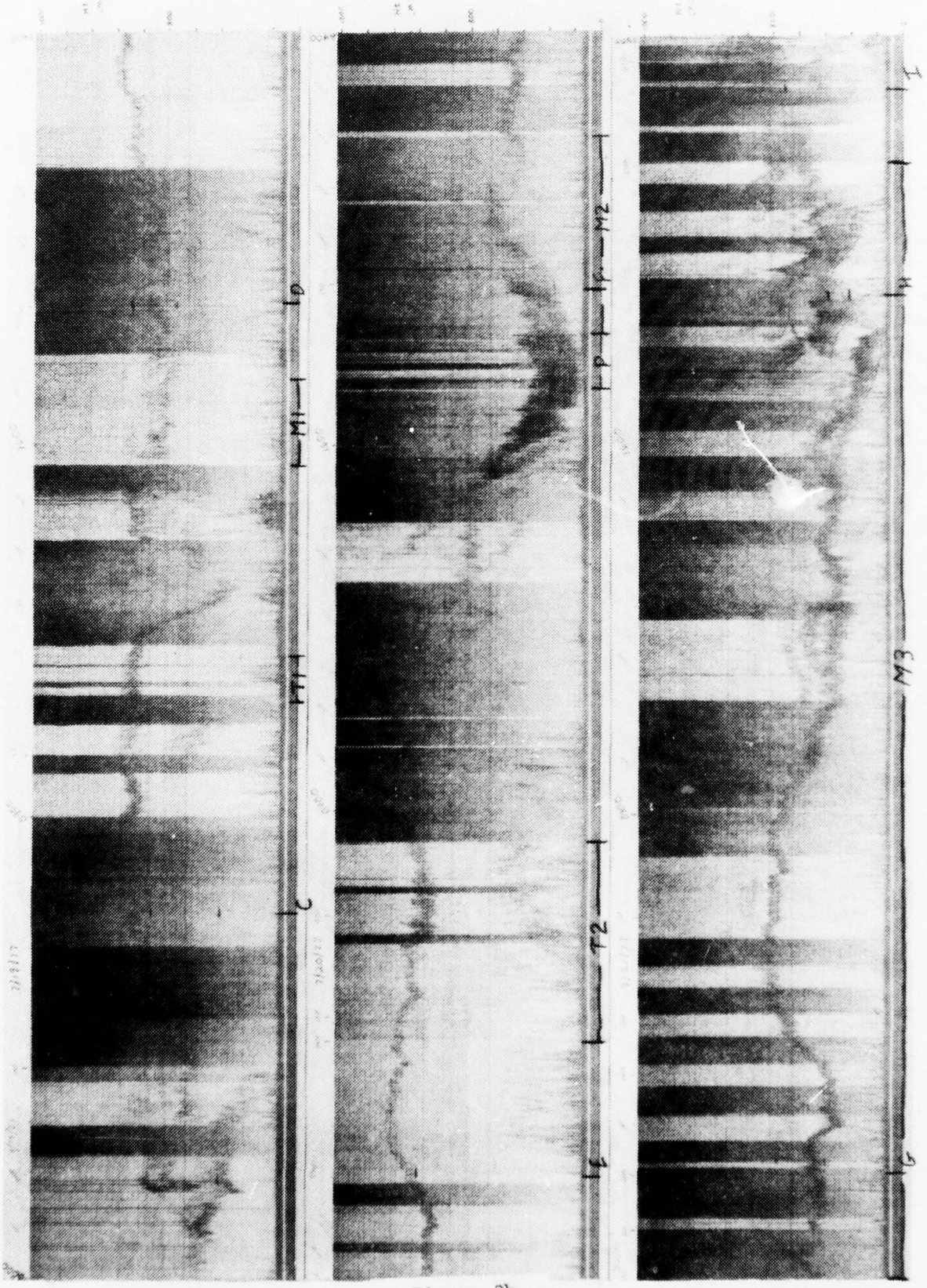

Figure 2b
A-34

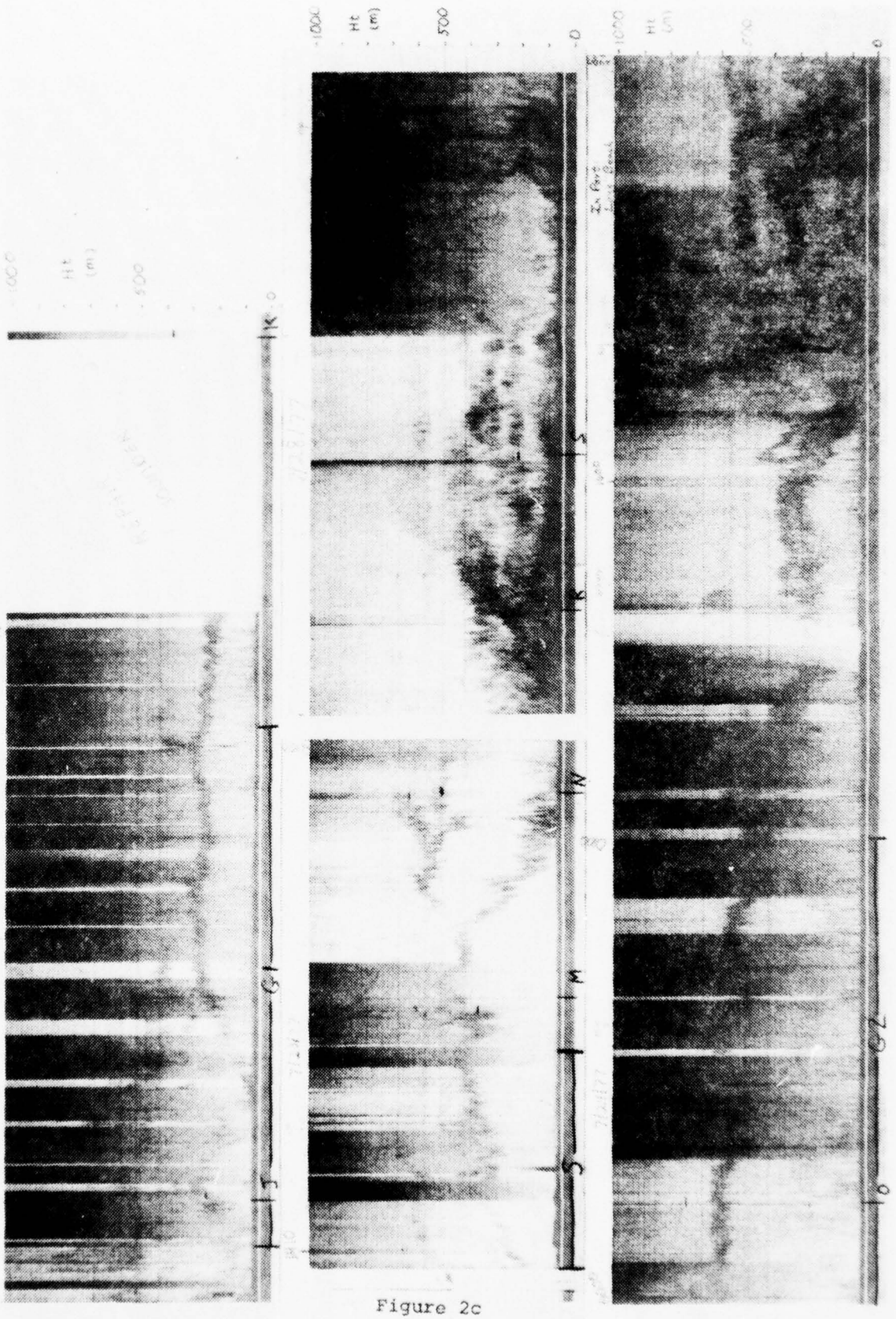

Figure 2c
A-35

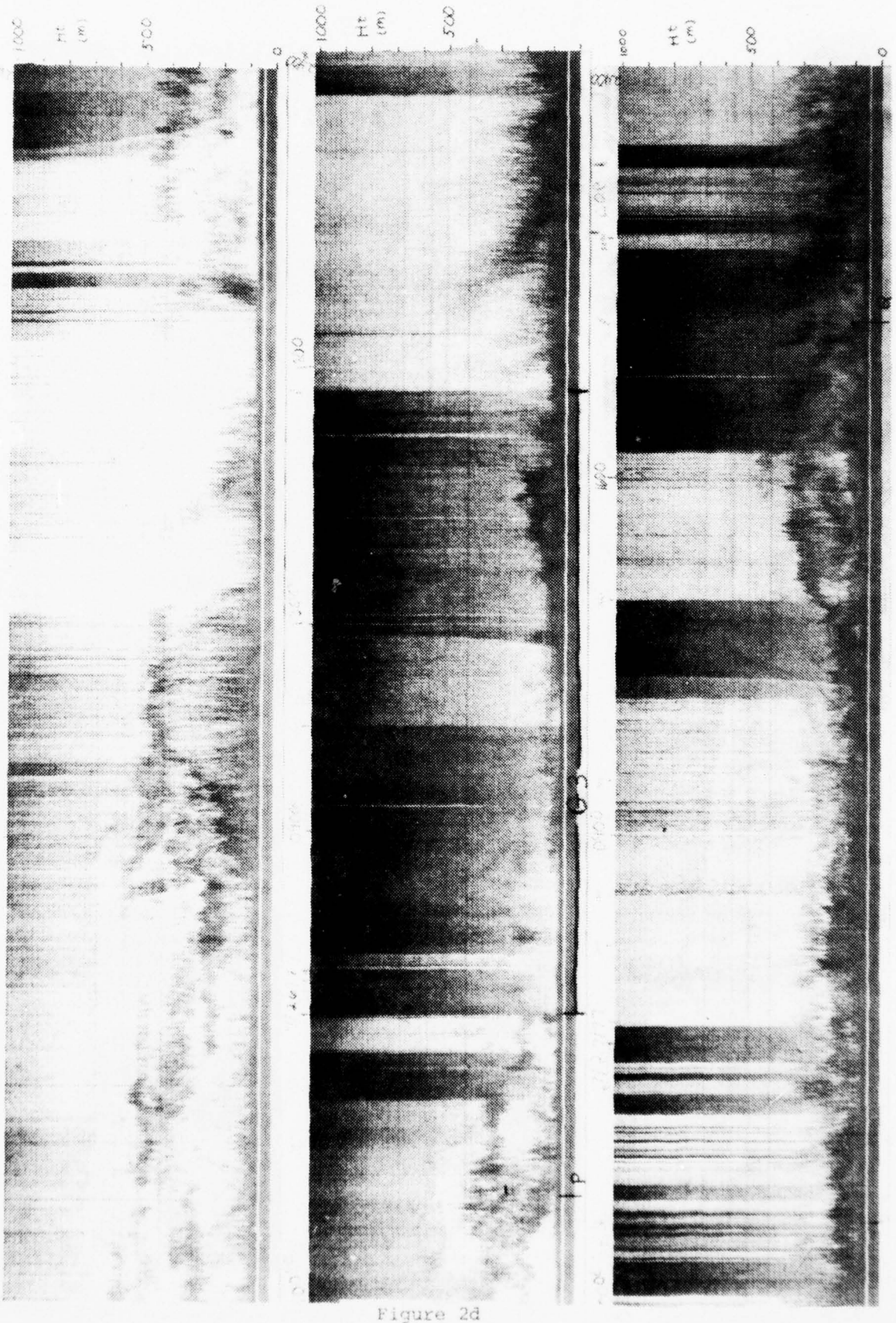

Figure 2d
A-36

TABLE IV

SUMMARY OF ACOUSTIC SOUNDER RESULTS

DATE/ TIME	THERMAL PLUMES	RETURN HEIGHTS 1	2	3	4	COMMENTS
7/16/77						
1120		S290				no thermal plumes until 1400
1140		S360				
1200		S370				
1220		S340	460			divides
1240		S380	420			
1300		S400	460			
1320		W300	380	480		return at 300m appears - 2nd return
1340		W300	W400	480		getting weak - 3rd return rising, weak
1400	260	S360	?	480		return 1 & 2 merge
1420	200	380	?	510		can't tell where #2 begins
1440	W160	360	?	520		
1500	220	300	?	W520		seems to be 4 returns but can't tell where it starts
1520	160	300	?	540		
1540	200	260	?	520		
1600	160	S320	420			return 3 & 4 merge together
1620	160	S300	400	500		
1640	W130	280	merged	W480	W580	
1700	250	320	500	600		
1720	240	300	merged	520	580	
1740	260	~290	~360	VW540		plumes merge with 1st return
1800	240	320	~400	530		return #2 merges with 1 around 400 m

1820	290	360	dark	560	620	
1840	120	180	300	~360	560	
1900	S100	160	320		VW580-600	
1920	S100	180	300	340	W~580	may be another return at 460 m
1940	140	~200	260			#3 merges with 2
2000	140	260	merged		340	
2020	VW 100	140	280	320	VW420	inversion rising from surface
2040	"	140	260	320	"	return 3 seems to have split
2100	~120	240	300	340	400	
2120		150	200		410	may have 5 return heights
2140		240	combined		VW450	3 is combined with 2 and another one
2200		160	290	340	~420-460	return 4 is hazy - not clear
2220		160	290	~340	440	
2240		260	~310 merged	~330	W460	no plumes
2300	VW200	290	~300	- 400	460	
2320	180	260				return 2,3,4 merged
2340	220	260				
2400	180	S270			360	
7/17/77						
0020		W200	280		400	inversion rising from surfaces
0040		230	S280		380	no plumes
0100			280		400	

0120	W80		320		420	can't discern return 1 & 3
0140	W100	280	310		~410(?)	
0200		260	280	merged		
0220	W100	290			460	there are now 4 returns - all merging
0240	W120	260	not clear			
0300	W160	240				no 5 returns
0320	W140	220		300		
0340		240	280	320	~400	
0400		220	460			
0420		240	merged		330	inversion from surface
0440	80	220		280	320	#5 hazy
0500	120	220		270	310	4 & 5 merged together
0520	140	250		310		
0540	160	260		340		
0600	60	260	310	420		
0620	80	280	merged			can't tell #3 & 4
0640	160	280	320			
0700		200				
0720		260		300		no plumes
0740	100	S200			340	
0800	160	210	390	350		
0820	200	300	350			
0840	~210	300	340			
0900		240				getting too dark to see much
0920		320				
0940						
1000						

1020		280	340	
1040				
1100		300		
1120		200W		may have 2nd return
1140	W80	200		
1200	100	180W	240	
1220	100	160W		
124C	120	180		
1300	120	220		very faint second return
1320	120	210		
1340	130	220		
1400	120	220		
1420	140	210		
1440	215	260		
1500	130	240	300	
1520	90	240	300	
1540	110	240	305	
1600	120	210	300	
1620	140	270	320	
1640	110	280		
1700	140	280		
1720	110	300		have 2nd return but can't judge - too dark
1740	130	300	380	
1800	120	260	360	
1820	140	280	380	
1840	160	300		
1900	140	320		

1920	140	300	
1940	140	280	
2000	150	300	
2020	140	300	
2040	260	280	
2100	160	320	
2120	120	310	
2140	200	300	
2200	160	300	
2220	150	300	
2240	130	280	
2300	180	280	
2320	120	300	
2340	200	290	
2400	160	280	
7/18/77			
0020	140	260W	
0040	120	260	
0100	120	255	
0120	125	145	return 1 descending to surface
0140	can't tell - too dark		may be 2 or 3 returns
0200			
0220			inversion - going to surface - plumes become darker, rising up blotch so can't tell which is which
0240	160(?)	220W	may have 2 or 3 returns
0300			

0320	140	160W			
0340	140	180	400		
0400		100	180	360	inversion rising from surface
0420	120	140	240		plumes rising to combine with inversion at 120-140m
0440	80	110W	240		too dark to see 3rd
0500	160	220			
0520	120	160			
0540	80	100	250		
0600	140	220			
0620	120	200			
0640	180	200	310		
0700					too dark to see anything
0720					
0740					
0800					
0820	120	160			
0840	130	200			
0900	100	240	340		
0920	90	210	340		
0940	100	240			2nd return may have combined with 1st
1000	100	220			
1020	120	200			
1040	140	160W			
1100	130	180			
1120	150	200			
1140	160	230			
1200	150	260			

1220		220
1240	160	230
1300	100	250
1320	120	210
1340	170	240
1400	160	240
1420	160	260
1440	160	240
1500	130	320
1520	140	300
1540	100	320
1600	180	330
1620	100	360
1640	120	340
1700	100	360
1720	120	340
1740	120	340
1800	120	350
1820	160	360
1840	130	360
1900	100	390
1920	120	400
1940	180	390
2000	W100	380
2020		400
2040	W100	410
2100	W120	400

2120	W100	420					
2140	W100	420					
2200	120	380					
2220	120	380					
2240	100	380					
2300	110	340					
2320		320					
2340	140	340					
2400	160	280					
7/19/77							
0020	140	330					
0040		300					
0100		320					dividing into 3 returns
0120	W150	270W					plumes are very faint
0140	W150	190W	360				can't tell where 3 returns start
0200	120	240W	480	520			
0220	160	240W	DARK				
0240	100	DARK					
0300	120	180	380				
0320	130	140	340W	460	540		inversion descending to surface
0340	140	~145	370W				3 & 4 merged with 2
0400	100		360	DARK			
0420		TOO	DARK				too dark to see until 0850
0440							
0500							
0520							
0540							

0600				
0620				
0640				
0700				
0720				
0740				
0800				
0820				
0820				
0840				
0900	220	S580		only 1 inversion now
0920	220	590		
0940	240	620		
1000	240	370	580	another return appeared at 370 m
1020	160	300	620	
1040		DARK		
1100		DARK		
1120	140	W240	610	
1140	210	at surface	600	1st return at surface
1200	180	"	600	
1220	180	"	580	
1240	160	disappeared	420	#2 dropping
1300	200	260		almost at surface
1320	200	220		
1340	160	300		
1400	140	340		

1420	170	200W		inversion very wide not sure if it's part of plume or inversion (200-660)
1440	190	200W		
1500	180	TOO DARK		
1520	160	"		
1540	180	~ 500		
1600	190	500		
1620	210	470	600	2nd return appeared
1640	220	500		#2 merged with #1
1700	220	500		
1720	220	480	560	
1740	240	420	510	
1800	220	410	DARK	
1820	160	460		
1840	160	510		
1900	160	540		
1920	160	DARK		
1940	180	500		
2000	220	500		
2020	240	510		
2040	200	540		
2100	160	560		
2120	180	590		
2140	200	600		
2200	180	590		
2220	140	600		
2240	200	580		
2300	130	650		

2320	150	650		
2340	200	640		
2400				
7/20/77				
0000	140	620		
0020	140	635		
0040	180	630		
0100	180	620		
0120	140	640		
0140	140	640		
0200	120	690		
0220	200	720		
0240	320	750		
0300	380	760		
0320	380	790		
0340	400	760		
0400	380	740		
0420	360	720		
0440	360	740		
0500	300	720		
0520	320	700		
0540	280	280	690	another return appears at ~ 280 m
0600	can't tell where plume ends & inversion begins		700	very faint - may have merged with plumes
0620	180	120	690	
0640	?	160	620	
0700	?	160	615	

0720	160	220	615			
0740	180	230	600			
0800	200	280	640			
0820	140	200W	660			
0840	140	DARK	700			
0900	120	W160	700			
0920	140	180	DARK			
0940	120	160	DARK			
1000	140	210	"			
1020	?	?	"			plumes are there but inversion is overlapping with it
1040	180	disappeared	"			
1100	140		"			
1120	120	DARK	"			may have 2 or 3 returns between 300-500 m
1140	140	?	"			
1200	130	?	"			
1220	160	360	"			
1240	180	360	"			
1300	100	360	420	TOO DARK		return became clear at 420 m
1320	100	280	440	TOO DARK		
1340	110	260	400	700		may have another return at 360 m and another between 520-610 m
1400	W90	320	440	570W	700	
1420	110	260	450	560	620	
1440	100	DARK				
1500	100	280	440	DARK	?	

1520	160	200	240	420	?	
1540	120	120		300		#2 overlapping with #1 same with #3 & #4
1600	100	120			300	#2 & 3 overlapping with #1
1620	90	100		235		
1640	80	120W				return dropped to surface became one big return
1700	70	80W				
1720	?	70W				inversion - overlapping with plumes
1740	?	80W				
1800	?	80W				
1820	100	120W				
1840	100	130W				
1900	100	140W				may have 2 wide returns overlapping
1920	100	160W				
1940	120	260W				
2000	120	280W				
2020	200	W240	380			another return appeared at 240 m
2040	120	W200	360			
2100	140	W220	300			
2120	150	240				#2 overlapping with #1
2140	160	240				
2200	120	280				
2220	140	340				
2240	140	320				
2300	130	300				
2320	200	270				
2340	140	300				

7/21/77

0000	140	280		
0020	150	290		
0040	160	310		
0100	160	290		
0120	130	270		
0140	120	270		
0200	140	280		
0220	150	280		
0240	160	300		
0300	320	200		
0320	320	220		
0340	?	260		dark band covering plumes
0400	?	240		inversion covering plumes
0420	?	320		band covering plumes
0440	?	380		band covering plumes
0500	210	360		
0520	dark band	450		
0540	"	455		
0600	320	460		
0620	150	dark band		
0640	120	480	640	
0700	260	460	560	
0720	260	460	560	
0740	300	460	520W	
0800	320	420		

0820	220	460			
0840	240	475			
0900	200	430			
0920	160	420			
0940	160	360			
1000	200	310			
1020	210	300			
1040	180	280			
1100	100	260			
1120	200	220	340		
1140	200	220	360		
1200	210	220	~ 300	400	#1 split into 2 returns
1220	200	230	~ 330	400	
1240	180	200	320	400	
1300	140	180W	blotch	dark	
1320	140	210	ended	ended	
1340	140	200			
1400	100	200			
1420	100	280			
1440	140	220			
1500	200	200			
1520	140	200			
1540	120	220	290		
1600	150	220	290		
1620	140	200	280		
1640	140	160			#2 overlapping
1700	120	140			

1720	90	120	220			
1740	100	~110	220	420		
1800		100	250			return at surface overlapping with plumes
1820		80	240	overlapping with #2	440	
1840	120	140	overlapping with #1	"	440	
1900	140	200	"	"	440	
1920	160	240	ended	ended	380	
1940	140	250W				#2 & 3 combined (?) with #1 - so did 4
2000	140	200W				may have another return ~ 400 & ~ 540 m
2020	140	160W	390W			
2040	130	140	~500	400	500	#1 stopped
2100	100	300	DARK	DARK		
2120	140	310	460			
2140	100	320W				#2 combined with #1
2200	110	330W				
2220	100	340W				
2240		DARK				
2300		DARK				may have 2 returns
2320	110	290	480W			
2340	140	190	290	440W		
7/22/77						
0000	160	200	370	480W		
0020	110	140	380	470W		
0040	100	140	?	460W		

0100		120	320	460W		
0120	100	120	DARK	DARK		
0140		160	320	DARK		
0200		180	DARK	500W		
0220	80	250	340	410	510W	another return at 410 m
0240		200	340	390	480W	
0300		180	DARK			
0320		80	DARK			
0340	100	140	DARK			
0400	110	220	DARK			
0420		at surface	290	400	580	
0440		"	240	DARK		
0500	100	120	300	380		#4 combined with #3
0520	130	140	290	360		
0540	100	190	280	DARK		
0600	130	220	DARK			
0620	110	220				#2 combined with #1
0640	100	240	DARK			
0700	110	240	DARK			
0720	100	240	DARK			
0740	110	240	DARK			
0800	160	260	360			
0820	110	230	DARK			
0840	100	230				
0900	100	200				
0920	80	220				
0940	100	220				
1000	120	220				

1020	100	260			
1040	100	260			
1100	120	250			
1120	140	220			
1140	140	220			
1200	140	210			
1220	150	210			
1240	150	200			
1300	160	180			
1320	110	160			
7/23/77					
1400		160	260	530	
1420		210		560	#2 combined with #1
1440		280	580		
1500		310	580		
1520		DARK			
1540	S260	290	?	560	may have 2 more returns
1600	90	260	combined with #1	640	
1620	120	300W	DARK		
1640	160	320			
1700	140	320			
1720	120	355			
1740	120	350			
[illegible]	110	400			
[illegible]	120	320			
[illegible]	100	270W			
[illegible]		400			

1920		480			
1940		400			
2000	240	390	W610		
2020	110	360	W410	W610	
2040		260	combined with #3	500	
2100		210	540		
2120		170	520		
2140		100W	500		
2200		80	500		
2220		80W at surface	300	555	
2240		at surface	390	500	580
2300		"	460	620	
2320	160	490			
2340	260	500			
2400	160	weak			
7/24/77					
0020	150	too weak			
0040		155	580		
0100		120	560		
0120	100	170	550		
0140	100	140	560		
0200	120	~125	560		
0220	120	?	550		
0240	100	120	240	570	
0300	120	160	?	540	
0320	100	at surface	DARK	540	

0340	100	120	DARK			
0400	120	140	"	500		
0420	100	140	"	DARK		
0440		at surface	stopped	"		overlapping with plumes
0500		"	560			
0520		"	DARK			
0540		"	"			
0600		"	480			
0620	120	DARK	500			
0640	100	"	500			
0700	90	"	540			
0720	100	140	520			
0740	150	175	500			
0800	DARK	DARK	DARK			
0820	110	"	"			
0840	120	"	490			
0900	120	"	400W			
0920	110	"	DARK			
0940	105	"	"			
1000	160	~165	300	400	550	
1020	100	DARK				
1040	110	"	280			
1100	100	"	"			
1120	120	200W	460			
1140	120	260W	500			
1200	140	220W				
1220	140	180W				

1240		weak				
1300		W250				
1320	160	220	350	640		
1340	180	220	320	580		
1400	160	200	320	580		
1420	140	220	320			
1440	120	160	300			return between 160-300 m
1500	140	160	260	~305		
1520	160	240				
1540	160	260				
1600	180	220				
1620	140	200				
1640	120	180	260	350		
1700	?	100	200	310		
1720		at surface	?	DARK		
1740		"	?	220	360	
1800		"	?	340		
1820	180	200	DARK			
1840	S200	300				
1900	S180	340	400			
1920	S210	220	340			
1940	S220	220	360			
2000	S240	280	360	DARK		
2020	120	140	280	500		
2040	S200	240	340	465		
2100	S260	280	380	440		
2120	S280	320	?	480		
2140	S280	340	?	470		
2200	S240	260	380	460		

2220	S200	?	?	400	480	
2240	S200	~195	300	420	~500	
2300	~140	~100W	300	420	~500	
2320	~100	at surface	240	440	?	
2340	90	120W	~240	440	?	
2400	120	130	220	300	380	6 returns here
				5	6	
				460	560	
7/25/77						
0020	140	160	240	380	420	
					5	
					560	
0040	110	160	240W	440	540	
0100	110	at surface	260W	480	560	
0120	140	"	260	340	480	#5 return at 560
0140	140	"	260	445		
0200	150	"	280			
0220	110	"	2	3	4	may have as many as 6 or 7 returns
			160	260	350	
				5	6	
				400	460	
0240	120	"	180	360	450	#4 & 5 combined with #3
0300	180	"	260	360	440	
0320	140	"	320	370	?	#4 combined with #3
0340	140	"	260	330W	?	
0400	110	"	280	310W	480	
0420	160	"	280W	465		
0440	100	"	210	280W	?	
0500	100	"	200	300	470	

0520	90	at surface	200	300W	460	
0540	100	"	~200	280	360	#5 return at 460
0600	150	220	280W	480		
0620	120	145	230	290		
0640	100	120	230	overlapping with #2		
0700	90	at surface	160	"	W340	
0720	120	"	180	330		#3 combined with #2
0740	130	"	180	300	420	#5 return at 500
0800	140(?)	"	180	320	400	
0820	200	DARK	200	380	500	plumes covering #1 return
0840	200	DARK	240	300	440	
					5 660	
0900	220	DARK	240	300	430	
					5 640	
0920	240	240	300	400W		
0940	260	~240	360W			
1000	?	160	270	380		
1020	220	260	overlapping	400		
1040	280	360	"	combined with #2		
1100	260	380	420			
1120	320	420				
1140	260	400				
1200	260	360				
1220	240	~380				
1240	200	400				

1300	280	400			
1320	~300	400			
1340	~200				
1400	190	W320			
1420	200	W260	W440		
1440	200	W300W			
1500	180	W300			
1520	200	W240			
1540	?				plumes and return overlapping
1600	?	at surface			
1620	180				
1640	220	W440			
1700	240	W360			
1720	220	at surface	360		
1740	180	340			
1800	150	300			
1820	160	340			
1840	160	360			
1900	140	320			
1920	200(?)	260			may be plume or return - not sure
1940	?	at surface	DARK		
2000		90			no plumes
2020		140	220	310	
2040		100	220	320	
2100		~110	210	340	
2120		100	250	380	
2140		90	230	370	

2200		170	240	380		
2220		160	?	340		
2240		140	?	340		
2300	110	140	300			
2320	W100	160	300			
2340		160	260W			
2400		160	280			
7/26/77						
0020		at surface	S150	~260		
0040		"	S150	250		
0100		"	S160	?		return #2 & 4 may have become 1
0120	100	"	S140	?		
0140		"	S85			
0200		"	S80	200	320	
0220		at surface	180	280		
0240		"	?	~220		
0300		"	240			
0320		"	260			
0340		110	250			
0400	100	110	270			
0420		90	DARK			
0440	90	160	"			
0500		at surface	180	280	340	420
0520		90	160	280		
0540		stopped	DARK	DARK		
0600		200	DARK			

0620		DARK	DARK	
0640		220	"	
0700		80	"	
0720		90	200	
0740		240		
0800	90	200		
0820	110	200		
0840	110	140	260	
0900	120	160		
0920	130	~ 140		
0940	100	110		
1000	120	at surface		
1020		"		no plumes
1040		"		
1100		"		
1120		80		
1140		at surface		
1200		"	110	
1220		"		
1240		"		
1300		"		
1320		"		
1340		"		
1400		"		
1420		"		
1440		"		
1500		"	120	
1520		"	DARK	

1540		at surface	180	
1600		"		
1620	100	110		
1640		at surface		
1700		"		
1720	120			
1740	120			
1740	120			
1800	140	160		
1820	120	at surface		may have another return
1840	120	"		
1900	?	"	440	
1920	?	"	380	
1940	?	?	300	don't know which is return or plume
2000	160	170		
2020	120	140		
2040		at surface		
2100		"		
2120		100		
2140		at surface		
2200		"		
2220		"		
2240		"		
2300		"		
2320		"		
2340		"		
2400		"		

7/27/77

0020		at surface			
0040		S90			may have another return
0100		S80	260		
0120		S80	250		
0140		S80	DARK		
0200		S80	W250		
0220		S70	too weak		
0240		S90	W300		
0300		S90	200		
0320		S80	overlapping		
0340		S80	140		
0400		S70	120		another return above #2 but is overlapping
0420		S70W	?	S150	
0440		at surface	200W		#2 seems to have merged with #1
0500		80W	180		
0520	100	S120	210		
0540	80	90	110	200	
0600		80		200	#2 is too low - seems to be at surface
0620	90	100	220		
0640		at surface	~ 210		
0700		"	~ 220		
0720		S80	200		
0740		at surface	220		
0800		S80	220		

0820		80	160	210		may have another return under #1
0840		90	150	200		
0900		80	100	160	W400	
0920		90	~140	? overlapping	W300	
0940		90	~120	190	W250	
1000		70	?	150	200	#2 is partly under #1, #5 at 300
1020		70	?	160	200	#5 at 320
1040		70		overlapping		
1100		70		200		
1120		80	120	230		
1140		100	120	220		
1200		at surface	~100	DARK		
1220		"	DARK	DARK		
1240		80	"	"		
1300		90	"	"		
1320		90	160	"		
1340		at surface	100	190	W340	
1400		80	140	220	W380	
1420		90	130	200	W380	
1440		S80	S230			
1500		90	S200W			
1520	100	110	260W	W400		
1540	110	130	290	W400		
1600	120	150	210	400		

1620	150	180	250	400		
1640	160	DARK	260	340		
1700	160	180	300			
1720	140	DARK	300			
1740	100	120	200W			
1800		80	190W			inversion rising from surface
1820		80	190			
1840		80	180	260W		
1900		at surface	130	240		
1920		80	120	240		
1940		100	S160W			
2000		at surface	S140W			
2020		"	S120W			
2040		"	S120W			
2100		"	S100W			
2120		"	S100W			may have another return ~200 m
2140		"	S90W	220		
2200		"	S95W	210		
2220		"	S100W	DARK		
2240		"	S100W	DARK		
2300		80	110	220		
2320		at surface	200			may have return between 110-200 m
2340		100	190			
2400		at surface	110	200		
7/28/77						
0020		at surface	DARK	200	~400	

0040		at surface	160	280			
0100		"	200	270			
0120		"	160	260			
0140		100	180	280			
0200		80W	~240	300			
0220		80W	260	overlapping			
0240		80	190	290	380		
0300		at surface	~200	280	380		
0320		"	160	280	~400		5 returns
0340		"	150	290	380		6 returns
					5		
					560		
0400		"	140	280	320		
				5	6		
				380	560		
0420		"	120	240	320		
				5	6		
				440	560		
0440		"	170	260	380		
				5	6		
				480	560		
0500		"	200	340	400		
					5		
					580		
0520		80	200	280	360		
					5		
					580		
0540		80	190	280	340		
					5		
					580		
0600		80	210	300			
0620	80	100	230	300	360		

AD-A054 239 NAVAL POSTGRADUATE SCHOOL MONTEREY CALIF F/G 13/2
EXPERIMENTAL INVESTIGATION OF THE MARINE BOUNDARY LAYER IN SUPP--ETC(U)
FEB 78 G E SCHACHER, C W FAIRALL
UNCLASSIFIED NPS61-78-002 NL

2 OF 3
AD
A054239

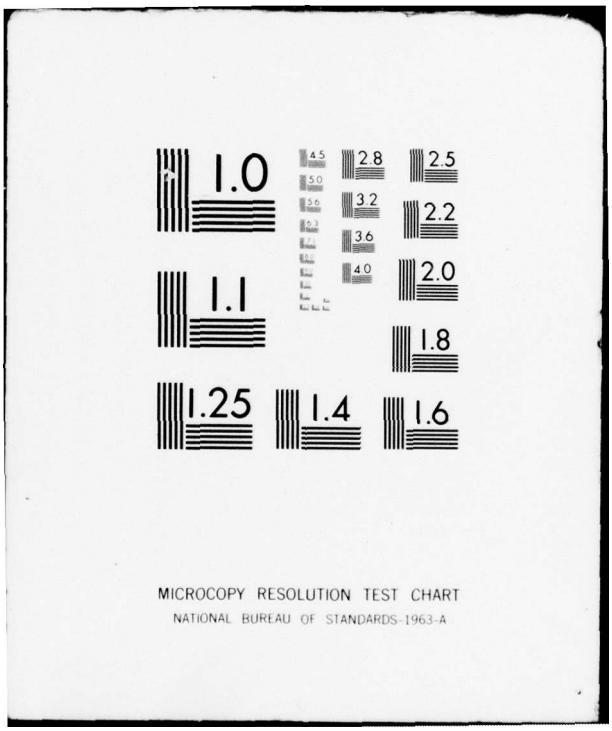
1.0
1.1
1.25
1.4
1.6
1.8
2.0
2.2
2.5
2.8
3.2
3.6
4.0
4.5
5.0
5.6
6.3
7.1
8.0
9.0
MICROCOPY RESOLUTION TEST CHART
NATIONAL BUREAU OF STANDARDS-1963-A

0640	90	100	200	300	380
0700		80	200	270	400
0720		80	210	260	400
0740		80	200	300	
0800		100	250		
0820	110				
0840	90	120			
0900		90			
0920	100				
0940	90	100			
1000	90				
1020	80	100			
1040	110	160	240		
1100	120	140			
1120	100	180			
1140	140	160			
1200	180	overlapping			
1220	90	180			

D. Radiosonde

Figures 3a - 3u show the radiosonde results up to elevation of 1000 meters. Results are not shown above this height because we are primarily interested in the marine inversion. These figures were derived directly from the radiosonde readout strip chart presentation so that fine detail can be observed. A good example is shown in Figure 3b where the results show a surface inversion, an elevated inversion with a 230 m base, and 10 changes in slope above the inversion. Detail of this type is not available in the normal presentation of radiosonde results where only major features are plotted on a much larger height scale.

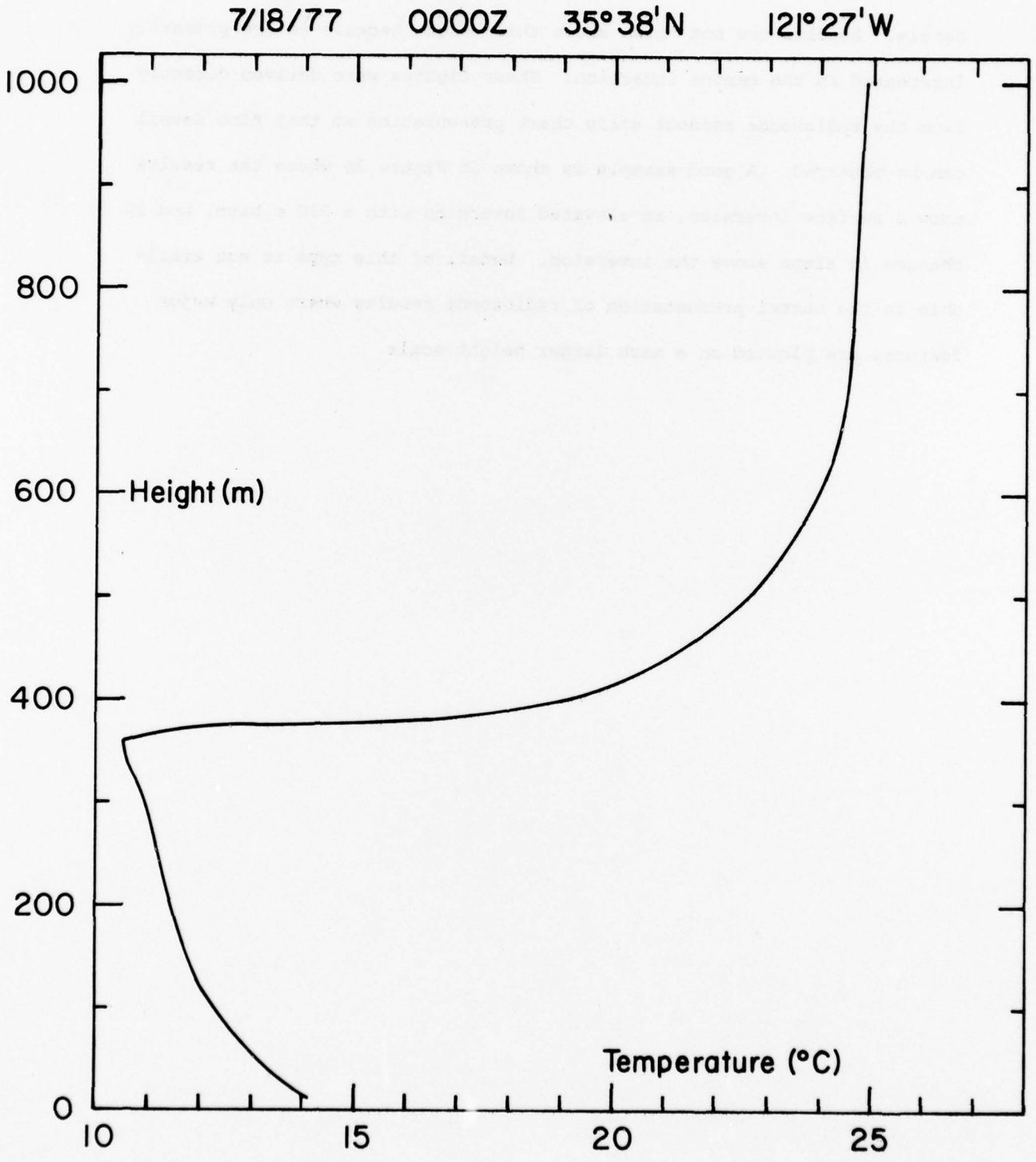

Figure 3a
A-70

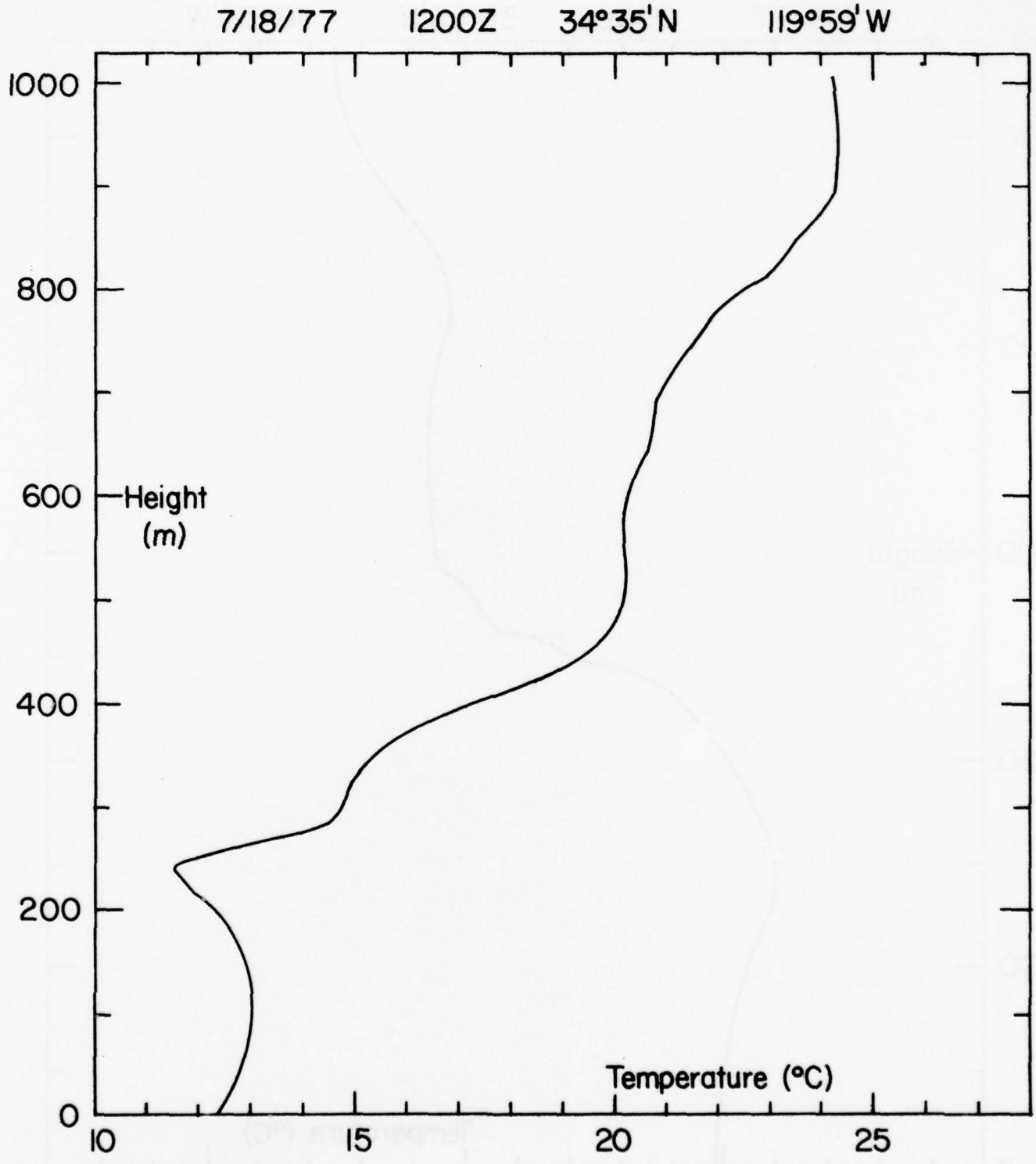

Figure 3b
A-71

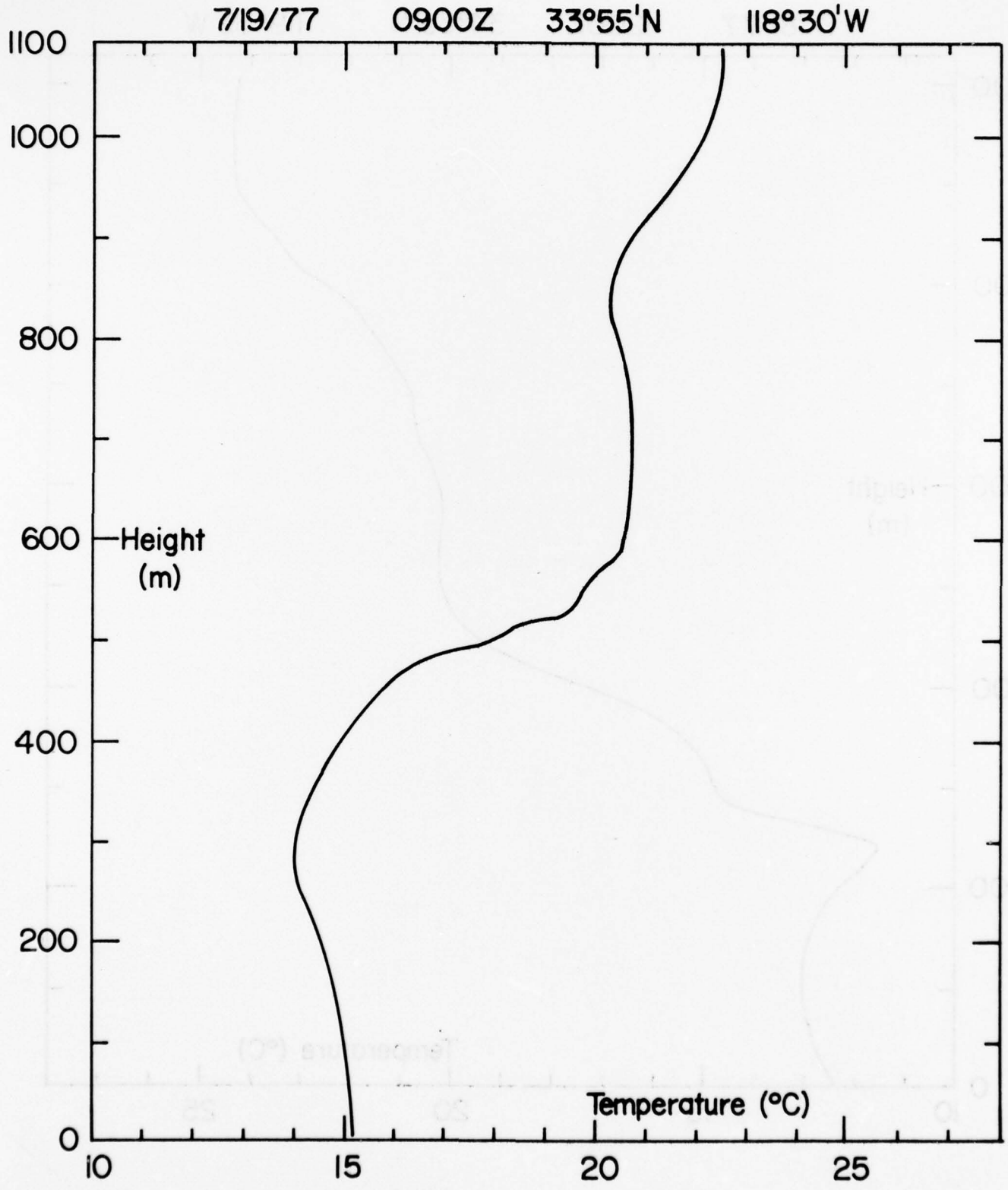

Figure 3c
A-72

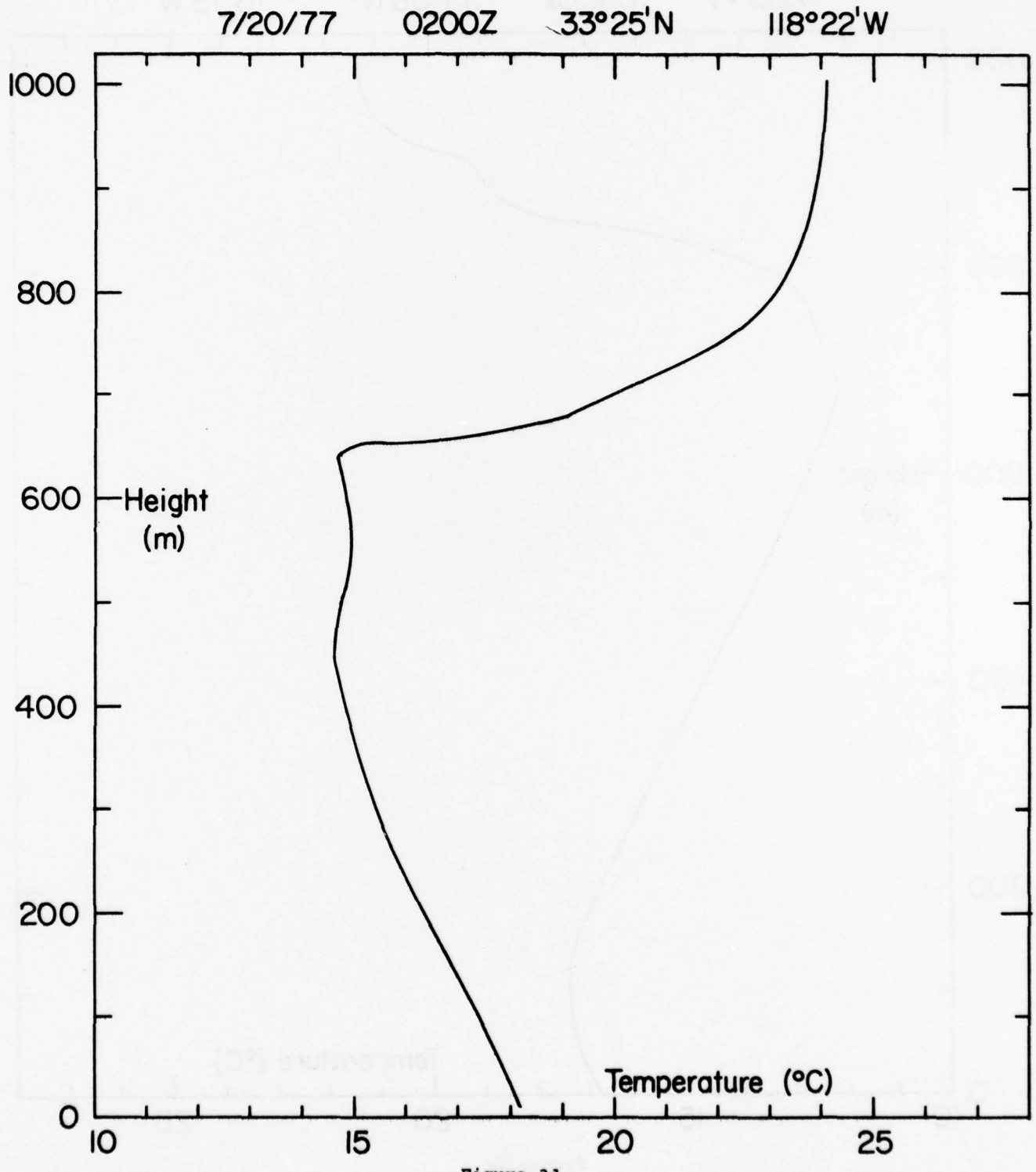

Figure 3d
A-73

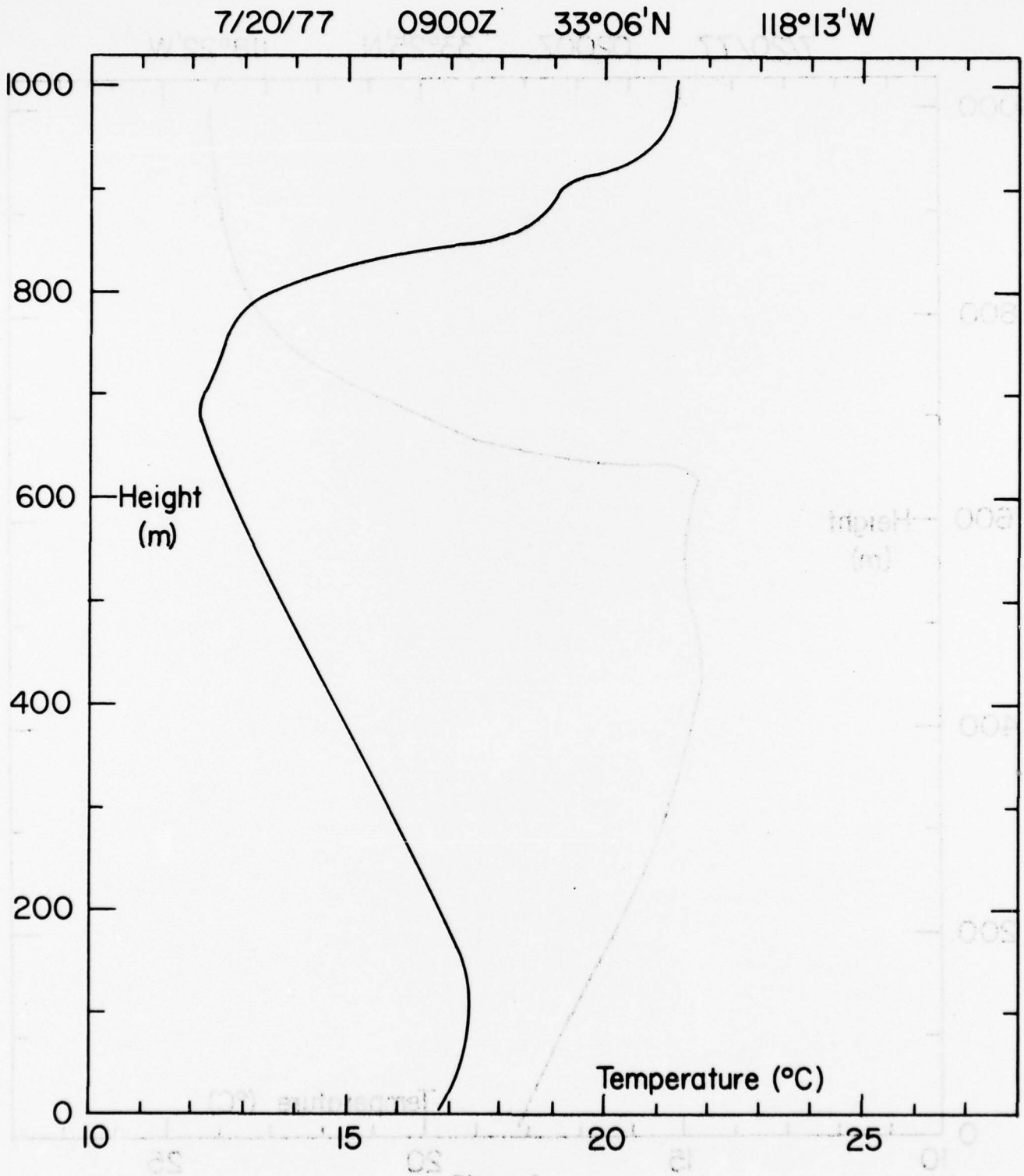

Figure 3e
A-74

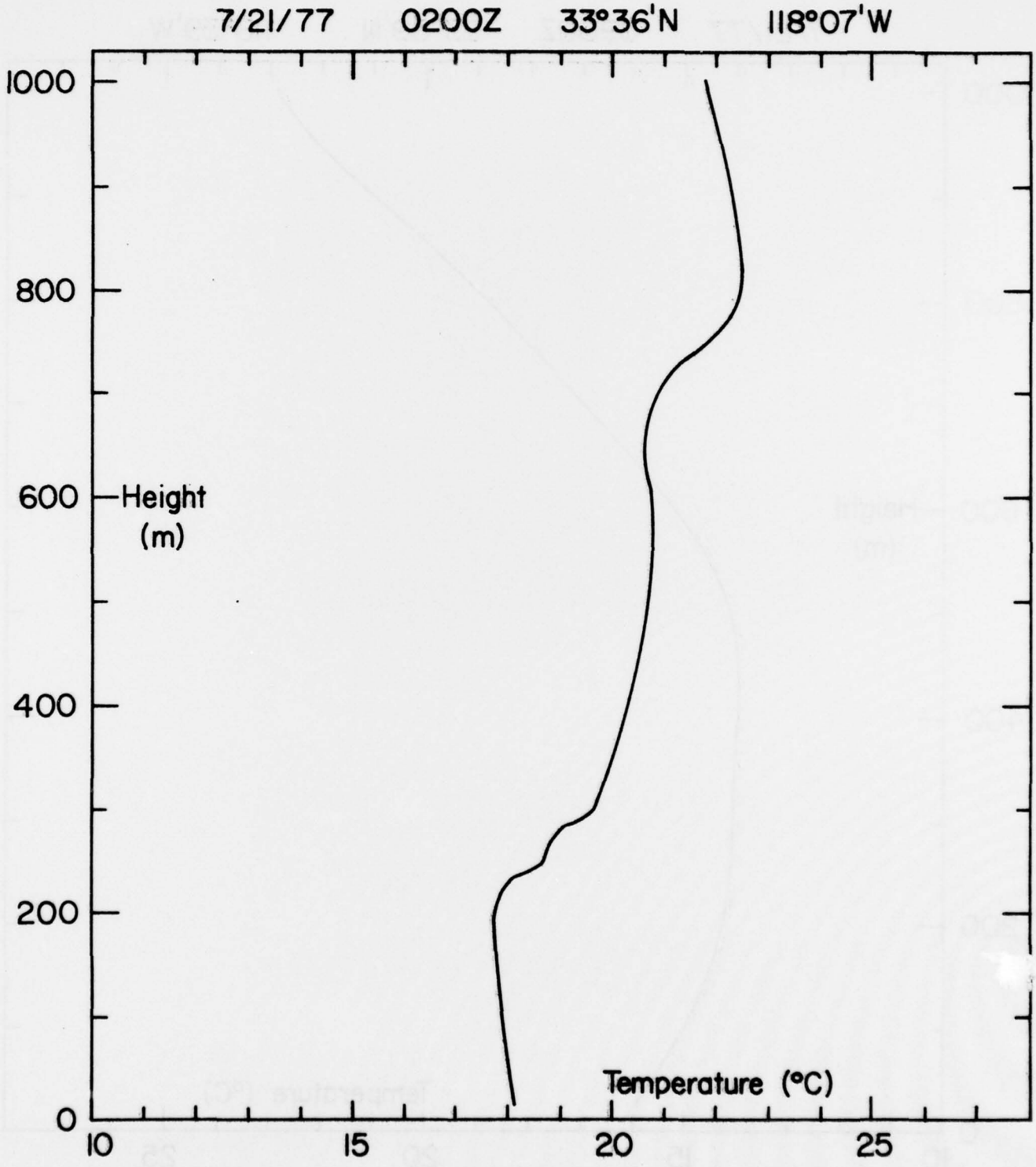

Figure 3f
A-75

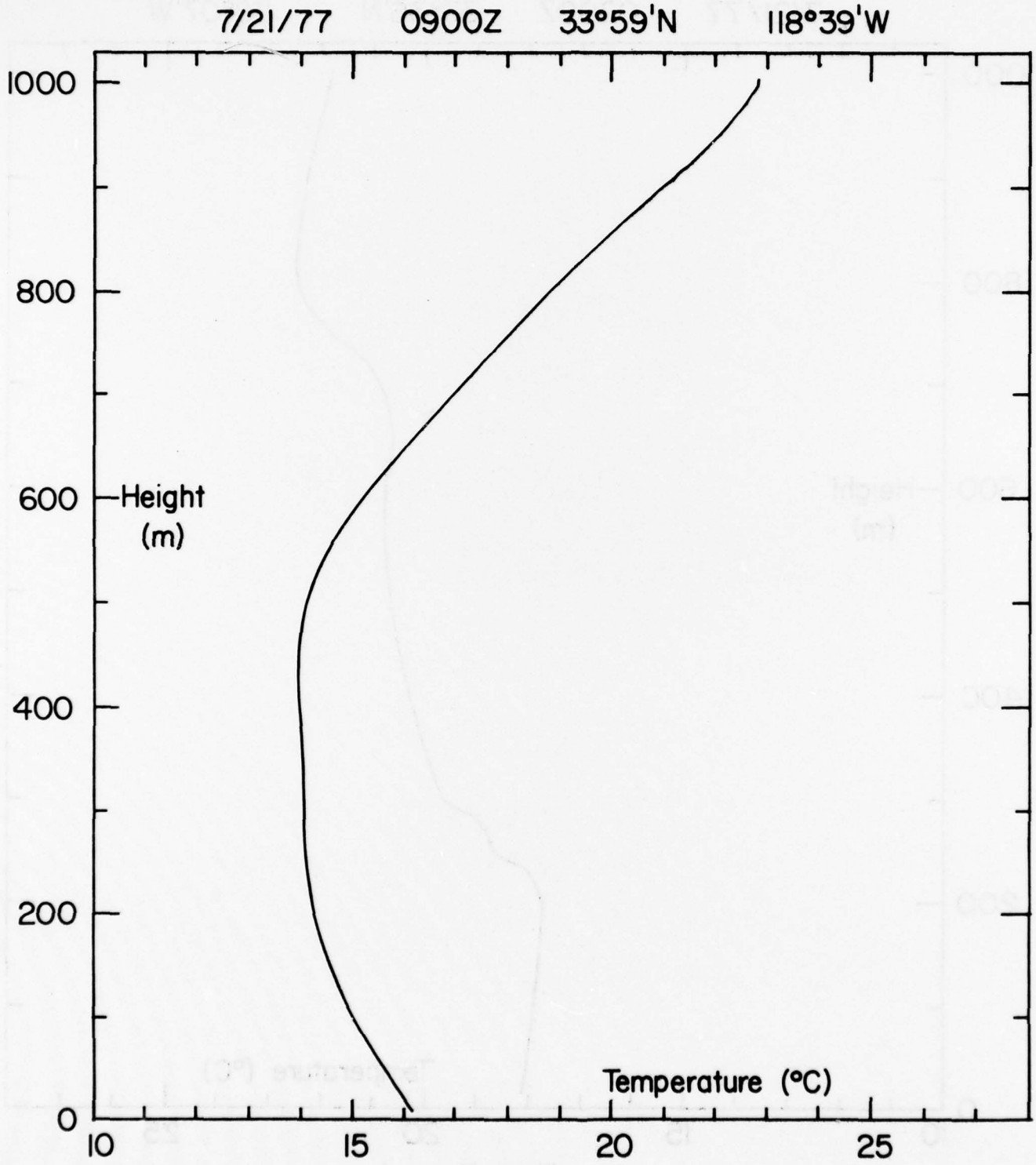

Figure 3g
A-76

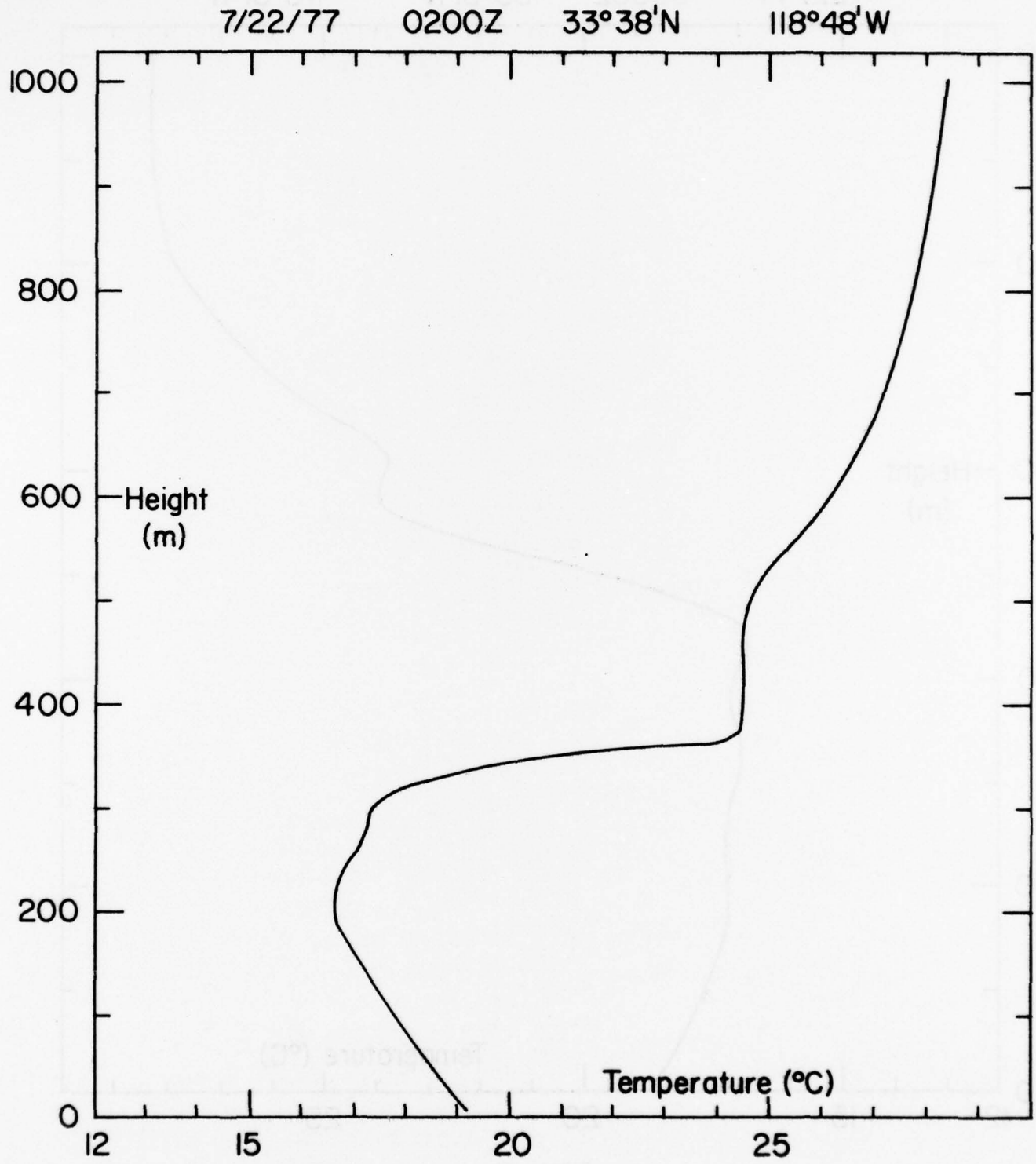

Figure 3h
A-77

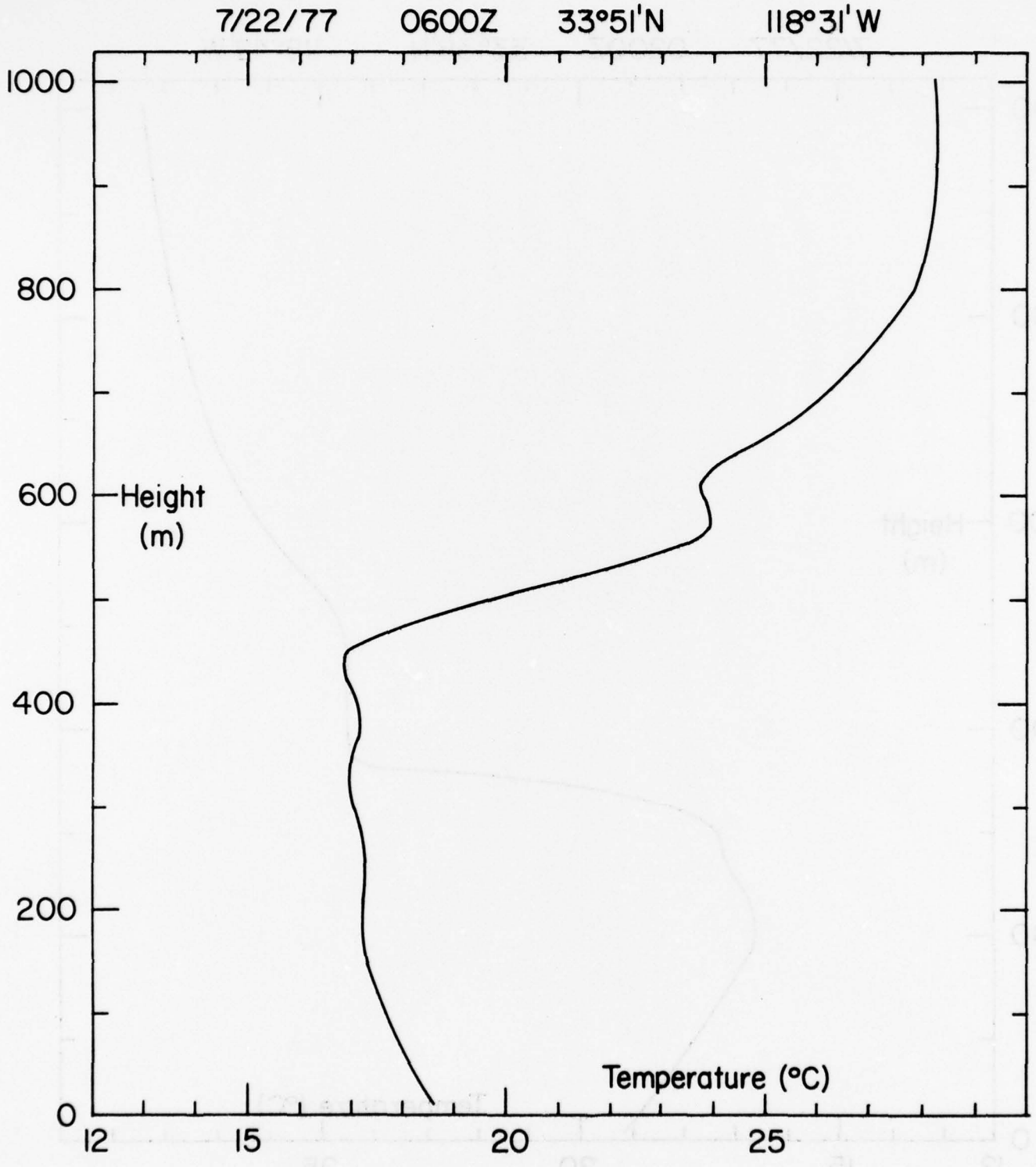

Figure 3i
A-78

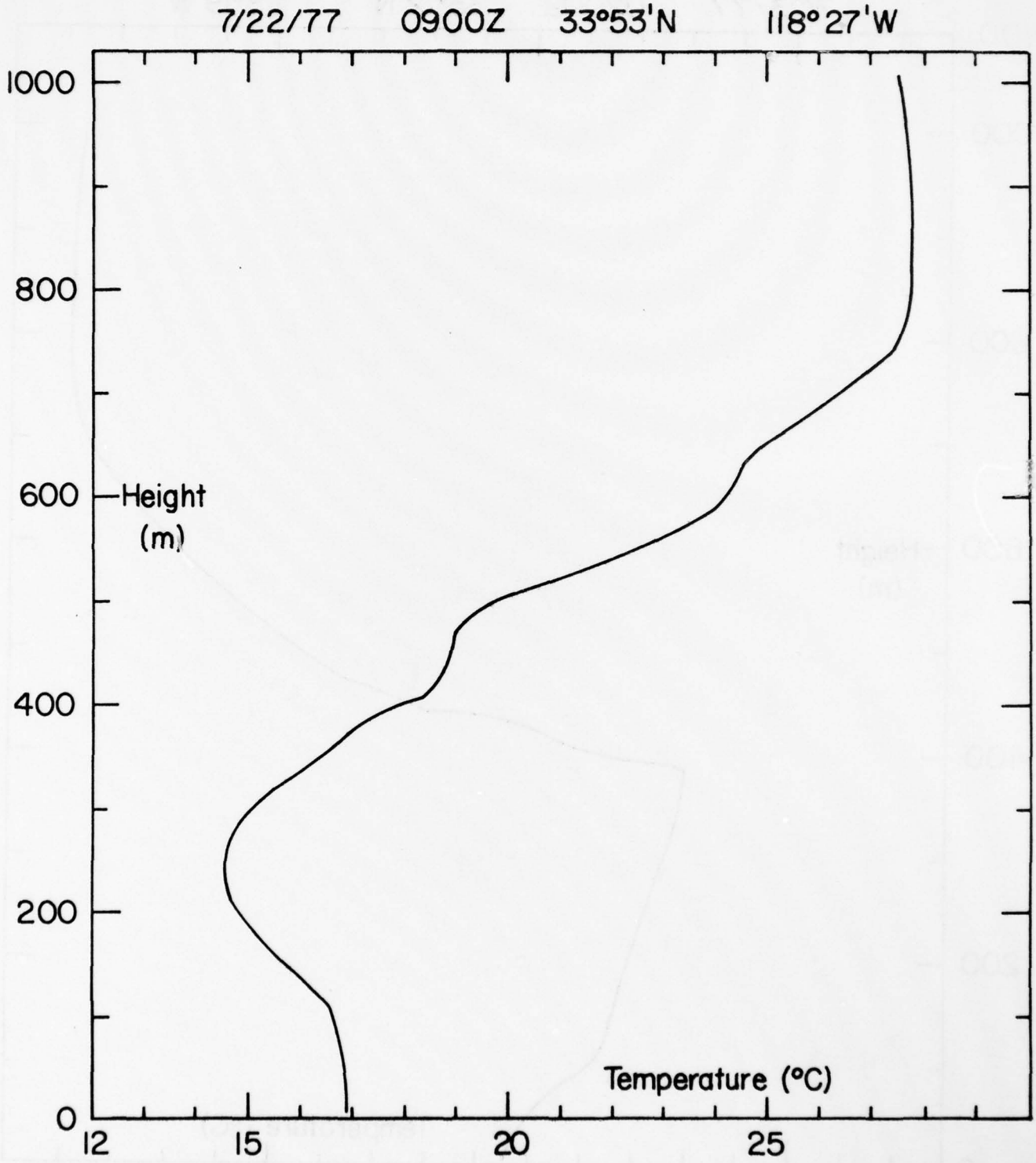

Figure 3j
A-79

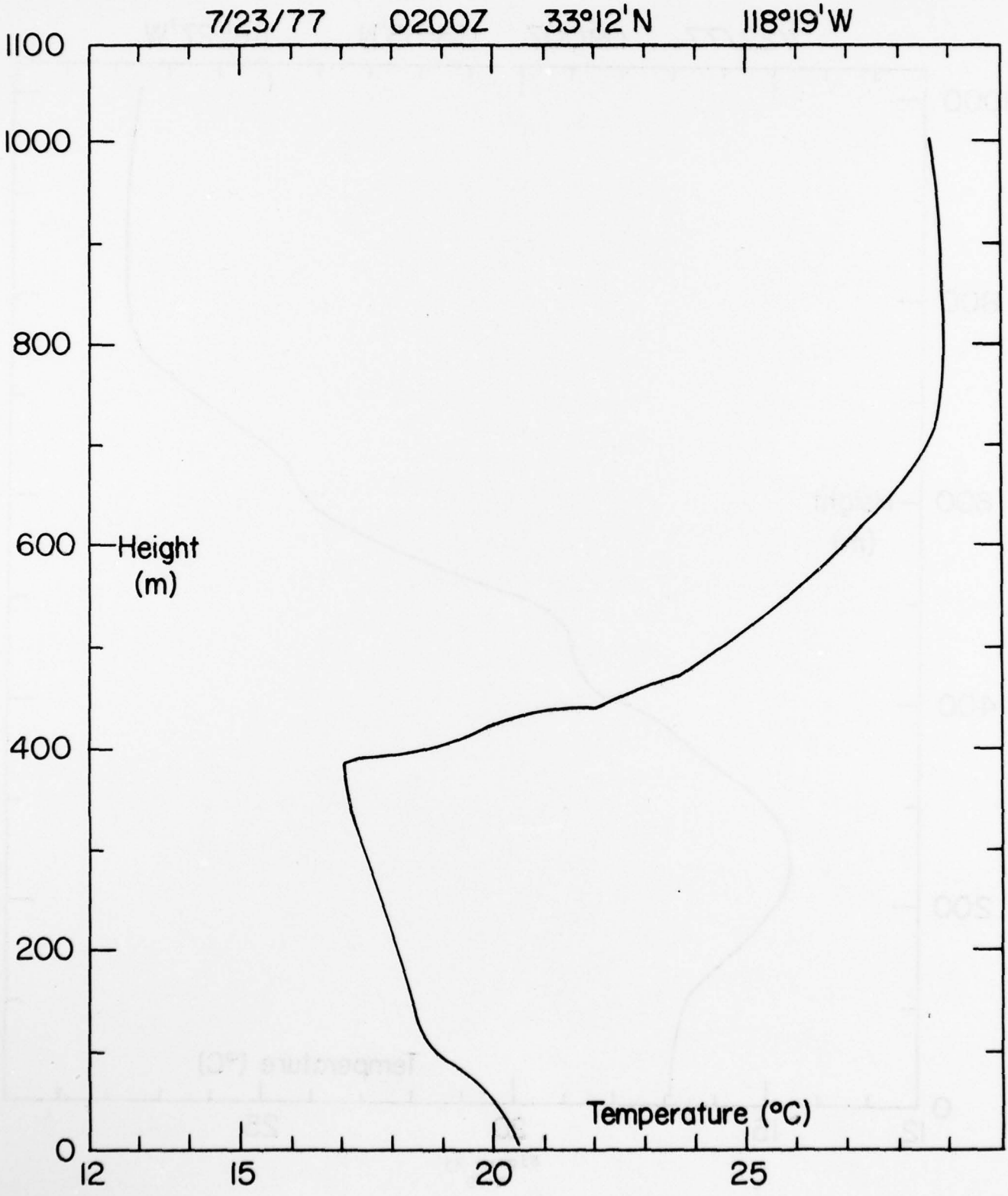

Figure 3k
A-80

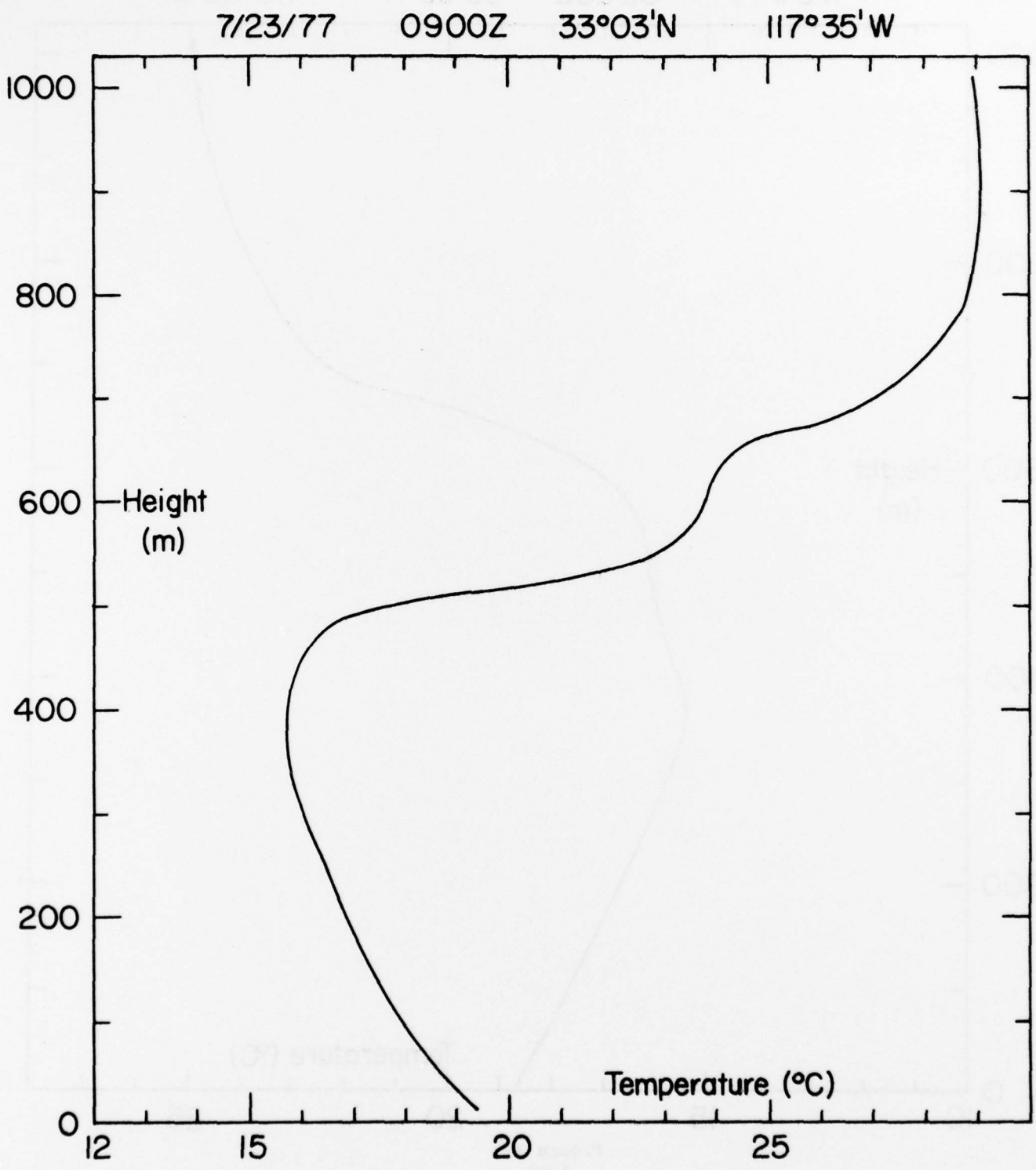

Figure 31
A-81

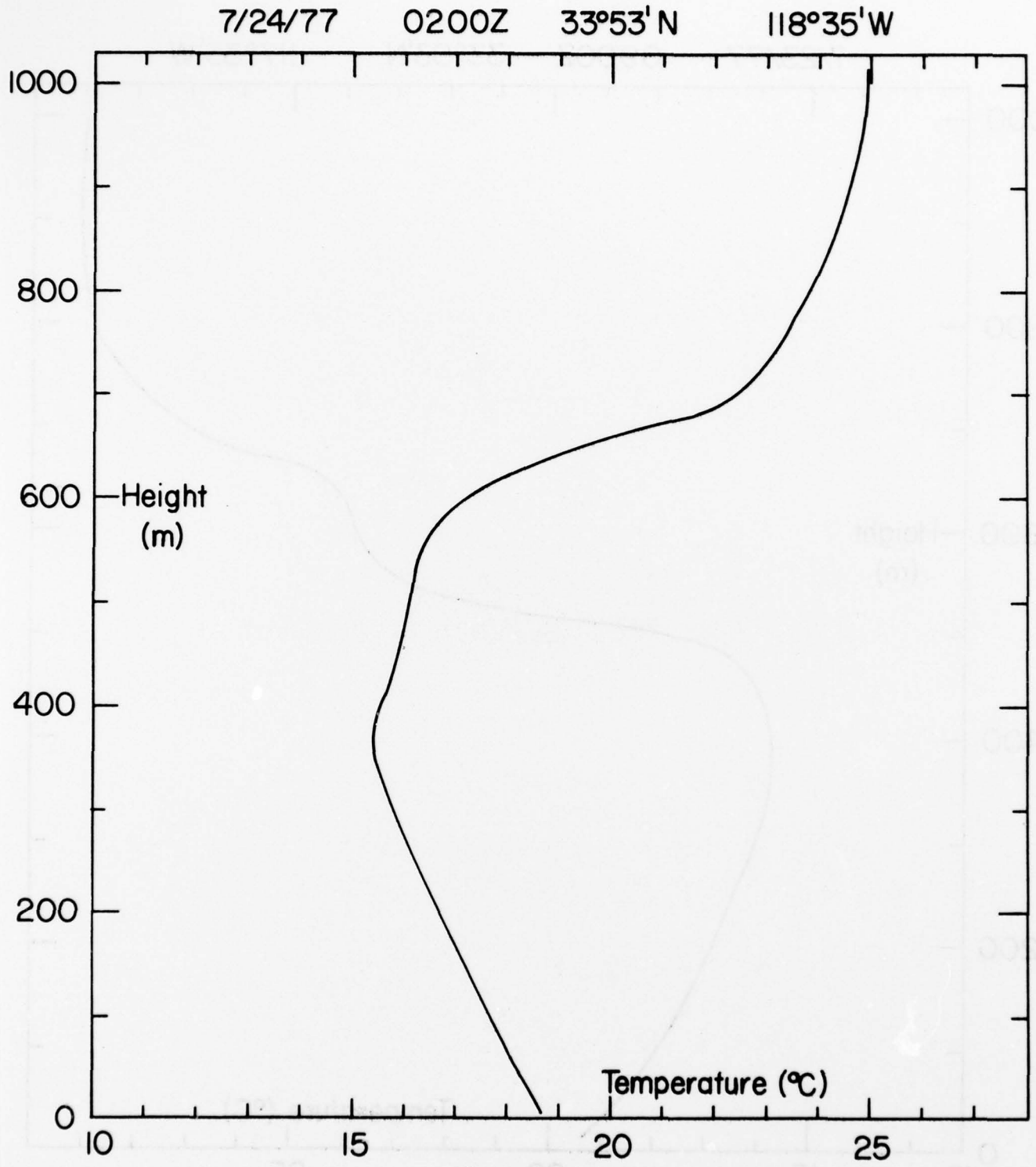

Figure 3m
A-82

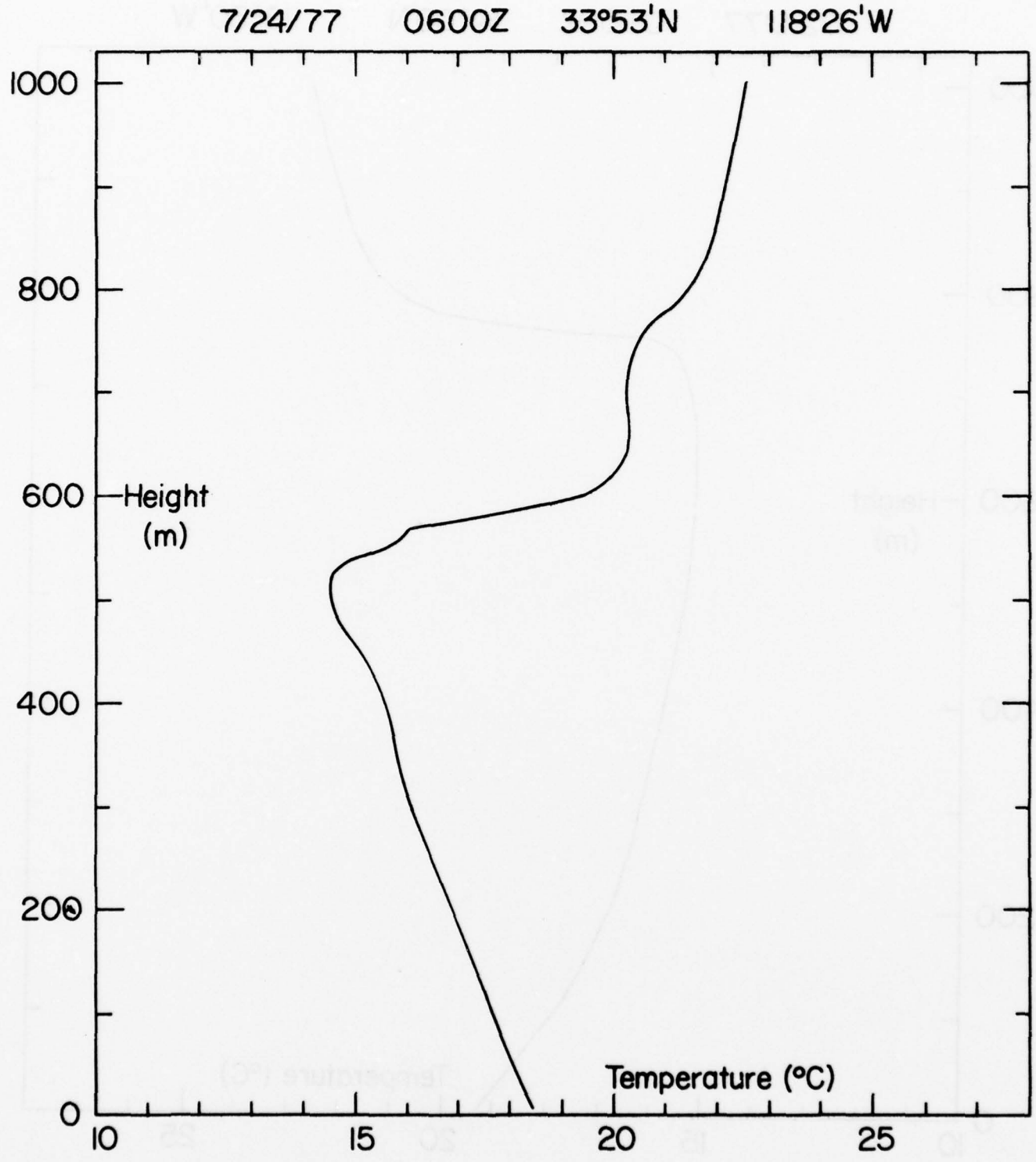

Figure 3n
A-83

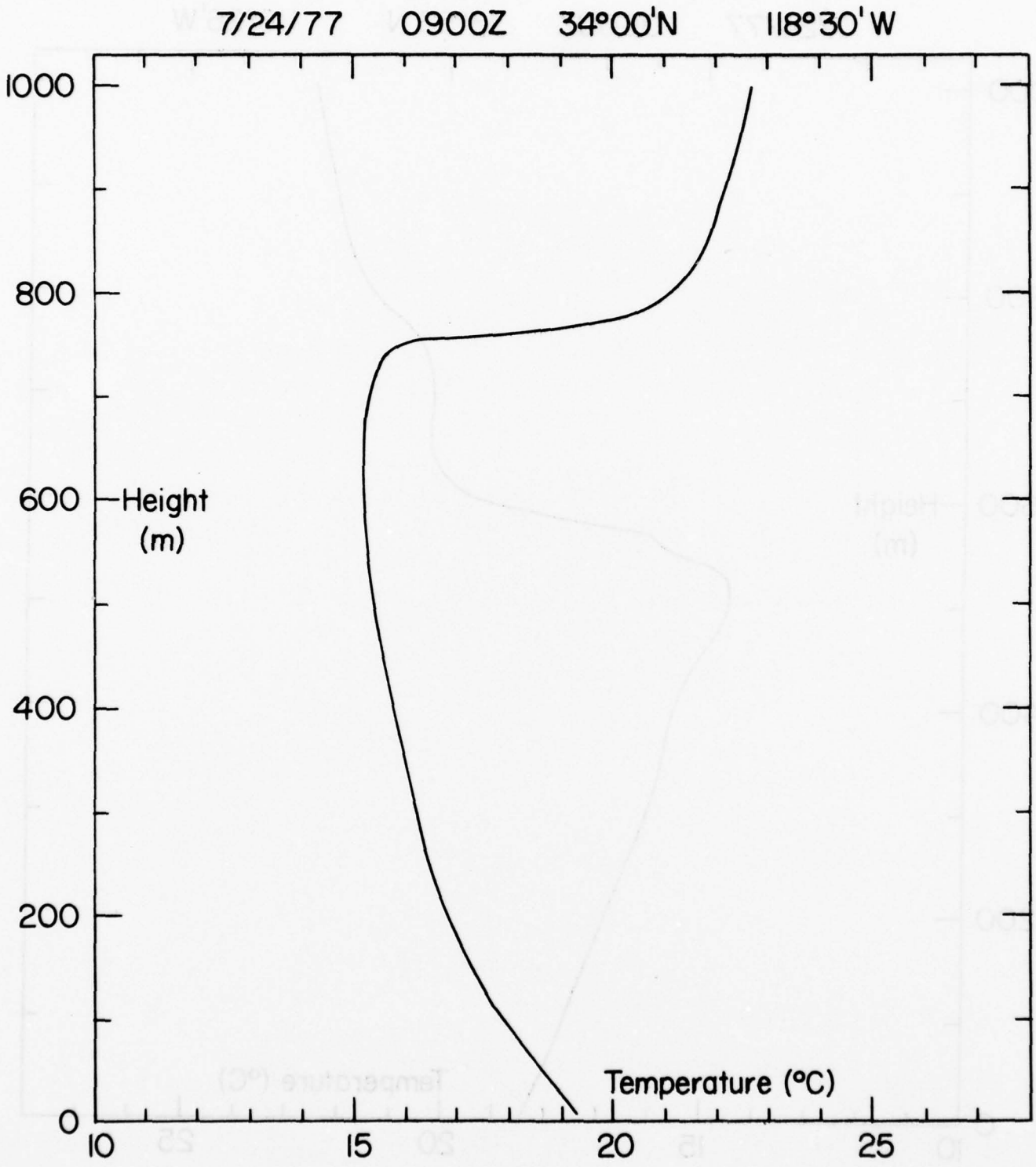

Figure 3o
A-84

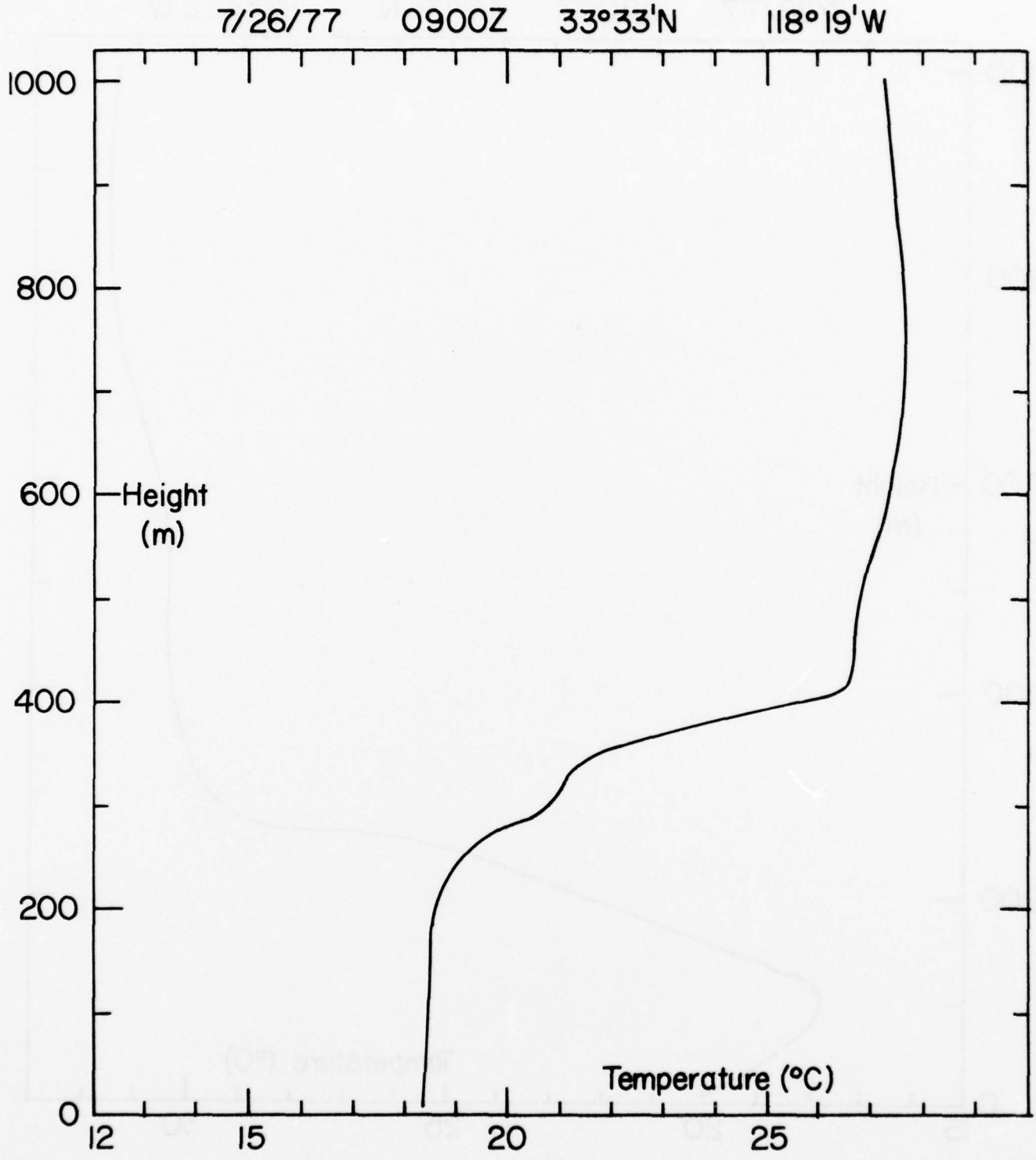

Figure 3p
A-85

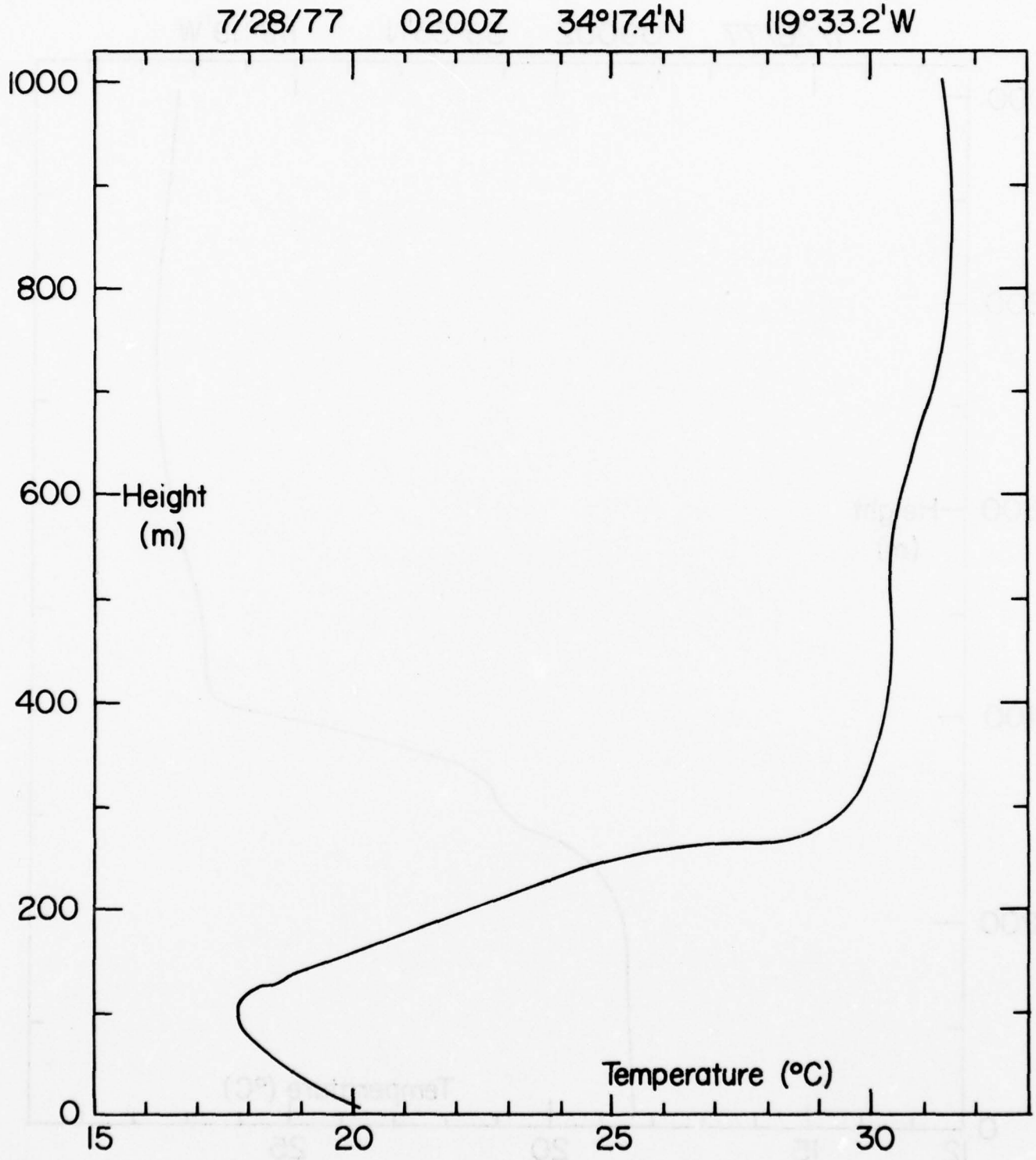

Figure 3q
A-86

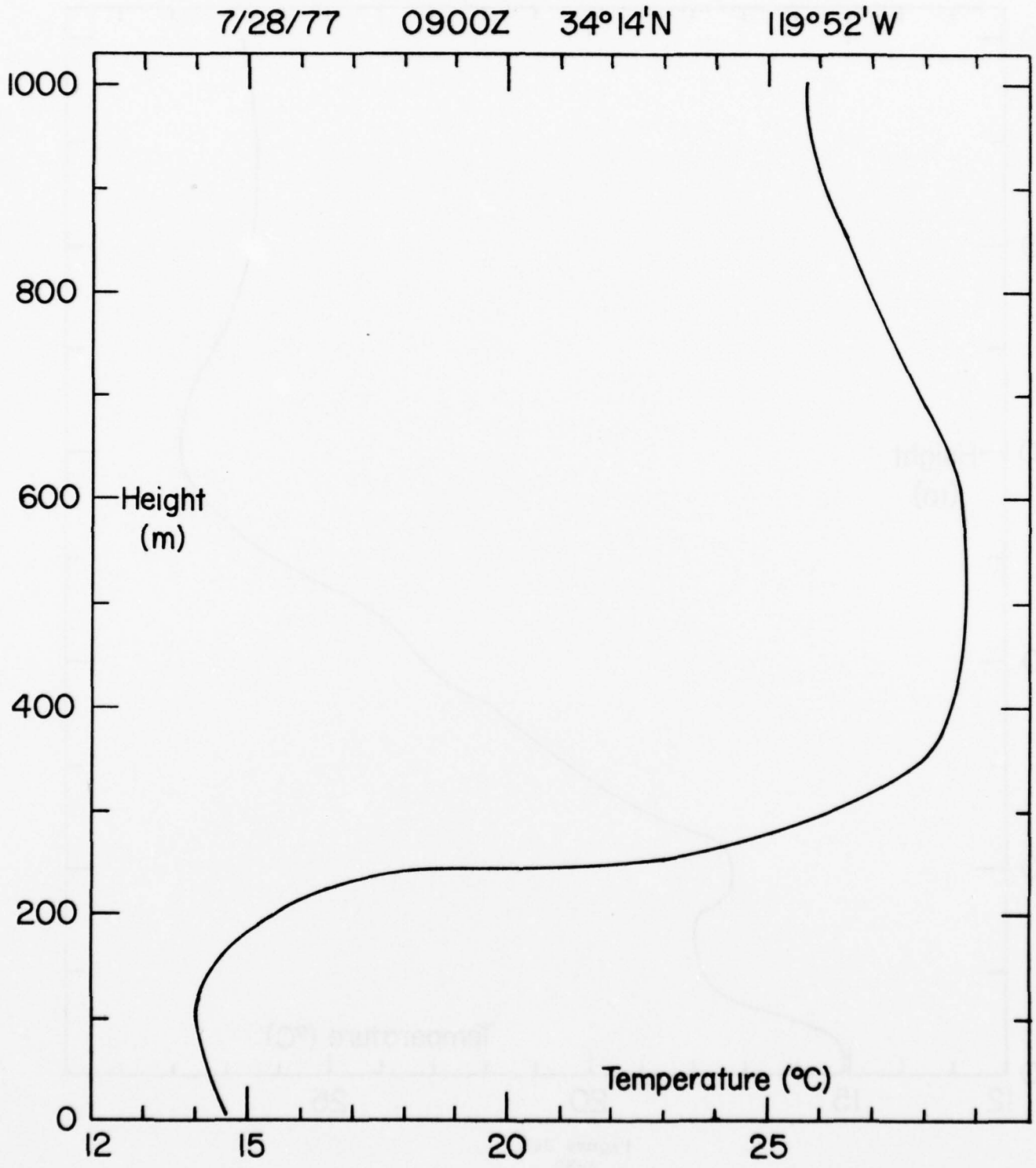

Figure 3r
A-87

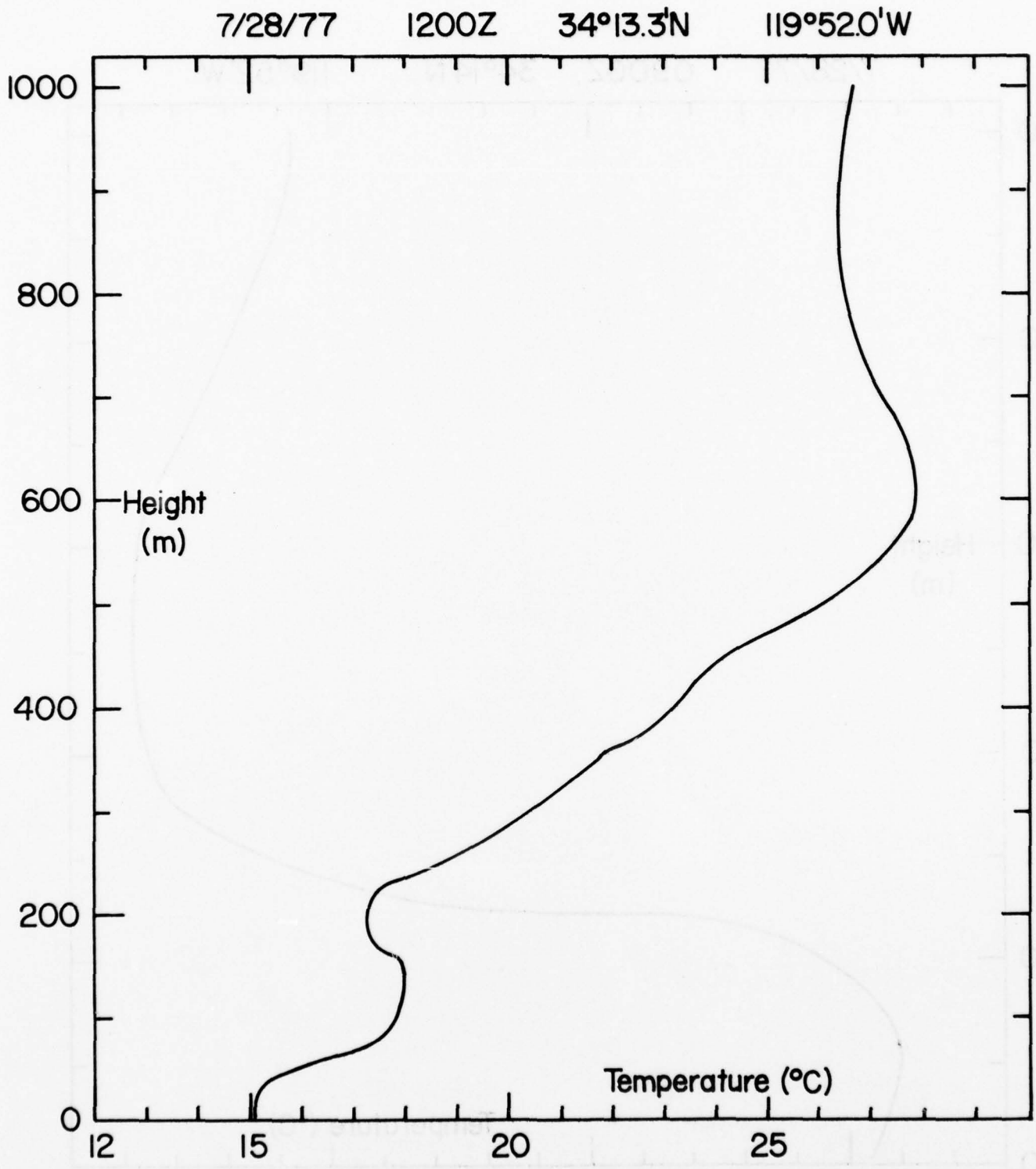

Figure 3s
A-88

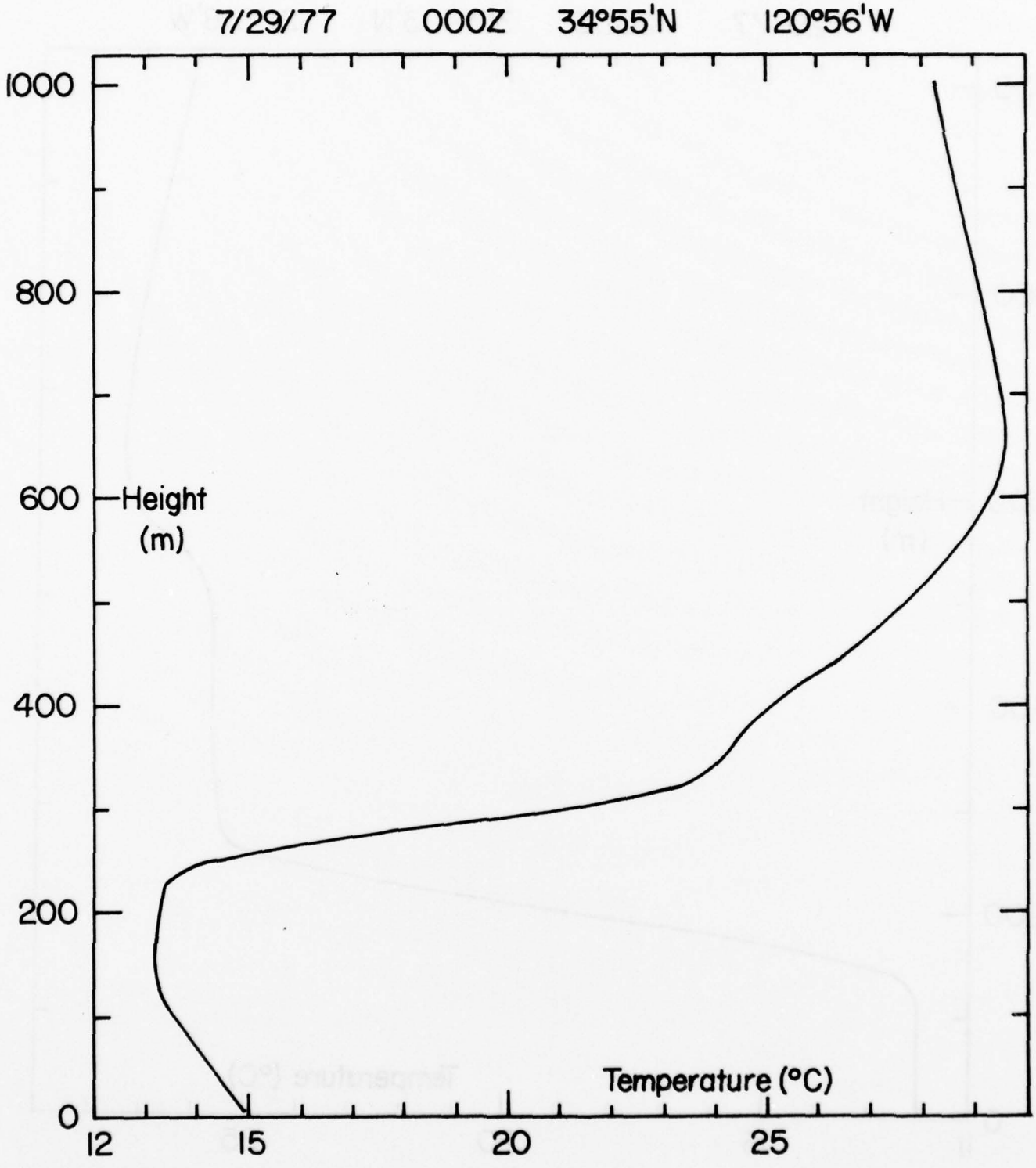

Figure 3t
A-89

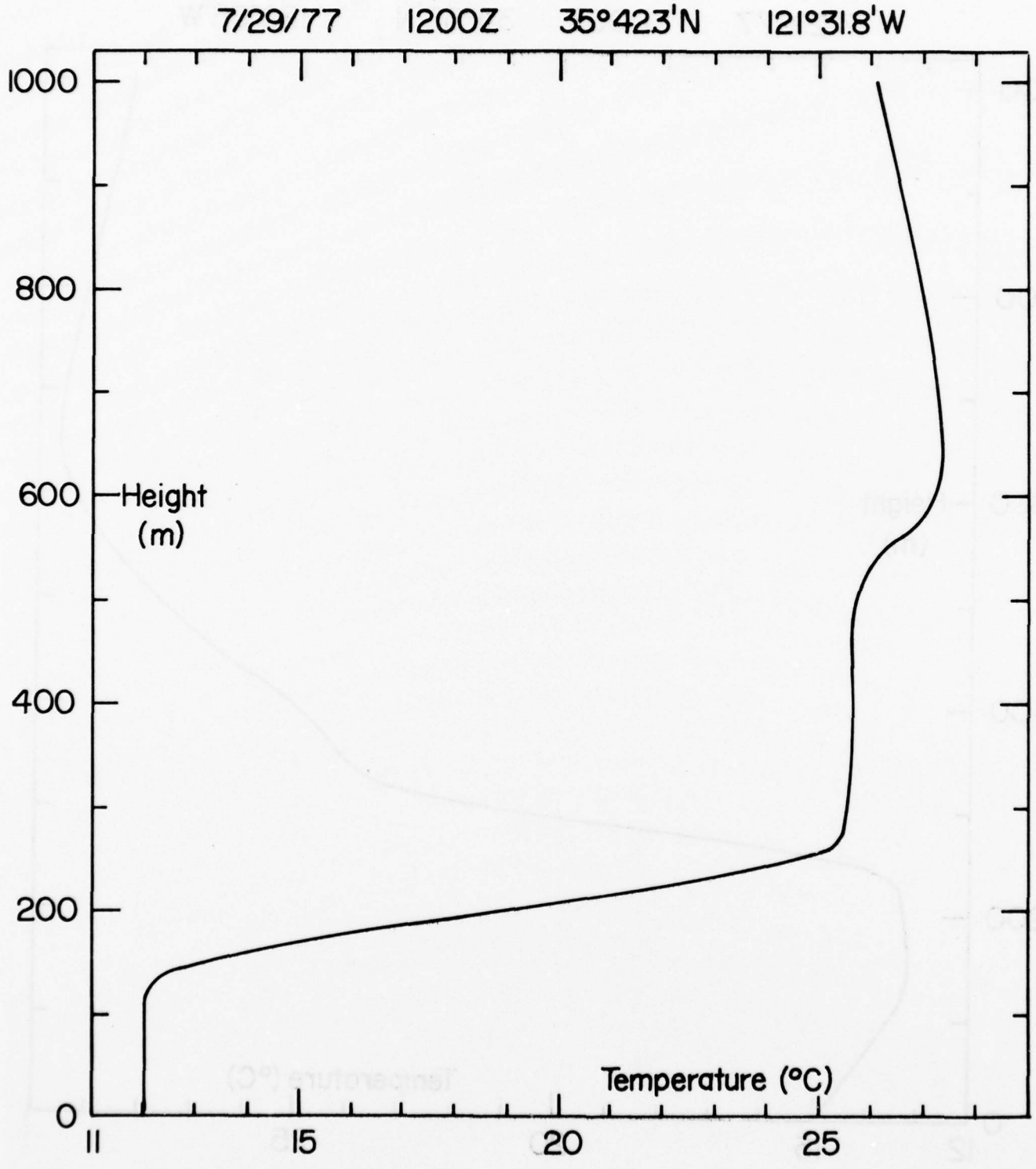

Figure 3u
A-90

E. Temperature and Humidity Data

Table V lists sea surface temperature, air temperature at the four shipboard levels and the average relative humidity from the four levels. Due to inherent inaccuracies in the humidity sensors it would be inappropriate to list the four values obtained from the levels. All temperatures are in °C. The only data presented in Table IV is for those time periods when it was possible to obtain good profiles and fluctuation data (those times when the relative wind was from a favorable direction). Data entries are missing for some times due to malfunctions of the teletype or, in the case of the sea surface and level 1 for the latter part of the cruise, due to system damage by high waves.

TABLE V

Sea Surface Temperature and Atmospheric Temperature and Relative Humidity

Time	T_S	T_1	T_2	T_3	T_4	H
7/18						
2025		16.41	16.37	16.34	16.25	90
2120	17.11	16.45	16.42	16.36	16.27	90
2145	16.49	16.49	16.47	16.42	16.33	90
2200		16.56	16.53	16.49	16.40	89
2220	16.42	16.51	16.47	16.42	16.34	90
2245			16.47	16.42	16.33	90
7/19						
0000	19.11		16.53	16.44	16.36	90
0020	18.54	16.34	16.47		16.28	90
0100		16.13	16.08	16.06	16.01	92
0140	16.70	15.80	15.89	15.94	15.90	93
0245	16.06	16.03	15.98	15.95	15.92	100
0420	17.04	16.58	16.56	16.51	16.43	90
0440	17.4	16.7	16.67	16.62	16.53	90
0500	17.70	16.71		16.63	16.33	89
0520	17.7	16.8	16.73	16.67	16.58	87
0600	16.81	16.92	16.90	16.89	16.80	85
0620	19.20	17.31	17.08			84
0640	19.00	17.51	17.40	17.34	17.24	83
0700	18.80	17.63	17.59	17.55	17.44	83
0720		17.82	17.76	17.75	17.62	82
0740	19.40	17.55	17.71	17.70	17.53	83
1350	20.4	18.46		18.36		82
1410	21.8		18.58	18.77	18.58	79
1620	21.1	18.7	18.59	19.12	18.71	79
1650	21.07	18.69	18.44	18.83	18.50	79
1710	20.99	18.56	18.35	18.58	18.27	79
1730			18.25	18.43	18.13	79

Time	T_S	T_1	T_2	T_3	T_4	H
7/19						
1940		18.5	18.47	18.42	18.31	86
2000	18.76	18.03			18.17	84
2040		17.85	17.79	17.70	17.54	87
2120		17.76	17.71	17.64	17.54	87
2140	19.88	17.77	17.70	17.65	17.55	87
2200			17.78		17.60	87
7/20						
0700	18.70	17.41	17.32	17.29	17.03	86
0740	19.2		17.51	17.47	17.27	86
0840	19.22	17.76	17.70	17.72	17.48	85
0900	19.3	18.02	18.02	17.98	17.84	85
0920	19.3	18.08	18.07	18.19	17.88	85
1020	19.63	18.33	18.33	18.40	18.12	84
1040	19.92		18.77	18.92	18.61	80
1240	20.2	19.1	19.19	19.25	19.0	78
1300	19.81	19.12	19.24	19.22	19.03	79
1320	19.67	19.08	19.22	19.24	19.04	88
1800	18.24	18.80	18.84	19.16	18.80	84
1900	17.80	18.86	18.78	18.87	18.28	83
1920	17.70	18.77	18.70	18.79	18.35	84
1940	18.40	18.70		18.65	18.28	84
2000		18.30	18.32	18.38	18.21	85
2020		18.40	18.27	18.18	17.74	86
2040			18.14	18.06	17.85	87
2120	18.24	18.11	18.08	18.00	17.83	88
2140			17.97	17.90	17.71	89
2200	18.63	17.91	17.84	17.79	17.64	89
2220	19.00	17.89	17.83		17.62	90
2230			17.71	17.71	17.55	91
2300	18.23		17.38	17.39	17.23	91
2400	17.20	16.59	16.59	16.58	16.57	94

Time	T_S	T_1	T_2	T_3	T_4	H
7/21						
0040	16.9	16.39	16.37	16.32	16.20	94
0100	16.6		16.01	16.04	15.88	93
0120	16.1	15.83	15.67	15.66	15.58	96
0405	17.7	16.42	16.47	16.38	16.24	98
0425		16.62	16.61	16.52	16.40	97
0445	18.4	17.04	17.08	16.97	16.83	96
0505	18.4	17.19	17.20	17.13	17.07	94
0545	18.2	17.55	17.57	17.51	17.39	91
0605		17.67	17.65	17.59	17.41	89
0625		16.75	16.69			89
0645	18.3	17.59	17.56	17.53	17.34	89
0705	18.19		17.52	17.48	17.33	89
0725			17.60	17.56	17.43	89
0745		17.87	17.79	17.77	17.63	89
0805			17.73	17.75	17.64	89
0825			17.71	17.72	17.57	90
0845	19.04		17.93	17.93	17.73	91
0905			17.99	18.03	17.76	89
0945	18.75	17.75	17.67	17.75	17.49	89
1005	18.16	17.63	17.53	17.73	17.44	88
1025	18.46		17.60	17.92	17.58	88
1045	18.4	17.76	17.63	17.97	17.60	88
1105	17.72	17.44	17.42	17.79	17.39	89
1305		17.66	17.51	17.94	17.66	90
1325	17.7	17.72	17.52	17.85	17.46	90
1345	17.86	17.97	17.80	17.97	17.46	90
1405	18.23	18.06	18.05	18.14	17.69	90
1505	18.9	18.53	18.29	18.60	18.22	88
1620			18.40	18.79	18.34	86
1720	18.72	18.51	18.26	18.55	18.03	85
1945	19.93	19.93	18.69	18.86	18.63	79
2030	19.84	18.45	18.39	18.31	18.18	85

Time	T_S	T_1	T_2	T_3	T_4	H
7/21						
2110			18.50	18.42	18.32	84
2130	19.5	18.49	18.46	18.40	18.29	85
2150			18.59	18.52	18.41	84
2250			18.28	18.21	18.15	89
2350			17.95	17.95	17.89	91
7/22						
0130			18.14	18.11	18.03	92
0150	17.2	18.02	18.02	18.01	17.93	91
0450	17.4	17.41	17.29	17.31	17.27	92
0550			17.24	17.21	17.12	93
0610	17.22	16.83	17.03	16.98	16.88	94
0710			16.61	16.60	16.48	96
0730			16.70	16.70	16.57	97
0750	18.86	16.67	16.65	16.68	16.54	97
0810			16.85	16.86	16.68	96
0830		16.72	16.64	16.74	16.58	96
0910		16.66	16.54	16.65	16.52	97
0930	17.3	16.74	16.63	16.77	16.59	97
0950			16.53	16.72	16.49	97
1010	18.02		16.75	16.91	16.66	97
1030	18.51	17.15	17.18	17.33	17.05	96
1050	18.6	17.54	17.64	17.81	17.51	94
1210		17.24	17.13	17.27	17.01	90
1230			17.19	17.41	17.18	91
1333		17.83		17.80	17.22	92
1350		18.01	17.92	18.15	17.59	91
1610		19.81	19.64	19.90	19.40	87
1630			19.77	20.51	19.94	87
1650			19.58	20.35	19.83	86

Time	T_S	T_1	T_2	T_3	T_4	H
7/22						
1710			19.68	20.20	19.85	85
1910		19.34	19.19	19.29	19.15	90
1950	19.9		18.78	18.73	18.53	91
2130		17.97	17.87	17.82	17.60	93
2150		17.78	17.64	17.58	17.33	94
7/23						
0310			18.19		17.83	94
0330			18.17	18.11	17.85	94
0350			18.24	18.19	17.91	94
0410			18.23	18.18	17.99	94
0430		18.25	18.19	18.15	17.93	94
0450		18.44	18.39	18.31	18.09	94
0630		18.56	18.55	18.49	18.28	91
0730	18.40	18.60	18.61	18.58	18.30	90
0750			18.67	18.65	18.42	89
0810		18.9	18.80	18.79	18.58	89
0910		19.06	19.04	18.97	18.78	88
0930			19.05	18.96	18.70	88
1410	18.2		19.25	19.36	18.95	86
1430	18.2	19.40	19.33		19.22	86
1440	18.23	19.51	19.38	19.58	19.15	87
1450	18.49	19.69	19.58	19.75	19.35	86
1505			19.69	19.83	19.46	85
1515			19.79	19.91	19.50	84
1525	19.1	20.02	19.86	20.10	19.57	84
1535			19.83	19.97	19.49	83
1645	20.36		19.87	20.29	19.93	83
1655		19.83	19.63	19.90	19.51	83
1705		19.62	19.47	19.68	19.34	83
1715			19.33	19.55	19.21	84

Time	T_S	T_1	T_2	T_3	T_4	H
7/23						
1725	19.2	19.23	19.18	19.43	19.12	85
1735	19.17	19.18	19.01	19.28	18.95	85
1745		19.10	18.93	19.11	18.82	87
1755	19.03	18.97	18.80	18.95	18.65	88
1805	19.2	18.86	18.74	18.87	18.59	88
2020	17.7	18.71	18.68	18.66	18.31	89
2040	17.7		18.67	18.64	18.27	89
2340		18.79	18.78	18.82	18.53	90
2400	18.4	19.05	18.91	18.89	18.60	90
7/24						
0020		19.09	19.06	19.04	18.86	91
0040			19.12	19.10	18.95	91
0100		19.19	19.16	19.15	18.99	90
0120	18.70	19.08	19.15	19.15	18.98	90
0240			19.18	19.13	18.95	87
0300		19.1	19.17	19.15	18.98	86
0320		19.04	18.99	19.00	18.84	87
0420		18.97	18.93	18.92	18.76	88
0440		18.81	18.75	18.75	18.61	88
0500			18.72	18.70	18.57	88
0520	18.7	18.81	18.77	18.73	18.59	89
0540			18.89	18.83	18.68	89
0600	19.2	18.98	18.95	18.91	18.74	88
0620			19.05	19.00	18.81	88
0640		19.01	18.99	18.95	18.77	87
0700			18.94	18.94	18.74	86
0820		19.03	18.96	19.26	18.91	81
0840		19.22	19.07	19.40	19.07	79
0900			19.15	19.63	19.23	77
0920			19.14	19.47	19.18	77
0940		19.32	19.07	19.46	19.05	78

Time	T_S	T_1	T_2	T_3	T_4	H
7/24						
1000		19.39	19.26	19.66	19.26	78
1020	19.15		19.28	20.01	19.41	79
1040			19.32	19.92	19.35	80
1100	18.75		19.58	19.87	19.45	80
7/25						
2220	17.7	19.77	19.82	19.82	19.27	83
2320	17.86	19.45	19.46	19.43	19.13	84
7/26						
0020	17.71	19.39	19.40	19.37	18.71	85
0120	18.22	19.05	19.07	19.13	18.80	87
0320	17.7	18.96	18.98	18.98	18.71	89
0420	18.1	18.86	18.82	18.84	18.59	90
0440			18.28	18.41	18.25	91
0500			17.99	18.26	18.12	89
0600	17.2	18.23	18.38	18.42	18.09	91
0620	17.8	18.17		18.51	18.21	93
0640			19.05	19.01	18.60	93
0700			19.76	19.91	18.58	87
0715			19.92	20.18	19.76	86
0725			19.79	20.27	19.76	86
0805			19.39	19.86	19.42	85
0815			19.33	19.81	19.38	83
0830			19.43	19.89	19.48	81
0840			19.32	19.85	19.38	81
0850			19.26	19.78	19.29	81
0940			18.86	19.01	18.68	83
1005			18.83	19.07	18.74	84
1015			18.77	19.03	18.70	84
1030			18.80	18.96	18.71	84
1040			18.98	18.99	18.81	83
1050			19.11	19.02	18.96	81

Time	T_S	T_1	T_2	T_3	T_4	H
7/26						
1105			19.12	19.06	19.02	81
1115			19.16	19.04	18.92	80
1130			19.23	19.10	18.88	78
1140			19.22	19.10	18.83	77
1155			19.11	19.05	18.79	78
1210			18.91	18.88	18.68	80
1235			18.60	18.58	18.35	80
1245			18.57	18.52	18.29	80
1300			18.55	18.53	18.29	78
1310			18.49	18.54	18.20	78
1320			18.47	18.57	18.22	77
1335			18.37	18.53	18.20	77
1350			18.12	18.31	17.95	76
1410			17.56	17.80	17.40	76
1420						77
1435			16.97	17.18	16.87	78
1450			16.92	17.16	16.83	79
1500			16.95	17.19	16.81	78
1515			16.81	17.09	16.69	78
1525			16.89	17.27	16.85	77
1540				17.61	17.17	76
1550			17.32	17.92	17.43	75

APPENDIX B: COMPUTED RESULTS

This section includes computed values of Richardson's number, the momentum and heat flux, diffusivity, and the dissipation rate and temperature structure function. The mean wind speed is included for convenience. Figures showing the temporal variation of Richardson's number and momentum flux, and the dependence of momentum flux on wind speed are also included.

Computed Results

Time	$\bar{U}$ knots	ε $10^{-4}\ \frac{m^2}{sec^3}$	C_T^2 $10^{-3}\ \frac{°C^2}{m^{2/3}}$	D m^2/sec	Ri	F_M $10^{-2}\ \frac{kg}{m\ sec^2}$	F_H Watt/m^2
7/19							
0000	3	2.2		.32	- .34	1.1	- 3.1
0020	2	1.8	2.3	.30	.06	.95	
0100	1	.2	.3	.15	- .08	.24	.87
0140	.5	1.1	.1	.25			
0245	3	1.3		.24	0	.71	1.5
0420		.2	.5	.15	- .56	.24	.28
0440	3	.86		.22	- .36	.51	- .15
0500	1	2.0		.30	- .02	.95	- 5.6
0520	3	1.7	.9	.29	- .39	.88	- 2.3
0600	2	1.8		.30	.01	.95	2.4
0620			1.3				
0640		2.9		.38	- .10	1.5	.21
0700	1	2.3		.34	- .18	1.2	- .79
0720		1.3	1.4	.27	- .28	.77	- .59
0740		4.1		.39		1.6	
1350	9	6.4	5.2	.46	- .07	2.2	- .14
1410	9	7.1		.47		2.3	
1610	6		4.0				
1620		5.7		.44		2.0	
1630	6		4.3				
1650	7.5	6.9	4.5	.46	- .06	2.2	.65
1710	7.0	7.1	20.	.46	- .24	2.2	- 7.7
1730		6.3	23.	.45	- .06	2.1	.63
1940	6	3.4		.37	- .16	1.4	- .99
2000	8.5	2.7		.34			
2040	5	4.6		.41	- .36	1.8	- 8.5
2120	3	3.3		.36	- .25	1.4	- 3.1
2140	3	1.8		.30	- .35	.95	- 2.3
2200		3.4		.37	- .30	1.4	- 4.7

Time	$\overline{U}$	ε	C_T^2	D	Ri	F_M	F_H
7/20							
0700	7	4.3		.39	- .46	1.6	-10
0740		2.5		.33	- .54	1.1	- 6.9
0840	3	2.2		.32	- .36	1.1	- 3.2
0850	3		9.7				
0900		2.1	2.0	.32	- .17	1.1	- .28
0920	4	1.9		.31	- .35	1.0	- 2.7
1020	3	5.1		.42	- .22	1.9	- 4.5
1040		5.3		.43	- .17	1.9	- 3.5
1240	4	1.8		.30	- .06	.95	1.5
1300	3.5	1.4		.27	.06	.77	2.7
1320		1.4		.27		.77	
1800	14	15		.60		3.8	
1900	12	32		.78	- .26	6.3	- 5.5
1920	14	22	1.3	.69	- .21	5.0	-30
1940	14	15	2.1	.61	- .21	3.7	-14
2000	11	15		.61		3.9	
2020	10	18	3.6	.65	- .40	3.9	-37
2040	7	4.6	3.1	.41	- .50	1.8	-14
2100	9	4.1	3.2	.39			
2120	7	4.8	2.9	.42	- .30	1.7	- 5.9
2140		2.5		.33	- .66	1.1	- 9.3
2200	4	3.0		.36	- .28	1.4	- 3.6
2220		3.7		.38	- .40	1.4	- 6.5
2230		3.7		.38	- .15	1.5	- 1.2
2300	4.5	4.0		.39	- .10	1.6	- .2
2400	5	5.7	.8	.44		2.0	
7/21							
0040	5	3.7		.38	- .12	1.5	- .5
0100	3.5	3.7		.38	- .12	1.5	- .4
0120	2	2.6		.33	- .34	1.1	- 3.2

Time	$\bar{U}$	ε	C_T^2	D	Ri	F_M	F_H
7/21							
0240	5		1.2				
0405		5.7		.44	- .13	1.8	- 1.2
0425		7.4		.48	- .14	2.4	- 3.7
0445	5	4.2		.40	- .20	1.7	- 3.4
0505	4	4.2	2.1	.40	- .04	1.7	1.8
0545	3	4.0		.39	- .09	1.6	.2
0605		2.4		.33	- .38	1.1	- 4.1
0625	0	2.5		.33	- .44	1.1	- 5.1
0645	0	6.2		.45	- .04	2.1	- .73
0705		1.2		.29	- .47	.88	- 3.2
0725		.9		.29	- .58	.56	- 1.7
0805		3.7		.38	- .11	1.5	- .28
0825	5	5.0		.42	- .10	1.9	- .48
0845	6	4.6	3.9	.41	- .30	1.8	- 7.2
0905	4	6.6	3.9	.46	- .31	2.2	-11.
0945		3.3	2.0	.36	- .39	1.4	- 5.9
1005	3	2.3	1.4	.33	- .23	1.1	- 1.2
1025	~0	2.5	2.3	.33		1.1	
1045	1.6	2.8	3.4	.35		1.3	
1105		3.3	2.4	.36		1.4	
1305	14	21	1.4	.68		4.8	
1325		34	2.4	.80	- .06	6.7	- 9.7
1345		28	3.2	.75	- .22	5.9	-41.
1405	13	25		.72	- .17	5.4	-26.
1505	15	31		.77	- .08	6.2	15.
1620		24	7.2	.71	.04	5.7	11.
1720	11	6.7	7.4	.47	- .51	2.3	-22.
1945	8	3.8	9.5	.39	- .50	1.6	-11.
2030		4.2	8.9	.39	- .35	1.4	- 5.3
2110	2	2.9		.35	- .32	1.3	- 4.0
2130		2.6	4.3	.34	- .22	1.2	- 1.5
2150		3.1		.36	- .33	1.2	- 3.4
2250	3	11		.55	- .05	3.2	- .48
2350	2	2.3		.33		1.1	

Time	$\overline{U}$	ε	C_T^2	D	Ri	F_M	F_H
7/22							
0130	3	2.2		.32	- .05	1.0	1.2
0150		5.3		.43	.03	1.9	4.3
0450		2.5	.95	.33	- .04	.77	1.3
0550		1.8		.30	- .09	1.1	.83
0610	3	3.6		.38	- .16	1.5	1.4
0710	0	3.6		.38	- .08	1.3	.66
0730	0	4.0		.39	- .08	1.3	.80
0750	0	2.9		.35	- .18	1.3	- 1.0
0810		5.1		.42	- .21	1.9	- 4.4
0830	4	4.6		.41	- .10	1.8	- .34
0910	2	7.1		.47	- .02	2.3	2.5
0930	1	7.3		.48	- .03	2.4	1.6
0950	3	10		.53		2.9	
1010	5	5.0		.42	.02	1.8	3.5
1030		4.7		.41	0	1.8	2.8
1050	3	7.3	1.9	.48		2.4	
1210	4	4.6		.41	- .22	1.8	- 4.2
1230		3.0		.36		1.4	
1330		1.8		.30	-1.8	.95	-22.
1350		.7		.22	-2.1	.51	- 9.3
1610	5.5	1.4		.28	-1.2	.82	-11.
1630		1.4		.28			
1650	4	1.6		.29			
1710	6	2.1		.32			
1910	7.5	1.8		.30	- .22	.95	- .61
1950	4.5	2.1		.32	- .72	1.1	- 9.4
2130	6	3.4		.37	- .93	1.4	-20.
2150	8	1.3		.27	-1.3	.77	-13.
7/23							
0310	4	4.8		.42	- .86	1.6	-24.
0330		3.7		.38	- .72	1.4	-15.
0350		3.1		.36	- .72	1.4	-14.

Time	$\overline{U}$	ε	C_T^2	D	Ri	F_M	F_H
7/23							
0410	4	4.0		.39	- .40	1.6	- 8.4
0430		4.8		.42	- .32	1.8	- 7.0
0450	5	3.6		.38	- .47	1.5	- 9.3
0630	5	3.2		.36	- .32	1.5	- 5.1
0730	5	3.8		.39	- .34	1.4	- 5.0
0750		5.9		.44	- .31	2.0	- 9.7
0810		4.0		.39	- .31	1.8	- 6.4
0910	6	13		.58	- .14	3.5	- 8.9
0930		13		.58	- .32	3.5	-26.
1410	6.5	2.7		.34	- .81	1.2	-14.
1430	6	3.6		.38		1.5	
1440		2.7	.4	.34	- .72	1.2	-11.
1450	4	3.6		.38	- .52	1.5	-11.
1505		2.9	.4	.35	- .54	1.3	- 8.6
1515	7.5	1.8		.32	- .93	1.1	-12.
1525		4.4	.5	.40	- .66	1.68	-18.
1535	7.5	5.3		.43	- .65	1.9	-22.
1645	9	7.0		.47			
1655	9	8.5	1.2	.50	- .18	2.6	- 7.7
1705		8.0	1.5	.47	- .22	2.3	- 8.1
1715		3.5		.37	- .09	1.4	- .47
1725	9.5	4.9		.42		1.9	
1735		4.0		.39	- .21	1.6	- 3.2
1745	4	4.0	1.1	.39	- .32	1.6	- 6.5
1755		4.3		.40	- .40	1.7	- 9.3
1805	4.5	2.7	1.5	.34	- .43	1.2	- 5.6
2020		2.0		.31	-1.1	1.0	-13.
2040		1.5		.28	-1.6	.82	-15.
2340	3	3.8		.39	- .35	1.6	- 7.3
2400		3.0		.36	- .66	1.4	-12.

Time	$\bar{U}$	ε	C_T^2	D	Ri	F_M	F_H
7/24							
0020	3	2.7		.34	- .24	1.2	- 2.1
0040		2.4		.33	- .26	1.1	- 2.0
0100	3.5	1.8		.30	- .22	.95	- .53
0120	3	1.9	.5	.31		1.0	
0240		2.2		.32	- .55	1.1	- 6.3
0300	3	2.0		.31	0	1.0	1.6
0320		8.0		.49	- .06	2.5	- 3.6
0420	2	22	1.4	.69	- .04	5.0	- .22
0440		11		.54	- .06	3.1	- .83
0500	3	2.1		.32	- .20	1.1	- .68
0520		1.9	.8	.31	- .30	1.0	- 2.0
0540		2.4		.33	- .45	1.1	- 5.3
0600	4	1.4		.27	- .46	.77	- 2.3
0620		1.6		.28	- .79	.82	- 6.0
0640		1.8		.30	- .37	.95	- 2.6
0700	1	2.1		.32	- .38	1.1	- 3.5
0820	1	1.8		.39	- .03	1.6	2.0
0840		3.5		.37	- .10	1.4	1.7
0900	4	2.5		.33			
0920		5.7		.44			
0940	2	2.4		.33	- .37	1.1	- 4.0
1000	2	3.5		.37	- .06	1.4	1.3
1020		5.2		.43			
1040	4.5	7.2		.48			
1100	4.5	6.9		.47	- .08	2.3	- .50
7/25							
2220		26	1.2	.73	- .16	5.6	-27.
2320	12	17	1.3	.63	- .18	4.2	-19.

Time	$\overline{U}$	ε	C_T^2	D	Ri	F_M	F_H
7/26							
0020	7	5.8	2.8	.44	- .72	2.0	-26.
0120	1	4.9		.42	- .26	1.9	- 6.4
0320		2.0	2.7	.31	- .49	1.0	- 4.7
0420		1.6	2.0	.29	- .66	.88	- 5.6
0440		1.2		.26			
0500	4	1.8		.30			
0600	2	1.0		.25	- .18	.66	.51
0620		1.6		.29			
0640		7.6		.49			
0700	4.5	12		.56	- .13	3.3	- 7.2
0715		3.7		.38	- .22	1.5	- 3.1
0725	2	6.2		.45	.15	2.1	0
0805	4	2.3		.33	.55	1.1	0
0815		3.1		.36	.54	1.4	0
0830		4.7		.41	.42	1.8	0
0840		4.4		.40	.47	1.7	0
0850	3	4.9		.42	.34	1.9	0
0940	4	4.4		.40	- .26	1.7	- 5.1
1005	4	4.4		.40	.05	1.7	
1015		7.4		.48	.06	2.4	
1030		12		.56	.03	3.3	
1040		26		.73	- .04	5.6	- 3.2
1050		23		.70	- .05	5.1	- 4.1
1105	4	18		.65	0	4.4	3.6
1115		24		.71	- .13	5.3	-18.
1130		54		.93	- .12	9.1	-44.
1140		54		.93	- .14	9.1	-51.
1155	10	54		.93	- .10	9.1	-35.
1210		43		.87	- .06	7.9	-16.
1235		77		1.05	- .06	12.	-31.
1245		81		1.07	- .07	12.	-39.

Time	$\overline{U}$	ε	C_T^2	D	Ri	F_M	F_H
7/26							
1300	11.5	19		.66	- .18	4.6	-21.
1310		61		.97	- .09	9.9	-37.
1320		35		.81	- .11	6.9	-24.
1335		61		.97	- .03	9.8	-10.
1350	10	67		1.0	- .03	11.	-10.
1410		54		.93	- .03	9.1	- 7.6
1420		48		.90			
1435		115		1.2	0	15.	7.1
1450		113		1.2	.01	15.	7.5
1500	16.5	133		1.3	.01	15.	13.
1515		138		1.3	0	18.	16.
1525		125		1.2	.03	15.	24.
1540		47		.89			
1550	9	7.1		.47		2.3	

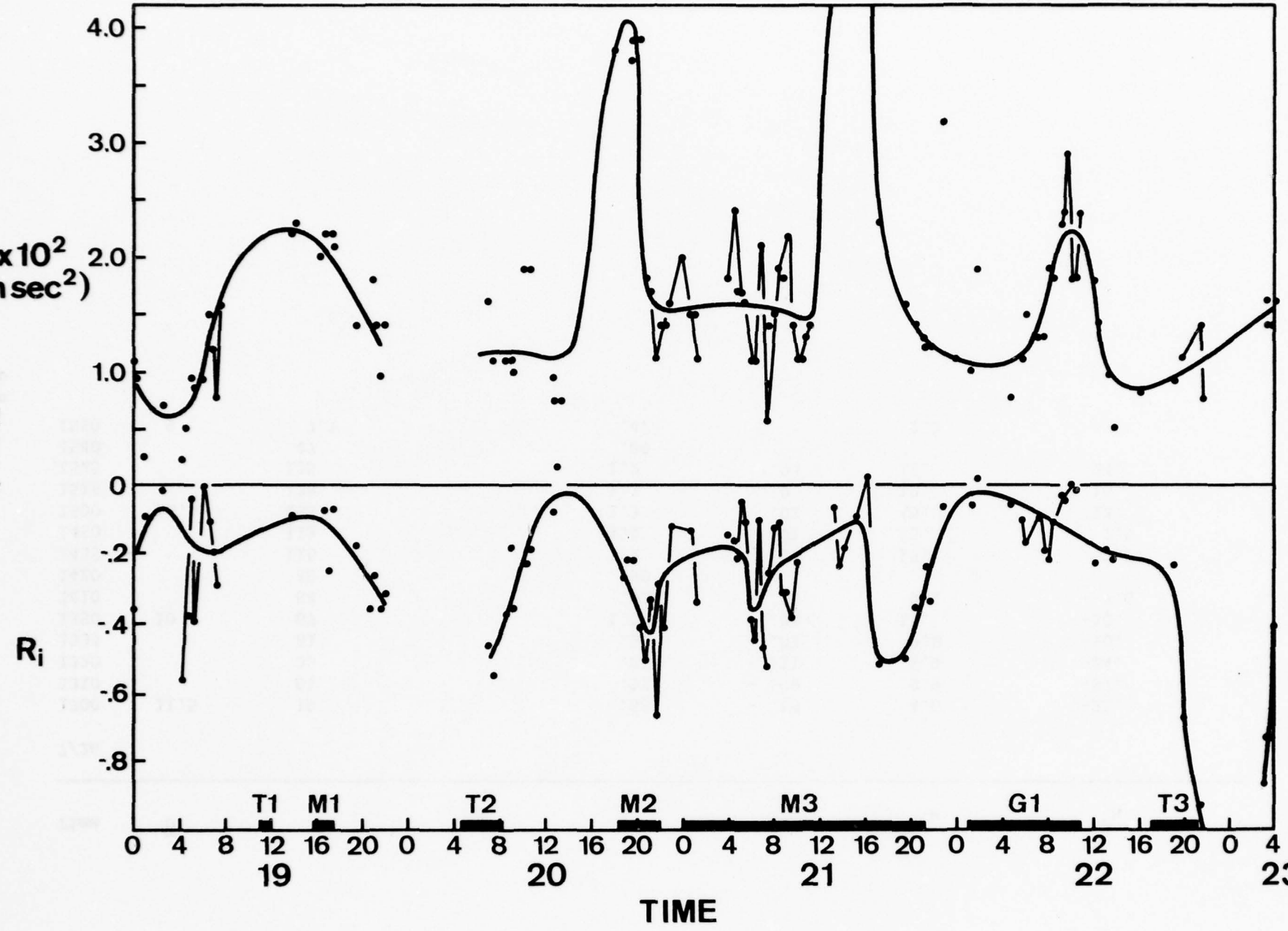

Figure 4a
B-10

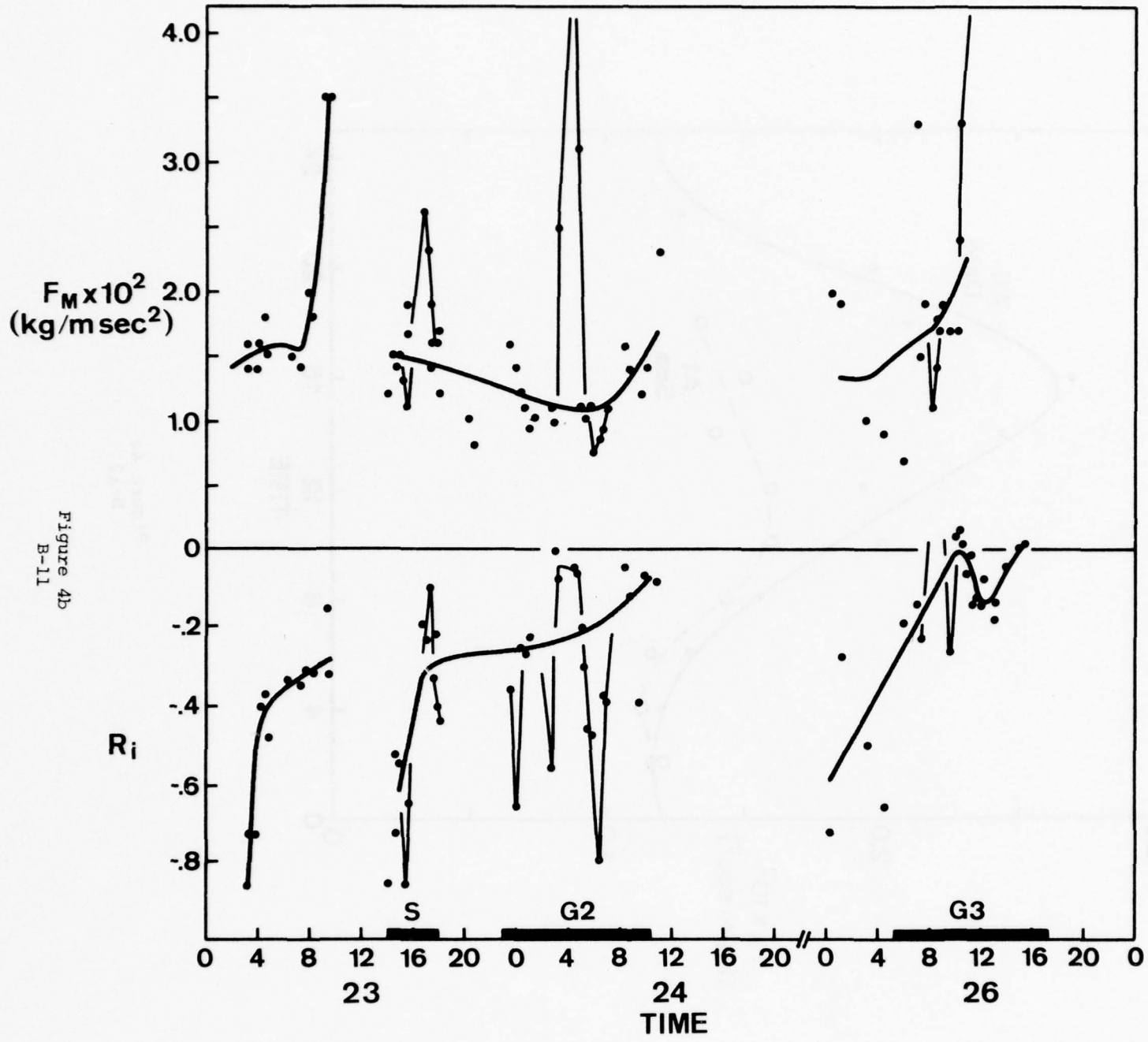

Figure 4b
B-11

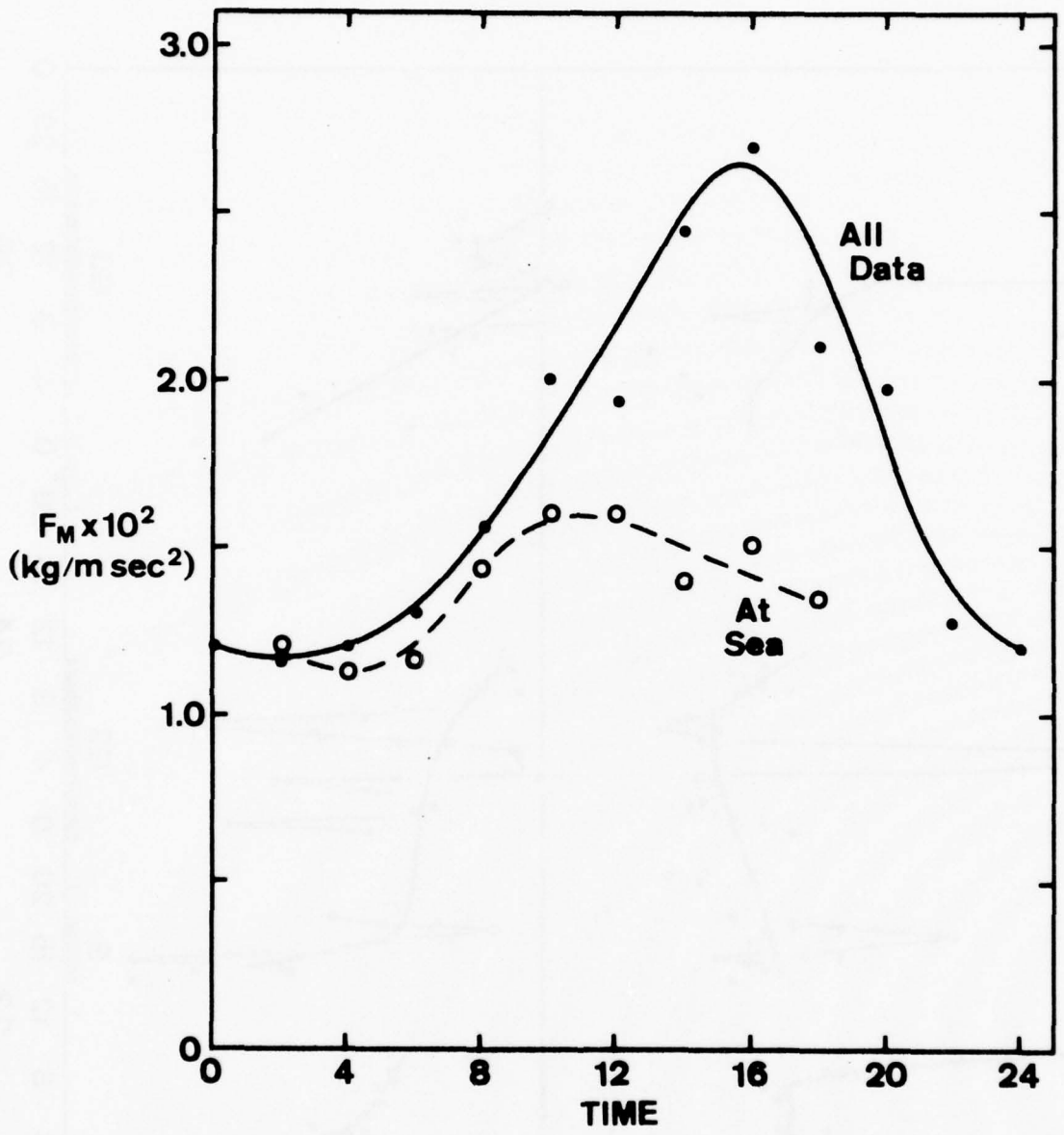

Figure 4c
B-12

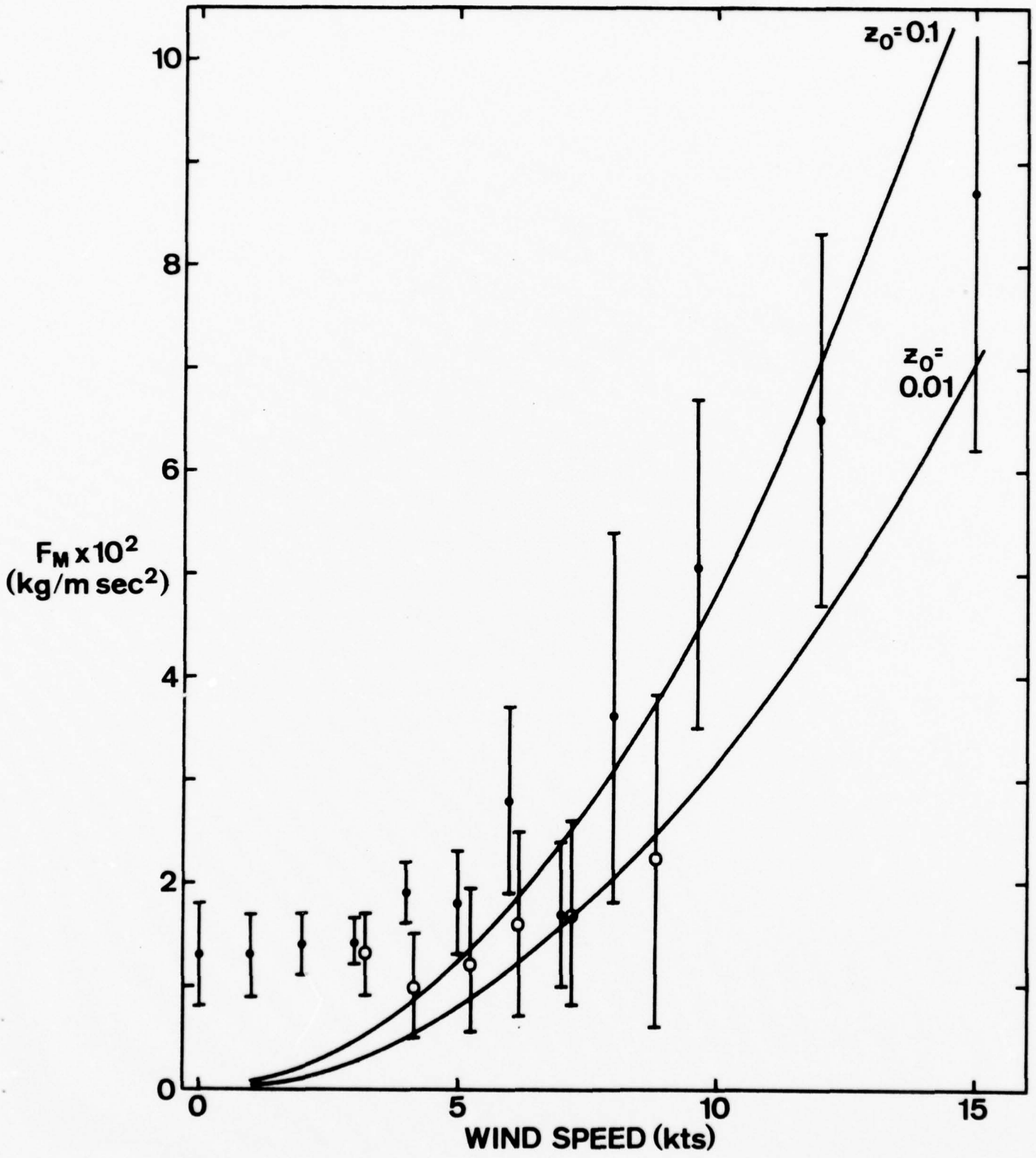

Figure 4d
B-13

APPENDIX C: AEROSOL RESULTS

This section is excerpted from a Masters Thesis written by LT Alan Simoncek, USN. It includes data and analysis for the cruise reported here and also for data obtained off the Florida Coast. Both are included for comparison purposes. All of the data was gathered by personnel from Calspan Corporation, Buffalo, New York.

TABLE OF CONTENTS

LIST OF TABLES

LIST OF FIGURES

ACKNOWLEDGEMENTS

Appreciation and thanks are extended to Dr. Kenneth L. Davidson for his support and guidance throughout this study. Dr. Chris Fairall and Dr. Gordon Schacher aided immeasurably by offering technical assistance and advice. Many thanks also to Mr. Gene Mack for providing the aerosol and meteorological data used in this investigation.

A special and heartfelt appreciation must go to my wife, Sue, and sons, David and Adam, for their constant expression of encouragement and understanding.

I. INTRODUCTION

The military is currently very interested in the performance of electro-optical weapons systems in an atmosphere of varying turbidity. For example, a number of electro-optical systems which utilize the visible as well as IR wavelengths are being developed by the Navy for use in surveillance and intelligence gathering operations in the marine boundary layer. These systems are limited by the extinction of the propagated energy due to absorption and scattering by aerosols. The effect of absorption depends on the composition of the particulates and wavelength of the energy and the effect of scattering depends on the concentration and size of the scatterers. For most applications the scattering processes in the atmosphere are caused by particles of size comparable to the wavelength of the radiation.

The size distribution of the marine aerosol is known to depend upon the wind speed, relative humidity, stability, and air mass trajectory. In order to evaluate accurately and predict the atmospheric effects on these electro-optic systems, it is necessary to know the dependence of the aerosol size distribution on the foregoing meteorological parameters.

The nature of the aerosol size distribution in a coastal marine environment is investigated in this study. Data from aerosol observations off the coast of Panama City, Florida and off the Southern California coast near the Channel Islands

were analyzed. These coastal regimes, which represent a mixture of continental and marine aerosols, should contain aerosol distributions somewhat different from the typical marine environment. The relationship of the coastal marine aerosol to wind speed, relative humidity, stability, and sub-synoptic circulation is examined. Furthermore, an attempt is made to evaluate the use of the friction velocity as a valid aerosol distribution predictor.

II. BACKGROUND

A. THE ATMOSPHERIC AEROSOL

With the recent increasing concern over the pollution of our atmospheric environment, the examination of the tropospheric aerosols has also increased. Particulate matter enters the atmosphere through either natural or man-made processes; approximately 10% of the total concentration is believed to originate from combustion and industrial processes while the natural sources, including soil dust, volcanoes, and oceans account for the remaining 90%. The size range of aerosols observed by current methods extends from 10^{-3} μ to 10^{3} μ radius (1 μ = 10^{-6}m = micron). Depending on their size, amount of soluble matter, and the relative humidity, these particles may act as condensation nuclei and aid in the precipitation process.

Mason (1975) classified condensation nuclei into three groups according to radius: Aitken (< 0.1 μ), Large (0.1 μ - 1 μ), and Giant (> 1 μ) particles. Essentially, Aitken nuclei are produced by man-made sources and larger nuclei by natural processes. Therefore, it is not surprising to see Aitken nuclei dominate the size distribution spectrum over continents. The marine aerosol above .1 μ is composed of sea-salt particles produced by spray and bubble bursting mechanisms on the water surface. These mechanisms are quite complex and their contribution to the size distribution will be discussed in detail later.

The vertical profiles of trace constituents that are produced over the continents have been shown to be rather uniform in space and time above 5 km. This "background" aerosol is affected slightly by anthropogenic activities and is far away from local natural sources. Its number concentration is almost identical with the concentration of Aitken nuclei over ocean areas. Past experiments have shown the concentration of the background aerosol to be about 300 cm^{-3} over remote ocean areas. However, a recent experimental cruise (R/V Meteor) by Junge and Jaenicke, 1971 in the mid Atlantic yielded observed concentrations of 600 cm^{-3}. Measurements by Hidy, et al. (1973) on San Nicolas Island, 130 km, west-southwest of Los Angeles, have shown the background aerosol to be a mixture of material from both marine and continental sources with an average concentration of 2400 cm^{-3}. Samples taken over oceans of the South Atlantic (Meszaros and Vissy, 1974) resulted in Aitken particle counts of between 300-450 cm^{-3}.

B. CHARACTERISTICS OF THE MARINE AEROSOL

An idealized size distribution of the continental and marine aerosol is supplied by Junge (1972) in Figure 1. The significant feature is the shift of the maximum of particles as a function of total particle concentration. Over the ocean the sea-salt aerosol, which is usually confined to the lower 2 km, is superimposed on the background aerosol. Junge reasoned that the concentration of the background

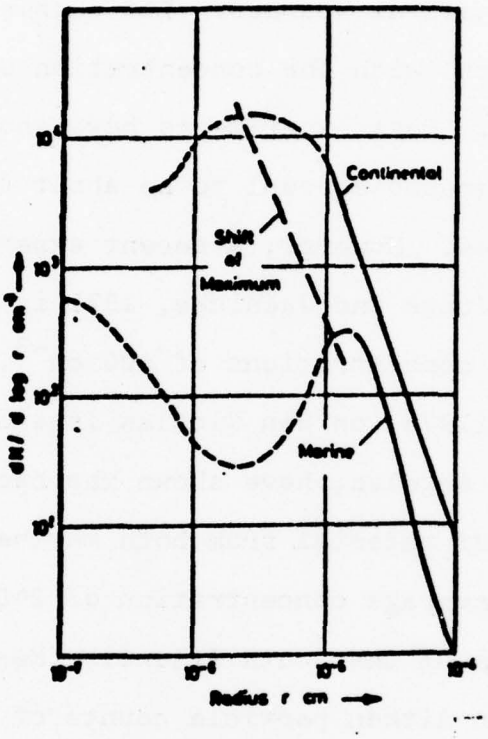

Figure 1. Idealized Size Distributions of Continental and Marine Aerosols

cloud nuclei decreases below the marine inversion due to the effect of washout, or coalescence, due to the larger water droplets in the cumulus clouds.

Another aspect of the aerosol distribution is the slope of the number density versus radius curve. Friedlander (1961) proposed a theory of self-preserving size distributions which helps to explain why all atmospheric size distributions are similar. He proposed that the similarities can be explained by solutions to the kinetic equation which describe the relationship between particle size distribution and time. Experimental results have indicated that the size distribution over a particular range of sizes of continental aerosol has a -4 slope and follows the relation

$$\frac{dN}{dr} = C\phi\, r^{-4} \qquad (1)$$

where N is the number of particles/cm^3, r the particle radius, C a constant, and ϕ the volume of particles per unit volume of aerosol.

Blifford (1970) measured the size and number distributions of atmospheric aerosols at various altitudes over the ocean 250 km west of Santa Barbara, California. Samples were taken by an aircraft equipped with a jet impactor and the data was obtained from direct microscopic counting techniques in the laboratory. The aerosol distribution at approximately 15 meters above the sea surface is presented in Figure 2. The curve has a rather steep negative slope at

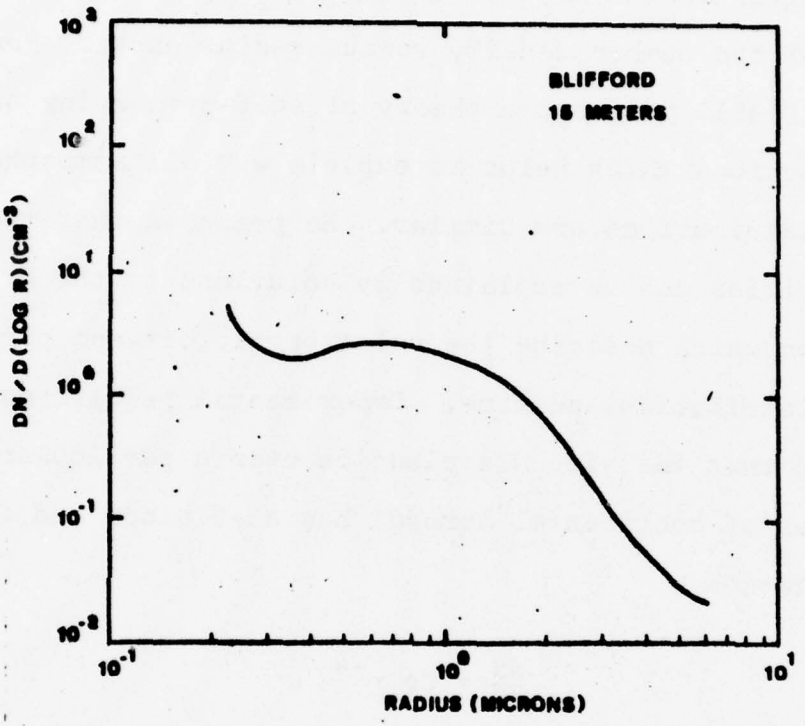

Figure 2. Size Distribution at 15 Meters, 250 km West of Santa Barbara

the small particle end which becomes slightly positive at around .4 μ radius. For particles larger than .8 μ, a fairly constant slope of about -2 to -3 is observed.

The results of the R/V Meteor experiment, where several aerosol counters were used, are shown in Figure 3. Above 10 μ the exponent of a power function fit to the data is approximately -6 and between 0.3 μ and 10 μ it is variable but on the average around -3. The maximum of the size distribution occurred at 0.3 μ with a secondary maximum at 0.03 μ.

It is possible that, due to increased human activity in the Northern Hemisphere, Junge and Jaenicke's Atlantic experiment did not explore the undisturbed marine environment. Meszaros and Vissy (1974) describe the results of aerosol samples taken over the oceans of the Southern Hemisphere by means of membrane filters. An example of the number concentration and size distribution over the Atlantic between (a) 0° and 20° South and (b) 40° and 60° South can be found in Figure 4. Chemical analyses were performed and it was observed that the maxima in the concentrations of all particles and of sodium chloride particles occur at approximately .1 μ radius in both cases. Up to .5 μ radius the slope of the distribution is approximately -5. Between 0.5 μ and 1.5 μ, however, the decrease of the concentration with increasing particle size is very moderate (-1 to -2), while for radii larger than 1.5 μ the slope is close to -3. This has been interpreted to indicate that the form of the

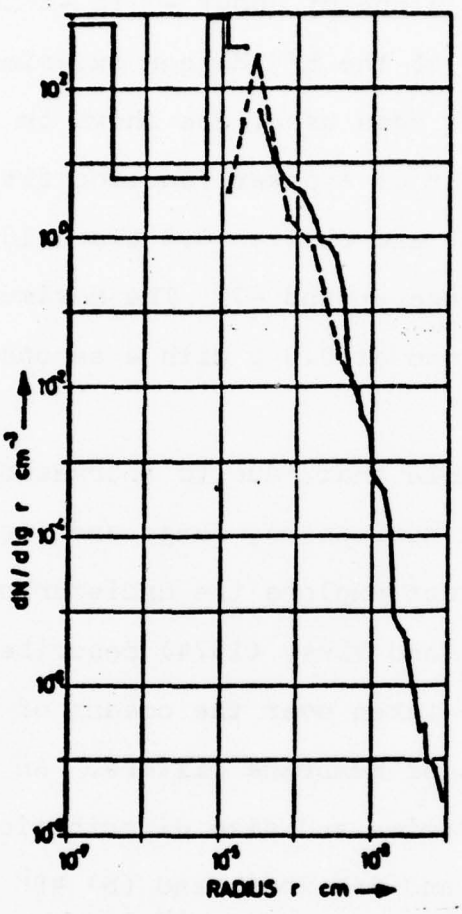

Figure 3. Results of the R/V Meter Cruise. Measurement Systems Used: o—o Combination of CCN Counter, Optical Counter, and Impactors: – – – Double Stage Impactor (Junge and Jaenicke, 1971)

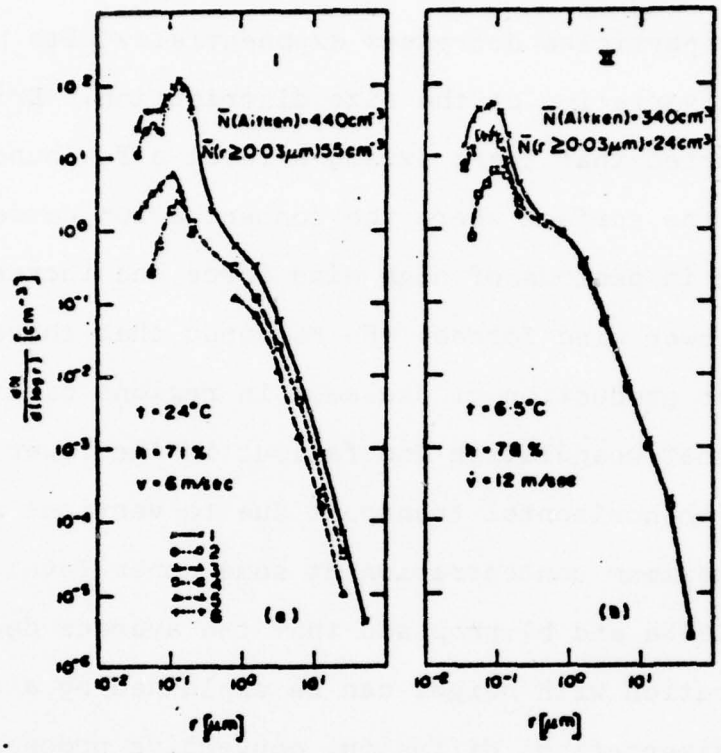

Figure 4. Size Distributions over Remote Ocean Areas (—— All Particles; —·— NaCl Particles)

distribution is produced by the combined effect of particles formed in different ways.

Oceanic measurements have shown that the concentration of sea-salt particles decreases exponentially with height, with little variation of the size distribution. Ericksson (1959) reported that there exists a level a few hundred feet above the surface where the concentration decreases with height in periods of high wind force and increases with height in lower wind forces. He reasoned that there is little or no production of sea-salt in regions of light winds and that coagulation and fallout in the lower levels combined with horizontal transport due to vertical shear produce a maximum concentration at some upper level.

Toba (1965a and b) proposed that the average decrease in concentration with height can be explained by a combination of sedimentation, diffusion, convective processes and the humidity distribution. He suggested that the line between the aerosol vertical distribution and the process of production of sea-salt particles at the sea surface is found within the lowest layer of the atmosphere where the eddy diffusivity and relative humidity sharply change.

The distribution of eddy diffusivity near the sea surface is closely related to the wind speed. The larger the eddy diffusivity near the surface the more sea-salt particles that will be supplied. Toba considered eddy diffusivity in the form

$$D = kU_*(Z + Z_o) \qquad (2)$$

where k is the von Karman constant, Z the height above the sea surface, Z_o the roughness length, and U_* the friction velocity which is a function of the momentum transfer over the sea.

The relative humidity in the first few meters over the ocean is known to decrease rapidly with height. The particles produced near the surface in a region of high humidity grow larger and thus have a greater terminal velocity due to gravity than those at the top of this layer.

During light winds the number concentration near the sea surface increases with height. Since it results from a non-steady state, an inversion of vertical gradient of the particle concentration is most likely to be found in small particles which have a longer residence time. Ericksson (1959) computed the fall velocities for given relative humidities, salinity, and radius. During high wind periods, giant size sea-salt particles are produced at the surface and through the diffusion process are mixed throughout the atmosphere. The largest particles may fall back into the ocean due to excessive terminal velocity or be entrained in the wave crests. Smaller particles are free to rise to cloud height where coalescence with larger cloud drops and washout usually occur.

Measurements of salt nuclei greater than 10^{-14} gm over the North Atlantic by Moore and Mason (1954) revealed the existence of two distinct types of size distributions (Type I and II). The curves for the observed Type I and Type II

nuclei distributions are reproduced in Figure 5. Type I distributions were observed for wind speeds between 6-15 m/sec and were thought to be residuals of spray droplets produced by breaking waves. The presence of a discontinuity or a sharp change of slope in the Type I distribution was explained in terms of a loss of the larger nuclei by sedimentation. In strong winds, the part of the curve to the right of the discontinuity probably represents a state of equilibrium between production and loss by sedimentation. In light winds and stable conditions the slope should be steeper due to the fact that the loss by sedimentation is greater than production and larger nuclei are not easily transported vertically under stable conditions. The Type II distributions were only observed when the wind speeds were less than 7 m/sec and resembled a high concentration continental aerosol. In winds of up to 15 m/sec the measured concentrations of large sea-salt nuclei rarely exceeded 10 cm^{-3}.

The effect of stability on the concentration of atmospheric condensation nuclei was well documented by Moore (1952). He used an Aitken counter to measure the relationship between concentration of nuclei and the intensity of vertical mixing over the North Atlantic. The results indicated a decrease by as much as a factor of 4 in the number of Aitken particles near the surface on days with cumulus clouds as compared to days with stratus clouds. This would indicate that convection plays an important role, at least in the transport of smaller particles.

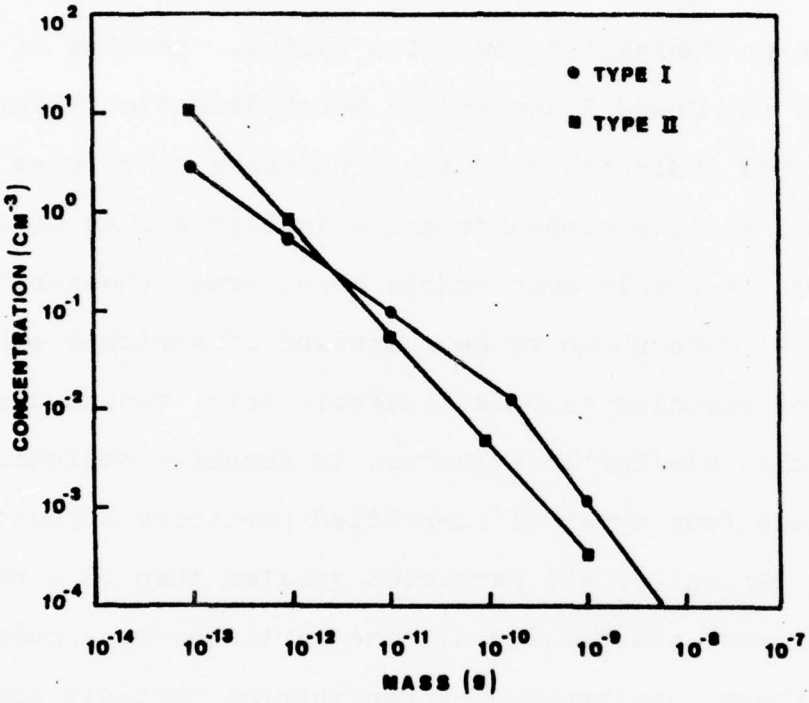

Figure 5. The Size Distribution of Moore and Mason's Type I and Type II Nuclei

Chemical analyses by various investigators have indicated that between 0.1 μ and 1.0 μ radius the marine aerosol is composed of a background component of continental origin and a sea-salt component. Sodium chloride was found to predominate above 1 μ radius while particles of continental origin predominate below 0.1 μ radius. Results of a cruise off the Grand Banks in the North Atlantic (Ruskin, et al., 1976) indicated that the continental particles are composed of sulfate compounds and a smaller amount of sulfuric acid. Aerosols over remote ocean areas (Meszaros and Vissy, 1974) were shown to be comprised of variable concentrations of ammonium sulfate, sulfuric acid, sodium chloride, and particles similar in structure to ammonium sulfate. The sum of these four types of identified particles accounted for 75-95 percent of all particles greater than .3 μ radius. In other words, practically all the particles in a pure marine atmosphere, undisturbed by continental particle sources, are soluble in water.

C. RELATIVE HUMIDITY EFFECTS

A solid particle which is composed wholly, or in part, of a pure water-soluble substance will undergo a sudden transition to a saturated solution droplet when some critical value of relative humidity, less than 100%, is reached. The relative humidity at which this transition occurs depends on the size and chemical composition of the particle. The smaller the particle, the lower the critical humidity. Below the transition point, solid particles acquire small amounts

of water by the process of adsorption. At relative humidities above the transition point, a particle (or, more properly, an aqueous solution droplet) grows by the absorption of water vapor (Fitzgerald, 1975).

A pure water droplet is said to be in equilibrium with its surroundings if it neither evaporates nor grows. This only occurs when the equilibrium vapor pressure over the surface of the droplet is equal to the vapor pressure of the surrounding air. Winkler (1973) describes the equilibrium growth of aerosol particles due to humidity as complex and depending on the relative proportion of soluble and insoluble material in the particles and on the chemical composition of the soluble component. Complex ionic mixtures, similar to those present in atmospheric aerosols, show material influences and lower the water vapor pressure to a much less degree than the same amount of pure salts. In such complex mixtures the various salts become dissolved only gradually with increasing relative humidity until at a sufficiently high humidity all soluble material is in solution.

Measurements have shown that with increasing humidity a sodium chloride crystal undergoes a phase transition to a saturated solution droplet at a relative humidity of approximately 78%. Figure 6 describes how the equilibrium radii of droplets containing specified masses of sodium chloride vary with the relative humidity. The equilibrium radius of the droplet increases with increasing humidity until the air becomes supersaturated by a critical amount, corresponding to

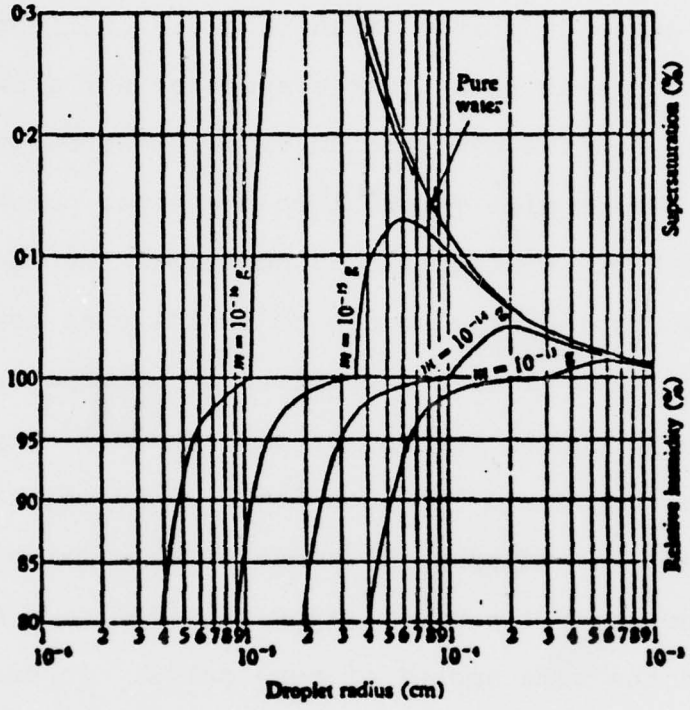

Figure 6. Equilibrium Relative Humidity and Corresponding Radii (Mason, 1975)

(This page intentionally blank)

the maximum of the curve in this figure. If this supersaturation were maintained, theoretically the droplet will grow without bound. With decreasing humidity a sodium chloride solution droplet crystallizes at a humidity between 35-45%. Since the relative humidity at a height of about 15 meters over the ocean surface goes below 40% very infrequently, sea-salt droplets will have little opportunity to crystallize (Fitzgerald and Ruskin, 1977).

Since the later discussion refers to the distribution of sea-salt particles by bolt mass weight of salt (grams), radius of dry crystals (μ) or radius at ambient humidity (μ), the scale in figure 7 is furnished as a reference.

D. THE PRODUCTION OF AIRBORNE SEA-SALT

Although the spectrum of the marine aerosol above .1 μ radius is known to consist of sea-salt particles, very little is certain about the concentration and mechanisms of production. Because of the smallness of the particles and limitations of the sampling equipment, earlier experiments did not measure the quantity of sea-salt particles much less than 10^{-12} gm.

Woodcock (1953) determined that the mass distribution of "giant" (> 10^{-12} gm) sea-salt nuclei varies with wind speed. Increases in the amount of air-borne salt near cloud bases were shown to be related to increases in wind speed at the sea surface, with the greatest proportionate increase in particle number occurring at the large end of the weight range. The results of Woodcock's measurements for wind forces of 1,

3, 5, and 7 on the Beaufort scale are shown in Figure 7. The line (a) gives the size distribution of continental aerosol for comparison. The line (b) is an extrapolated size distribution of the marine aerosol. Chemical analysis of Woodcock's bulk aerosol samples between .1 μ and 1 μ indicated a maximum of sea-salt around 0.3 μ and a lower limit in the vicinity of .1 μ radius. These distributions indicate total concentrations of all sea-salt particles of no higher than a few per cubic centimeter (Junge, 1972). According to Mason (1975), over a rough sea the concentration of sea-salt particles greater than 2 μ radius rarely exceeds 1 cm^{-3} and the total concentration of all salt particles rarely exceeds 10 cm^{-3}.

Moore (1952) observed a distinct correlation between wind speed and concentration of sea-salt larger than 10^{-11} gm up to wind speeds of 15 m/sec. He also found a linear increase in concentration of particles larger than 10^{-9} gm with increase in wave height. Results of experiments by Monahan (1968) reveal an abrupt increase in concentration of sea water droplets larger than 45 μ radius at a wind speed of approximately 9 m/sec, measured 47 cm above the sea surface.

Moore (1952) also analyzed the visibility observations at two ocean weather ships and determined that the opacity for a given humidity increases with wind speed. He attributed this increase to an observed increase in the concentration of large nuclei. Another result indicated that at lower humidities, the increase in opacity was more pronounced, and Moore believed this was due to the dehydration of larger droplets. These conclusions would indicate that the aerosol

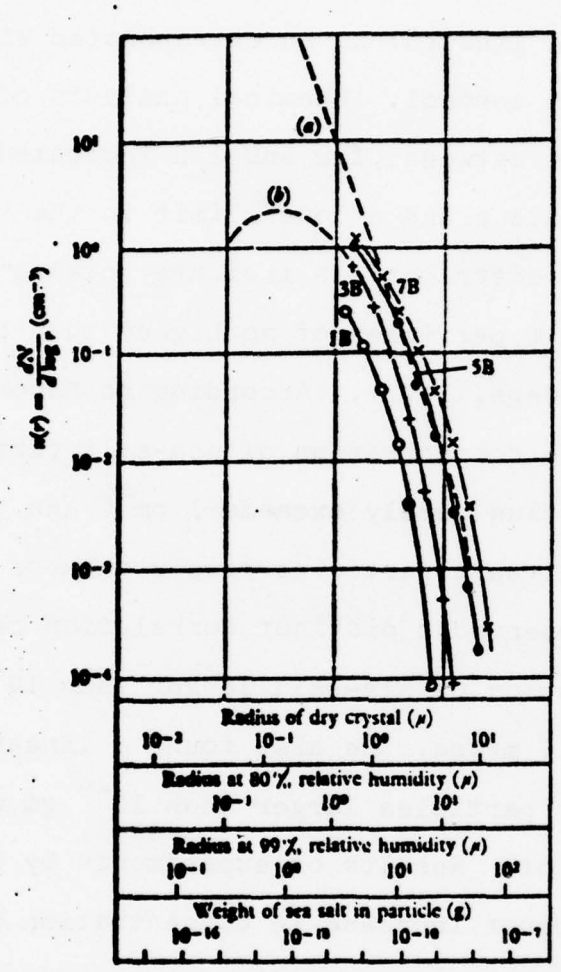

Figure 7. Size Scale and Average Size Distribution of Sea-Salt Nuclei Measured by A.H. Woodcock (Mason, 1975)

distribution is more variable and sensitive to wind speed in drier air, and this feature should be most noticeable in the larger size ranges.

As the wind speed increases over the ocean, gravity waves are generated and begin to break at a critical wind speed generally agreed upon to be near 7 m/sec. Air that is entrained by these breaking "whitecaps" rises to the surface sometime later in the form of bubbles. The principal mechanisms of sea-salt production are thought to be the direct spraying of droplets off the crests of breaking waves and the bursting of bubbles in areas of whitecaps and foam. Droplets produced by direct spraying are generally larger than 45 μ and, due to large fall velocities, are not airborne long enough to evaporate and become light enough to be transported upward (Monahan, 1968). Toba's model (1965b) showed that the net production of sea-salt particles at the sea surface seems to increase with particle mass even beyond 10^{-8} gm (20 μ), but that the transport by eddy diffusion is not sufficient to carry the particles upward against gravity beyond this size. The presence of particles larger than 10^{-8} gm in the atmosphere is generally attributed to coalescence of sea-salt droplets within and below clouds.

Some examples of residence times for different sea-salt particle sizes taken from Junge (1972) are found in Table I. It would seem then that particles in the .1 μ - 20 μ range, at least, are produced by the bursting of bubbles.

In efforts to photograph the rupture of the surface bubble film, Kientzler, et al. (1954) found that their camera

exposure was too long to capture this rapid phenomenon. However, they were able to see the formation of the "Rayleigh" jet which projects upward, continues to rise as a thin column, and then breaks into droplets of varying sizes. Day (1964) describes this process in the following manner. Each bubble, as it reaches the surface, develops a spherical film-cap which drains, thins, and bursts. Fragments of the film are thrown out and are dragged upward by the air which escapes from the bubble orifice. Water, rushing down the sides of the bubble cavity, emerges from the center as a narrow jet. A schematic of this process is shown in Figure 8. The larger drops (L) are formed by disintegration of the jet (J). Smaller particles (S) are formed by bursting of the bubble film.

Kientzler's experiment was significant in that no droplets of large enough size to be resolved by the film and optical system were observed from .2 - 1.8 mm diameter bubbles until after the jet formation. This was interpreted to indicate that the larger droplets are not produced when the bubble film is broken. On the average, the droplets produced by the jet mechanism were approximately 1/10 of the original bubble size. 1 mm diameter bubbles were observed to produce droplets of approximately 50 μ radius. The smallest observed were of 2 μ radius and deduced to have been formed by a bubble of approximately .04 mm diameter. Therefore, the jet mechanism can be considered a source of salt particles greater than 10^{-12} gm (1 μ).

	Residence Time τ, days			
	M = 10^{-8} grams	M = 10^{-11} grams	M = 10^{-14} grams	M = 10^{-9} grams
Toba's value w_f for 80% relative humidity	86	17	2.9	0.32
Toba's value w_f for 91.4% relative humidity	59	11	2.1	0.23
Eriksson's estimate from sedimentation	82	16	2.6	0.4
Eriksson's estimate from production	3.5	1.0	0.6	0.5
Our estimate*	1.9	1.6	1.0	0.26

Table is taken from *Toba* [1965a, Table 2]. The variable M is the mass of particles.

Table 1. Residence Times of Sea-Salt Particles over the Oceans

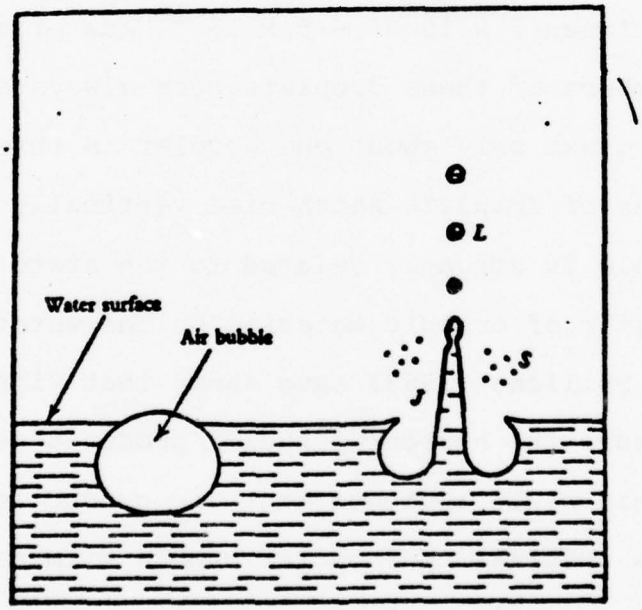

Figure 8. The Formation of Sea-Salt Droplets by the Bursting of Bubbles (Mason, 1975)

Mason (1954) utilized a cloud chamber to study bubble behavior in both distilled and salt water. After expansion, a dense cloud of tiny droplets was observed rising vertically in the space above the salt water, but not above the distilled water. Bubbles of 3 mm diameter produced 100-200 of these condensation nuclei, the majority of which are estimated to have salt contents between 10^{-15} gm and 2×10^{-14} gm. This would correspond to droplets of approximately .1 μ to .3 μ radius at 80% relative humidity. Mason also observed a second group of droplets produced by the shattering of the bubble film. These were projected sideways at an angle of ten to 15 degrees above the horizontal and slightly larger, containing between 2×10^{-12} - 5×10^{-10} gms of salt. However, the numbers of these droplets were always small, on the average, there was only about one droplet in this size range.

The number of droplets which rise vertically from a bursting bubble is strongly related to the state of compression of the film of organic material on the water surface. Paterson and Spillane (1969) have shown that with an increase of film pressure the number of nuclei produced decreases markedly. This would indicate that the production of sea-salt droplets originating from the bubble film mechanism would be suppressed in regions of high organic activity on the sea surface. Aerosol samples taken by Woodcock (1972) over Hawaiian and Alaskan seas may help explain where the transition between the jet and film sea-salt production mechanisms occurs. His observations, using an improved slide collection

technique, show an increased average particle production for sea salt particles less than 2×10^{-14} gm (.3 μ radius) in Hawaii where marine organic productivity is low. In contrast, the mean distribution curve for particles over the organically rich Gulf of Alaska fails to indicate an increased slope of the concentration curve among particles of the same size range. These curves are shown in Figure 9. The presence of surface active films arising from the biologically productive Alaskan waters is thought to suppress the production of film droplets.

Statistical analysis by Meszaros and Vissy (1974) showed that with increasing particle radius the correlation between wind speed and chloride concentration increased. This meant that smaller chloride particles are formed by the bubble film mechanism than by direct spraying. The distribution curve gives evidence that the transition between these two chloride formation mechanisms lies between .2 μ and .4 μ. Thus the maximum at .1 μ gives the maximum of chloride particles formed by the bubble film process.

Moore (1952) found evidence that the particle concentrations below 1 μ are not correlated with wind speed. This would indicate that most of the particles between .1 μ and 1 μ are not produced by bursting bubbles. Other experiments using the effects of relative humidity on particle growth indicate that a considerable proportion of marine particles between .1 μ and 1 μ must differ in composition from sea-salt (Junge, 1972). Meszaros and Vissy (1974) found that, in this size range, sodium chloride varied from 4-50% of the

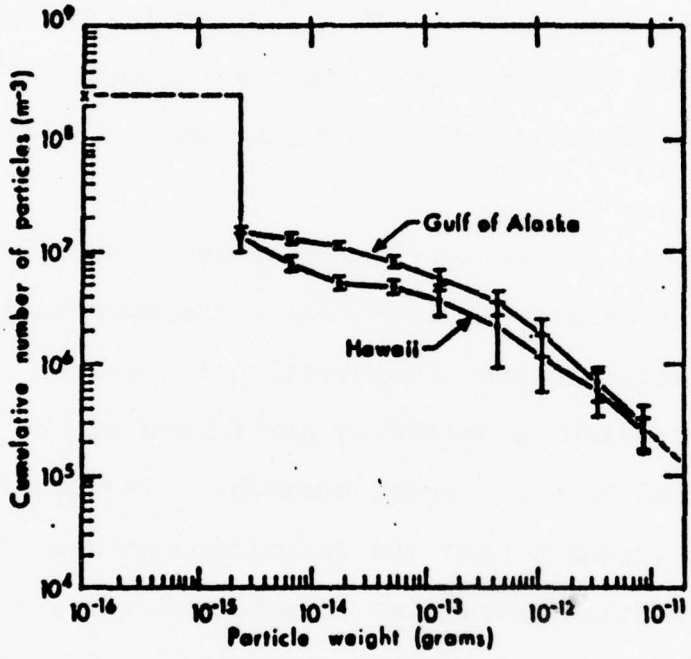

Figure 9. Distribution Curves over Alaskan and Hawaiian Waters (Woodcock, 1972)

concentration for all particles. The observations by Hidy et al. (1974) off the coast of Southern California revealed that 11% of the aerosol sampled contained sea-salt, the remainder being a combination of sulfates, nitrates and soil dust.

E. AEROSOL MODEL

Recently, various aerosol models have been developed in an attempt to accurately describe marine aerosol distributions as a function of one or more parameters. This is essential for the calculation of optical propagation through the atmosphere as aerosols scatter and absorb energy. Since the aerosol distribution is known to be dependent on relative humidity and wind speed, these two variables usually are the key parameters of each model.

One model in particular has been developed by Fitzgerald and Ruskin (1977) on the basis of the North Atlantic observations. They applied the effects of relative humidity on the equilibrium growth of aerosol particles to the sea-salt mass distribution determined by Lovett (1975) in the North Atlantic. Lovett presents empirical log radius mass distributions in the form of the following power law:

$$\frac{dN}{d \log r_d} = C\, r_d^{-\nu} \qquad (3)$$

where r_d is the dry particle radius and C and ν depend on the wind speed V in the following manner:

$$\nu = 3.317 - .03\, V \qquad (4)$$

and $$C = 0.2 - 0.0196\ V + 0.0121\ V^2 \qquad (5)$$

These expressions are valid only over a wind speed range of 3-17 m/sec^{-1}.

Formulae have been derived (Fitzgerald, 1975) for the equilibrium size of aerosol particles composed of a single pure salt as a function of relative humidity. For a sodium chloride particle the relationship between particle radius and relative humidity may be expressed as

$$r = \alpha\ r_d^{\beta} \qquad (6)$$

where α and β are functions of the relative humidity as described by Fitzgerald (1975). Equations (3) and (6) are combined to describe the aerosol size distribution as a function of relative humidity and wind speed, giving

$$\frac{dN}{d \log r} = \frac{c}{\beta} (\alpha^{\nu/\beta}) (r^{-\nu/\beta}) . \qquad (7)$$

Comparison between the aerosol distributions derived from the above model and those observed in two coastal marine environments is made within this study.

III. TURBULENCE THEORY

A. BOUNDARY LAYER CONSIDERATIONS

The importance of turbulent exchange processes in the surface boundary layer has long been recognized. Panofsky (1969) describes atmospheric turbulence as consisting of horizontal and vertical eddies by which the air is mixed. The two mechanisms by which eddies are formed in the atmosphere are heating from below and wind shear. Heating produces convection and the change in wind speed with height produces mechanical turbulence. Because there is no wind at ground level, and there is usually some wind above the ground, mechanical turbulence is common. This type of turbulence increases with increasing wind speed (at a given height) and is greater over rough terrain than over smooth terrain. The terrain roughness is usually characterized by a roughness length, Z_o , which is proportional to the size of the eddies that can exist. The relative importance of heat convection and mechanical turbulence is characterized by the Richardson number, R_i . The Richardson number is a measure of the relative rate of conversion of convective to mechanical energy. For example, negative Richardson numbers of large magnitude indicate that convection predominates resulting in strong vertical motion. As the mechanical turbulence increases, the Richardson number approaches zero.

Finally, as the Richardson number becomes positive, the thermal stratification becomes stable and damps the mechanical turbulence. For $R_i > 0.25$, vertical mixing disappears.

The effect of the wind on the underlying surface is termed the shearing or Reynolds stress, τ, and is characterized by a downward momentum transfer. The Reynolds stress may be represented by

$$\tau = -\rho \langle u'w' \rangle \qquad (8)$$

where u' = fluctuating horizontal wind velocity

w' = fluctuating vertical wind velocity

ρ = density of air

It is convenient to express Reynolds stress in terms of the friction velocity U_* so that

$$\tau = \rho U_*^2 \qquad (9)$$

where U_* is constant throughout a region of constant momentum flux. Hence, U_* is a measure of the downward transfer of momentum in the lower 50 meters of the atmosphere. Over the ocean an increase in the near surface winds would lead to a greater momentum and energy transfer for surface wave and sea-salt aerosol production. The relationship between the turbulent transfer of heat and moisture in the marine boundary layer and the generation and transfer of aerosols is not well known and, unfortunately, is not investigated in this study.

B. MOMENTUM TRANSFER, U_*, RELATIONS

A thorough discussion of the boundary layer expressions is presented in several references, e.g. Lumley and Panofsky (1964). The similarity approach of Monin and Obukhov (1954) is used to define a representative length scale, L , for the surface layer of the atmosphere,

$$L = \frac{-U_*^3 \, T_o}{kg \, \overline{w'T'}} \qquad (10)$$

where g = gravitational acceleration

T = ambient temperature

k = von Karman constant = 0.35

The selection of the Monin-Obukhov length as a stability scaling parameter is based on the assumption that friction velocity, U_* , and vertical heat flux ($\overline{w'T'}$) are constant in the surface layer. This scaling length, using dimensional analysis, leads to the development of a dimensionless function, $\phi_m(Z/L)$, which can be used to represent the mean horizontal wind variation with height, $d\bar{u}/dZ$, in the surface layer. The following expression is the empirical relationship for the wind shear in this development,

$$\frac{d\bar{u}}{dZ} = \frac{U_*}{kZ} \phi_m(Z/L) \qquad (11)$$

As vertical turbulent heat flux ($\overline{w'T'}$) decreases to zero, indicating neutral stability, $\phi_m(Z/L)$ must approach 1 if Equation (11) is to take on its expected form under neutral conditions. Assuming that convective mixing is negligible

under neutral conditions it follows that for values of ϕ_m (Z/L) near 1 or Z << 1 mechanical turbulence is of primary importance. Thus, the absolute magnitude of L becomes an indicator of the vertical extent to which mechanical turbulence controls the turbulent regime.

Observational experiments by Businger et al. (1971) produced a definite relationship between the Richardson number, R_i ,

$$R_i = \frac{g(\partial\theta_v/\partial Z)}{\bar{\theta}(\partial u/\partial Z)^2} \tag{12}$$

and the Monin-Obukhov length, L , where θ_v is the virtual temperature. The following expressions are approximations for the unstable and stable conditions respectively,

$$Z/L = R_i \tag{13}$$

$$Z/L = \frac{R_i}{1-\alpha R_i} \tag{14}$$

where α is an empirically derived constant equal to 0.5.

Of interest in this study is the rate of viscous molecular turbulent kinetic energy dissipation, ε . Wyngaard, et al. (1971) considered the dependence of ε on momentum fluxes and height in deriving the following empirical expression

$$\varepsilon = U_*^3/kZ\ \phi_\varepsilon\ (Z/L) \tag{15}$$

Since Z/L and R_i are functionally related, equations (11) and (15) can be rewritten as

$$\frac{d\bar{u}}{dZ} = \frac{U_*}{kZ}\ f_m\ (R_i) \tag{16}$$

and $$\varepsilon = U_*^3/kZ\ f_\varepsilon\ (R_i) \qquad (17)$$

where f_m and f_ε are stability corrections equal to 1 under neutral conditions. In near neutral conditions, the turbulent kinetic energy production is assumed to be equal to the rate of molecular dissipation of turbulent kinetic energy and from equations (16) and (17) the following relation is valid

$$\varepsilon = U_*^2(\partial\bar{u}/\partial Z) \qquad (18)$$

Assuming neutral conditions, the combinations of equations (16) and (18) yields

$$U_* = (\varepsilon kZ)^{1/3} \qquad (19)$$

Now the friction velocity U_* can be estimated from either mean wind profiles using the integrated form of equation (16) or from velocity fluctuation data involving turbulent energy dissipation by using equation (19). The latter approach is used in this study.

IV. DATA COLLECTION

A. DURATION AND LOCATION

Aerosol and meteorological data for this study were made available through Calspan Corporation, Buffalo, New York, from two separate experiments. During a ten day period in February 1977, Calspan Corporation provided limited meteorological and cloud physics support during a study of marine boundary layer phenomena conducted on the Gulf of Mexico (Mack and Katz, 1977). The experiment was performed on the Naval Coastal Systems Laboratory's (NCSL) offshore platform "Stage I" located approximately 20 km SW of Panama City, Florida as depicted in Figure 10.

A second experiment which provided data for this study was conducted along the coastal waters of Southern California (Figure 11) during a 12 day period in July 1977 aboard the Naval Postgraduate School (NPS) R/V Acania. Under contract from NPS, Calspan Corporation provided limited meteorological and aerosol physics support during a study of air quality parameters and marine boundary layer characteristics (Mack, 1977). This region contains primary shipping lanes and a number of drilling platforms all of which contribute to atmospheric contamination.

The following discussion will be limited to equipment used to measure the meteorological parameters actually analyzed in this study. A listing of the Panama City and

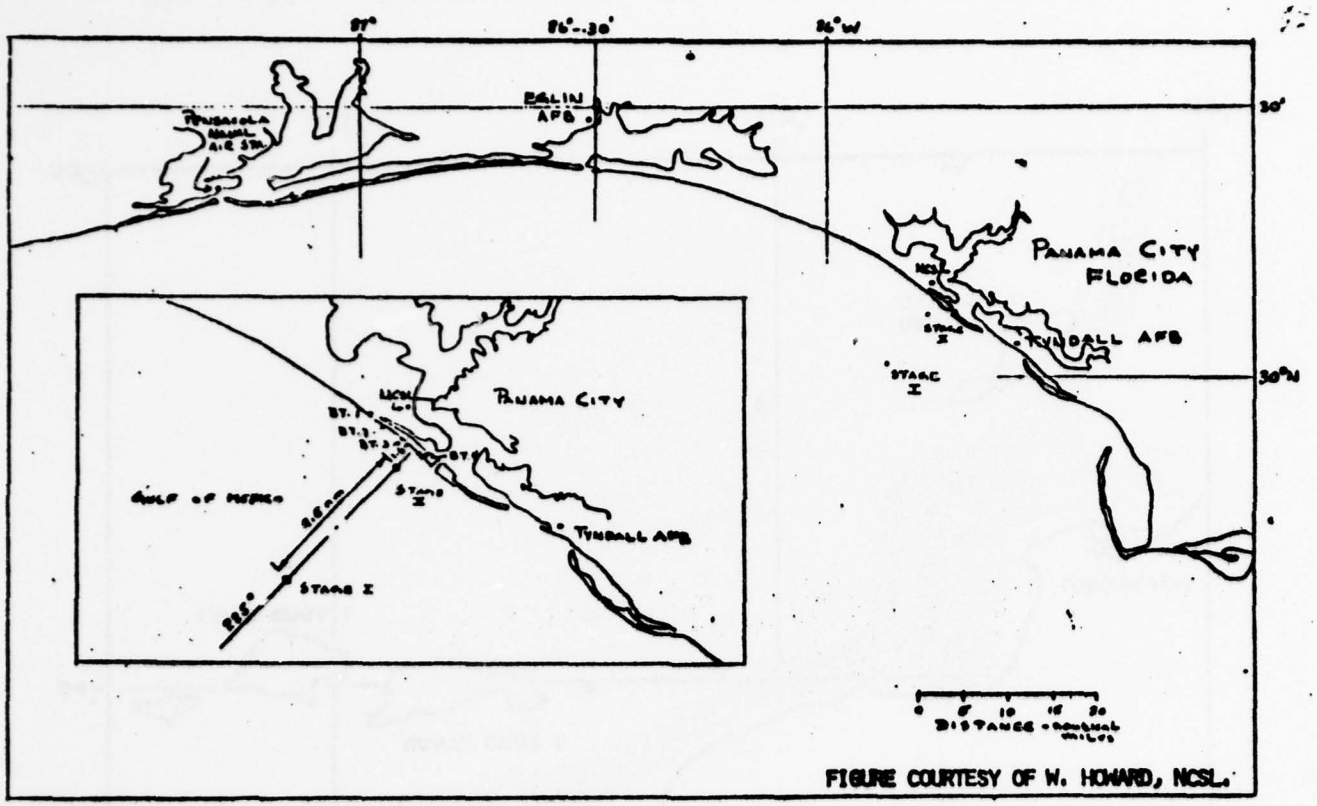

Figure 10. Location of NCSL Offshore Platform "Stage I"

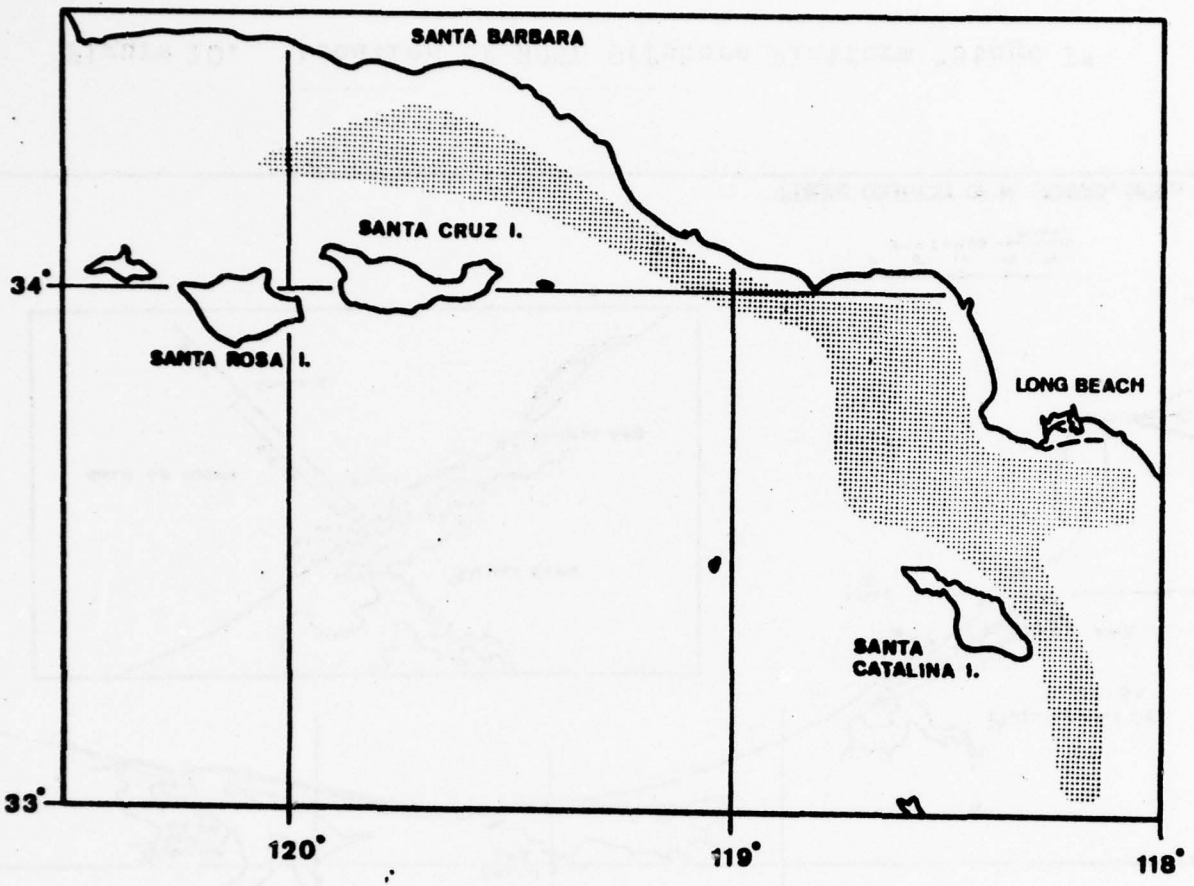

Figure 11. Location of Southern California Cruise

Southern California data may be found in Tables V and VI, respectively, at the end of the text.

B. PANAMA CITY INSTRUMENTATION

"Stage I" provided a stable platform for measuring the meteorological parameters necessary to describe and study the aerosol distribution and behavior in the marine boundary layer. The instrumentation installed by Calspan included a Sling Psychrometer, Bechman-Whitley wind system, Gardner small particle detector, and Royco Model 225 Particle Counter. The wind speed and direction was monitored continuously at the 20 meter level while wet and dry bulb temperatures were obtained hourly at the 17 meter level. A Foxboro temperature system (4 sensors) provided continuous temperature measurements at 4 levels; sea surface, 4.5, 9.0 and 24.5 meters. This data was recorded in an hourly log. Ten minute averaged aerosol size spectra were obtained continuously with the Royce counter at the 17 meter level, and a printout of aerosol concentration in 5 size intervals was provided every ten minutes. The Gardner Counter measured the concentration of particles greater than .0025 μ diameter on an hourly basis.

The majority of the time the Royco instrument operated in "threshold" mode where number concentration (per 2.8 liters) of particles greater than the following size ranges were measured: 0.5 μm, 0.7 μm, 1.4 μm, 3.0 μm, and 5.0 μm diameter. For a shorter period of time the instrument was operated in the "window" mode producing number concentrations between the

above size ranges. The particle counter and sensor are shown in Figure 12. The environmental air was drawn continuously through a sampling line of 3 meter length and 5 cm inside diameter. The flow rate through the counter's sensing volume was set at 2.8 liters per minute.

The Royco Model 225 sampler utilizes a near forward scattering optical system (Figure 13) which is ideal for monitoring large volumes of ambient gases where suspended particles can vary widely in composition, size, and optical properties. The aerosol is drawn through the sensor into a beam of focused light. As each particle passes through the illuminated volume, it scatters a pulse of light which is then detected by a photomultiplier tube. The photomultiplier output is then processed elctronically to produce a pulse height spectrum from which the particle size spectrum is deduced. The height of each pulse is proportional to the square of the diameter of the particle.

Whitby and Liu (1973) note that the important characteristics of an optical counter are the sampling flow rate and the size of the optical viewing volume. The sampling flow rate determines the minimum counting period needed to obtain a statistically accurate count, and the size of the optical viewing volume determines the maximum aerosol concentration the instrument can accept without loss of particle count due to "coincidence", i.e., the loss of particle count due to the presence of more than one particle in the optical viewing volume at the same time. The viewing volume of the Royco 225 is 4.0 mm^3 and the collection aperture half angle is 25 degrees.

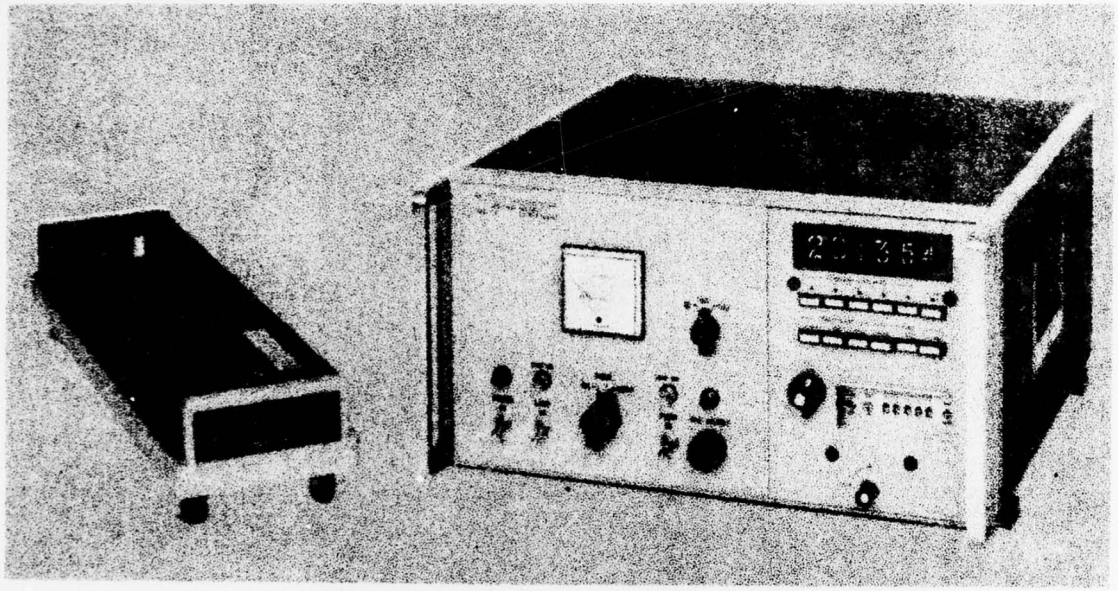

Figure 12. Royco 225 Particle Counter and Sensor

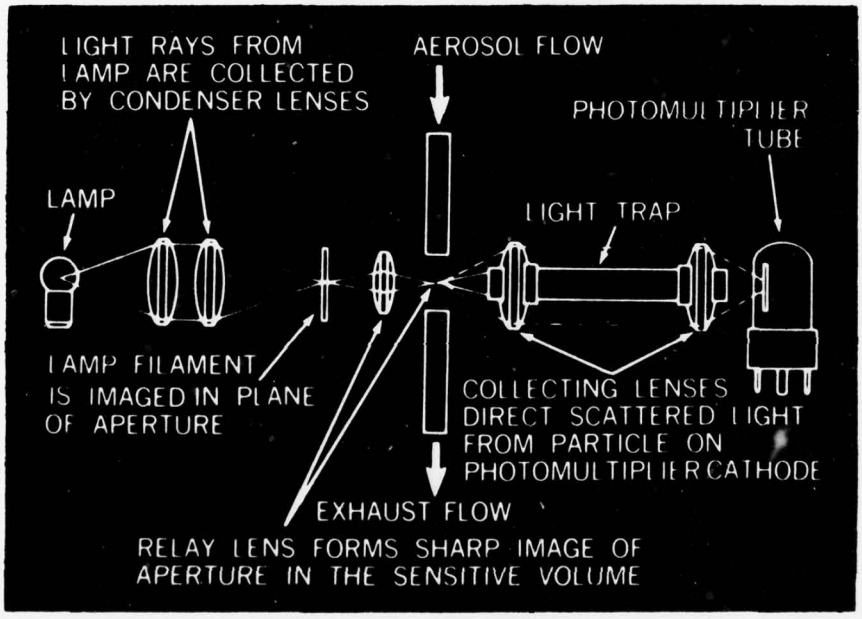

Figure 13. Near Forward Scattering Optical System

This model is also equipped with a sheath air inlet which diverts part of the aerosol stream through an external filter before reentry to the viewing volume. This sheath improves the performance of the instrument by preventing the recirculation of particles in the optical chamber and by confining the aerosol stream to a narrower region. Thus, the broadening of the pulse spectrum due to variation in illuminating intensity is reduced.

C. SOUTHERN CALIFORNIA INSTRUMENTATION

The location of the sensors aboard the R/V Acania are shown in Figure 14. Again, a Royco Model 225 Optical Particle Counter was used to measure the aerosol concentration of the coastal marine boundary layer. This instrument was operated continuously in the threshold mode where number concentration (per .28 liters) of aerosols greater than the following size ranges were measured: 0.3 μm, 0.6 μm, 1.2 μm, 3.0 μm, and 5.0 μm diameter. The mainframe and sensor were located near the bridge of the Acania with the origin of the sampling line positioned forward of the pilot house roof at a height of 7 meters above the sea surface. The sampling line was 6 meters long with an inside diameter of 5 cm. The air was sampled through the viewing volume at a rate of .28 liters per minute. A Gardner small particle detector was again used to measure the Aitken nuclei concentration.

A sling psychrometer was used to measure the wet/dry bulb temperatures and relative humidity determined from psychometric tables for a height of 5 meters. The mean wind

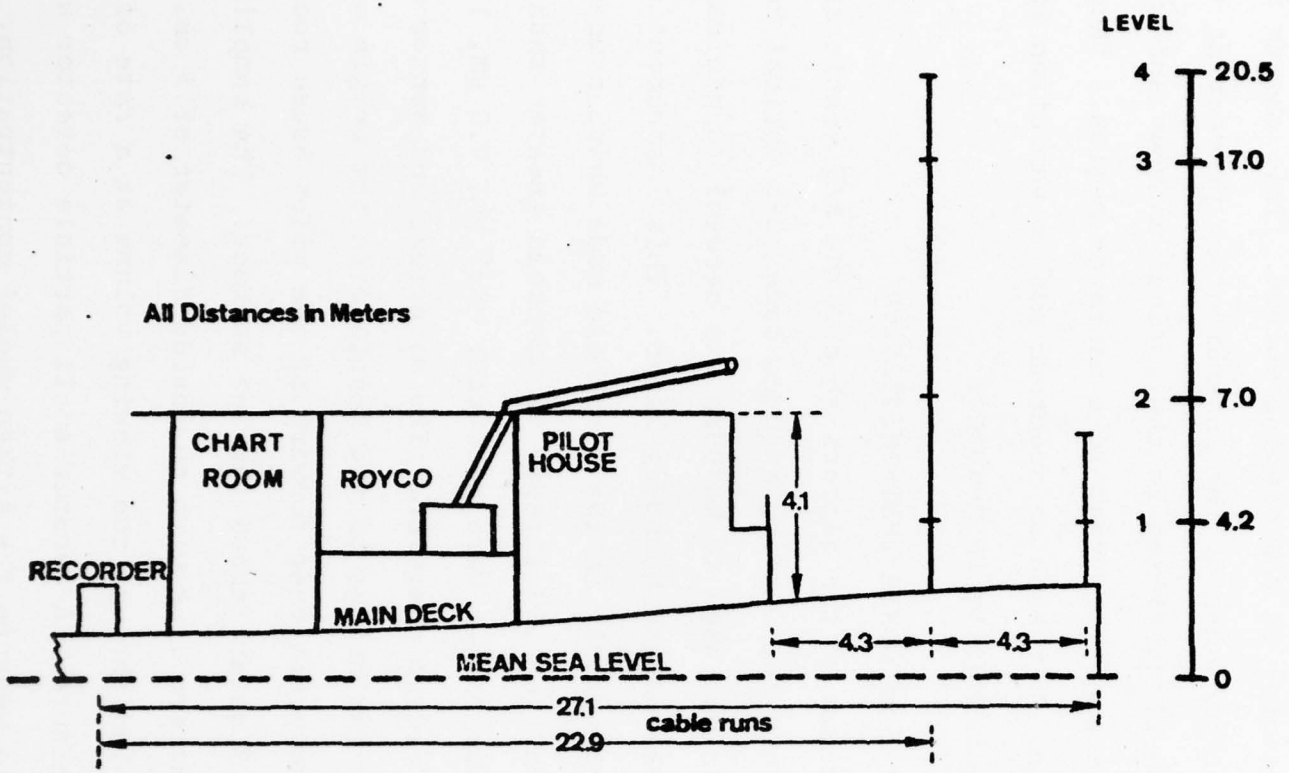

Figure 14. Sensor Locations on Board the R/V Acania

measurements were obtained at four levels using cup anemometer wind profile register systems supplied by the NPS. Calspan recorded the wind, humidity, and aerosol measurements in an hourly log.

Velocity fluctuation measurements were obtained with Thermo-Systems Model 1210 hot wire anemometer probes mounted with hot film sensors (platinum coated, 60 mil quartz fibers) installed by the NPS. The anemometer was a Thermo-Systems Model 1054B. The sensors were small enough to resolve the viscous dissipation scale without making corrections for wire length. Wind fluctuation data were recorded on a 14 channel tape recorder. The placement of these sensors required exceptionally long cable runs. Therefore, adjustments were made in the bridges for resistance and capacitance of the wirelength to insure a correct response.

The mean and fluctuation wind data were logged by the NPS developed MIDAS (Microprogrammable Integrated Data Acquisition System). This system is fully automated to sample the tailored list of sensors every 30 seconds and 20 minute averaged output values were printed.

AD-A054 239 NAVAL POSTGRADUATE SCHOOL MONTEREY CALIF F/G 13/2
EXPERIMENTAL INVESTIGATION OF THE MARINE BOUNDARY LAYER IN SUPP--ETC(U)
FEB 78 G E SCHACHER, C W FAIRALL
UNCLASSIFIED NPS61-78-002 NL

3 OF 3
AD
A054239

END
DATE
FILMED
6 -78
DDC

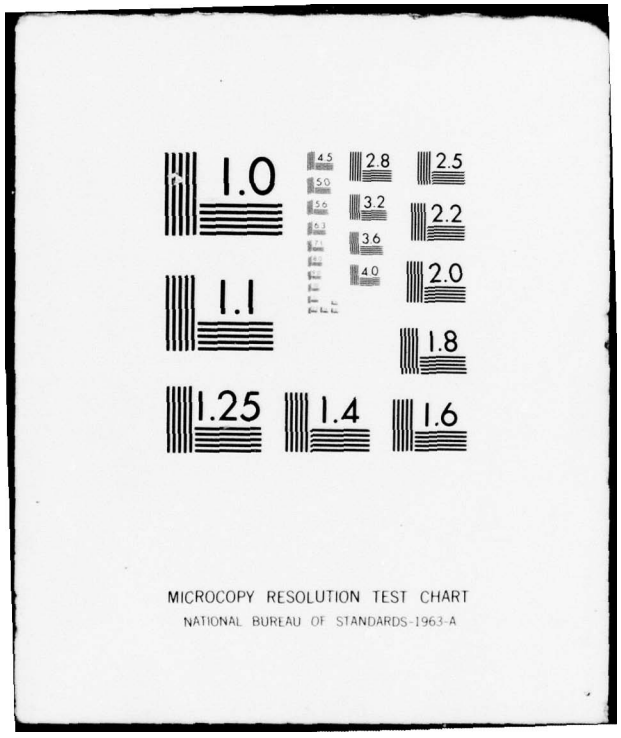
1.0
1.1
1.25
1.4
1.6
1.8
2.0
2.2
2.5
2.8
3.2
3.6
4.0
4.5
5.0
5.6
6.3
7.1
MICROCOPY RESOLUTION TEST CHART
NATIONAL BUREAU OF STANDARDS-1963-A

V. ANALYSES PROCEDURES

A. VELOCITY FLUCTUATION ANALYSIS

The dissipation of turbulent kinetic energy, ε , can be related to the mean wind velocity at any given level, $\bar{u}$, and the RMS value of the velocity fluctuation, $\overline{u'^2}$, in a frequency band specified by a lower frequency limit, f_ℓ , and an upper frequency limit, f_u (Fairall, et al., 1977). The relationship is

$$\varepsilon = \frac{(4/3)^{3/2} \, (u'_{RMS})^3}{(\bar{u}/2\pi)[f_\ell^{-2/3} - f_u^{-2/3}]^{3/2}} \qquad (20)$$

In this procedure recordings were made of both the cup anemometer wind speed and the corresponding hot wire voltage output. The sensor wind speed is given by

$$v = V_o^2 + B(\bar{u})^{\frac{1}{2}} \qquad (21)$$

where v is the hot wire voltage output, and V_o^2 and B are constants obtained by laboratory calibration using a TSI Model 1125 Calibrator. Differentiation of equation (21) produces the following relationship between the velocity fluctuation and the voltage fluctuation:

$$u'_{RMS} = \frac{4v(\bar{u})^{\frac{1}{2}}}{B} \, v'_{RMS} \qquad (22)$$

Substitution into equation (20) yields

$$\varepsilon = \frac{(4/3)^{3/2}[4\nu(\bar{u})^{1/2})/B]^3 \ (v'_{RMS})^3}{(\bar{u}/2\pi)[f_\ell^{-2/3} - f_u^{-2/3}]^{3/2}} \qquad (23)$$

Values of f_ℓ = 5 Hz and f_u = 200 Hz were selected for the cruise and since amplifiers with known gains, G , were required, further reduction leads to

$$\varepsilon = (3.53\text{x}10^3)[V_o^2 + B(\bar{u})^{1/2}]^{3/2}(\bar{u})^{1/2}[v'_{RMS}/BG]^3 \qquad (24)$$

The friction velocity, U_* , was then calculated from equation (19) for each of three levels and averaged to produce over 400 values from 19-27 July. Voltage fluctuation data from level 3 proved to be erroneous and were not included in the calculations. Obviously erroneous values of U_* owing to erratic behavior were also neglected. U_* values were then averaged about the aerosol observation times to correspond to a given aerosol distribution.

B. AEROSOL ANALYSIS

Analyses were performed on 215 aerosol samples during the SC cruise which were confined to the time period of the valid velocity fluctuation measurements. The observations included date and time, humidity, relative wind speed and direction, ship's speed and heading, Aitken concentration, and aerosol concentration as determined by the Royco 225 optical counter (Table VI). Wind and ship's speeds were recorded in knots.

The analyzed aerosol observations for the PC experiment were limited to 137 cases during the period 18-23 February. Cold frontal passage at approximately 0000Z, 24 February and subsequent advection of continental dust through 25 February were reasons for neglecting the aerosol samples for these days. Aerosol counts prior to 18 February were determined with the Royco instrument in the window mode and were not included in this study. Observations were generally made hourly and recorded in a log. They included date and time, humidity, wind speed and direction (knots), Aitken concentration, and data from the optical particle counter (Table V).

Computer programs were developed to plot the aerosol size distribution as a function of radius (R) in microns versus $dN/d \log R$ (cm^{-3}) where N is the number of particles greater than a given radius as measured by the Royco instrument. The program also included provisions to plot size distributions predicted by Fitzgerald's model. For this the observed relative humidity and wind speeds were used with equation (7). Initially the average aerosol distributions for both the SC and PC experiments were computed and compared to the respective predicted model distributions.

Subsequently, the variations in the average aerosol distributions with respect to four different categories of wind speed, relative humidity, and friction velocity were plotted for the SC data. The categories chosen for each of the above respective parameters are as follows: 0-2, 2-5, 5-8, 8-12 m/sec; 90-99, 80-90, 70-80, and 60-70 percent; and 0-.15, .15-.25, .25-.35, .35-.70 m/sec.

Friction velocity data was not available from the PC experiment; therefore, variations in the aerosol distributions were plotted with respect to categories of wind speed and humidity only. Because of essentially different meteorological conditions, the categories were chosen as follows: 0-3, 3-7, 7-10, and 10-15 m/sec; and 85-99, 70-85, 55-70 and 40-55 percent.

Visual inspection of these plots may indicate satisfactory relationships between the aerosol concentration and the above parameters. However, a statistical means of viewing these relationships was also deemed necessary. Wind speed, humidity, and U_* values were cross correlated with number concentration of particles in graduated size ranges. This procedure was accomplished by a Biomed Regression/Correlation computer program which produced corresponding correlation coefficients.

The nature of the diurnal variation of the aerosol concentration during the SC and PC experiments was investigated in this study. A computer program averaged the aerosol concentrations, wind speeds, humidities, and friction velocities about each hour and plots showing variations with time are produced. The aerosol plots depict the number of particles per cm^3 within specified size ranges versus time. The SC data produced curves representing the number of particles between the following size ranges: .15-.30 μ, .30-.60 μ, .60-1.5 μ, and 1.5-2.5 μ radius. Diurnal variation of concentration for the PC data utilized the following slightly different size ranges: .25-.35 μ, .35-.70 μ, .70-1.5 μ, and 1.5-2.5 μ radius.

Finally, diurnal variations of the aerosol size distribution for the SC and PC experiments were calculated using techniques similar to those described above. Average size distributions for the following two time periods were plotted: 0000-1200 hrs and 1200-2400 hrs.

C. ERROR ANALYSIS

The optical particle counter has an advantage over the membrane filter or impactor sampling techniques. For example, the latter require the samples to be taken to a lab for microscopic inspections and the aerosols may possibly be disturbed or altered due to contamination. Although the optical counter provides continuous "in situ" aerosol measurements, there are ample causes for counting errors. Because light scattering is a function of size, shape, and refractive index of the particles, careful calibration is necessary.

The Royco 225 model counter used in these experiments was calibrated using monodisperse latex spheres of known refractive index (1.6). Laboratory experiments by Lieberman and Allen (1969) showed a good correlation between the theoretical response curve for a near forward optical system and measurements using latex sphere and glass beads of refractive index 1.6 (Figure 15). Of most significance is the "fold" in the curve or zone of multi-valued response in the region of 1 μ diameter. Figure 16 is provided to illustrate how the response curve varies with particles of different refractive index. It is evident that when measuring particles of refractive index 1.6, a zone of ambiguity exists between

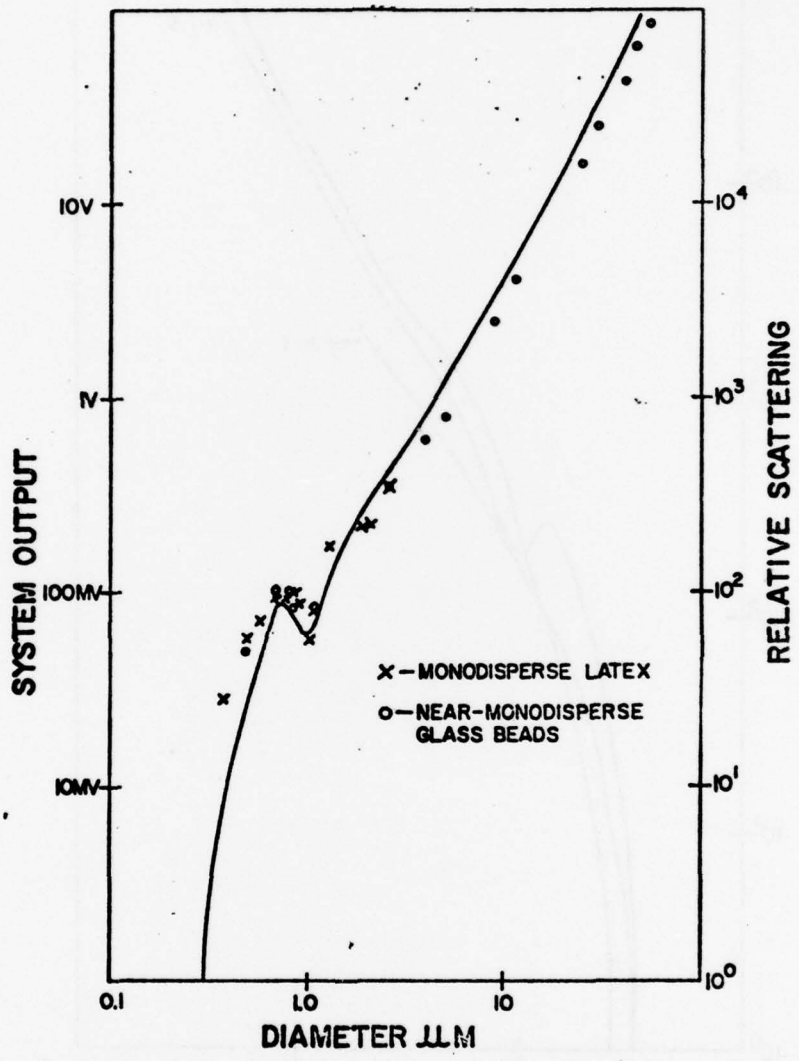

Figure 15. Theoretical Response Curve and Experimental Results for a Forward Scattering System

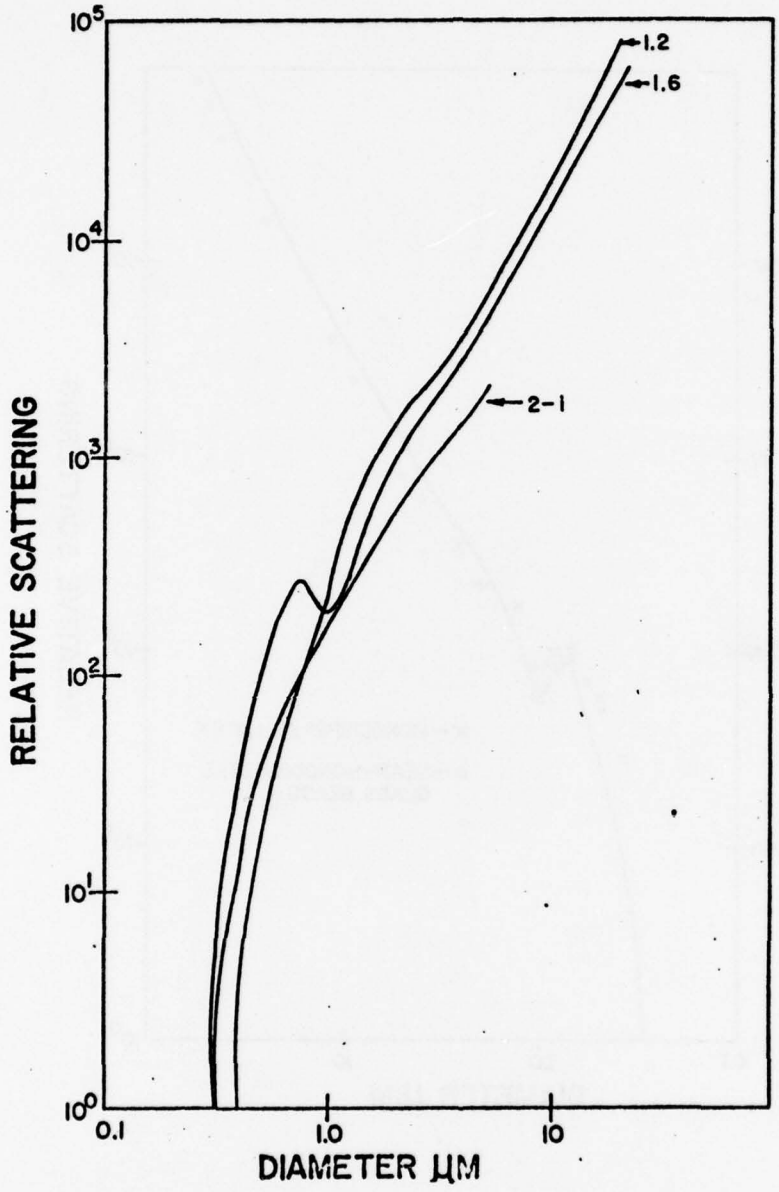

Figure 16. Dependency of the Response of a Forward Scattering System on Refractive Index

approximately .3 μ and .6 μ radius and may vary with the aerosol refractive index. Lieberman and Allen (1969) state that the instrument will still produce valid data if the zone is encompassed within a size range or channel. Since the SC counter measured between .3 μ and .6 μ radius and the PC counter between .35 μ and .70 μ radius, it is assumed that this multi-valued zone is compensated for.

Counting errors can also arise from flow rate considerations. If the particle sizes are large and the number of particles small, enough particles must be counted to obtain good statistical resolution. When a small random number of particles is counted, the statistical error in counting is equal to the ratio of 1 over the square root of the number of particles counted (Zinky, 1962). The counter should be operated over a longer time period (10 minutes) to sample a larger volume or an increase in the flow rate will reduce the error. It then seems quite possible that the flow rate of the counter used in the SC cruise (.28 liter/min) provided too small of a sampling volume to obtain an accurate count of the larger particles.

Zinky (1962) also states that a vertically aligned inlet tube is recommended to prevent any deposition in the line due to settling. It has already been mentioned that the sampling lines used in each experiment were considerably long and aligned horizontally. Many of the larger particles may not have remained airborne long enough to reach the illuminated volume.

Errors in the calculation of the friction velocity may have come from various sources. Since calculation of U_* from Equation (19) is only valid for near-neutral conditions, any substantial departure of the Richardson number from zero would result in inaccurate values. The measurement of the dissipation of turbulent kinetic energy was large dependent on the accuracy of the voltage output. The signal response is sensitive to electromagnetic energy, and any local radio or radar transmission may introduce noise to the system. Additionally, under the light wind conditions which prevailed on the SC experiment, the lateral motion of the anemometers due to ship pitch and roll may have resulted in erroneously high readings.

VI. RESULTS

The data from the Southern California (SC) cruise proved to represent an atmosphere somewhat different from a typical marine environment. The Aitken particle population averaged almost 8500 cm^{-3} which is about 4 times higher than that observed by Hidy, et al. 130 km west southwest of Los Angeles. This high concentration is suspected to be due to a combination of pollution from merchant ships' exhaust, combustion from the drilling platforms, and offshore flow from the nearby populated coastal cities.

The average wind speed and relative humidity were 3 m/sec and 86 percent, respectively. This data was used to compute the prediction from Fitzgerald's model (Eq. 7) which is compared to the average SC distribution in Figure 17. The vertical bars represent one standard deviation either side of the mean. There is generally good agreement between the two below .4 μ radius, with a larger experimentally observed concentration above this range. Although sea-salt production should have been minimal during this time period because of low wind speeds, the characteristic hump at around 1 μ, to a certain extent, reflects the contribution by sea salt nuclei. A similarity exists here with Moore and Mason's (1954) observation of a discontinuity where the slope changes and becomes rather steep in the region of the larger size range. The larger concentration in this range may be solely

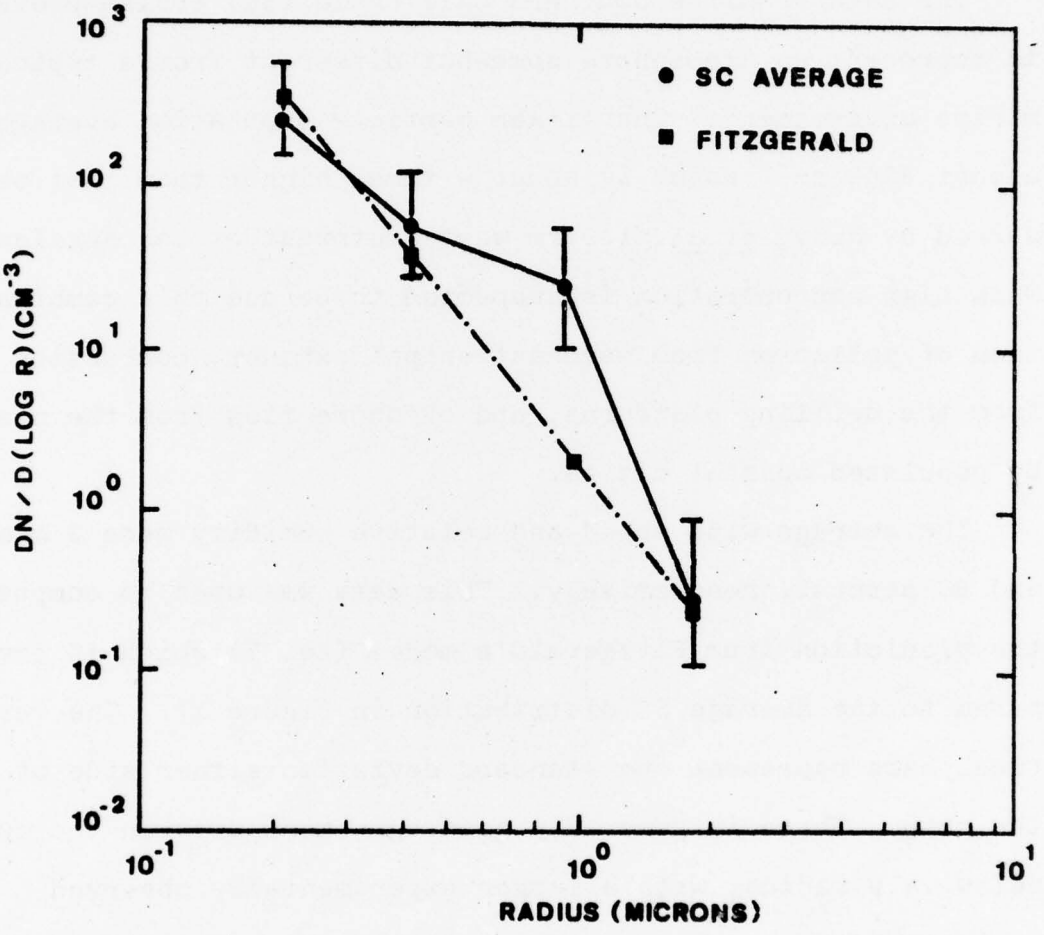

Figure 17. Average Aerosol Size Distribution for the SC Experiment and Distribution Predicted by Fitzgerald's Model

due to the influence of atmospheric contaminants such as combustion by-products, soil dust, or smoke. Considering previous experiments, this range does indeed contain a mixture of both continental and marine aerosols possibly resulting in the increase over Fitzgerald's model.

As previously mentioned, the low flow rate of the optical counter may account for the low concentrations at 2 μ. However, since the wind speed reached 8 m sec^{-1} only 6 times, this may have been a truly representative concentration of droplets as agreement is also shown with Fitzgerald's curve.

Figure 18 presents the synoptic situation for three days at the beginning, middle, and end of the experiment. A persistent thermal low is located in the desert area of Southern California and the isobaric pattern off the coast reflects a rather weak gradient. Therefore, smaller scale circulations should prevail in this area of little or no synoptic forcing.

Plots showing the variations of the average distributions with respect to wind speed, relative humidity, and friction velocity (U_*), are shown separately in Figures 19, 20, 21. The number of observations in each category is placed in parentheses. These figures indicate that the size distribution has a better relationship with the relative humidity than to the wind speed and U_* . Correlation coefficients between these parameters and the number concentration of particles in a given size interval are produced in Table II. Since diurnal variations tend to reflect a negative relationship between relative humidity and wind

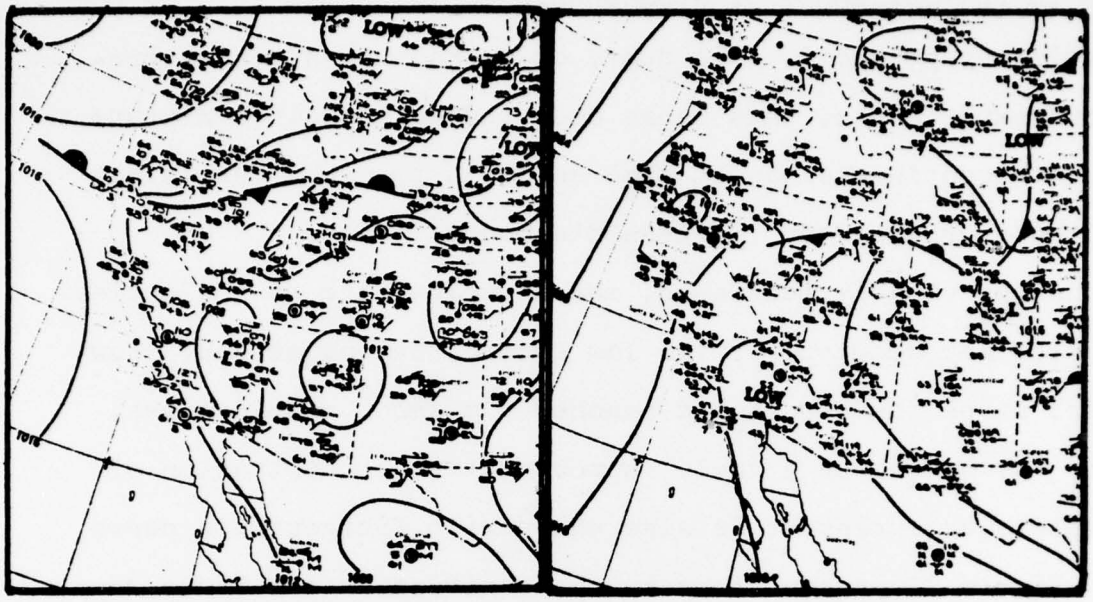

19 JUL

23 JUL

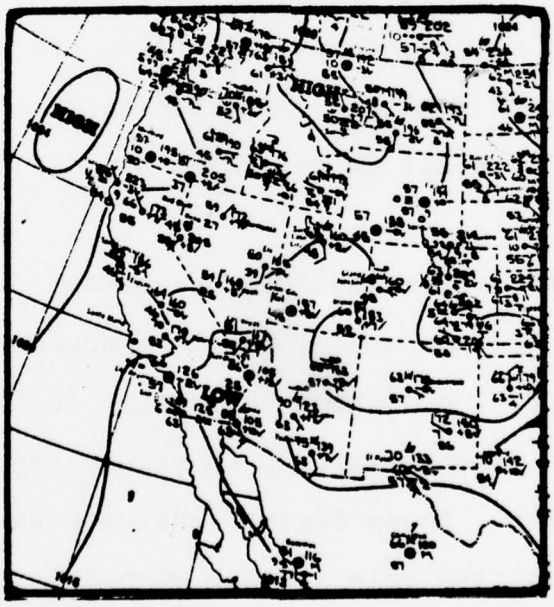

26 JUL

Figure 18. Synoptic Situation during the SC Experiment

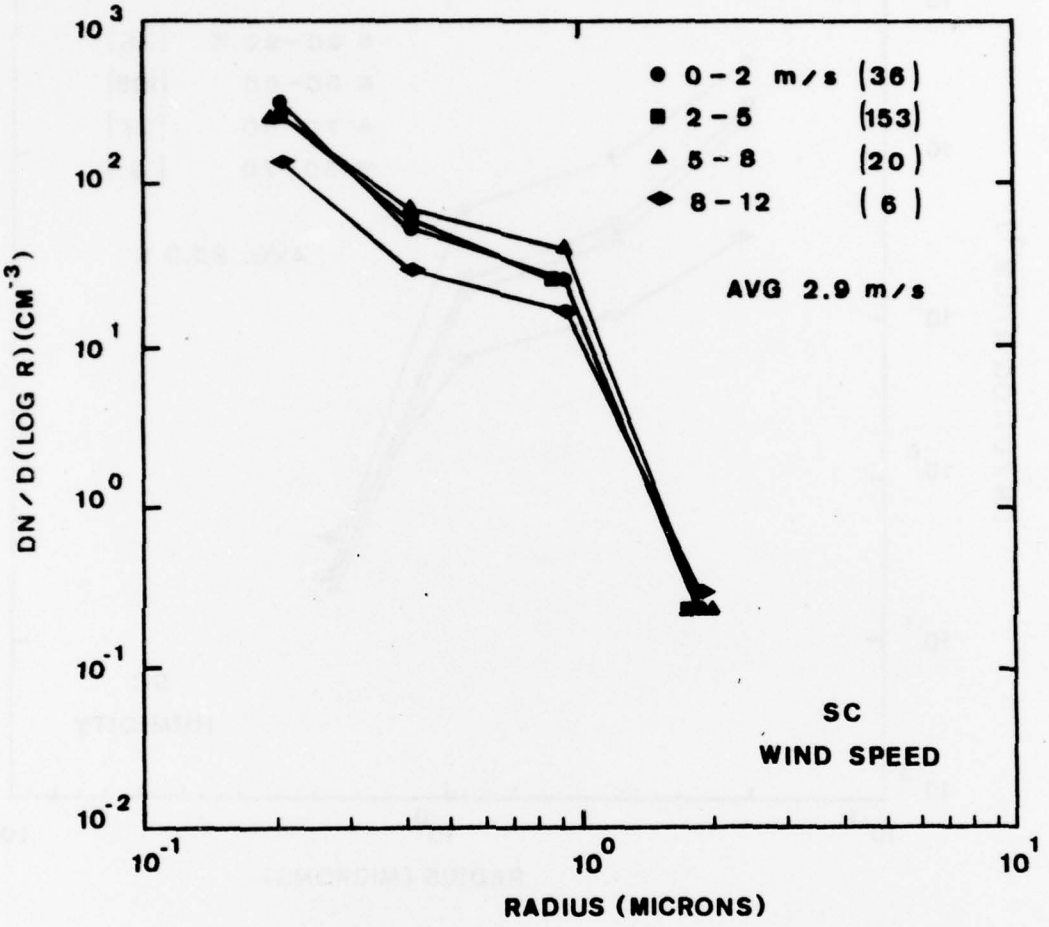

Figure 19. Variation of SC Size Distribution with Wind Speed

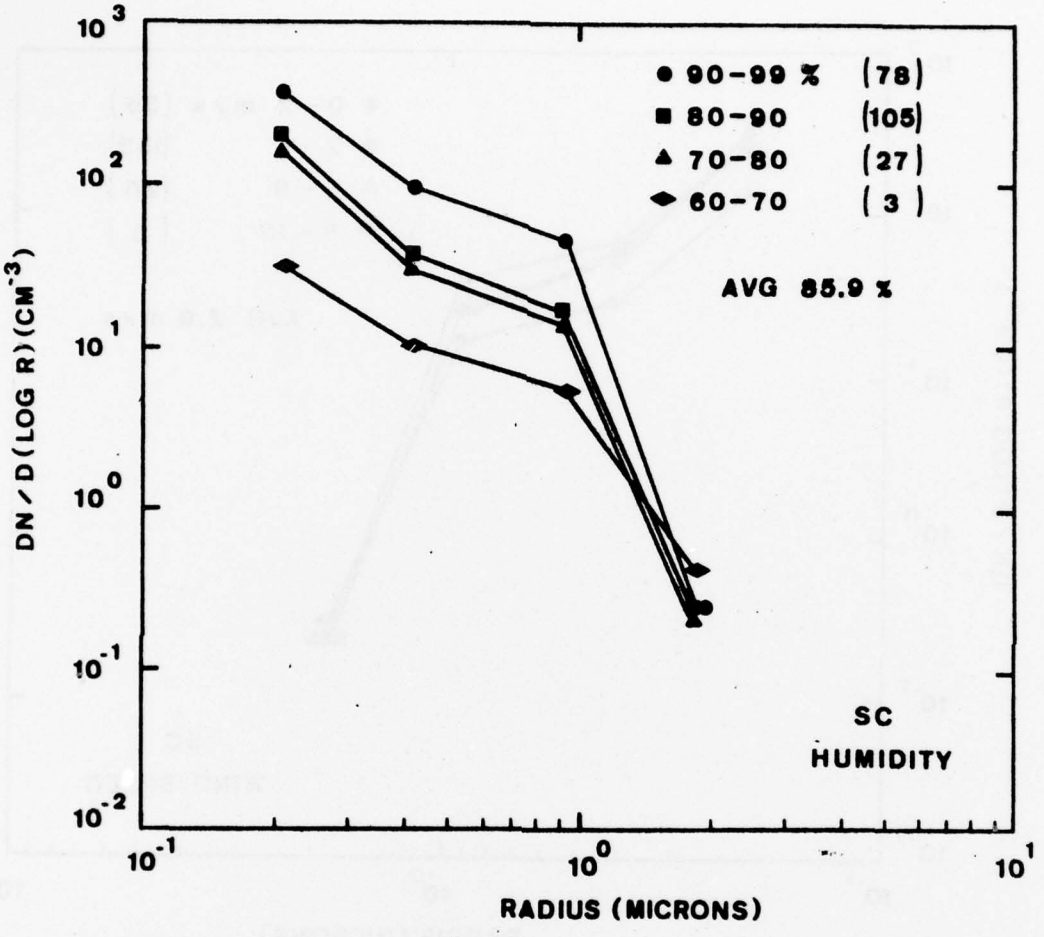

Figure 20. Variation of SC Size Distribution with Relative Humidity

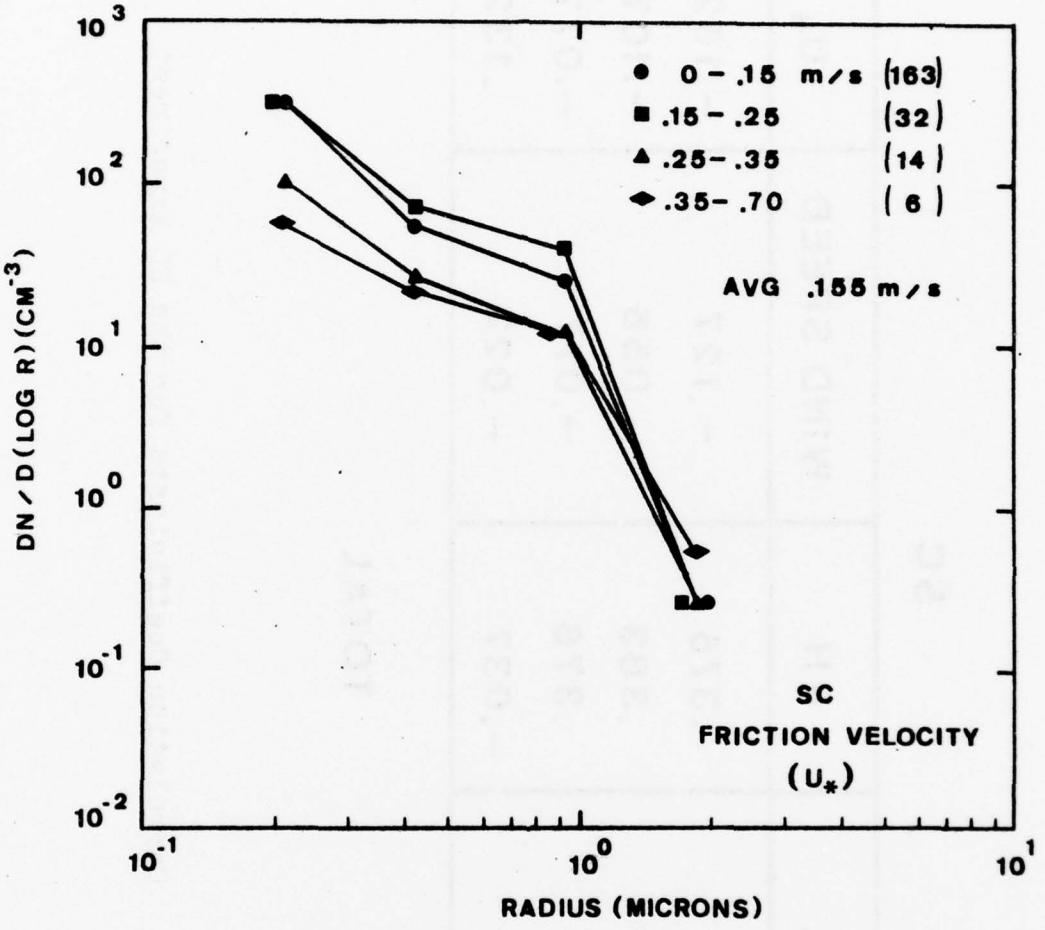

Figure 21. Variation of SC Size Distribution with Friction Velocity

SC

INTERVAL	RH	WIND SPEED	U_*
.15 – .30 μ	.375	–.127	–.162
.30 – .60 μ	.383	–.056	–.107
.60 – 1.5 μ	.376	–.017	–.077
1.5 – 2.5 μ	–.037	–.022	.132

TOTAL

Table II. Correlation Coefficients for the SC Experiment

speed, the results in this table are not surprising. The negative correlation of relative humidity with the concentrations in the large size range indicates that sedimentation of large droplets, which grow with increasing humidity, is most important when the wind speed and sea surface production of salt nuclei are weak. Although these larger droplets also exhibit a small positive correlation with U_* while the wind speed correlation remains negative, this result does not appear to be significant.

An attempt was made to examine the influence of stability on the size distribution. The summer months are characterized by the occurrence of stratus and fog off-shore below the marine inversion. Two days are compared with the assumption that they represent the unstable and stable atmospheres. According to the daily observation log, stratus clouds in the morning becoming stratocumulus by afternoon were observed on 19 July. 26 July was characterized by clear skies. The average distribution for both days is presented in Figure 22. The correlation coefficients between concentration and wind speed and U_* show a trend toward positive values from the stable to the unstable day with U_* eventually becoming positively correlated in the unstable day (Table III). The increase in the size distribution on 26 July in the size range greater than .3 μ seems to be due to increase in the average wind speed and occasional gustiness as whitecaps were reported during the afternoon. The stable stratification assumed in this case allows generated sea-salt nuclei to accumulate and the concentration to increase at the 7 meter

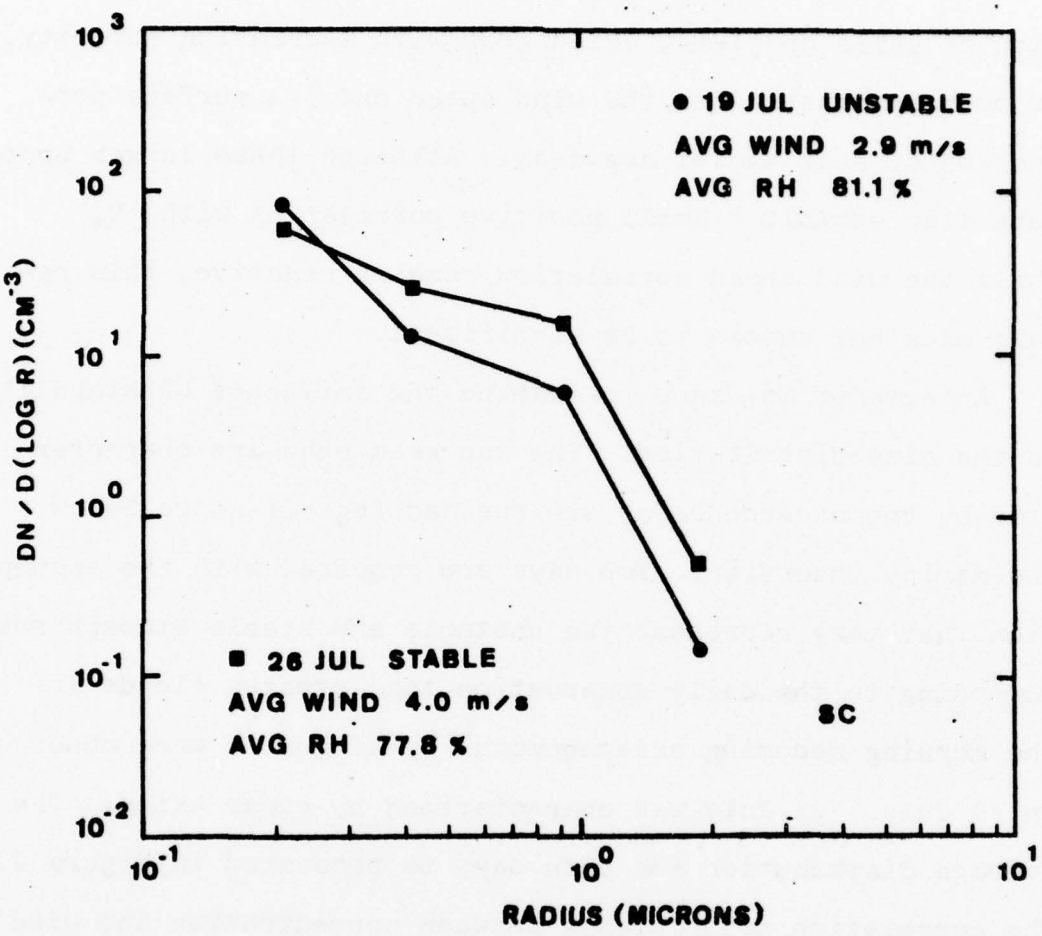

Figure 22. Average Size Distributions on 19 July and 26 July

SC

INTERVAL	RH	WIND SPEED	U_*
.15 – .30 μ	.814	–.205	.129
.30 – .60 μ	.837	–.184	.165
.60 – 1.5 μ	.792	–.110	.147
1.5 – 2.5 μ	–.104	–.049	.075

19 JUL UNSTABLE

SC

INTERVAL	RH	WIND SPEED	U_*
.15 – .30 μ	.610	–.395	–.372
.30 – .60 μ	.754	–.499	–.535
.60 – 1.5 μ	.835	–.615	–.634
1.5 – 2.5 μ	.355	–.413	–.273

26 JUL STABLE

Table III. Correlation Coefficients for 19 July and 26 July

level. The lower average wind speed associated with the unstable period does not allow for much sea-salt production. An unstable atmosphere can lead to convective processes which may vertically transport aerosols and create higher concentrations at an upper level as proposed by Ericksson (1959) and Toba (1965a & b). Hence, a decrease in the size distribution on 19 July is observed. This evidence gives credence to the possibility that friction velocity is a better indication of aerosol size distribution than wind speed. On both days the correlation of the concentration with humidity is lowest in the largest size interval. This relationship is most pronounced on the unstable days and may be explained by sedimentation due to mixing and resulting increased coalescence.

The averaged diurnal variations of wind speed, relative humidity, friction velocity, and aerosol concentration are shown in Figures 23, 24, and 25. Again the negative relationship of aerosols to wind speed and U_* in the size range of generally less than 1 μ is indicated. A satisfactory relationship with relative humidity is not evident and this is probably due to transport by a secondary circulation. A land-sea breeze type of effect could account for the observed decrease in concentration of the particles smaller than 1.5 μ. As the heating over the land generates an on-shore flow along the coast, the wind increases and persists through the afternoon. The average wind direction derived from the observations of five random days during the experiment is shown in Figure 26. A westerly wind is

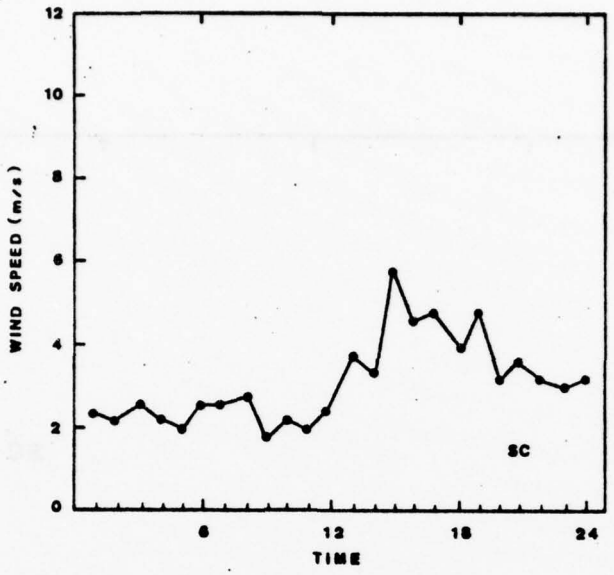

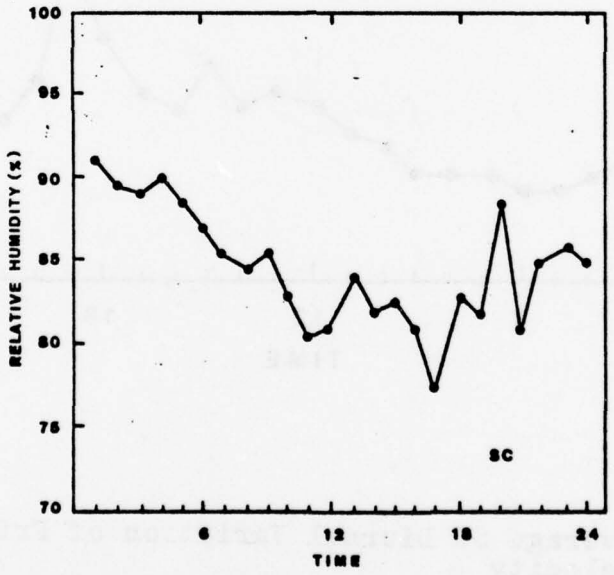

Figure 23. Average SC Diurnal Variations of Wind Speed and Relative Humidity

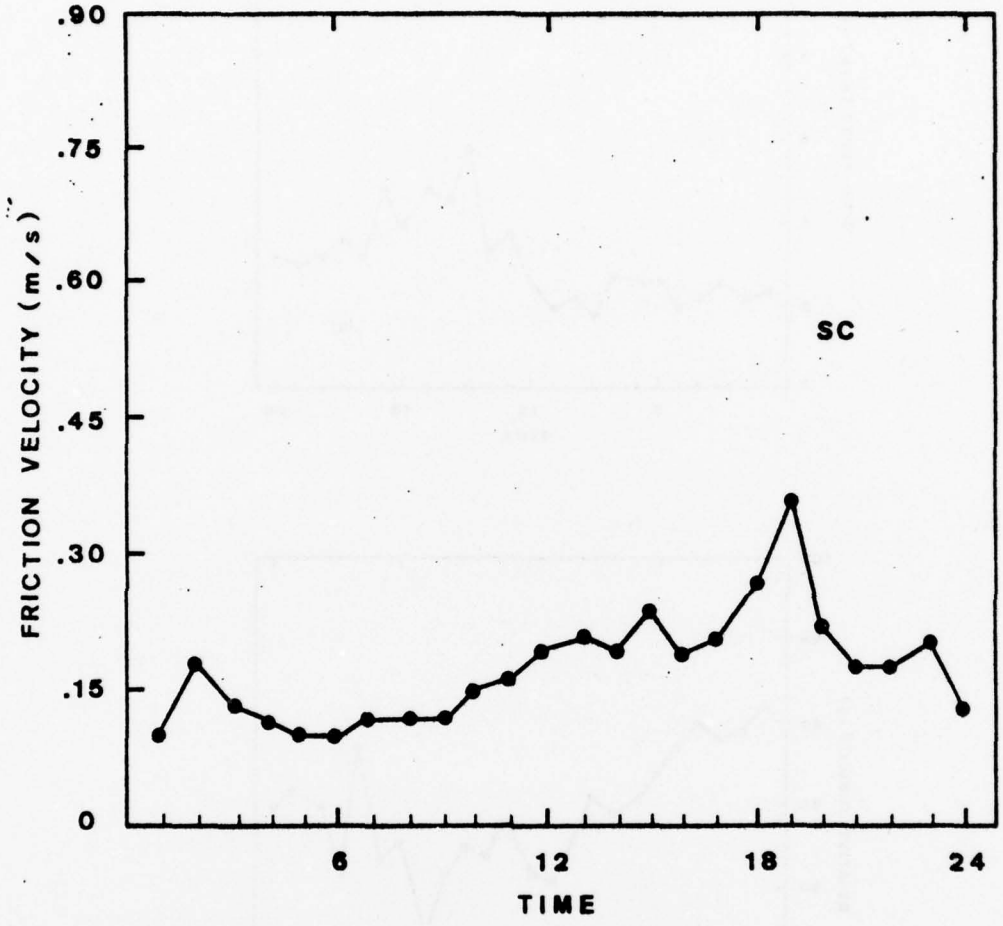

Figure 24. Average SC Diurnal Variation of Friction Velocity

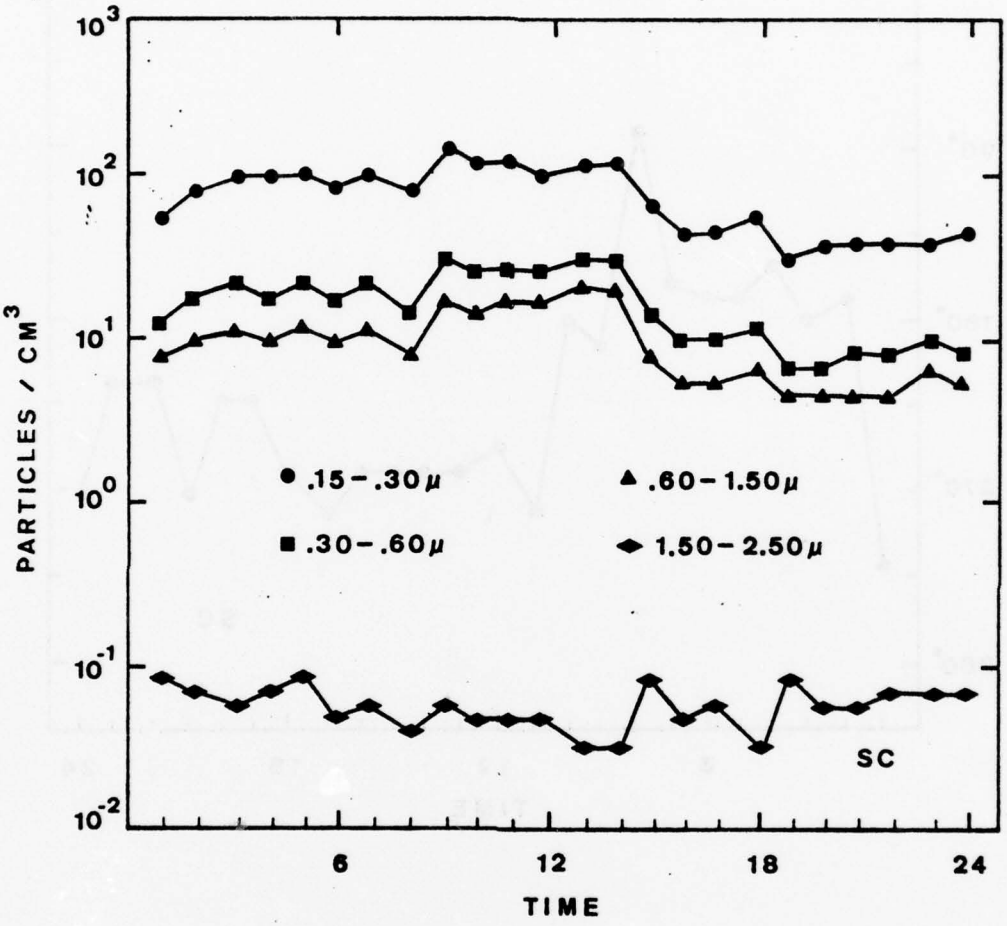

Figure 25. Average SC Diurnal Variations of Particle Concentrations

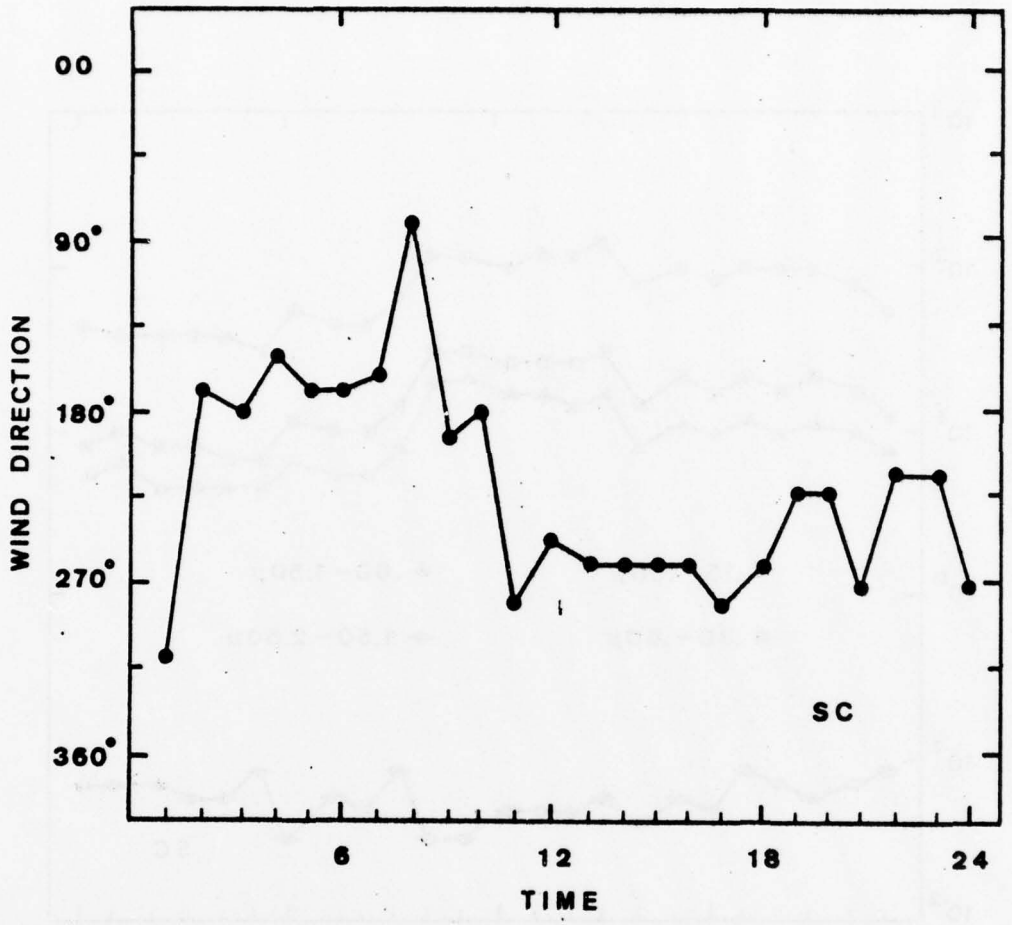

Figure 26. Average SC Wind Direction

seen to dominate during the peak wind periods. The decrease in the aerosol population may be explained by a horizontal divergence effect in the marine boundary layer as largest accelerations are found near the coast. The average size distributions displayed in Figure 27 reflect the decrease in the aerosol population due to this sub-synoptic circulation. Although the relative humidity increases slightly in the early evening hours, the smaller nuclei show a stronger relationship with the wind speed. This again implies that a large part of the coastal marine aerosol is of continental origin. The outflow of circulation aloft is probably responsible for the introduction of continental particulates to the marine environment. The minor peaks in the small particle concentration and also the somewhat greater increase in the large particles during the afternoon should be attributed to sea-salt production.

The Panama City (PC) observations more closely resembled a marine environment. The Aitken particle count was lower and averaged 2600 cm^{-3} while the distribution curve showed a marked change from the Southern California data. Winter time synoptic scale features predominate in this region of the Gulf Coast. Cold frontal passages and an accompanying influx of continental air into the Gulf of Mexico are frequent occurrences. Subsequent movement of the high pressure ridge into Florida and off its eastern seaboard provides the circulation which reestablishes moist southerly flow and return of the marine aerosol. Figure 28 provides the synoptic analyses for the period of the experiment. Stable

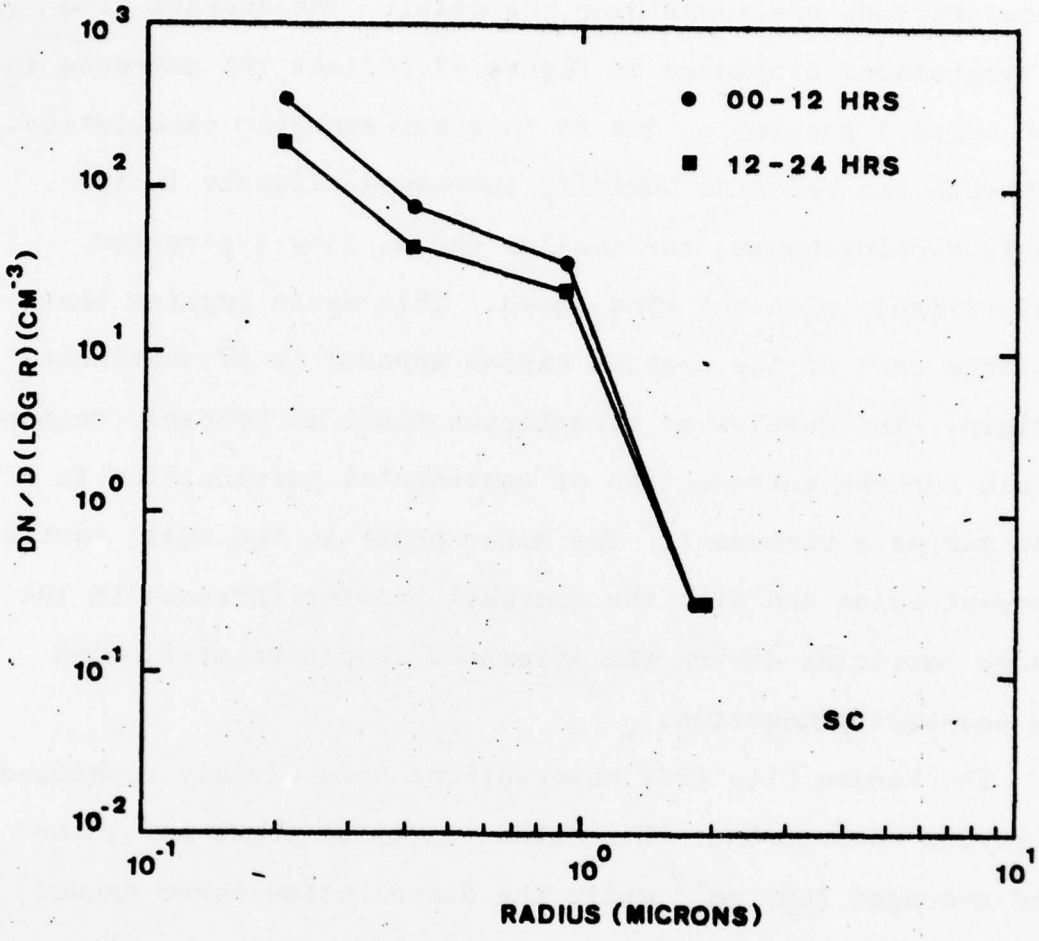

Figure 27. Average SC Diurnal Variation of the Aerosol Size Distribution

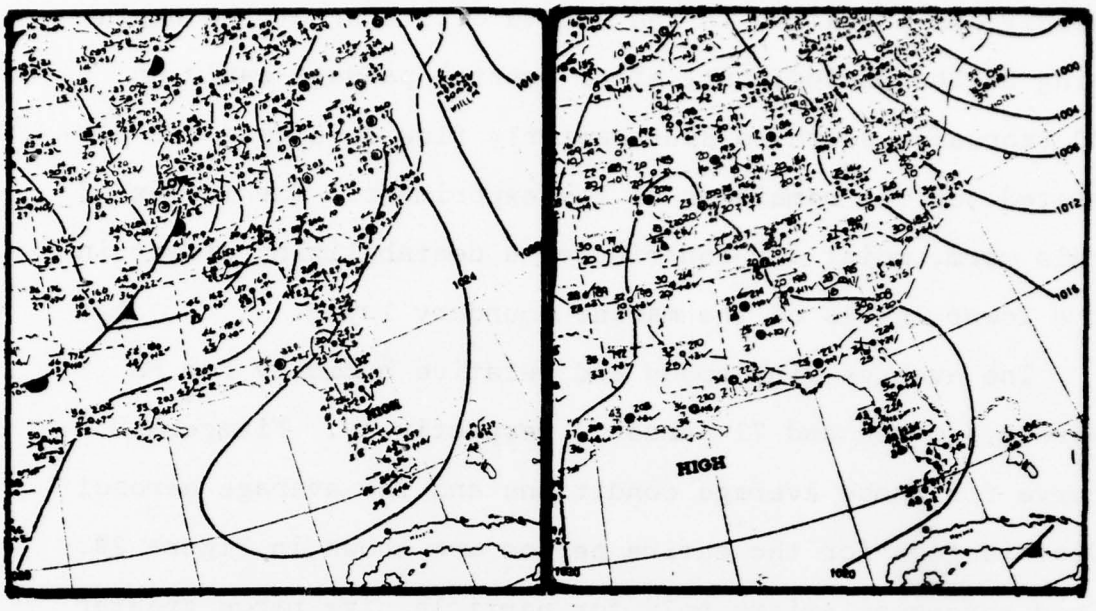

18 FEB

21 FEB

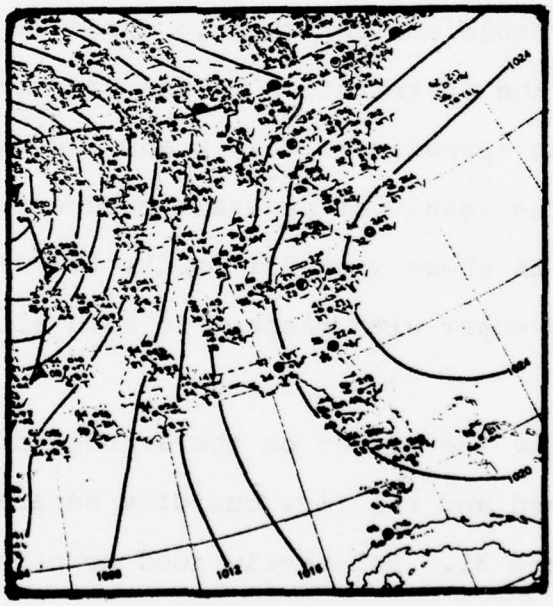

23 FEB

Figure 28. Synoptic Situation during the PC Experiment

conditions prevailed in the Panama City area at the beginning of the period; but, after frontal passage early on 20 February, south to southeasterly flow developed and persisted for the remainder of the experiment. The influx of this warm, moist air contributed a destabilizing effect in the lower levels of the marine boundary layer.

The average wind speed and relative humidity for PC were 8.4 m/sec and 71 percent, respectively. Fitzgerald's curve for these average conditions and the average aerosol distribution for the entire period are shown in Figure 29. Good agreement exists only for particle size range greater than .9 μ radius. The observed concentrations are approximately an order of magnitude lower than Fitzgerald's prediction for aerosols smaller than .5 μ radius. A significant aspect of the distribution is the positive slope observed between approximately .5 μ and 1 μ radius which appears to be the result of sea-salt production. Actually, good agreement is shown with Blifford's (1970) observation off the Pacific coast with respect to both slope and number concentration.

Plots showing the effect on the average distributions due to wind speed and relative humidity separately are shown in Figures 30 and 31. Relatively good correlations seem to exist between these parameters and the aerosol distributions. Correlation coefficients are presented in Table IV. The synoptic scale effects predominate over diurnal variations and wind speed and relative humidity are both positively correlated to the concentration. The highest correlation of

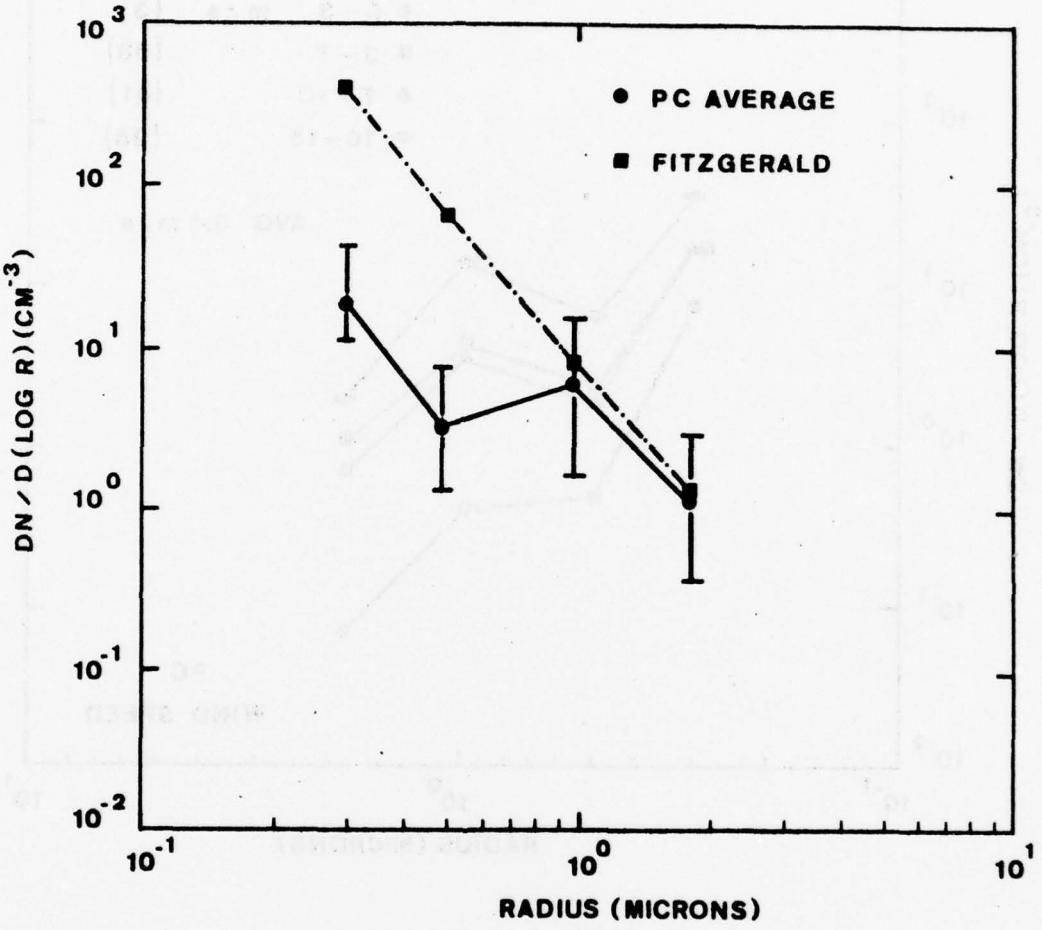

Figure 29. Average Aerosol Size Distribution for the PC Experiment and Distribution Predicted by Fitzgerald's Model

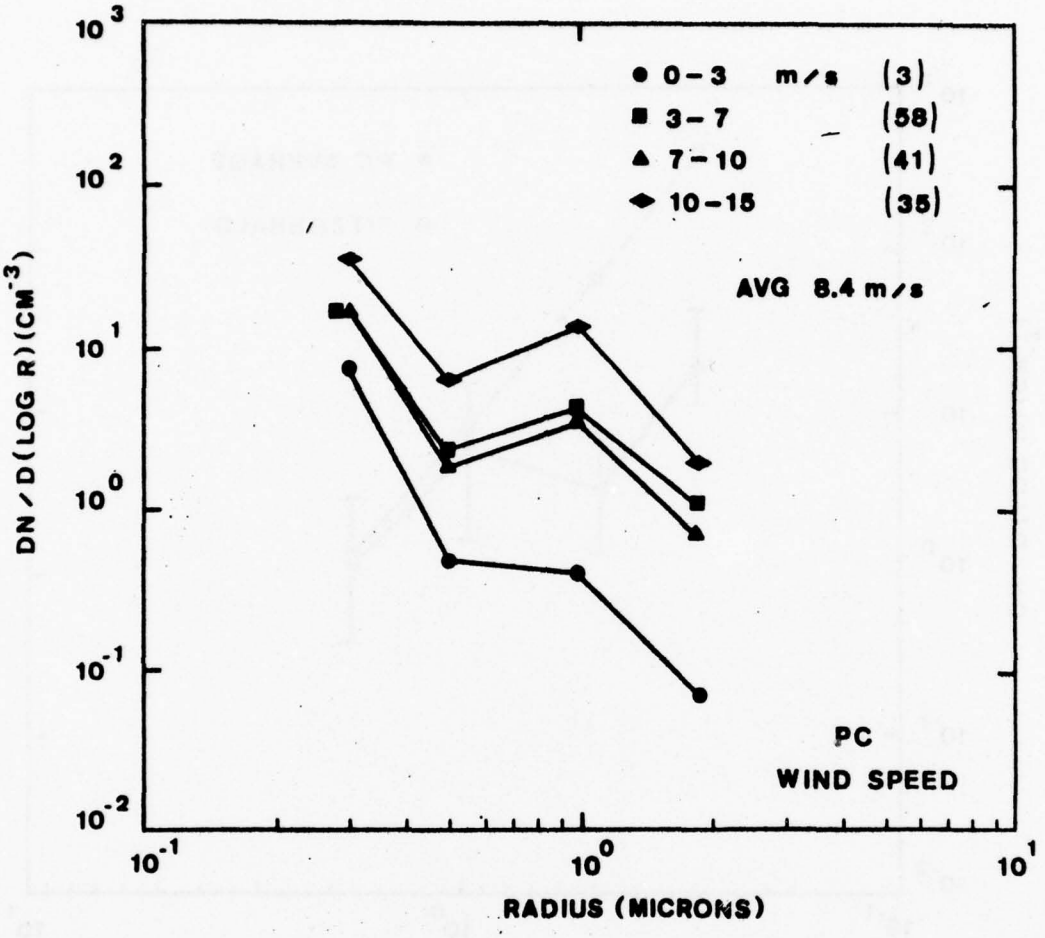

Figure 30. Variation of PC Size Distribution with Wind Speed

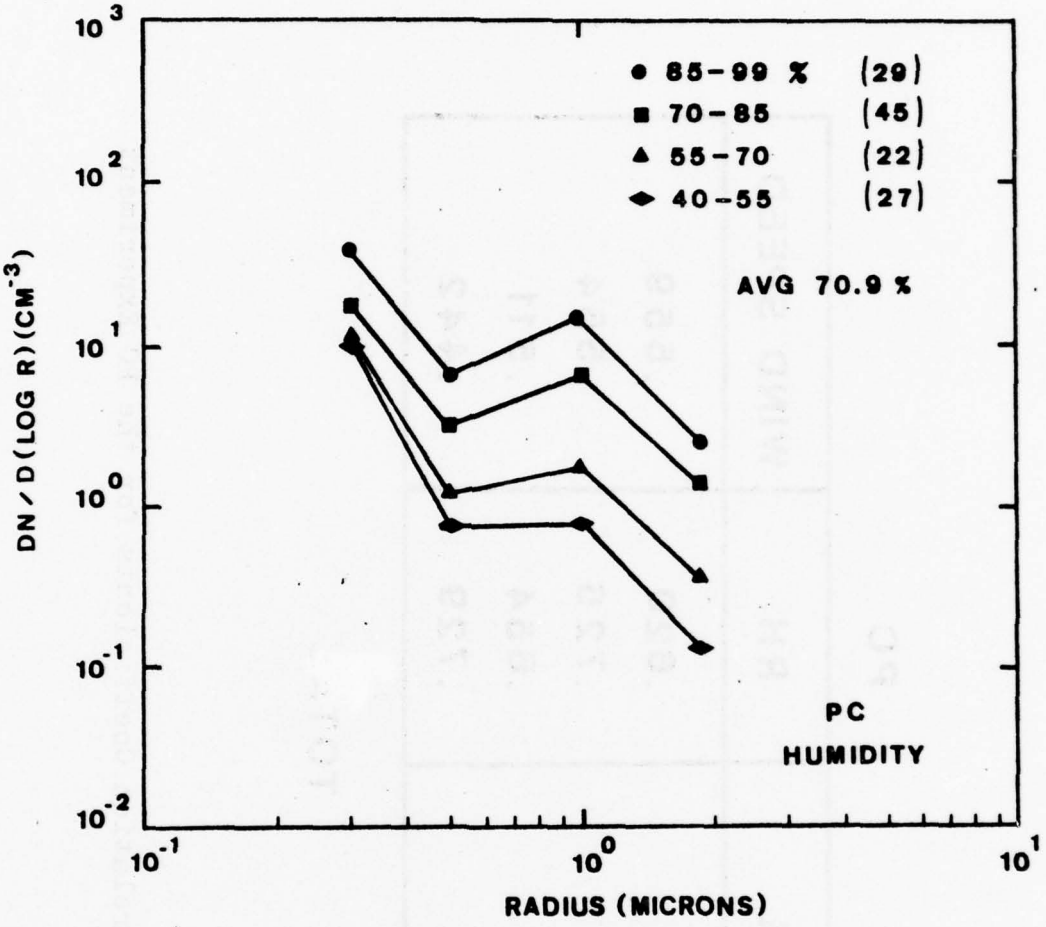

Figure 31. Variation of PC Size Distribution with Relative Humidity

PC

INTERVAL	RH	WIND SPEED
.25 – .35 μ	.620	.559
.35 – .70 μ	.726	.554
.70 – 1.5 μ	.654	.511
1.5 – 2.5 μ	.729	.442

TOTAL

Table IV. Correlation Coefficients for the PC Experiment

concentration to humidity at Panama City is witnessed in the 1.5 μ to 2.5 μ interval. This result may indicate that equilibrium tends to exist between production and sedimentation in this interval as hypothesized by Moore and Mason (1954). Disagreement exists in that the steeper negative slope is found during periods of strongest wind. The plot showing the effect of relative humidity on the size distributions results in small variations in the .25 μ - .35 μ interval. This probably indicates that the majority of these particles represent a mixture of continental and marine nuclei.

The stability influence was investigated by comparing observations on 18 February and 21 February. Temperature measurements at various levels on the platform made it possible to examine the lapse rates and determine the stability. The average distributions for these days grouped according to wind speed, and respective correlation coefficients are shown in Figures 32 and 33. The low humidities on 21 February resulted from the earlier intrusion of continental air, but southeast to southwest flow persisted most of the day. Although this trajectory helped to advect in warmer air, production of sea-salt dropped off as the wind decreased considerably below 7 m/sec. A much larger decrease is observed in the distribution curve on 21 February as compared to 18 February when the wind speed decreased below 7 m/sec. This agrees well with Moore's (1952) finding that the change in opacity is well marked during periods of low humidity. Also the decrease in the slope of the curve between .5 μ and

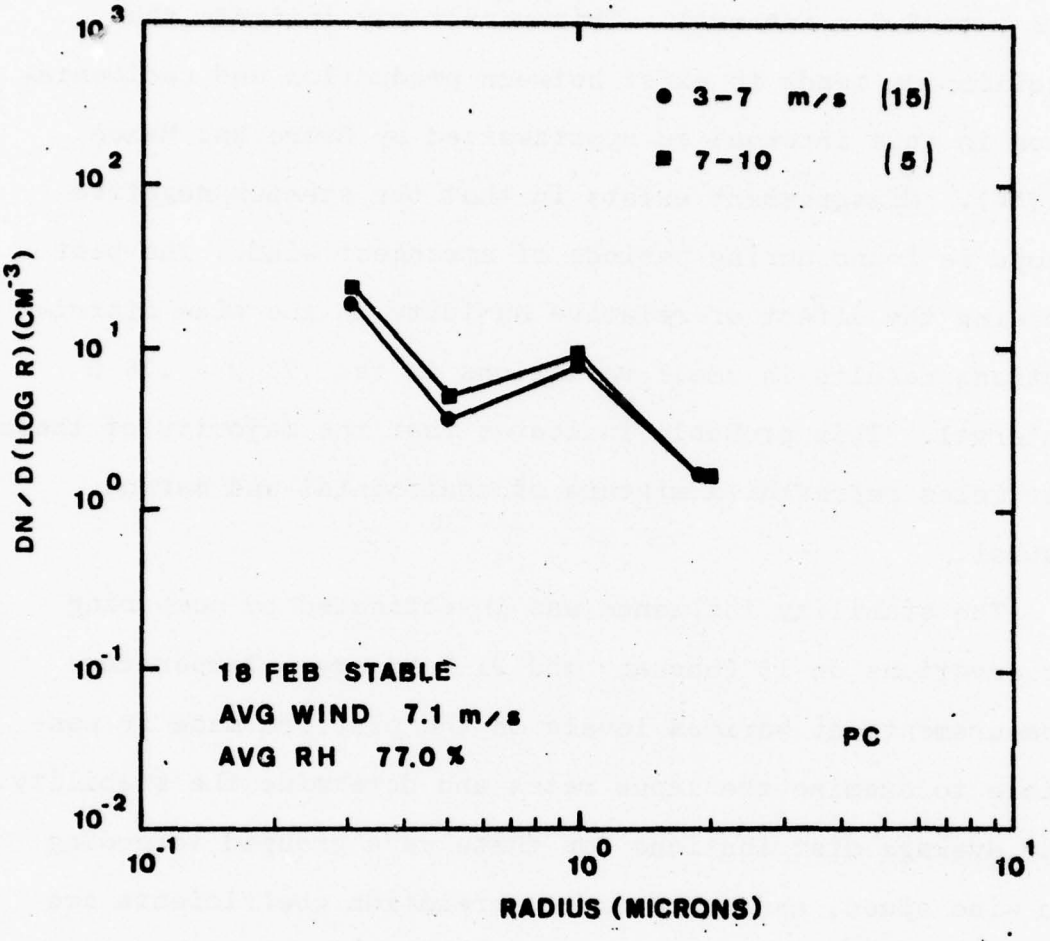

PC

INTERVAL	RH	WIND SPEED
.25-.35μ	.169	.065
.35-.70μ	.104	.334
.70-1.5μ	.279	.605
1.5-2.5μ	.385	.442

18 FEB STABLE

Figure 32. Correlation Coefficients and Variation of the Size Distribution with Wind Speed, 18 February

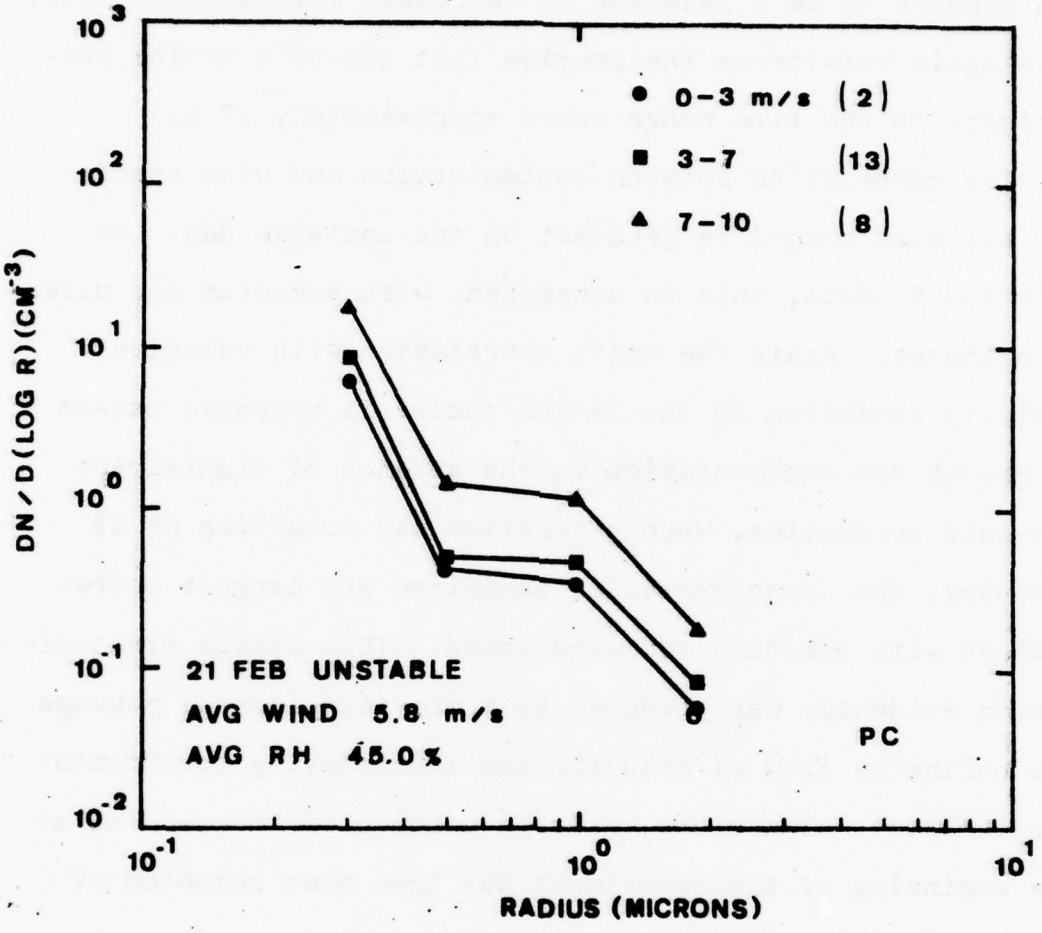

PC

INTERVAL	RH	WIND SPEED
.25-.35μ	.746	.615
.35-.70μ	.692	.651
.70-1.5μ	.558	.737
1.5-2.5μ	.253	.571

21 FEB UNSTABLE

Figure 33. Correlation Coefficients and Variation of the Size Distribution with Wind Speed, 21 February

1 μ appears to be a function of decreased relative humidity. This again reinforces the premise that sea-salt nuclei predominate in the size range above approximately .7 μ.

The correlation between concentration and wind speed for all size ranges is greatest on the unstable day. As with the SC data, this is consistent with momentum and diffusion theory. Again the small correlation with relative humidity exhibited by the larger nuclei is probable caused by growth and sedimentation in the absence of significant sea-salt production. When generation was occurring on 18 February, the large particles exhibited the largest correlations with humidity and wind speed. This stable stratification evidently was produced by a previous frontal passage and northerly flow of cold air and accompanying continental particulates. Therefore, a large portion of the aerosol at the beginning of the experiment may have been composed of non-hygroscopic material.

Figures 34 and 35 display the average diurnal changes in wind speed, relative humidity, and aerosol concentration. Again positive correlations are noted as relative humidity and wind speed, although containing quite a bit of scatter, tend to vary accordingly. Of most significance would be the obviously high concentration of droplets in the .7 μ - 1.5 μ range. Noting that the average wind seldom went below 7 m/sec, this would indicate that sea-salt nuclei production is greatest in this size range. A diurnal representation of the average aerosol distribution is presented in Figure 36.

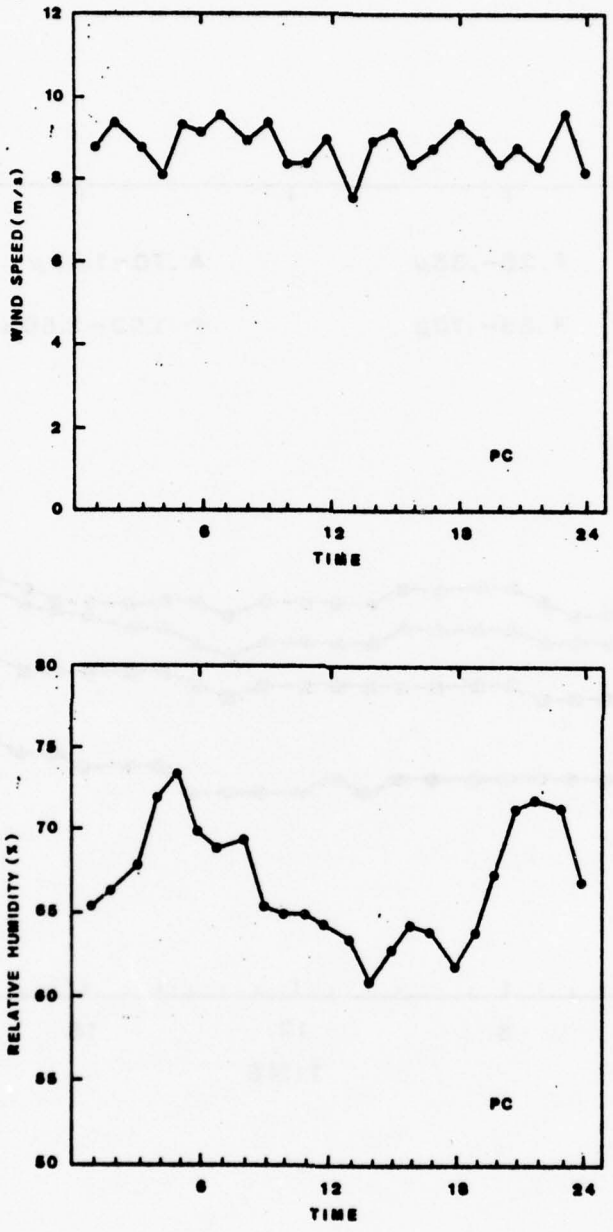

Figure 34. Average PC Diurnal Variations of Wind Speed and Relative Humidity

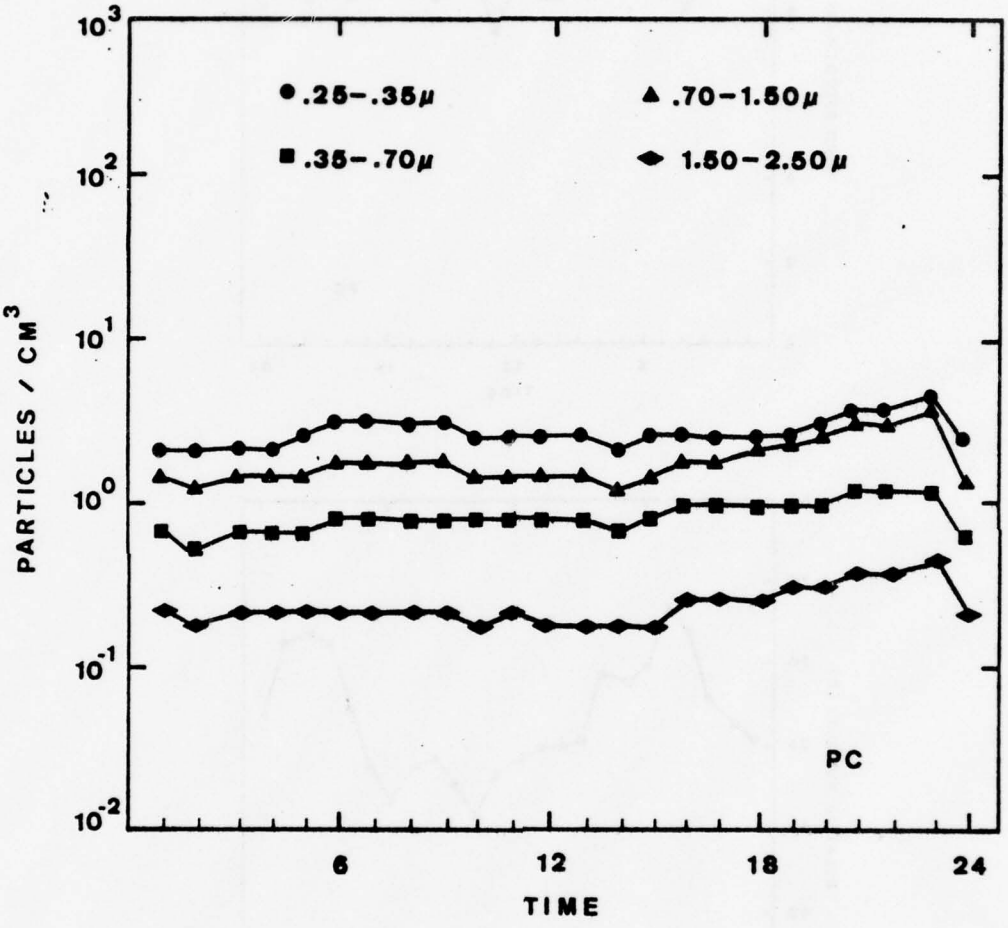

Figure 35. Average PC Diurnal Variations of Particle Concentrations

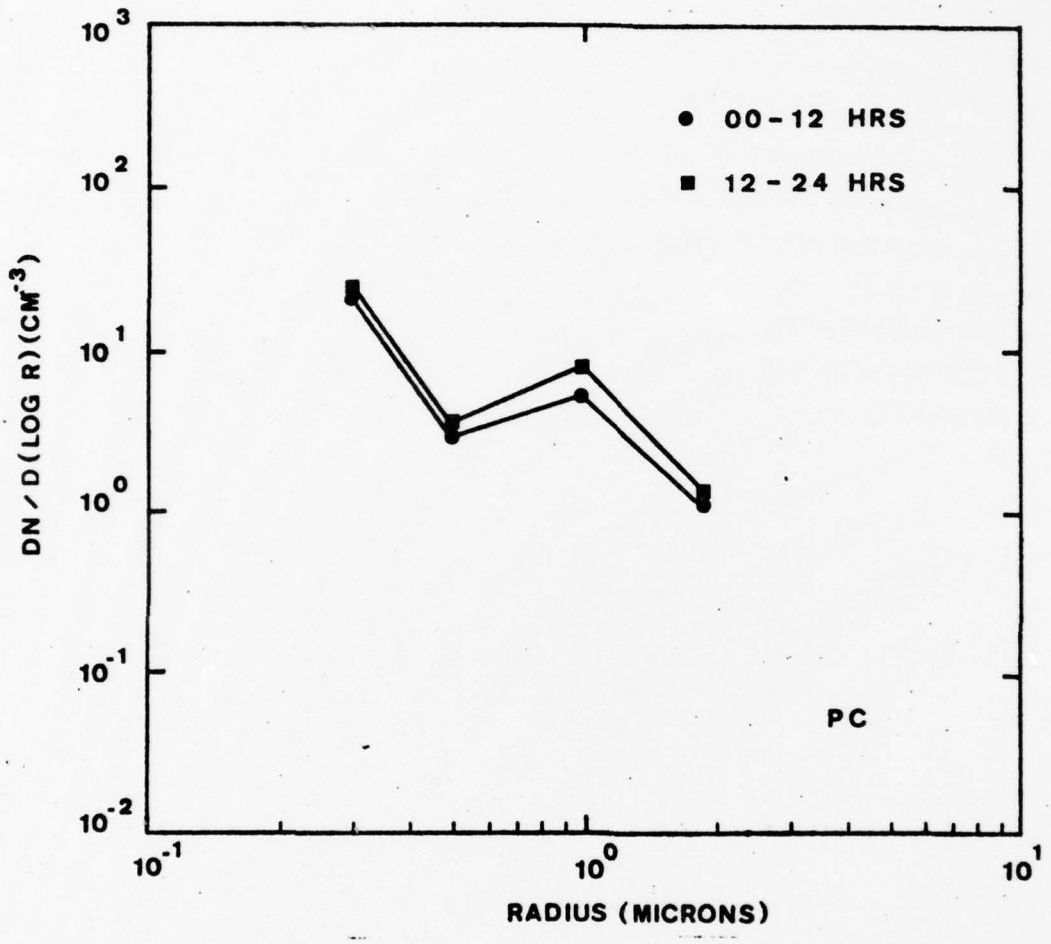

Figure 36. Average PC Diurnal Variation of the Aerosol Size Distribution

Any transport of aerosols due to a land-sea breeze effect should be ruled out as a satisfactory relationship does not seem to exist.

VII. CONCLUSIONS

The coastal marine aerosol is shown to be a highly variable function of the interaction between synoptic and mesoscale processes. Important meteorological parameters such as wind speed, relative humidity, and stability are dependent upon secondary circulations between land and sea in the absence of large scale forcing.

The minimum concentration in the size distribution curves at .4 μ - .5 μ radius may indicate that this size is indeed the transition zone between the two bubble bursting sea-salt producing mechanisms. Since the slope on either side of this zone is steeper during the Panama City experiment, wind speeds of greater than 7 m/sec result in the generation of sea-salt particles larger than .25 μ radius. Sedimentation of particles larger than 1.5 μ appears to be most significant during periods of low wind speed. During strong winds a state of equilibrium between sedimentation and production exists for these larger particles.

Relative humidity variations have the largest effect on the aerosol size distribution in the absence of sea-salt production. The concentration of the coastal marine aerosol is most sensitive to wind speed effects at low relative humidity. Friction velocity seems to be a better indication of the aerosol size distribution than wind speed under unstable atmospheric conditions. Also during light wind

periods, instability appears to result in a decrease in concentration at the observation height. Enhanced diffusion during periods of sea-salt production causes vertical transport of sea-salt from the sea surface and an increase in concentration.

Any effect of surface organic film possibly suppressing the production of small sea-salt particles could not be examined because of the absence of significant generation off the Southern California coast.

Table V. Panama City Data

DATE & TIME	RH	WIND DIR & SPEED	AITKEN CON	# PARTICLES / 2.8 L	>.5	>.7	>1.4	>3.0	>5.0
18 C	77	28015	3000		21C75	11206	7935	1287	200
18 100	68	28018	2300		21791	12419	8953	1324	216
18 200	72	27517	2000		18261	10588	7682	1147	179
18 300	72	28014	0		22634	13397	9792	1598	308
18 400	72	28514	0		23305	13914	10351	1644	265
18 500	83	29015	1500		23266	13930	10350	1588	270
18 600	83	28014	1600		24627	14956	11146	1701	294
18 700	76	28518	1800		25487	15548	11471	1570	228
18 800	78	28515	1800		24018	14461	10607	1450	220
18 900	73	28017	1600		23508	14357	10342	1491	225
18 1000	70	27515	0		22752	13351	9447	1317	190
18 1100	73	25015	0		21002	11973	8285	1161	174
18 1200	73	26514	1700		19602	10473	7014	1067	144
18 1300	73	260 E	1600		18490	8917	5471	879	109
18 1500	74	25013	2100		17104	8210	5095	722	76
18 1600	84	28011	1900		19002	10300	6921	1068	127
18 1700	78	28514	2000		18102	10248	7048	1117	158
18 2100	86	27014	1800		23647	13933	10385	1685	290
18 2200	84	27514	1700		23440	13872	10274	1655	299
18 2300	84	27015	1700		22644	13309	9635	1447	240
19 0	81	26516	1600		22648	13433	9744	1480	257
19 100	82	28018	1500		20363	11832	8320	1236	209
19 200	83	28017	0		18567	10848	7658	1163	180
19 300	84	28015	0		20337	11916	8591	1314	203
19 400	84	28013	0		20082	11917	8739	1486	220
19 500	85	28013	0		17003	9872	7170	1245	212
19 600	86	28013	1600		15437	8631	6196	1047	174
19 700	86	27512	1500		15227	8438	6035	1014	194
19 800	87	27013	1500		13565	7784	5624	1002	190
19 400	87	26512	3200		12605	6852	4832	804	126
19 1000	86	26512	1350		12267	6684	4695	781	133
19 1100	85	26510	0		12084	6339	4314	716	92
19 1200	83	25011	0		10293	5103	3402	567	84
19 1300	82	26511	1300		10085	4854	3057	485	65
19 1400	77	25512	1500		11280	5547	3588	592	73

DATE & TIME	RH	WIND DIR & SPEED	AITKEN CON	# PARTICLES / 2.8 L	>.5	>.7	>1.4	>3.0	>5.0
19 1500	77	27516	1400		11553	6074	2956	621	75
19 1600	74	25015	1900		13707	7262	4518	818	119
19 1700	81	24014	1600		13113	6951	4752	822	115
19 1800	83	24014	1500		14767	8359	6040	1100	191
19 1900	86	24514	2400		15396	8762	6422	1134	196
19 2000	85	25014	3900		16218	8251	5521	1060	184
19 2100	81	27015	5000		22721	9815	6807	1206	199
19 2200	86	28512	5200		27510	12120	8448	1448	240
20 200	69	35028	0		9030	2810	1640	201	37
20 300	66	35025	0		8603	2198	1196	160	23
20 400	62	35523	0		6051	1542	822	82	11
20 500	58	35021	8000		8187	1998	1067	139	19
20 600	51	35319	0		9283	2094	1125	142	21
20 700	51	35519	0		10768	2421	1153	138	16
20 800	51	35018	0		8003	1788	878	93	19
20 900	58	33516	0		7142	1327	686	59	12
20 1000	45	34017	0		6425	1375	681	57	8
20 1100	37	32019	0		5229	1248	736	125	36
20 1200	35	31521	0		4256	972	586	77	25
20 1300	35	31019	0		3806	1027	637	135	35
20 1400	30	31516	0		3155	871	536	89	18
20 1500	31	30020	0		2532	680	416	60	23
20 1600	32	30517	0		2671	712	457	74	16
20 1700	26	30515	0		4768	934	534	68	17
20 1800	24	32013	0		4334	1005	565	78	14
20 1900	29	35012	0		3243	598	684	167	54
20 2000	33	32010	0		3482	893	530	92	22
20 2100	45	29017	0		7045	2528	1586	260	51
20 2200	49	28518	0		6583	2076	1238	169	23
20 2300	45	33026	0		9442	2659	1636	254	52
21 0	44	33021	0		9384	2823	1667	267	74
21 100	42	32518	2700		7582	2674	1691	304	79
21 200	39	35016	2700		5155	1323	724	64	11
21 300	44	518	0		5417	715	276	5	1
21 400	45	1518	0		8835	1702	821	49	7

DATE & TIME		RH	WIND DIR & SPEED	AITKEN CON	# PARTICLES / 2.8 L	>.5	>.7	>1.4	>3.0	>5.0
21	5C0	57	5017	2400		16227	3181	1482	135	29
21	6C0	51	6516	2200		14496	3144	1565	171	42
21	7CC	51	8516	2200		15791	3463	15CE	104	11
21	8C0	52	10511	3300		10451	2C86	963	57	8
21	9CC	47	135 9	5000		6777	1385	688	64	9
21	1CC0	42	130 8	0		5764	1212	633	67	12
21	11C0	45	155 6	0		4743	988	511	56	6
21	12CC	42	175 6	8000		3550	910	454	62	10
21	13C0	37	215 7	9000		2672	567	300	35	7
21	14CC	4C	205 8	7000		2650	546	324	40	4
21	15C0	4C	240 8	0		2465	502	26E	33	2
21	16CC	35	24C 9	0		2843	597	310	39	7
21	17CC	36	24510	4500		2585	678	371	41	11
21	18C0	43	24010	4000		3C40	702	402	55	7
21	19C0	43	22510	2900		3282	808	451	64	10
21	2CCC	49	23511	3100		3133	780	435	69	10
21	21CC	47	22510	2800		3124	797	467	76	8
21	22CC	47	21510	3000		3321	888	520	71	10
21	23CC	48	20010	3000		3396	880	492	73	11
22	C	48	20C 9	2800		3404	856	485	71	11
22	1CC	55	18011	2700		336C	903	520	75	11
22	2CC	55	16511	2200		2902	846	510	89	6
22	3CC	59	14513	0		3556	1218	766	112	7
22	4CC	64	14014	0		3735	1478	971	135	18
22	5CC	71	13517	2000		5366	2287	1517	256	32
22	6CC	68	14019	2000		6182	2747	1508	278	42
22	7CC	66	14C19	2000		6688	3031	2049	341	61
22	8CC	66	14021	2000		7297	3365	2262	311	54
22	9CC	61	13822	1800		7299	3345	2223	298	30
22	1CCC	62	13522	2100		6784	3129	2050	278	28
22	11CC	65	13522	0		8611	4341	3010	402	61
22	12C0	69	13522	2300		8665	3906	2565	336	34
22	13CC	66	13522	2500		9368	4203	2663	375	45
22	14CC	66	13822	3600		8305	3451	2225	333	34
22	15CC	66	13322	0		8253	3500	2207	335	38

DATE & TIME		Rh	WIND DIR & SPEED	AITKEN CON	# PARTICLES / 2.8 L	>.5	>.7	>1.4	>3.0	>5.0
22	1600	65	14518	2400		8193	3551	2283	326	34
22	1700	71	13025	3200		9455	4276	2846	443	49
22	1800	70	12026	3000		9013	3528	2632	332	44
22	1900	70	11826	3000		10166	4562	3072	421	56
22	2000	76	14021	2500		10704	4593	3058	450	60
22	2100	73	15022	3300		8087	3483	2251	273	21
22	2200	73	13017	2000		8393	4419	3067	508	82
22	2300	82	12815	1700		10198	5447	3882	678	111
23	0	85	12018	2000		11839	6411	4566	678	87
23	100	86	11821	1700		12617	7048	5002	686	86
23	200	82	12522	2000		14337	8001	5818	835	129
23	300	84	13018	0		17257	9785	7192	1125	154
23	400	86	11516	0		18069	10235	7559	1076	191
23	500	88	11027	3500		18055	9643	7041	901	116
23	600	82	11527	2800		24655	14118	9970	1180	158
23	700	82	11028	3200		27584	15405	10982	1297	179
23	800	83	11024	3100		34453	18582	13313	1685	209
23	900	88	11028	3300		34011	18410	13031	1562	170
23	1000	86	11525	0		31144	16629	11121	1223	102
23	1100	86	11027	2700		36249	19615	13208	1332	107
23	1200	86	11531	2600		36675	20600	13926	1504	132
23	1300	85	13026	2400		37036	21113	14636	1696	188
23	1400	91	12525	2400		37751	21301	14592	1712	145
23	1500	91	11528	1800		41249	22854	15325	1493	134
23	1600	92	12025	1700		48270	28627	20153	2185	234
23	1700	91	11526	1600		48641	29137	20620	2117	208
23	1800	91	12528	1800		52317	31873	23169	2510	275
23	1900	91	14025	1700		60162	37378	28007	3312	505
23	2000	94	13325	1500		68055	42388	32516	4167	690
23	2100	94	14026	1300		70670	44713	34658	3822	518
23	2200	94	14528	0		75264	46227	36507	3174	281
23	2300	94	15528	1200		95524	56409	45316	5071	516

Table VI. Southern California Data

DATE & TIME		RH	REL WIND DIR & SPD	SHIPS HEAD & SPD	AITKEN CON	# PARTICLES / .28 L	>.3	>.6	>1.2	>3.0	>5.0
19	C	85	287 3	270 0	3000		12344	2531	933	10	0
19	100	92	290 1	270 0	1500		14239	2526	896	10	0
19	200	87	260 1	270 0	1700		15632	2975	1039	5	0
19	300	85	192 1	270 0	3500		12690	2660	995	11	0
19	400	85	180 10	180 9	0		13914	2475	797	10	0
19	500	85	180 10	180 9	0		14444	2485	841	6	0
19	600	80	340 7	140 9	0		6461	1455	578	7	0
19	700	82	15 8	140 9	0		6028	1371	550	10	0
19	800	81	360 9	205 9	0		5612	1673	624	9	0
19	1000	77	215 1	353 2	0		9261	1509	545	6	0
19	1100	76	172 9	175 9	3800		6753	1305	479	6	0
19	1120	76	172 9	175 9	0		7046	1429	565	11	0
19	1130	76	172 9	175 9	8500		6789	1321	526	10	0
19	1140	76	172 2	155 2	2200		6530	1290	495	12	0
19	1150	76	172 2	155 2	3000		6374	1321	489	10	0
19	1200	74	168 3	168 2	1300		6215	1357	579	14	0
19	1300	79	168 3	168 2	1200		6173	1291	503	12	0
19	1400	78	168 3	168 2	1500		6215	1304	458	5	0
19	1430	78	234 7	254 0	2900		6760	1466	583	22	0
19	1600	78	305 6	317 0	2100		8352	1618	585	7	0
19	1700	80	284 2	274 0	1300		6632	1340	504	12	0
19	1800	82	190 1	133 9	1200		7095	1491	575	14	0
19	2000	86	220 8	167 9	1100		8226	1658	610	10	0
19	2100	86	175 5	147 9	1800		11758	2088	728	5	0
19	2200	83	160 1	147 0	1400		11950	2139	723	16	0
19	2300	80	315 0	147 0	0		11620	2033	689	12	0
20	0	82	183 1	147 0	0		9526	1780	643	7	0
20	100	82	67 2	147 0	0		9986	1747	637	11	0
20	200	84	290 2	147 0	0		11699	1512	662	10	0
20	300	82	90 4	147 0	0		19871	4111	1473	8	0
20	400	84	280 5	0 0	0		23000	4668	1636	8	0
20	500	84	280 4	0 0	0		22081	4189	1431	5	0
20	555	84	270 3	0 0	5100		23114	4664	1628	8	0
20	610	84	270 3	0 0	8000		24119	4936	1784	5	0
20	625	84	270 3	0 0	4800		25023	5273	1922	8	0

DATE & TIME	RH	REL WIND DIR & SPD	SHIPS HEAD & SPD	AITKEN CON	# PARTICLES / .28 L	>.3	>.6	>1.2	>3.0	>5.0
20 650	84	270 3	0 0	0		23370	4879	1707	6	0
20 700	82	285 5	0 0	2400		23558	5028	1761	8	0
20 710	82	285 5	0 0	1950		22378	4658	1654	8	0
20 720	82	305 2	0 0	2700		21453	4445	1564	3	0
20 740	82	310 1	0 0	6000		22713	4723	1725	7	0
20 750	82	240 1	0 0	2400		21528	4536	1665	5	0
20 800	82	240 1	0 0	2200		22292	4675	1690	7	0
20 820	82	230 3	0 0	3000		24133	4141	1925	10	0
20 835	82	315 5	345 9	3900		22244	4640	1637	9	0
20 905	85	340 7	342 9	2900		22825	4953	1835	12	0
20 1000	82	310 8	350 9	1650		23006	5059	1865	14	0
20 1100	78	20 4	343 9	5500		13184	2310	793	7	0
20 1200	78	325 3	340 9	3600		12649	2228	733	5	0
20 1300	79	310 6	332 9	2500		14505	2066	629	6	0
20 1400	80	280 2	0 0	1600		15433	1917	550	3	0
20 1730	78	255 3	0 0	0		19117	3568	1393	7	0
20 1750	81	27510	350 0	9200		20619	4238	1448	8	0
20 1815	81	27510	350 0	0		16965	4032	1371	1	0
20 1900	86	27014	272 4	5800		21875	4718	1653	4	0
20 2005	87	27510	270 5	7000		26296	5768	2040	10	0
20 2050	85	280 5	0 0	5100		25881	6759	2438	7	0
20 2200	89	280 2	0 0	1900		27090	6880	2616	16	0
20 2300	88	300 3	0 0	3100		67724	20710	8710	16	0
21 0	93	330 7	360 9	2900		32913	8312	3119	14	0
21 100	94	305 2	0 0	4100		45895	12409	4761	5	0
21 200	95	225 2	265 9	0		51710	14480	5750	5	0
21 300	97	135 4	0 0	4400		55620	17560	7350	3	0
21 345	93	100 5	100 2	0		46050	12860	5264	5	0
21 500	90	125 2	0 0	5000		57565	16326	6641	19	0
21 545	90	160 2	0 0	5000		38950	9370	3548	17	0
21 645	87	170 1	0 0	2600		25423	5767	2250	16	0
21 800	87	170 1	0 0	0		34360	7496	2685	10	0
21 900	85	30 6	360 7	0		37857	7756	2730	15	0
21 1000	87	20 5	360 9	0		87734	25760	10098	15	0
21 1115	90	270 5	0 0	8200		98190	32021	13122	15	0

DATE & TIME	RH	REL WIND DIR & SPD	SHIPS HEAD & SPD	AITKEN CON	# PARTICLES / .28 L	>.3	>.6	>1.2	>3.0	>5.0
21 1215	90	260 8	0 0	7600		107112	36552	15930	11	0
21 1300	90	260 6	265 5	5000		110540	35506	16729	9	0
21 1400	90	274 6	254 6	7300		116775	37650	16250	1	0
21 1445	87	280 4	0 0	21000		65554	16527	6258	5	0
21 1600	85	260 2	0 0	4200		31756	7017	2589	13	0
21 1700	86	270 5	0 0	4300		11364	3261	1257	14	0
21 1800	85	265 9	0 0	9500		6360	2645	1179	17	0
21 1925	82	250 6	0 0	6400		5863	2685	1230	30	0
21 2010	85	225 7	0 0	5000		6259	2865	1307	21	0
21 2115	84	295 1	0 0	5300		6557	3069	1502	28	0
21 2200	88	80 9	53 9	4700		6587	2543	1464	25	0
21 2300	94	100 1	0 0	4800		8985	3256	1491	21	0
21 2315	94	100 1	0 0	4800		8739	3106	1416	16	0
21 2325	94	15 8	360 9	5200		11636	3648	1570	24	0
22 30	93	10 1	0 0	5600		10065	3569	1474	21	0
22 100	91	20 1	0 0	5200		9586	3214	1418	18	0
22 130	91	145 9	165 9	9000		12750	3889	1703	35	0
22 140	91	145 9	165 9	18500		34791	7800	2960	18	0
22 150	90	145 9	160 9	14500		58358	13095	4711	11	0
22 200	90	145 9	160 9	19000		72729	17835	6563	17	0
22 215	90	180 1	0 0	7300		50905	11661	4030	16	0
22 230	92	180 1	0 0	10000		61164	14380	5195	16	0
22 245	92	95 6	0 0	14000		68500	16653	5900	14	0
22 300	94	95 6	25 9	11000		65880	15400	5500	14	0
22 315	94	65 8	25 9	28000		72405	17859	6529	12	0
22 330	93	122 3	0 0	27000		70800	16380	5523	16	0
22 345	93	122 3	0 0	27000		57280	12460	4100	10	0
22 355	92	300 5	267 9	19000		42050	8785	2657	27	0
22 415	92	15 1	0 0	16000		30585	7054	2250	19	0
22 445	92	15 1	0 0	0		73900	18800	7060	14	0
22 515	95	120 3	0 0	21000		74348	15837	7487	18	0
22 600	95	130 9	138 9	5500		64051	16194	6190	15	1
22 645	95	10 7	360 9	9000		78139	20548	7623	10	0
22 715	95	20 1	0 0	16000		100065	25740	11800	11	0
22 800	93	20 1	0 0	9600		81079	21612	7799	12	0

DATE & TIME	RH	REL WIND DIR & SPD	SHIPS HEAD & SPD	AITKEN CON	# PARTICLES / .28 L	>.3	>.6	>1.2	>3.0	>5.0
22 835	93	20 1	0 0	0	104567	30760	11584	15	0	
22 850	93	20 1	0 0	0	104660	31147	12517	15	0	
22 910	93	20 1	0 0	0	120771	36450	14258	20	0	
22 945	93	20 1	0 0	0	89714	22441	8413	6	0	
22 1015	93	20 1	0 0	0	96659	27513	10500	10	0	
22 1040	93	20 1	0 0	0	100800	28583	10641	8	0	
22 1130	93	20 1	0 0	0	104968	31062	12386	9	0	
22 1200	92	170 2	52 0	0	84874	24125	9211	3	0	
22 1300	90	45 3	104 9	0	90750	25340	9591	8	0	
22 1400	85	180 5	155 9	6400	114549	33457	12966	9	0	
22 1500	86	225 7	155 9	79000	37164	6476	2095	26	0	
22 1600	89	155 2	153 9	6200	14650	3333	1137	5	0	
22 1700	84	215 8	179 9	3100	26285	5464	1946	9	0	
22 1755	85	275 5	0 0	10500	17685	3778	1328	5	0	
22 1810	85	260 3	0 0	4000	9248	2549	1182	9	0	
22 1900	91	140 3	0 0	3800	10718	2870	1127	13	0	
22 1915	91	150 3	0 0	8100	11925	3114	1242	20	0	
22 1930	91	150 3	0 0	6000	12038	3151	1266	23	0	
22 1945	91	150 3	0 0	9300	12081	2564	1257	20	0	
22 1950	90	145 6	0 0	14000	12468	3145	1220	19	0	
22 2020	90	255 2	0 0	4400	15438	3562	1453	12	0	
22 2115	92	120 9	100 9	4300	14500	3471	1295	14	0	
22 2200	97	11515	100 9	10000	14504	3245	1251	10	0	
22 2300	89	13512	100 9	11500	11953	2697	1093	7	0	
23 0	87	13512	100 9	5100	11140	2751	1065	8	0	
23 100	87	13010	95 9	4200	13020	2710	918	6	0	
23 200	92	135 8	90 9	3800	33570	6770	2222	8	0	
23 235	92	160 2	0 0	5800	63264	14772	5139	10	0	
23 315	92	330 3	325 9	2900	63350	14540	5240	17	0	
23 400	92	340 4	324 9	4700	46733	10112	3350	5	0	
23 530	92	340 4	324 9	3600	38071	7235	2269	3	0	
23 600	92	325 3	300 9	0	29975	5441	1575	0	0	
23 700	92	310 2	300 9	0	35975	6897	2170	5	0	
23 800	89	315 3	290 9	0	32127	5870	1860	5	0	
23 900	80	345 2	315 9	0	22542	3820	1070	5	0	

DATE & TIME		RH	REL WIND DIR & SPD	SHIPS HEAD & SPD	AITKEN CON	# PARTICLES / .28 L	>.3	>.6	>1.2	>3.0	>5.0
23	1CCC	78	33C 4	300 9	0		25258	4480	1253	5	0
23	14CC	82	250 5	0 0	7300		18968	4242	1570	17	0
23	15CC	85	215 8	215 5	2700		13656	3353	1327	21	0
23	16CC	82	300 7	360 9	5100		16043	3675	1411	27	0
23	165C	86	265 8	0 0	8000		40053	9837	3524	17	0
23	18CC	87	245 9	262 9	6400		76597	18645	6462	12	0
23	2CCC	88	250 1	0 0	3000		18165	4097	1571	18	0
23	21CC	86	300 1	0 0	2800		20170	4800	1805	16	0
23	22CC	90	330 1	0 0	3500		21142	4760	1852	21	0
23	23CC	91	200 1	0 0	4100		22894	5540	2212	23	0
24	8	93	5 3	160 4	6000		26669	6232	2352	20	0
24	30	93	305 6	318 4	13800		34045	8019	3021	22	0
24	1CC	90	27C 1	0 0	15500		75830	16535	7371	28	0
24	13C	90	135 6	100 5	18000		66626	16280	6169	20	0
24	155	85	180 2	0 0	17500		31474	5770	2160	23	0
24	23C	85	15C 2	0 0	19500		36695	6711	2382	23	0
24	3CC	86	225 7	245 9	16000		35510	6150	2032	11	0
24	33C	86	135 2	0 0	17500		45800	8344	2665	23	0
24	4CC	86	23C 6	245 9	15500		46516	9750	3090	11	0
24	430	86	24C 9	246 9	10000		34785	7334	2560	20	0
24	5CC	87	6C 5	50 9	5000		43400	9248	3200	24	0
24	53C	87	25 4	38 9	6900		46142	9792	3456	19	0
24	55C	85	31C 2	0 0	6200		62980	14200	5069	19	0
24	63C	85	170 6	147 9	12000		55820	13200	4600	15	0
24	7CC	84	160 8	167 9	14000		45738	9260	3000	15	0
24	8CC	80	14C 8	150 9	0		54937	10550	3289	14	0
24	83C	8C	14C 8	150 9	0		37551	8447	2111	10	0
24	9C0	76	75 2	0 0	0		30717	5212	1866	10	0
24	93C	76	75 2	0 0	0		32532	5742	1957	10	0
24	1CCC	77	320 8	325 9	0		41046	8516	2050	15	0
24	103C	77	32C 8	325 9	0		63024	11604	3446	15	0
24	110C	77	32011	330 9	0		75771	16170	5225	15	0
24	12C0	71	135 1	10C 9	0		92097	26258	10170	30	0
25	21CC	83	27C11	245 1	3800		10826	2636	712	7	0
25	223C	83	285 8	305 1	3600		8284	3261	1161	18	0

DATE & TIME		RH	REL WIND DIR & SPD	SHIPS HEAD & SPD	AITKEN CON	# PARTICLES / .28 L	>.3	>.6	>1.2	>3.0	>5.0
25	23CC	83	28C10	0 0	0		9490	3630	1378	30	0
26	C	83	290 6	0 0	0		9317	3784	1531	40	0
26	1CC	87	45 1	0 0	0		9486	4147	1890	50	0
26	2CC	86	225 1	0 0	0		13584	5317	2390	40	0
26	3CC	90	240 1	0 0	0		10170	4661	2259	40	0
26	4CC	90	360 9	340 9	0		9960	4600	2300	40	0
26	5CC	86	300 2	0 0	10000		11768	5540	2660	51	0
26	6CC	91	270 6	270 9	5600		11050	5090	2650	47	0
26	7CC	86	275 5	297 9	3000		10505	4825	2394	55	1
26	8C0	86	315 9	295 9	4500		9229	4167	2088	26	0
26	9CC	86	30C1C	295 9	6000		14336	5851	2650	36	0
26	10C0	85	30012	295 9	7300		14455	6019	2791	36	0
26	11CC	81	30012	255 9	12200		11144	4776	2256	24	0
26	12CC	82	29017	295 9	10500		10352	4365	1975	19	0
26	13C0	81	29016	284 9	9600		10857	4545	2059	12	0
26	14CC	77	27C17	278 9	5600		10953	4605	2077	15	0
26	15CC	77	24514	0 0	5400		12162	5280	2464	21	0
26	16CC	71	23512	278 8	4400		11940	5086	2280	19	0
26	17C0	52	29021	278 8	20000		7640	2542	1205	26	0
26	18CC	60	30514	70 0	7800		5229	1917	850	55	0
26	21CC	51	32512	70 3	0		5391	1320	520	25	0
26	22C0	62	325 8	80 3	0		4700	1446	573	25	0
26	23C0	62	325 4	80 3	0		3186	1067	452	15	0
27	C	73	150 3	90 2	7300		5085	2654	1097	26	0
27	104	95	13C 4	0 0	10000		7280	3094	1506	45	0
27	119	95	115 3	0 0	8400		6134	2455	1215	23	0
27	145	94	200 2	0 0	7600		6321	2358	1047	24	0
27	2CC	93	210 1	0 0	7000		7694	3097	1384	23	0
27	212	92	235 8	253 4	5800		5576	3850	1682	24	0
27	223	82	24C 1	0 0	6800		10586	4300	1849	25	0
27	25C	82	24C 1	0 0	7100		10122	4147	1820	25	0
27	3C6	84	315 1	0 0	6700		10280	4209	1890	23	0
27	324	85	31C 1	0 0	16000		10808	4253	1851	26	0
27	335	90	310 1	0 0	52000		10212	3996	1690	15	0
27	356	90	31C 1	0 0	23000		10383	4025	1807	40	0

DATE & TIME	RH	REL WIND DIR & SPD	SHIPS HEAD & SPD	AITKEN CON	# PARTICLES / .28 L	>.3	>.6	>1.2	>3.0	>5.0
27 417	5C	30 1	0 0	35000		10864	4320	1930	35	0
27 440	5C	80 1	0 0	23500		12414	4915	2272	34	0
27 5CC	85	275 4	0 0	0		9864	4105	1908	25	0
27 6CC	80	270 2	0 0	0		9689	4014	1958	15	0
27 7CC	75	255 2	0 0	0		12690	4986	2504	25	0

APPENDIX C:

REFERENCES

1. Blifford, I. H., 1970: "Tropospheric Aerosols", J. Geophys. Res., 75, 3099-3103.

2. Businger, J. A., J. C. Wyngaard, Y. Izumi, and E. F. Bradley, 1971: "Flux-Profile Relationships in the Atmospheric Surface Layer," J. Atmos. Sci., 28, 181-189.

3. Day, J. A., 1964: "Production of Droplets and Salt Nuclei by the Bursting of Air-Bubble Films," Q. J. Roy. Meteor. Soc., 90, 72-78.

4. Ericksson, E., 1959: "The Yearly Circulation of Chloride and Sulphur in Nature; Meteorological, Geochemical and Pedological Implications," Tellus, 11, 375-403.

5. Fairall, C. W., K. L. Davidson, J. Houlihan, and G. E. Schacher, 1977: Turbulence and Drag Coefficient over the Ocean. Unpublished, Environmental Physics Group, Naval Postgraduate School, Monterey, California, 19 pp.

6. Fitzgerald, J. W., 1975: "Approximation Formulas for the Equilibrium Size of an Aerosol Particle as a Function of its Dry Size and Composition and the Ambient Relative Humidity," J. Appl. Meteorol., 14, 1044-1049.

7. Fitzgerald, J. W. and R. E.Ruskin, 1977: A Marine Aerosol Model for the North Atlantic, Naval Research Laboratory Memorandum Report 3430, Washington, D. C., 104-110.

8. Friedlander, S. K., 1961: "Theoretical Considerations for the Particle Size Spectrum of the Stratospheric Aerosol," J. Meteorol., 18, 753-759.

9. Hidy, G. M., P. K. Mueller, H. H. Wang, J. Karney, S. Twiss, M. Imada, and A. Alcocer, 1974: "Observations of Aerosols over Southern California Coastal Waters," J. Appl. Meteorol., 13, 96-106.

10. Junge, C. E., 1972: "Our Knowledge of the Physico-Chemistry of the Undisturbed Marine Environment," J. Geophys. Res., 77, 5183-5200.

11. Junge, C. E. and R. Jaenicke, 1971: "New Results in Background Aerosols Studies from the Atlantic Expedition of the R. V. Meteor, Spring, 1969," Aerosol Sci., 2, 305-314.

12. Kientzler, C. F., A. B. Arons, D. C. Blanchard, and A. H. Woodcock, 1954: "Photographic Investigation of the Projection of Droplets by Bubbles Bursting at a Water Surface," Tellus, 6, 1-7.

13. Lieberman, A., and R. J. Allen, 1969: Theoretical and Experimental Light Scattering Data for a Near Forward System. Presented at American Association for Contamination Control, May 19-22, 15 pp.

14. Lovett, R. F., 1975: The Occurrence of Airborne Sea Salt and its Meteorological Dependence. M. S. Thesis, Heriot-Watt University, United Kingdom, 194 pp.

15. Lumley, J. L. and H. A. Panofsky, 1964: The Structure of Atmospheric Turbulence, Interscience Publishers, John Wiley and Sons, London, 239 pp.

16. Mack, E. J., 1977: Measurements of Aerosol Characteristics in the Marine Boundary Layer along the Offshore Margin of Southern California, Calspan Corp., Buffalo, N.Y., Prepared For: Naval Postgraduate School, Monterey, California, 44 pp.

17. Mack, E. J. and U. Katz, 1977: Measurements of Aerosol and Micrometeorological Characteristics of the Marine Boundary Layer in the Gulf of Mexico, Calspan Corp., Buffalo, N.Y., Prepared For: Naval Avionics Facility, Indianapolis, Indiana, 58 pp.

18. Mason, B. J., 1954: "Bursting of Air Bubbles at the Surface of Sea Water," Nature, 174, 470-471.

19. Mason, B. J., 1975: Clouds, Rain and Rainmaking, Cambridge University Press, Cambridge, 189 pp.

20. Meszaros, A. and K. Vissy, 1974: "Concentration, Size Distribution and Chemical Nature of Atmospheric Aerosol Particles in Remote Oceanic Areas," Aerosol Sci., 5, 101-109.

21. Monahan, E. C., 1968: "Sea Spray as a Function of Low Elevation Wind Speed," J. Geophys. Res., 73, 1127-1137.

22. Monin, A. S. and A. M. Obukhov, 1954: "Basic Laws of Turbulent Mixing in the Ground Layer of the Atmosphere," Akademiia Navk SSSR, Leningrad, Geofizicheskii Institut, Trudy No. 24 (151), 163-187, English Translation by Miller, J., 1959.

23. Moore, D. J., 1952: "Measurements of Condensation Nuclei over the North Atlantic," Q. J. Roy. Meteor. Soc., 78, 596-602.

24. Moore, D. J. and B. J. Mason, 1954: "The Concentration, Size Distribution and Production Rate of Large Salt Nuclei over the Oceans," Q. J. Roy. Meteor. Soc., 80, 583-590.

25. Panofsky, H.A., 1969: "Air Pollution Meteorology," American Scientist, 57, 269-285.

26. Panofsky, H. A., A. K. Blackadar, and G. G. McVehil, 1960: "The Diabatic Wind Profile," Q. J. Roy. Meteor. Soc., 86, 390-398.

27. Paterson, M. P. and K. T. Spillane, 1969: "Surface Films and the Production of Sea-Salt Aerosol," Q. J. Roy. Meteor. Soc., 95, 526-534.

28. Ruskin, R. E., R. K. Jeck, and H. E. Gerber, 1976: Progress Report on Sea Salt Measurement September 1975 - January 1976, Naval Research Laboratory Memorandum Report 3270, Washington, D. C., 10 pp.

29. Toba, Y., 1965a: "On the Giant Sea-Salt Particles in the Atmosphere, 1, General Features of the Distribution," Tellus, 17, 131-145.

30. Toba, Y., 1965b: "On the Giant Sea-Salt Particles in the Atmosphere, 2, Theory of the Vertical Distribution in the 10-m Layer over the Ocean," Tellus, 17, 365-382.

31. Whitby, K. T. and B. Y. Liu, 1973: Advances in Instrumentation and Techniques for Aerosol Generation and Measurement, P. L. Pub. No. 216, University of Minnesota, 34 pp.

32. Winkler, P., 1973: "The Growth of Atmospheric Aerosol Particles as a Function of the Relative Humidity---II. An Improved Concept of Mixed Nuclei," Aerosol Sci., 4, 373-387.

33. Woodcock, A. H., 1953: "Salt Nuclei in Marine Air as a Function of Altitude and Wind Force," J. Meteorol., 10, 362-371.

34. Woodcock, A. H., 1972: "Smaller Salt Particles in Oceanic Air and Bubble Behavior in the Sea," J. Geophys. Res., 77, 5316-5321.

35. Wyngaard, J. C., Y. Szumi, and S. A. Collins, 1971: "Behavior of the Refractive Index Structure Parameter near the Ground," Jour. Opt. Soc. America, 61, 1646-1650.

36. Zinky, W. R., 1962: "A New Tool for Air Pollution Control: The Aerosol Particle Counter," J. Air Pollution Control Assoc., 12, 578-583.

References

Equipment:

Houlihan, T., K. L. Davidson, C. W. Fairall, and G. E. Schacher, "Experimental aspects of a shipboard system used in investigation of overwater turbulence and profile relationships", Submitted to J. Applied Meteorology, January 1978.

Fairall, C. W. and G. E. Schacher, "Frequency response of hot wires used for atmospheric turbulence measurements in the marine environment", Rev. Sci. Instrum. 47, 12-17 (1977).

Plunkett, J. R., "A microprogrammable data acquisition and control system (MIDAS II A) with application to mean meteorological data", M.S. Thesis, Naval Postgraduate School, Monterey, California (1976).

Schacher, G. E. and C. W. Fairall, "Use of resistance wires for atmospheric turbulence measurements in the marine environment", Rev. Sci. Instrum. 47, 703-707 (1976).

Corbin, J. H., "Measurements of near surface turbulence and possible wave influence", M.S. Thesis, Naval Postgraduate School, Monterey, California (1977).

Welsh, P. T., "An investigation of ship related motion and its effect on turbulence measurements", M.S. Thesis, Naval Postgraduate School, Monterey, California (1974).

Theory:

Businger, J. A., J. C. Wyngaard, Y. Izumi, and E. F. Bradley, "Flux profile relationships in the atmospheric surface layer", J. Atmos. Sci. 28, 181-189 (1971).

Fairall, C. W., K. L. Davidson, T. M. Houlihan, and G. E. Schacher, "Atmospheric turbulence measurements in marine fog during CEWCOM-76", Naval Postgraduate School Report, NPS61-77-004.

Kraus, E. B., Atmosphere-Ocean Interaction, Clarendon Press, Oxford, Ch. 5 (1972).

Lumley, J. L. and H. A. Panofsky, The Structure of Atmospheric Turbulence, Interscience, New York (1964).

Hughes, M. M., "An investigation of optically relevant turbulence parameters in the marine boundary layer", M.S. Thesis, Naval Postgraduate School, Monterey, California (1976).

NPS Theses:

Johnston, W. E., "Estimating boundary layer fluxes from dissipations of turbulent kinetic energy and temperature variance", M.S. Thesis, Naval Postgraduate School, Monterey, California (1974).

Karch, G. W., "An examination of turbulent dissipation in the marine boundary layer", M.S. Thesis, Naval Postgraduate School, Monterey, California (1976).

Lund, A. B., "Spectral estimates of marine turbulence data", M.S. Thesis, Naval Postgraduate School, Monterey, California (1975).

Schutt, W. L., "An investigation of small scale humidity fluctuations in the marine boundary layer", M.S. Thesis, Naval Postgraduate School, Monterey, California (1976).

Smedley, G. W., "Investigations of vertical profiles of mean temperature, wind and humidity", M.S. Thesis, Naval Postgraduate School, Monterey, California (1975).

Cavanaugh, M. P., "Examination of shipboard measurements of the vertical profiles of mean temperature, humidity, and wind speed", M.S. Thesis, Naval Postgraduate School, Monterey, California (1974).

Atkinson, H. E., III, "Turbulent flux estimates from shipboard mean wind and temperature profiles and dissipation rates", M.S. Thesis, Naval Postgraduate School, Monterey, California (1976).